

# A Combination of Cold Ion Spectroscopy and Ion Mobility for the Study of Complex Peptides and Small Proteins

THÈSE N° 5427 (2012)

PRÉSENTÉE LE 28 SEPTEMBRE 2012

À LA FACULTÉ DES SCIENCES DE BASE

LABORATOIRE DE CHIMIE PHYSIQUE MOLÉCULAIRE

PROGRAMME DOCTORAL EN CHIMIE ET GÉNIE CHIMIQUE

ÉCOLE POLYTECHNIQUE FÉDÉRALE DE LAUSANNE

POUR L'OBTENTION DU GRADE DE DOCTEUR ÈS SCIENCES

PAR

Georgios PAPADOPOULOS

acceptée sur proposition du jury:

Dr R. Hovius, président du jury  
Prof. T. Rizzo, directeur de thèse  
Prof. D. Clemmer, rapporteur  
Prof. Y. Tsybin, rapporteur  
Dr G. von Helden, rapporteur



ÉCOLE POLYTECHNIQUE  
FÉDÉRALE DE LAUSANNE

Suisse  
2012



# Abstract

We present in this work experiments that push the limits of cold ion spectroscopy to the study of complex peptides and small proteins in the gas phase. Although the low temperature attainable in a cold ion trap greatly simplifies the electronic spectra of large molecules, conformational heterogeneity can still be a significant source of congestion, complicating spectroscopic analysis. To overcome this hurdle, we propose an *in tandem* combination of ion mobility spectrometry and photofragment spectroscopy. This permits for conformational separation prior to laser interrogation.

Towards this end, we describe a proof-of-principle experiment where we combine high-Field Asymmetric waveform Ion Mobility Spectrometry (FAIMS) with electronic spectroscopy. We demonstrate that using FAIMS to separate gas-phase peptide conformers before injecting them into a cold ion trap allows one to decompose a dense spectrum into contributions from different conformational families. In the inverse sense, cold ion spectroscopy can be used as a conformation-specific detector for ion mobility, allowing one to separate an unresolved mobility peak into contributions from different conformational families. The doubly protonated peptide bradykinin serves as a good test case for the marriage of these two techniques as it exhibits a considerable degree of conformational heterogeneity that results in a highly congested electronic spectrum. Our results demonstrate the feasibility and advantages of directly coupling ion mobility with spectroscopy and provide a diagnostic of conformational isomerization of this peptide after being produced in the gas phase by electrospray.

In a second series of studies we show the potential but also the limitations of our spectroscopic approach for investigating small, naturally occurring proteins, by applying it to ubiquitin, a protein of 76 amino acids. We present electronic photofragment spectra of various protonation states of ubiquitin and we compare our results to literature data acquired by ion mobility spectrometry. These experiments show that the information obtained by laser interrogation of molecules of this size is limited and could be enhanced by a combination with ion mobility techniques. Although some of the results obtained may be important in characterizing small proteins in the gas phase, these experiments are at an early stage and the application of photofragment spectroscopy on proteins needs more investigation.

**Keywords:** electronic spectroscopy, ion mobility spectrometry, FAIMS, spectral congestion, conformational separation, tandem mass spectrometry, cold ions, gas phase peptides, gas phase proteins.

# Résumé

Au cours de ce travail nous présenterons des expériences qui repoussent les limites de la spectroscopie de photodissociation d'ions à basse température en phase gazeuse appliquée à des peptides complexes et des protéines. La basse température utilisée dans notre piège à ion simplifie grandement le spectre électronique des grandes molécules en les plaçant dans leurs états fondamentaux. Cependant, l'hétérogénéité des conformères présent peut compliquer l'analyse spectroscopique en superposant l'ensemble des spectres de chacun des conformères, rendant l'attribution des raies difficile, voir impossible. Nous présenterons dans cette thèse une méthode permettant cette attribution, en combinant la spectroscopie de photodissociation avec une technique de mobilité ionique. Cette dernière permet la séparation des conformères avant l'excitation laser.

Pour cela, nous avons mis au point une expérience au cours de cette thèse. Celle-ci utilise la mobilité ionique de forme d'onde asymétrique et à haut champ (appelé "FAIMS") avec la spectroscopie électronique. Nous démontrerons que cette technique permet la décomposition d'un spectre électronique originalement dense en spectre plus simple représentant chaque famille de conformères. Inversement, la spectroscopie peut être utilisée comme détecteur pour la mobilité ionique d'un conformère spécifique permettant de séparer un pic non-résolu aux contributions de différentes familles de conformères. La bradykinine doublement protonée est un bon test pour le mariage de ces deux techniques. En effet, elle possède un haut degré d'hétérogénéité de conformères, il en résulte une superposition importante de spectres électroniques. Nous avons utilisé ce peptide pour démontrer la faisabilité d'une telle technique et fournir un diagnostic d'isomérisation de conformères de ce peptide après la production en phase gazeuse par electrospray.

Dans une seconde partie, nous montrerons les avantages mais aussi les limites de notre approche spectroscopique utilisée pour investiguer de petites protéines en l'appliquant sur l'ubiquitin, une protéine de 76 acides aminés. Nous présenterons les spectres électroniques de photodissociation de divers états protonés de l'ubiquitin et nous comparerons nos résultats avec ceux de la spectrométrie de la mobilité ionique. Les expériences montrent que l'information obtenue par la spectroscopie de molécules de cette taille est limitée et pourrait être amélioré en utilisant une combinaison de techniques de la mobilité ionique (telle que celle présenté dans la première partie). Bien qu'il soit possible d'obtenir des informations pour caractériser des petites protéines en phase gazeuse, ces expériences, au moment de l'écriture de cette thèse, sont encore à

leur début. Il apparaît que l'utilisation de spectroscopie de photodissociation aux protéines de plus grande taille nécessite un important développement.

**Mots-clés:** spectroscopie électronique, spectrométrie de la mobilité ionique, FAIMS, congestion du spectre, séparation des conformères, spectrométrie de masse en tandem, ions froids, peptides en phase gazeuse, protéines en phase gazeuse.

# Table of contents

<b>1 Introduction</b>	<b>5</b>
1.1. Methods of studying biomolecules in the gas phase	6
1.2. Spectroscopy of biomolecules in the gas phase	8
1.3. High-Field Asymmetric waveform Ion Mobility Spectrometry (FAIMS)	11
1.4. Goals and outline	13
1.5. References	14
<b>2 Experimental apparatus</b>	<b>23</b>
2.1. Overview of the tandem mass spectrometer	23
2.2. Electrospray ionization	26
2.3. Ion transmission in the mass spectrometer	28
2.3.1. Quadrupole mass analyzers	28
2.3.2. Higher order multipoles	30
2.4. Description of laser setup and spectroscopic schemes	31
2.4.1. Generation of ultraviolet radiation	31
2.4.2. Generation of infrared radiation	32
2.4.3. Spectroscopic scheme	32
2.5. References	34
<b>3 High-Field Asymmetric waveform Ion Mobility Spectrometry (FAIMS)</b>	<b>37</b>
3.1. Ion separation in IMS	37
3.1.1. Principle of operation	37
3.1.2. Multidimensional IMS separations	39
3.2. Ion separation in FAIMS	40
3.2.1. Principle of operation	40
3.2.2. The standard high-field effect	42
3.2.3. Clustering and declustering of ions	45
3.2.4. Collisional and dipole alignment	45
3.3. FAIMS geometries	47
3.3.1. Focusing in cylindrical geometries	47
3.3.2. “dome” FAIMS	49
3.3.3. “side-to-side” FAIMS	50
3.4. Parameters that govern FAIMS performance	52
3.4.1. The asymmetric waveform	53
3.4.2. The analytical gap width	54
3.4.3. The carrier gas flow speed/length of the gap	54
3.4.4. The composition of the carrier gas	55
3.4.5. Instrumental modifications for high-resolution FAIMS	56
3.5. Comparison of IMS with FAIMS	57
3.6. References	58
<b>4 Spectroscopy of mobility-selected biomolecular ions</b>	<b>63</b>
4.1. Introduction	63
4.2. Coupling of ion mobility and cold ion spectroscopy	66
4.3. Bradykinin and its structure in the gas phase	70
4.4. Experimental details	72
4.5. Bradykinin in “side-to-side” FAIMS	72

4.6. FAIMS as a conformational filter for cold ion spectroscopy.....	79
4.7. Cold ion spectroscopy as a high resolution ion mobility detector.....	85
4.8. Conclusions.....	87
4.9. References.....	89
<b>5 Using the conformational distribution of bradykinin as a probe of isomerization .....</b>	<b>93</b>
5.1. Introduction .....	93
5.2. Experimental details.....	94
5.3. Gas phase conformational distribution of [bradykinin + 2H] <sup>2+</sup> without FAIMS.....	95
5.4. Investigation of the cross-conformer contamination.....	98
5.4.1. Introduction .....	98
5.4.2. Increasing FAIMS resolution .....	100
5.4.3. Reducing heating in FAIMS.....	103
5.5. Quasi-equilibrium distribution in the gas phase .....	107
5.6. Kinetic-trapping of ions and implications concerning their solution structure.....	109
5.7. Conclusions.....	111
5.8. References.....	112
<b>6 Electronic photofragment spectroscopy of cold ubiquitin.....</b>	<b>115</b>
6.1. Introduction .....	115
6.2. Ubiquitin and its structure in the gas phase.....	116
6.3. Experimental details.....	120
6.4. nESI mass spectra of ubiquitin.....	120
6.5. Photofragmentation spectra of ubiquitin in phe and tyr absorption regions .....	121
6.6. UV fragmentation vs UV excitation assisted by IRMPD .....	125
6.7. Spectra of different charge states of ubiquitin.....	129
6.8. The influence of the injection voltage .....	131
6.9. Conclusions.....	136
6.10. References.....	137
<b>7 Conclusions and perspectives .....</b>	<b>141</b>
7.1. References.....	143
<b>List of abbreviations.....</b>	<b>145</b>
<b>Curriculum vitae.....</b>	<b>147</b>







## Introduction

The biological function and specificity of each protein depends strongly on its higher-order structure. The structure of a protein is often described in a hierarchical way. Short-range interactions between residues, which are near neighbors in the primary sequence of amino acids, determine secondary structure. The three-dimensional arrangement is then described in terms of combination and orientation of secondary structural elements.<sup>1</sup> The interplay between intramolecular interactions and interactions with the solvent drives protein folding and is also responsible for the integrity of the higher-order, biologically active state of a biomolecule.<sup>2</sup> However, the native, functional state of a protein is not a single structure, but rather an ensemble of structures (conformational sub-states) having the same overall folding pattern but differing in details (e.g., orientations of amino acid side chains).<sup>3</sup> The sub-states that constitute the native ensemble are in thermal equilibrium, and fluctuations between them are essential for protein function and play a major role in allostery.<sup>4-7</sup>

Protein folding involves the transformation of an one-dimensional chain of amino acids into a three-dimensional shape.<sup>8,9</sup> In principle, the information on the structure of the final state is contained in the primary sequence of amino acids,<sup>10</sup> but it is not trivial to predict the shape of the folded protein from the adjacent constituents of the linear chain.<sup>11,12</sup> Nevertheless, in order to understand the function of a protein it is essential to determine its geometry.

For many proteins, X-ray crystallography can be used to obtain their structure at atomic-scale resolution.<sup>13,14</sup> This approach presumes that the native structure is not altered or distorted upon crystallization. Recently, the use of picosecond time-resolved X-ray crystallography has been developed and allowed the real-time observation of a protein as it performs its function.<sup>15-18</sup> In solution, atomic-scale resolution of the structure of a biomolecule can be obtained from multidimensional Nuclear Magnetic Resonance (NMR) experiments.<sup>19-22</sup> Techniques like Fourier Transform Infrared Spectroscopy (FTIR)<sup>23</sup> and Circular Dichroism (CD)<sup>24,25</sup> can provide lower resolution structural information, such as the presence of different secondary structural elements (e.g.  $\alpha$ -helices and  $\beta$ -sheets) and their relative amounts in a folded protein.

While the above methods probe biomolecular structure in condensed phases, a large effort has been invested in studying biomolecules in the gas phase.<sup>26</sup> The work described in this thesis falls into the latter category. In the subsequent sections we will discuss some advantages offered by the investigation of solvent-free biomolecules in the gas phase and present some methods used for characterizing them. We will focus mainly on the two techniques that are used in this thesis, namely laser spectroscopy and high-Field Asymmetric waveform Ion Mobility Spectrometry (FAIMS).

## 1.1. Methods of studying biomolecules in the gas phase

As mentioned above, the subtle balance between inter- and intramolecular interactions determines the folded, “native” shape of a biomolecule. By isolating biomolecules in the gas-phase, one can disentangle these two contributions and study only their intrinsic behavior, for example the inherently preferred conformations as well as conformational changes in the absence of solvent. Moreover, there is a growing amount of evidence that, under some conditions, solvent-free biomolecules are found in metastable states right after the removal of the solvent, suggesting that they may represent solution phase structures.<sup>27,28</sup> Thus, probing these metastable states may provide insight into the structures adopted by the molecule in solution. Subsequently, the effects of the solvent on the structure and dynamics can be investigated in a step-wise fashion, by adding a controlled number of solvent molecules in the solvation shell of the biomolecule.<sup>29</sup>

The advent of Matrix-Assisted Laser Desorption/Ionization (MALDI)<sup>30,31</sup> and Electrospray Ionization (ESI, see Section 2.2)<sup>32-34</sup> has enabled the transfer of large, non-volatile and thermally labile molecules from the solution to the gas phase as closed-shell molecular ions. Once the gas phase charged species is produced it can subsequently be analyzed using mass spectrometric methods.<sup>35</sup> In this way, one can determine accurately the molecular mass of an intact protein as well as obtain information on its amino acid sequence by detecting and identifying fragments that result either from collision-induced<sup>36-39</sup> laser-induced dissociation<sup>40</sup> or other techniques (ECD etc.). However, the sequence of building blocks of a protein reveals little information about its three-dimensional architecture. The latter can be explored by several other methods.

One technique that can be used to reveal molecular conformation is gas phase hydrogen/deuterium (H/D) exchange.<sup>41-47</sup> In these studies biomolecular ions are allowed to collide for a certain time with an exchange reagent containing deuterium, such as D<sub>2</sub>O or ND<sub>3</sub>.<sup>42,48</sup>

During collisions the labile hydrogens of the protein ion can be exchanged. These include hydrogens of amine, amide, carboxyl and hydroxyl groups of the backbone and those that are bound to N, O and S atoms of the side chains. Exchange is faster for those that are not involved in intramolecular hydrogen bonding and are exposed to the surface of the ion. This process is detected as an increase in the mass of the ion. Different extents of H/D exchange reveal the presence of different conformations.<sup>47</sup> Using this technique, a number of gas phase conformations was revealed for multiply charged proteins like ubiquitin<sup>49</sup> and cytochrome *c*.<sup>42,43</sup> Implicit to the interpretation of the experimental results is that exchange rates and surface accessibility are correlated.<sup>50</sup> This method can also detect transitions between conformations that transiently expose “hidden” exchange sites.<sup>51</sup> H/D exchange measurements can also be performed in solution<sup>52</sup> with the exchange rates being measured by NMR<sup>53,54</sup> or mass spectrometry.<sup>55-57</sup> This way, the higher-order structure as well as conformational dynamics of proteins in solution can be inferred.

Another technique that is used to provide insight into the structure and conformation of gas phase biomolecules is Ion Mobility Spectrometry (IMS),<sup>58-61</sup> which is discussed in Section 3.1. IMS measures the time during which an ion drifts through a tube filled with a buffer gas under the influence of an electric field.<sup>62,63</sup> Larger ions drift slower than smaller ones and thus the drift time is connected to the size of the ion, or, more precisely, to its collision cross section. The latter can be compared to calculated cross sections from trial geometries generated by computers, allowing the assignment of the ion structure.<sup>62,64,65</sup> With this method different conformations of proteins were detected and identified, for example in studies of several charge states of cytochrome *c*,<sup>60,66</sup> ubiquitin<sup>67</sup> and bovine pancreatic trypsin inhibitor.<sup>66</sup> Using IMS methods, model peptides that form stable helical<sup>68</sup> or more complex helix-turn-helix<sup>69,70</sup> structures in the gas phase have been designed. IMS can also be used to probe conformational changes in the gas phase.<sup>71,72</sup> Combinations of the techniques of IMS and H/D exchange have also been employed for the two-dimensional characterization of gas phase biomolecules.<sup>50,51</sup>

A third technique that can shed light into the gas phase structures of biomolecules is Blackbody Infrared Radiative Dissociation (BIRD).<sup>73-78</sup> In these experiments, the selected ions are trapped for long times in vacuum, absorb blackbody radiation from the vacuum chamber walls and eventually dissociate.<sup>73</sup> Measurement of the dissociation rate as a function of the chamber temperature yields Arrhenius activation energies and pre-exponential factors.<sup>74</sup> Comparison of these quantities for a selected molecule with those obtained for carefully selected molecular analogues can provide data from which structural information can be inferred.<sup>74,76</sup> For example, by comparing the Arrhenius parameters for singly protonated bradykinin and several of its

analogues where selected residues were replaced, Williams and coworkers found evidence that it exists as a zwitterion in the gas phase.<sup>74</sup>

While the above methods offer undeniable assistance in the identification of general properties of gas phase biomolecules, they provide only limited structural information. The mechanism of H/D exchange is also influenced by other parameters than surface accessibility, making the correlation of the extent of H/D exchange to the compactness of a structure difficult.<sup>47</sup> Furthermore, ion mobility techniques reside on a single observable (the collision cross section) for the identification of conformational types, hence the detailed information is limited, while the BIRD technique provides only indirect information about the structure. Spectroscopic methods, on the other hand, can provide more detailed structural information for amino acids and small peptides, since the optical properties of a specific molecule are very sensitive to its arrangement. A short review of spectroscopic studies of gas phase biological molecules follows in the next section.

## 1.2. Spectroscopy of biomolecules in the gas phase

The interrogation of biomolecules by laser spectroscopy in the gas phase is an active field of research since the mid-1980s.<sup>79-83</sup> Recent reviews have covered many of its facets and only key experiments will be mentioned here.<sup>84-89</sup> Early experiments in the group of Levy employed electronic spectroscopy in order to investigate the conformational preferences of amino acid tryptophan and its derivatives in the cold, isolated environment of a molecular beam.<sup>79,80,90</sup> The molecular beam of tryptophan was produced by heating the solid sample in front of the nozzle of the supersonic helium expansion. While thermal instability inhibited the transfer of larger molecules in the gas phase, the use of laser desorption allowed for the production of larger and more complex systems and their subsequent interrogation by laser spectroscopy.<sup>83,91-93</sup>

An important leap forward for the field was the introduction of IR-UV<sup>94,95</sup> and UV-UV<sup>95</sup> double resonance spectroscopy by Zwier. In combination with cooling in supersonic expansions, these spectroscopic schemes led to an explosion of studies of neutral peptides.<sup>96-114</sup> With UV-UV double resonance the electronic spectrum can be deconvoluted to contributions from different isomers,<sup>94,115</sup> while with IR-UV double resonance conformer-specific vibrational spectra can be recorded. Comparison of experimental and calculated vibrational spectra can be used for structural assignment.<sup>115-118</sup> For both above techniques, a UV laser is set on a transition

originating from a specific conformer, and thus UV transitions from different isomers have to be clearly resolved. Recently, Zwier introduced an IR-IR-UV triple resonance scheme for the recording of conformation specific spectra of molecules that have indistinguishable electronic spectra.<sup>119</sup> Mons and others have used IR-UV to identify hydrogen bonding patterns in model peptides adopting  $\beta$ -turns,<sup>104,120</sup>  $\gamma$ -folds,<sup>105</sup> and helices<sup>108,121</sup> in the gas phase, while Gerhards and coworkers identified signatures of  $\beta$ -sheet structures.<sup>97,122-124</sup> Recently, Rjis *et al.* used mid-IR radiation from a free-electron laser in an IR-UV scheme to observe and characterize a neutral peptide that adopts a zwitterionic structure in the gas phase.<sup>113</sup>

Zwier and coworkers have reached beyond the identification of structural isomers, by conducting population transfer experiments between different stable conformations.<sup>125-130</sup> In these studies a specific conformational population is excited by an IR pulse<sup>125</sup> or by stimulated emission pumping,<sup>127</sup> and as a result part of it can isomerize to other conformations. Subsequently the resulting conformational distribution is probed spectroscopically. In that way, the conformational dynamics and the barriers to isomerization between conformers can be investigated.

The development of electrospray ionization (ESI)<sup>32,131</sup> made possible the production of large, protonated species for spectroscopic studies in the gas phase. The electrosprayed species are produced in the form of closed shell ions and thus are easier to manipulate with the help of static or radio-frequency (RF) electric fields. A number of groups have used the combination of these two techniques for electronic and vibrational studies of gas phase biomolecules.<sup>29,132-170</sup>

The group of Parks and coworkers observed laser induced fluorescence from electrosprayed ions stored in a quadrupole trap and used this technique to probe their conformational dynamics.<sup>132-134</sup> The group of Andersen was the first to use action spectra in order to investigate the electronic properties of the protonated and deprotonated forms of the green fluorescent protein chromophore, produced by electrospray and stored in an electrostatic ion storage ring.<sup>135,136</sup> The recording of highly resolved electronic spectra of complex and large ions requires that one needs to cool the ions to low temperatures (for a relevant discussion see Section 6.1). The spectra of Andersen and coworkers exhibited broad features because of the high internal temperatures of the ions in the storage ring. In 2004, Weinkauff and coworkers recorded the first electronic photofragment spectrum of protonated tryptophan stored in a cold ( $\sim 140$  K) Paul trap.<sup>137</sup> Despite the low temperature of the ions, the spectra exhibited broad structure. Rizzo and coworkers recorded electronic spectra of protonated tyrosine and tryptophan stored in a 22-pole linear ion trap that was cooled to  $\sim 6$  K.<sup>138</sup> Although the spectrum of tyrosine exhibited sharp, vibrationally resolved features, that of tryptophan showed broad bands, which was attributed to the fast de-excitation of the excited state.<sup>139,140</sup>

The use of photofragment spectroscopy requires that absorption of a photon leads to its fragmentation, a process which is likely to become slower for molecules of increasing size.<sup>171</sup> Dugourd and coworkers have introduced a technique that can be used to obtain electronic spectra of deprotonated peptides and large proteins in the gas phase, as an alternative to photofragmentation spectroscopy.<sup>87,141-143</sup> This involves monitoring of the photoinduced electron detachment channel<sup>144,145</sup> as a function of the laser excitation wavelength.<sup>141-143</sup> Electron detachment seems to be independent of the mass of the ion, and proteins as large as human serotransferrin (77 kDa) have been examined.<sup>141</sup> However, with this technique low-resolution electronic spectra are recorded because the photodetachment leads to an ultrafast deactivation of the excited state.

McLafferty and coworkers were the first to perform vibrational photofragmentation spectroscopy on peptides and proteins stored in a Fourier transform ion cyclotron resonance (FT-ICR) mass spectrometer.<sup>146,147</sup> They employed infrared multiphoton dissociation (IRMPD) using an optical parametric oscillator (OPO) for the generation of near-IR light. Although the ions were at room temperature, they observed vibrational bands that were  $\sim 30 \text{ cm}^{-1}$  wide, sufficiently narrow to distinguish many of the light atom stretch bands.<sup>146,147</sup> Using radiation from a free-electron laser, von Helden and coworkers extended the use of IRMPD spectroscopy to the amide I and amide II regions of the infrared to record vibrational spectra of several charge states of potassiumated cytochrome *c* ions.<sup>148</sup> In these experiments, infrared absorption was monitored by the loss of the potassium adduct. The vibrational features they observed suggested a high content of  $\alpha$ -helical structure. The use of IR light from free-electron lasers to perform IRMPD spectroscopy on trapped ions for their structural determination has been intensely explored.<sup>148-158</sup>

In recent work, Johnson and coworkers employed the messenger tagging technique<sup>159</sup> to record highly-resolved vibrational spectra of small peptides and biologically relevant systems.<sup>160-162</sup> In these experiments, the ions are produced by electrospray and cooled in a cold quadrupole ion trap, while absorption of IR laser radiation produced by an OPO is detected as loss of the “tag” molecule.

von Helden and coworkers have recently developed a promising technique that has the potential to cool ions to temperatures as low as 0.37 K.<sup>163</sup> This involves a linear ion trap where mass selected electrosprayed ions are confined. A stream of liquid helium droplets is sent along the trap axis and the droplets are doped with the ions. The droplets have an equilibrium temperature of 0.37 K that is maintained by evaporative cooling, effectively cooling the ions. Ions as large as cytochrome *c* have been embedded inside the droplets. The doped He droplets can subsequently be investigated by spectroscopic means.



Rizzo and coworkers have shown that highly resolved electronic spectra of ions cooled in a 22-pole ion trap can be recorded using photofragmentation spectroscopy.<sup>138</sup> In these spectra, features from individual isomers can be detected, allowing the use of IR-UV double resonance spectroscopy to record conformer specific and highly resolved vibrational spectra.<sup>29,85,164-169,172</sup> Stearns *et al.* have used this technique to investigate conformational preferences of protonated amino acids<sup>166</sup> and small peptides.<sup>165</sup> They also identified spectroscopic signatures of helix formation in the gas phase in polyalanine peptides with a C-terminal lysine,<sup>164,168</sup> proposed by Jarrold to adopt such a structure in the gas phase.<sup>68</sup> Nagornova *et al.* used this method in combination with high-level calculations to reveal the intrinsic structure of gramicidin S in the gas phase.<sup>169,172</sup> Recently, they recorded electronic and vibrational spectra of this peptide solvated with as many as 50 water molecules, bridging the gap between the gas phase and solution.<sup>29</sup>

Thus far, this technique has been applied to the investigation of molecules of up to 17 amino acids that adopt a limited number of conformations in the gas phase.<sup>167,170</sup> More floppy, complex and larger biomolecules adopt a number of conformations that make the spectra increasingly complex possessing overlapping transitions of all the individual conformers (see Section 4.1 for a relevant discussion). This prevents the study of larger systems with IR-UV double resonance which may lead to the recording of highly-resolved vibrational spectra that could help elucidating their structure.

In this work we push the limits of photofragment spectroscopy to the study of complex peptides and small proteins. Towards this end we propose using ion mobility techniques for conformer selection prior to investigation by laser spectroscopy. This will help in recording simplified electronic spectra in which one or only a few conformations contribute. In Chapters 4 and 5 we explore the marriage of the two techniques, employing high-Field Asymmetric waveform Ion Mobility Spectrometry (FAIMS) for separation of conformers before their laser interrogation. FAIMS is briefly reviewed below.

### 1.3. High-Field Asymmetric waveform Ion Mobility Spectrometry (FAIMS)

The technique that we use in conjunction with spectroscopy to study biomolecules in the gas phase is high-Field Asymmetric waveform Ion Mobility Spectrometry (FAIMS), also called differential ion mobility.<sup>173</sup> Owing to its capabilities as a post-ionization separation method,

FAIMS has received much attention over the last years,<sup>174,175</sup> with the first monograph appearing in the literature only recently.<sup>173</sup> The principle of ion separation in FAIMS was first described by Buryakov *et. al.*,<sup>176</sup> while further elucidation came from the pioneering work of Guevremont and coworkers.<sup>177-179</sup> Recent major advances in the understanding of the FAIMS separation is done by Shvartsburg and coworkers in the group of Smith at the Pacific Northwest National Laboratory (PNNL).<sup>173,180-182</sup> The details of FAIMS separation are presented in Chapter 3 and only a brief introduction along with a review of its separation capabilities will be given here.

In drift-tube Ion Mobility Spectrometry (IMS), a pulse of ions drifts through a buffer gas under the influence of a low electric field that pulls them gently towards a detector.<sup>60,61,183,184</sup> The ion motion is hindered by collisions with the buffer gas. Larger ions have more collisions and reach the detector at longer times compared to smaller ions. The velocity that an ion acquires is directly proportional to the strength of the electric field, with the proportionality constant called ion mobility,  $K$ . Thus, in IMS ions are separated by differences in their ion mobilities, and this parameter can be directly associated to their shape.<sup>58,60,64</sup> On the other hand, FAIMS exploits the deviation of the mobility of an ion with varying electric field.<sup>173</sup> The separation parameter in FAIMS is the Compensation Voltage (CV) that reflects the change in the mobility of an ion under the influence of a high electric field compared to its value at low field.<sup>177</sup> Despite the efforts being made to shed light on the detailed mechanism of FAIMS separation,<sup>180,185</sup> it has not yet been possible to connect the experimentally determined CV value to an ion's properties.<sup>173</sup> While this is a major drawback of this technique, this is balanced by its unusual separation ability.<sup>174</sup>

FAIMS separates ions at atmospheric pressure and room temperature.<sup>176,177,179</sup> It can be used in conjunction with mass spectrometry (MS) in order to separate ions prior to their introduction into the vacuum chamber. Its physical location is therefore between an atmospheric pressure ion source, like electrospray ionization (ESI), and the orifice of the mass spectrometer. The ESI-FAIMS-MS configuration has been introduced first by Guevremont and coworkers.<sup>179</sup> FAIMS can suppress the background ions produced by ESI by orders of magnitude, improving the signal-to-noise ratio of the mass spectrum and lowering the detection limits of specific ions.<sup>186</sup> This was demonstrated in analyses of complex peptide mixtures from tryptic digests of pure proteins<sup>187</sup> and protein mixtures.<sup>188</sup>

Because the separation is not directly related to  $m/z$ , FAIMS has been used for distinguishing and quantifying structural isomers like Leucine and Isoleucine,<sup>189</sup> diastereoisomers of ephedrine,<sup>190</sup> isomers of phtalic acid<sup>191</sup> and disaccharides of the same mass but also clusters of simple peptides.<sup>192</sup> FAIMS has been employed for separation of conformations of several proteins like ubiquitin,<sup>193-195</sup> cytochrome  $c$ <sup>196</sup> and lysozyme<sup>197</sup> in several charge states, as well as  $\beta_2$ -

microglobulin,<sup>198</sup> displaying the sensitivity of the separation to the three dimensional structure of biomolecules. It has been used in combination with gas phase H/D exchange measurements to detect four conformations of doubly protonated bradykinin,<sup>199</sup> having a very similar cross section and thus unresolved by IMS until only recently.<sup>200,201</sup> However, recent, higher resolution FAIMS measurements allowed the identification of six conformations of doubly protonated bradykinin.<sup>202-206</sup> Its combination with H/D exchange has also been used to identify more conformations of cytochrome *c* ions than any of these techniques alone.<sup>196</sup> FAIMS has also been shown to separate sequence-isomers of peptides,<sup>207,208</sup> isomeric metabolites,<sup>209</sup> isotopomers,<sup>210</sup> and phosphopeptides with identical amino acid sequence but differing in the modification sites<sup>211-214</sup>

The difference of the mobility of an ion at high electric field compared to its value at low field is independent of the value of mobility itself,<sup>173</sup> making FAIMS orthogonal to drift tube IMS. FAIMS-IMS configurations provide higher separation power than either technique alone and have been used for the analysis of complex mixtures of tryptic peptides<sup>215</sup> and proteins.<sup>216</sup> Shvartsburg *et al.* used this configuration for the investigation of conformers of several charge states of ubiquitin.<sup>216-219</sup> They also probed the field heating during FAIMS separation, employing as a “thermometer” the conformation of ubiquitin as characterized in the IMS stage.<sup>218,219</sup>

As mentioned above, FAIMS can continuously separate and transmit one type of ion into a mass spectrometer and functions at atmospheric pressure and room temperature. Although we acknowledge some of its disadvantages compared to drift tube IMS, we decided to use FAIMS as a first test to investigate the marriage of ion mobility and spectroscopy.

## 1.4. Goals and outline

In the two previous sections some experimental techniques that are used to characterize gas phase biomolecules were presented. Emphasis was given to spectroscopic and FAIMS studies. The purpose of this work is to push the limits of photofragment spectroscopy of cold species to the study of larger and more complex systems like small proteins. As the molecular size increases, the presence of a plethora of stable conformers renders the spectra increasingly complex, inhibiting spectroscopic analysis. To overcome this problem, we propose the use of ion mobility techniques to separate conformers prior to their laser investigation. Towards this end, we design a proof-of-principle experiment to demonstrate the feasibility of the above approach. This comprises a combination of a FAIMS stage with laser photofragment spectroscopy in a cold RF

ion trap. We explore the feasibility, advantages and limitations of coupling the two techniques using a complex peptide as a test molecule.

In a second series of studies, we investigate by means of electronic photofragment spectroscopy a small protein of 76 amino acids that shows a wealth of conformations. We show that molecules of this size can be cooled effectively in our cold trap. However, conformational heterogeneity congests the spectrum to such a large extent that most bands in the electronic spectra appear broad, despite the low temperature of the ions. This inhibits the use of IR-UV double resonance spectroscopy, making the addition of ion mobility techniques mandatory for simplifying the spectra of molecules in this size regime.

In Chapter 2 we describe the experimental apparatus built in our lab for the study of cold, biomolecular ions with laser spectroscopy.

In Chapter 3 we present the principle of FAIMS operation, along with several instrumental parameters and their effect on the separation.

In Chapter 4 we discuss the problems one is faced with in the spectroscopic investigation of molecules of increased size and we propose using ion mobility techniques to mitigate some of them. We employ FAIMS separation of conformers prior to their introduction into a cold ion trap for spectroscopic investigation. As a test molecule we use doubly protonated bradykinin. We explore the advantages and limitations of coupling the two techniques.

In Chapter 5 we use the conformational distribution of bradykinin, as it is reflected in the electronic spectrum, to probe heating processes in FAIMS and in our mass spectrometer.

In Chapter 6 we discuss some of the limitations of electronic photofragment spectroscopy in probing small, naturally occurring proteins. Then we continue to apply our spectroscopic technique to ubiquitin, a protein of 76 amino acids, showing electronic spectra of several of its charge states.

Finally, Chapter 7 summarizes the results of this work.

## 1.5. References

- (1) Barry Robson, J. G. *Introduction to Proteins and Protein Engineering*, 1986.
- (2) Igor A. Kaltsov, S. J. E. *Mass Spectrometry In Biophysics*; John Wiley & Sons, Inc., Hoboken, New Jersey, 2005.
- (3) Frauenfelder, H. *The Physics of Proteins: An Introduction to Biological Physics and Molecular Biophysics*; Springer, 2010.

- (4) Ansari, A.; Berendzen, J.; Bowne, S. F.; Frauenfelder, H.; Iben, I. E. T.; Sauke, T. B.; Shyamsunder, E.; Young, R. D. *Proc. Natl. Acad. Sci. U. S. A.* **1985**, *82*, 5000.
- (5) Frauenfelder, H.; Wolynes, P. G.; Austin, R. H. *Rev. Mod. Phys.* **1999**, *71*, S419.
- (6) Frauenfelder, H.; McMahon, B. H.; Austin, R. H.; Chu, K.; Groves, J. T. *Proc. Natl. Acad. Sci. U. S. A.* **2001**, *98*, 2370.
- (7) Hilser, V. J. *Science* **2010**, *327*, 653.
- (8) Plotkin, S. S.; Onuchic, J. N. *Q. Rev. Biophys.* **2002**, *35*, 111.
- (9) Christopher M. Dobson, A. a. M. K. *Angew. Chem., Int. Ed.* **1998**, *37*, 868.
- (10) Anfinsen, C. B. *Science* **1973**, *181*, 223.
- (11) Schulz, G. E. *Ann. Rev. Biophys. Chem.* **1988**, *17*, 1.
- (12) Bonneau, R.; Baker, D. *Annu. Rev. Biophys. Biomol. Struct.* **2001**, *30*, 173.
- (13) Kendrew, J. C.; Dickerson, R. E.; Strandberg, B. E.; Hart, R. G.; Davies, D. R.; Phillips, D. C.; Shore, V. C. *Nature* **1960**, *185*, 422.
- (14) Perutz, M. F.; Rossmann, M. G.; Cullis, A. F.; Muirhead, H.; Will, G.; North, A. C. T. *Nature* **1960**, *185*, 416.
- (15) Bourgeois, D.; Vallone, B.; Schotte, F.; Arcovito, A.; Miele, A. E.; Sciara, G.; Wulff, M.; Anfinrud, P.; Brunori, M. *Proc. Natl. Acad. Sci. U. S. A.* **2003**, *100*, 8704.
- (16) Schotte, F.; Lim, M.; Jackson, T. A.; Smirnov, A. V.; Soman, J.; Olson, J. S.; Phillips, G. N.; Wulff, M.; Anfinrud, P. A. *Science* **2003**, *300*, 1944.
- (17) Hummer, G.; Schotte, F.; Anfinrud, P. A. *Proc. Natl. Acad. Sci. U. S. A.* **2004**, *101*, 15330.
- (18) Schotte, F.; Soman, J.; Olson, J. S.; Wulff, M.; Anfinrud, P. A. *J. Struct. Biol.* **2004**, *147*, 235.
- (19) Williamson, M. P.; Havel, T. F.; Wüthrich, K. *J. Mol. Biol.* **1985**, *182*, 295.
- (20) Wuthrich, K. *Science* **1989**, *243*, 45.
- (21) Wuethrich, K. *Acc. Chem. Res.* **1989**, *22*, 36.
- (22) Tzakos, A. G.; Grace, C. R. R.; Lukavsky, P. J.; Riek, R. *Annu. Rev. Biophys. Biomol. Struct.* **2006**, *35*, 319.
- (23) Braiman, M. S.; Rothschild, K. J. *Ann. Rev. Biophys. Chem.* **1988**, *17*, 541.
- (24) Beychok, S. *Annu. Rev. Biochem.* **1968**, *37*, 437.
- (25) Greenfield, N. J. *Nat. Protocols* **2007**, *1*, 2876.
- (26) Schermann, J.-P. *Spectroscopy and Modeling of Biomolecular Building Blocks*; Elsevier, 2008.
- (27) Wyttenbach, T.; Bowers, M. T. *J. Phys. Chem. B* **2011**, *115*, 12266.
- (28) Breuker, K.; McLafferty, F. W. *Proc. Natl. Acad. Sci. U. S. A.* **2008**, *105*, 18145.
- (29) Nagornova, N. S.; Rizzo, T. R.; Boyarkin, O. V. *Science* **2012**, *336*, 320.
- (30) Karas, M.; Bachmann, D.; Bahr, U.; Hillenkamp, F. *Int. J. Mass Spectrom. Ion Processes* **1987**, *78*, 53.
- (31) Karas, M.; Hillenkamp, F. *Anal. Chem.* **1988**, *60*, 2299.
- (32) Fenn, J. B.; Mann, M.; Meng, C. K.; Wong, S. F.; Whitehouse, C. M. *Science* **1989**, *246*, 64.
- (33) Fenn, J. B.; Mann, M.; Meng, C. K.; Wong, S. F.; Whitehouse, C. M. *Mass Spectrom. Rev.* **1990**, *9*, 37.
- (34) Fenn, J. B. *Angew. Chem., Int. Ed.* **2003**, *42*, 3871.
- (35) Matsuo, T.; Seyama, Y. *J. Mass Spectrom.* **2000**, *35*, 114.
- (36) Fenselau, C. *Ann. Rev. Biophys. Chem.* **1991**, *20*, 205.
- (37) Biemann, K. *Annu. Rev. Biochem.* **1992**, *61*, 977.
- (38) Laskin, J.; Futrell, J. H. *Mass Spectrom. Rev.* **2003**, *22*, 158.
- (39) Kumar Kolli, V.; Orlando, R. *J. Am. Soc. Mass Spectrom.* **1995**, *6*, 234.

- (40) Little, D. P.; Speir, J. P.; Senko, M. W.; Oconnor, P. B.; McLafferty, F. W. *Anal. Chem.* **1994**, *66*, 2809.
- (41) Winger, B. E.; Light-Wahl, K. J.; Rockwood, A. L.; Smith, R. D. *J. Am. Chem. Soc.* **1992**, *114*, 5897.
- (42) Wood, T. D.; Chorush, R. A.; Wampler, F. M.; Little, D. P.; O'Connor, P. B.; McLafferty, F. W. *Proc. Natl. Acad. Sci. U. S. A.* **1995**, *92*, 2451.
- (43) McLafferty, F. W.; Guan, Z.; Haupts, U.; Wood, T. D.; Kelleher, N. L. *J. Am. Chem. Soc.* **1998**, *120*, 4732.
- (44) Freitas, M.; Hendrickson, C.; Emmett, M.; Marshall, A. *J. Am. Soc. Mass Spectrom.* **1998**, *9*, 1012.
- (45) Freitas, M.; Marshall, A. *Int. J. Mass Spectrom.* **1999**, *182-183*, 221.
- (46) Freitas, M. A.; Hendrickson, C. L.; Emmett, M. R.; Marshall, A. G. *Int. J. Mass Spectrom.* **1999**, *185-187*, 565.
- (47) Robinson, E. W.; Williams, E. R. *J. Am. Soc. Mass Spectrom.* **2005**, *16*, 1427.
- (48) Geller, O.; Lifshitz, C. *J. Phys. Chem. A* **2005**, *109*, 2217.
- (49) Cassady, C. J.; Carr, S. R. *J. Mass Spectrom.* **1996**, *31*, 247.
- (50) Valentine, S. J.; Clemmer, D. E. *J. Am. Chem. Soc.* **1997**, *119*, 3558.
- (51) Bohrer, B. C.; Atlasevich, N.; Clemmer, D. E. *J. Phys. Chem. B* **2011**, *115*, 4509.
- (52) Englander, S. W. *Annu. Rev. Biophys. Biomol. Struct.* **2000**, *29*, 213.
- (53) Englander, S. *Science* **1993**, *262*, 848.
- (54) Wand, A. J.; Roder, H.; Englander, S. W. *Biochemistry* **1986**, *25*, 1107.
- (55) Katta, V.; Chait, B. T. *J. Am. Chem. Soc.* **1993**, *115*, 6317.
- (56) Zhang, Z.; Smith, D. L. *Protein Sci.* **1993**, *2*, 522.
- (57) Kaltashov, I. A.; Bobst, C. E.; Abzalimov, R. R. *Anal. Chem.* **2009**, *81*, 7892.
- (58) von Helden, G.; Hsu, M. T.; Gotts, N.; Bowers, M. T. *J. Phys. Chem.* **1993**, *97*, 8182.
- (59) von Helden, G.; Wyttenbach, T.; Bowers, M. T. *Science* **1995**, *267*, 1483.
- (60) Clemmer, D. E.; Hudgins, R. R.; Jarrold, M. F. *J. Am. Chem. Soc.* **1995**, *117*, 10141.
- (61) Clemmer, D. E.; Jarrold, M. F. *J. Mass Spectrom.* **1997**, *32*, 577.
- (62) Bowers, M. T.; Kemper, P. R.; von Helden, G.; Vankoppen, P. A. M. *Science* **1993**, *260*, 1446.
- (63) Jarrold, M. F. *J. Phys. Chem.* **1995**, *99*, 11.
- (64) Shvartsburg, A. A.; Jarrold, M. F. *Chem. Phys. Lett.* **1996**, *261*, 86.
- (65) Mesleh, M. F.; Hunter, J. M.; Shvartsburg, A. A.; Schatz, G. C.; Jarrold, M. F. *J. Phys. Chem.* **1996**, *100*, 16082.
- (66) Shelimov, K. B.; Clemmer, D. E.; Hudgins, R. R.; Jarrold, M. F. *J. Am. Chem. Soc.* **1997**, *119*, 2240.
- (67) Myung, S.; Badman, E. R.; Lee, Y. J.; Clemmer, D. E. *J. Phys. Chem. A* **2002**, *106*, 9976.
- (68) Hudgins, R. R.; Ratner, M. A.; Jarrold, M. F. *J. Am. Chem. Soc.* **1998**, *120*, 12974.
- (69) Kaleta, D. T.; Jarrold, M. F. *J. Am. Chem. Soc.* **2003**, *125*, 7186.
- (70) Jarrold, M. F. *Phys. Chem. Chem. Phys.* **2007**, *9*, 1659.
- (71) Valentine, S. J.; Anderson, J. G.; Ellington, A. D.; Clemmer, D. E. *J. Phys. Chem. B* **1997**, *101*, 3891.
- (72) Zilch, L. W.; Kaleta, D. T.; Kohtani, M.; Krishnan, R.; Jarrold, M. F. *J. Am. Soc. Mass Spectrom.* **2007**, *18*, 1239.
- (73) Price, W. D.; Schnier, P. D.; Williams, E. R. *Anal. Chem.* **1996**, *68*, 859.
- (74) Schnier, P. D.; Price, W. D.; Jockusch, R. A.; Williams, E. R. *J. Am. Chem. Soc.* **1996**, *118*, 7178.

- (75) Jockusch, R. A.; Schnier, P. D.; Price, W. D.; Strittmatter, E. F.; Demirev, P. A.; Williams, E. R. *Anal. Chem.* **1997**, *69*, 1119.
- (76) Schnier, P. D.; Klassen, J. S.; Strittmatter, E. F.; Williams, E. R. *J. Am. Chem. Soc.* **1998**, *120*, 9605.
- (77) Jockusch, R. A.; Lemoff, A. S.; Williams, E. R. *J. Phys. Chem. A* **2001**, *105*, 10929.
- (78) Lemoff, A.; Williams, E. *J. Am. Soc. Mass Spectrom.* **2004**, *15*, 1014.
- (79) Rizzo, T. R.; Park, Y. D.; Levy, D. H. *J. Am. Chem. Soc.* **1985**, *107*, 277.
- (80) Rizzo, T. R.; Park, Y. D.; Peteanu, L.; Levy, D. H. *J. Chem. Phys.* **1985**, *83*, 4819.
- (81) Rizzo, T. R.; Park, Y. D.; Levy, D. H. *J. Chem. Phys.* **1986**, *85*, 6945.
- (82) Rizzo, T. R.; Park, Y. D.; Peteanu, L. A.; Levy, D. H. *J. Chem. Phys.* **1986**, *84*, 2534.
- (83) Cable, J. R.; Tubergen, M. J.; Levy, D. H. *J. Am. Chem. Soc.* **1987**, *109*, 6198.
- (84) de Vries, M. S.; Hobza, P. *Annu. Rev. Phys. Chem.* **2007**, *58*, 585.
- (85) Rizzo, T. R.; Stearns, J. A.; Boyarkin, O. V. *Int. Rev. Phys. Chem.* **2009**, *28*, 481
- (86) Polfer, N. C.; Oomens, J. *Mass Spectrom. Rev.* **2009**, *28*, 468.
- (87) Antoine, R.; Dugourd, P. *Phys. Chem. Chem. Phys.* **2011**, *13*.
- (88) Polfer, N. C. *Chem. Soc. Rev.* **2011**, *40*, 2211.
- (89) Simons, J. P. *Mol. Phys.* **2009**, *107*, 2435.
- (90) Park, Y. D.; Rizzo, T. R.; Peteanu, L. A.; Levy, D. H. *J. Chem. Phys.* **1986**, *84*, 6539.
- (91) Li, L.; Lubman, D. M. *Rev. Sci. Instrum.* **1988**, *59*, 557.
- (92) Nir, E.; Hunziker, H. E.; de Vries, M. S. *Anal. Chem.* **1999**, *71*, 1674.
- (93) Cohen, R.; Brauer, B.; Nir, E.; Grace, L.; de Vries, M. S. *J. Phys. Chem. A* **2000**, *104*, 6351.
- (94) Carney, J. R.; Hagemester, F. C.; Zwier, T. S. *J. Chem. Phys.* **1998**, *108*, 3379.
- (95) Carney, J. R.; Zwier, T. S. *J. Phys. Chem. A* **2000**, *104*, 8677.
- (96) Snoek, L. C.; Kroemer, R. T.; Hockridge, M. R.; Simons, J. P. *Phys. Chem. Chem. Phys.* **2001**, *3*, 1819.
- (97) Unterberg, C.; Gerlach, A.; Schrader, T.; Gerhards, M. *J. Chem. Phys.* **2003**, *118*, 8296.
- (98) Hünig, I.; Seefeld, K. A.; Kleinermanns, K. *Chem. Phys. Lett.* **2003**, *369*, 173.
- (99) Carcabal, P.; Kroemer, R. T.; Snoek, L. C.; Simons, J. P.; Bakker, J. M.; Compagnon, I.; Meijer, G.; von Helden, G. *Phys. Chem. Chem. Phys.* **2004**, *6*, 4546.
- (100) Chin, W.; Mons, M.; Dognon, J.-P.; Piuzzi, F.; Tardivel, B.; Dimicoli, I. *Phys. Chem. Chem. Phys.* **2004**, *6*, 2700.
- (101) Fricke, H.; Gerlach, A.; Unterberg, C.; Rzepecki, P.; Schrader, T.; Gerhards, M. *Phys. Chem. Chem. Phys.* **2004**, *6*, 4636.
- (102) Řeha, D.; Valdés, H.; Vondrášek, J.; Hobza, P.; Abu-Riziq, A.; Crews, B.; de Vries, M. S. *Chemistry – A European Journal* **2005**, *11*, 6803.
- (103) Bakker, J. M.; Plutzer, C.; Hunig, I.; Haber, T.; Compagnon, I.; von Helden, G.; Meijer, G.; Kleinermanns, K. *ChemPhysChem* **2005**, *6*, 120.
- (104) Chin, W.; Compagnon, I.; Dognon, J. P.; Canuel, C.; Piuzzi, F.; Dimicoli, I.; von Helden, G.; Meijer, G.; Mons, M. *J. Am. Chem. Soc.* **2005**, *127*, 1388.
- (105) Chin, W.; Dognon, J. P.; Canuel, C.; Piuzzi, F.; Dimicoli, I.; Mons, M.; Compagnon, I.; von Helden, G.; Meijer, G. *J. Chem. Phys.* **2005**, *122*, 054317.
- (106) Abo-Riziq, A.; Crews, B. O.; Callahan, M. P.; Grace, L.; de Vries, M. S. *Angew. Chem., Int. Ed.* **2006**, *45*, 5166.
- (107) Chin, W.; Mons, M.; Dognon, J. P.; Mirasol, R.; Chass, G.; Dimicoli, I.; Piuzzi, F.; Butz, P.; Tardivel, B.; Compagnon, I.; von Helden, G.; Meijer, G. *J. Phys. Chem. A* **2005**, *109*, 5281.

- (108) Brenner, V.; Piuzzi, F.; Dimicoli, I.; Tardivel, B.; Mons, M. *J. Phys. Chem. A* **2007**, *111*, 7347.
- (109) Häber, T.; Seefeld, K.; Kleinermanns, K. *J. Phys. Chem. A* **2007**, *111*, 3038.
- (110) Fricke, H.; Funk, A.; Schrader, T.; Gerhards, M. *J. Am. Chem. Soc.* **2008**, *130*, 4692.
- (111) von Helden, G.; Compagnon, I.; Blom, M. N.; Frankowski, M.; Erlekam, U.; Oomens, J.; Brauer, B.; Gerber, R. B.; Meijer, G. *Phys. Chem. Chem. Phys.* **2008**, *10*, 1248.
- (112) Fricke, H.; Schwing, K.; Gerlach, A.; Unterberg, C.; Gerhards, M. *Phys. Chem. Chem. Phys.* **2010**, *12*, 3511.
- (113) Rijs, A. M.; Ohanessian, G.; Oomens, J.; Meijer, G.; von Helden, G.; Compagnon, I. *Angew. Chem., Int. Ed.* **2010**, *49*, 2332.
- (114) Abo-Riziq, A.; Grace, L.; Crews, B.; Callahan, M. P.; van Mourik, T.; Vries, M. S. d. *J. Phys. Chem. A* **2011**, *115*, 6077.
- (115) Dian, B. C.; Longarte, A.; Mercier, S.; Evans, D. A.; Wales, D. J.; Zwier, T. S. *J. Chem. Phys.* **2002**, *117*, 10688.
- (116) Jockusch, R. A.; Kroemer, R. T.; Talbot, F. O.; Simons, J. P. *J. Phys. Chem. A* **2003**, *107*, 10725.
- (117) Rodrigo, C. P.; James, W. H.; Zwier, T. S. *J. Am. Chem. Soc.* **2011**, *133*, 2632.
- (118) Robertson, E. G.; Hockridge, M. R.; Jelfs, P. D.; Simons, J. P. *Phys. Chem. Chem. Phys.* **2001**, *3*, 786.
- (119) Shubert, V. A.; Zwier, T. S. *J. Phys. Chem. A* **2007**, *111*, 13283.
- (120) Brenner, V.; Piuzzi, F.; Dimicoli, I.; Tardivel, B.; Mons, M. *Angew. Chem., Int. Ed.* **2007**, *46*, 2463.
- (121) Chin, W.; Piuzzi, F.; Dognon, J. P.; Dimicoli, L.; Tardivel, B.; Mons, M. *J. Am. Chem. Soc.* **2005**, *127*, 11900.
- (122) Gerhards, M.; Unterberg, C.; Gerlach, A.; Jansen, A. *Phys. Chem. Chem. Phys.* **2004**, *6*, 2682.
- (123) Gerhards, M.; Unterberg, C.; Gerlach, A. *Phys. Chem. Chem. Phys.* **2002**, *4*, 5563.
- (124) Gerhards, M.; Unterberg, C. *Phys. Chem. Chem. Phys.* **2002**, *4*, 1760.
- (125) Dian, B. C.; Longarte, A.; Zwier, T. S. *Science* **2002**, *296*, 2369.
- (126) David, A. E.; David, J. W.; Brian, C. D.; Timothy, S. Z. *J. Chem. Phys.* **2004**, *120*, 148.
- (127) Dian, B. C.; Clarkson, J. R.; Zwier, T. S. *Science* **2004**, *303*, 1169.
- (128) Dian, B. C.; Florio, G. M.; Clarkson, J. R.; Longarte, A.; Zwier, T. S. *J. Chem. Phys.* **2004**, *120*, 9033.
- (129) Dian, B. C.; Longarte, A.; Winter, R. P.; Zwier, T. S. *J. Chem. Phys.* **2004**, *120*, 133.
- (130) Zwier, T. S. *J. Phys. Chem. A* **2006**, *110*, 4133.
- (131) Yamashita, M.; Fenn, J. B. *J. Phys. Chem.* **1984**, *88*, 4451.
- (132) Danell, A. S.; Parks, J. H. *Int. J. Mass Spectrom.* **2003**, *229*, 35.
- (133) Iavarone, A. T.; Duft, D.; Parks, J. H. *J. Phys. Chem. A* **2006**, *110*, 12714.
- (134) Iavarone, A. T.; Patriksson, A.; van der Spoel, D.; Parks, J. H. *J. Am. Chem. Soc.* **2007**, *129*, 6726.
- (135) Nielsen, S. B.; Lapierre, A.; Andersen, J. U.; Pedersen, U. V.; Tomita, S.; Andersen, L. H. *Phys. Rev. Lett.* **2001**, *8722*, 228102.
- (136) Andersen, L. H.; Lapierre, A.; Nielsen, S. B.; Nielsen, I. B.; Pedersen, S. U.; Pedersen, U. V.; Tomita, S. *Eur. Phys. J. D* **2002**, *20*, 597.
- (137) Nolting, D.; Marian, C.; Weinkauff, R. *Phys. Chem. Chem. Phys.* **2004**, *6*, 2633.
- (138) Boyarkin, O. V.; Mercier, S. R.; Kamariotis, A.; Rizzo, T. R. *J. Am. Chem. Soc.* **2006**, *128*, 2816.



- (139) Kang, H.; Jouvét, C.; Dedonder-Lardeux, C.; Martrenchard, S.; Gregoire, G.; Desfrancois, C.; Schermann, J. P.; Barat, M.; Fayeton, J. A. *Phys. Chem. Chem. Phys.* **2005**, *7*, 394.
- (140) Mercier, S. R.; Boyarkin, O. V.; Kamariotis, A.; Guglielmi, M.; Tavernelli, I.; Cascella, M.; Rothlisberger, U.; Rizzo, T. R. *J. Am. Chem. Soc.* **2006**, *128*, 16938.
- (141) Bellina, B.; Compagnon, I.; Joly, L.; Albrieux, F.; Allouche, A. R.; Bertorelle, F.; Lemoine, J.; Antoine, R.; Dugourd, P. *Int. J. Mass Spectrom.* **2010**, *297*, 36.
- (142) Joly, L.; Antoine, R.; Allouche, A.-R.; Broyer, M.; Lemoine, J.; Dugourd, P. *J. Am. Chem. Soc.* **2007**, *129*, 8428.
- (143) Matheis, K.; Joly, L.; Antoine, R.; Lépine, F.; Bordas, C.; Ehrler, O. T.; Allouche, A.-R.; Kappes, M. M.; Dugourd, P. *J. Am. Chem. Soc.* **2008**, *130*, 15903.
- (144) Antoine, R.; Joly, L.; Tabarin, T.; Broyer, M.; Dugourd, P.; Lemoine, J. *Rapid Commun. Mass Spectrom.* **2007**, *21*, 265.
- (145) Gabelica, V.; Tabarin, T.; Antoine, R.; Rosu, F.; Compagnon, I.; Broyer, M.; De Pauw, E.; Dugourd, P. *Anal. Chem.* **2006**, *78*, 6564.
- (146) Oh, H.; Breuker, K.; Sze, S. K.; Ge, Y.; Carpenter, B. K.; McLafferty, F. W. *Proc. Natl. Acad. Sci. U. S. A.* **2002**, *99*, 15863.
- (147) Oh, H.-B.; Lin, C.; Hwang, H. Y.; Zhai, H.; Breuker, K.; Zabrouskov, V.; Carpenter, B. K.; McLafferty, F. W. *J. Am. Chem. Soc.* **2005**, *127*, 4076.
- (148) Oomens, J.; Polfer, N.; Moore, D. T.; van der Meer, L.; Marshall, A. G.; Eyler, J. R.; Meijer, G.; von Helden, G. *Phys. Chem. Chem. Phys.* **2005**, *7*, 1345.
- (149) Oomens, J.; Meijer, G.; von Helden, G. *J. Phys. Chem. A* **2001**, *105*, 8302.
- (150) Kapota, C.; Lemaire, J.; Maître, P.; Ohanessian, G. *J. Am. Chem. Soc.* **2004**, *126*, 1836.
- (151) Lucas, B.; Gregoire, G.; Lemaire, J.; Maître, P.; Ortega, J. M.; Rupenyan, A.; Reimann, B.; Schermann, J. P.; Desfrancois, C. *Phys. Chem. Chem. Phys.* **2004**, *6*, 2659.
- (152) Polfer, N. C.; Paizs, B.; Snoek, L. C.; Compagnon, I.; Suhai, S.; Meijer, G.; von Helden, G.; Oomens, J. *J. Am. Chem. Soc.* **2005**, *127*, 8571.
- (153) Polfer, N. C.; Oomens, J.; Moore, D. T.; von Helden, G.; Meijer, G.; Dunbar, R. C. *J. Am. Chem. Soc.* **2006**, *128*, 517.
- (154) Seydou, M.; Gregoire, G.; Liquier, J.; Lemaire, J.; Schermann, J. P.; Desfrancois, C. *J. Am. Chem. Soc.* **2008**, *130*, 4187.
- (155) Gabelica, V.; Rosu, F.; De Pauw, E.; Lemaire, J.; Gillet, J. C.; Pouilly, J. C.; Lecomte, F.; Gregoire, G.; Schermann, J. P.; Desfrancois, C. *J. Am. Chem. Soc.* **2008**, *130*, 1810.
- (156) Balaj, O. P.; Kapota, C.; Lemaire, J.; Ohanessian, G. *Int. J. Mass Spectrom.* **2008**, *269*, 196.
- (157) Pagel, K.; Kupser, P.; Bierau, F.; Polfer, N. C.; Steill, J. D.; Oomens, J.; Meijer, G.; Koks, B.; von Helden, G. *Int. J. Mass Spectrom.* **2009**, *283*, 161.
- (158) Kupser, P.; Pagel, K.; Oomens, J.; Polfer, N.; Koks, B.; Meijer, G.; von Helden, G. *J. Am. Chem. Soc.* **2010**, *132*, 2085.
- (159) Kamrath, M. Z.; Relph, R. A.; Guasco, T. L.; Leavitt, C. M.; Johnson, M. A. *Int. J. Mass Spectrom.* **2011**, *300*, 91.
- (160) Kamrath, M. Z.; Garand, E.; Jordan, P. A.; Leavitt, C. M.; Wolk, A. B.; Van Stipdonk, M. J.; Miller, S. J.; Johnson, M. A. *J. Am. Chem. Soc.* **2011**, *133*, 6440.
- (161) Leavitt, C.; Wolk, A.; Kamrath, M.; Garand, E.; Van Stipdonk, M.; Johnson, M. J. *Am. Soc. Mass Spectrom.* **2011**, *22*, 1941.
- (162) Garand, E.; Kamrath, M. Z.; Jordan, P. A.; Wolk, A. B.; Leavitt, C. M.; McCoy, A. B.; Miller, S. J.; Johnson, M. A. *Science* **2012**, *335*, 694.
- (163) Bierau, F.; Kupser, P.; Meijer, G.; von Helden, G. *Phys. Rev. Lett.* **2010**, *105*, 133402.

- (164) Stearns, J. A.; Boyarkin, O. V.; Rizzo, T. R. *J. Am. Chem. Soc.* **2007**, *129*, 13820.
- (165) Stearns, J. A.; Guidi, M.; Boyarkin, O. V.; Rizzo, T. R. *J. Chem. Phys.* **2007**, *127*, 154322.
- (166) Stearns, J. A.; Mercier, S.; Seaiby, C.; Guidi, M.; Boyarkin, O. V.; Rizzo, T. R. *J. Am. Chem. Soc.* **2007**, *129*, 11814.
- (167) Guidi, M.; Lorenz, U. J.; Papadopoulos, G.; Boyarkin, O. V.; Rizzo, T. R. *J. Phys. Chem. A* **2009**, *113*, 797.
- (168) Stearns, J. A.; Seaiby, C.; Boyarkin, O. V.; Rizzo, T. R. *Phys. Chem. Chem. Phys.* **2009**, *11*, 125.
- (169) Nagornova, N. S.; Rizzo, T. R.; Boyarkin, O. V. *J. Am. Chem. Soc.* **2010**, *132*, 4040.
- (170) Guidi, M. PhD Thesis, EPFL, 2010.
- (171) Griffin, L. L.; McAdoo, D. J. *J. Am. Soc. Mass Spectrom.* **1993**, *4*, 11.
- (172) Nagornova, N. S.; Guglielmi, M.; Doemer, M.; Tavernelli, I.; Rothlisberger, U.; Rizzo, T. R.; Boyarkin, O. V. *Angew. Chem., Int. Ed.* **2011**, *50*, 5383.
- (173) Shvartsburg, A. A. *Differential Ion Mobility Spectrometry*; CRC Press: Boca Raton FL, 2009.
- (174) Guevremont, R. *J. Chromatogr. A* **2004**, *1058*, 3.
- (175) Kolakowski, B. M.; Mester, Z. *The Analyst* **2007**, *132*, 842.
- (176) Buryakov, I. A.; Krylov, E. V.; Nazarov, E. G.; Rasulev, U. K. *Int. J. Mass Spectrom. Ion Processes* **1993**, *128*, 143.
- (177) Purves, R. W.; Guevremont, R.; Day, S.; Pipich, C. W.; Matyjaszczyk, M. S. *Rev. Sci. Instrum.* **1998**, *69*, 4094.
- (178) Guevremont, R.; Purves, R. W. *Rev. Sci. Instrum.* **1999**, *70*, 1370.
- (179) Purves, R. W.; Guevremont, R. *Anal. Chem.* **1999**, *71*, 2346.
- (180) Shvartsburg, A. A.; Tang, K.; Smith, R. D. *J. Am. Soc. Mass Spectrom.* **2004**, *15*, 1487.
- (181) Shvartsburg, A. A.; Tang, K.; Smith, R. D. *Anal. Chem.* **2004**, *76*, 7366.
- (182) Shvartsburg, A. A.; Noskov, S. Y.; Purves, R. W.; Smith, R. D. *Proc. Natl. Acad. Sci. U. S. A.* **2009**.
- (183) Kemper, P.; Bowers, M. *J. Am. Soc. Mass Spectrom.* **1990**, *1*, 197.
- (184) von Helden, G.; Hsu, M.-T.; Kemper, P. R.; Bowers, M. T. *J. Chem. Phys.* **1991**, *95*, 3835.
- (185) Guevremont, R.; Purves, R. *J. Am. Soc. Mass Spectrom.* **2005**, *16*, 349.
- (186) Barnett, D. A.; Guevremont, R.; Purves, R. W. *Appl. Spectrosc.* **1999**, *53*, 1367.
- (187) Guevremont, R.; Barnett, D. A.; Purves, R. W.; Vandermeij, J. *Anal. Chem.* **2000**, *72*, 4577.
- (188) Barnett, D.; Ells, B.; Guevremont, R.; Purves, R. *J. Am. Soc. Mass Spectrom.* **2002**, *13*, 1282.
- (189) Barnett, D. A.; Ells, B.; Guevremont, R.; Purves, R. W. *J. Am. Soc. Mass Spectrom.* **1999**, *10*, 1279.
- (190) Schneider, B. B.; Covey, T. R.; Coy, S. L.; Krylov, E. V.; Nazarov, E. G. *Int. J. Mass Spectrom.* **2010**, *298*, 45.
- (191) Barnett, D. A.; Purves, R. W.; Ells, B.; Guevremont, R. *J. Mass Spectrom.* **2000**, *35*, 976.
- (192) Guevremont, R.; Purves, R. W. *J. Am. Soc. Mass Spectrom.* **1999**, *10*, 492.
- (193) Purves, R. W.; Barnett, D. A.; Guevremont, R. *Int. J. Mass Spectrom.* **2000**, *197*, 163.
- (194) Purves, R. W.; Barnett, D. A.; Ells, B.; Guevremont, R. *J. Am. Soc. Mass Spectrom.* **2000**, *11*, 738.

- (195) Purves, R. W.; Barnett, D. A.; Ells, B.; Guevremont, R. *J. Am. Soc. Mass Spectrom.* **2001**, *12*, 894.
- (196) Purves, R. W.; Ells, B.; Barnett, D. A.; Guevremont, R. *Can. J. Chem.* **2005**, *83*, 1961.
- (197) Robinson, E. W.; Sellon, R. E.; Williams, E. R. *Int. J. Mass Spectrom.* **2007**, *259*, 87.
- (198) Borysik, A. J. H.; Read, P.; Little, D. R.; Bateman, R. H.; Radford, S. E.; Ashcroft, A. *E. Rapid Commun. Mass Spectrom.* **2004**, *18*, 2229.
- (199) Purves, W. R.; Barnett, A. D.; Ells, B.; Guevremont, R. *Rapid Commun. Mass Spectrom.* **2001**, *15*, 1453.
- (200) Kemper, P. R.; Dupuis, N. F.; Bowers, M. T. *Int. J. Mass Spectrom.* **2009**, *287*, 46.
- (201) Pierson, N. A.; Valentine, S. J.; Clemmer, D. E. *J. Phys. Chem. B* **2010**, *114*, 7777.
- (202) Shvartsburg, A. A.; Tang, K.; Smith, R. D. *Anal. Chem.* **2010**, *82*, 32.
- (203) Shvartsburg, A. A.; Smith, R. D. *Anal. Chem.* **2010**, *83*, 23.
- (204) Shvartsburg, A. A.; Prior, D. C.; Tang, K.; Smith, R. D. *Anal. Chem.* **2010**, *82*, 7649.
- (205) Shvartsburg, A. A.; Danielson, W. F.; Smith, R. D. *Anal. Chem.* **2010**, *82*, 2456.
- (206) Shvartsburg, A. A.; Li, F.; Tang, K.; Smith, R. D. *Anal. Chem.* **2006**, *78*, 3706.
- (207) Blagojevic, V.; Chramow, A.; Schneider, B. B.; Covey, T. R.; Bohme, D. K. *Anal. Chem.* **2011**, *83*, 3470.
- (208) Shvartsburg, A. A.; Creese, A. J.; Smith, R. D.; Cooper, H. J. *Anal. Chem.* **2011**, *83*, 6918.
- (209) Parson, W. B.; Schneider, B. B.; Kertesz, V.; Corr, J. J.; Covey, T. R.; Van Berkel, G. *J. Rapid Commun. Mass Spectrom.* **2011**, *25*, 3382.
- (210) Shvartsburg, A. A.; Clemmer, D. E.; Smith, R. D. *Anal. Chem.* **2010**, *82*, 8047.
- (211) Shvartsburg, A. A.; Creese, A. J.; Smith, R. D.; Cooper, H. J. *Anal. Chem.* **2010**, *82*, 8327.
- (212) Yue, X.; Andrew, J. C.; Julie, A. H.; Helen, J. C. *Rapid Commun. Mass Spectrom.* **2009**, *23*, 1963.
- (213) Shvartsburg, A. A.; Singer, D.; Smith, R. D.; Hoffmann, R. *Anal. Chem.* **2011**, *83*, 5078.
- (214) Ibrahim, Y. M.; Shvartsburg, A. A.; Smith, R. D.; Belov, M. E. *Anal. Chem.* **2011**, *83*, 5617.
- (215) Tang, K.; Li, F.; Shvartsburg, A. A.; Strittmatter, E. F.; Smith, R. D. *Anal. Chem.* **2005**, *77*, 6381.
- (216) Shvartsburg, A. A.; Tang, K.; Smith, R. D. In *Mass Spectrometry of Proteins and Peptides: Methods and Protocols* 2008; Vol. 492, p 417.
- (217) Shvartsburg, A. A.; Li, F.; Tang, K.; Smith, R. D. *Anal. Chem.* **2006**, *78*, 3304.
- (218) Shvartsburg, A. A.; Li, F.; Tang, K.; Smith, R. D. *Anal. Chem.* **2007**, *79*, 1523.
- (219) Robinson, E. W.; Shvartsburg, A. A.; Tang, K.; Smith, R. D. *Anal. Chem.* **2008**, *80*, 7508.



## Experimental apparatus

In this chapter we present the home-built tandem mass spectrometer that was used to perform the experiments that are described in Chapters 4, 5 and 6. We begin with an overview of the machine followed by a more detailed description of some of its essential parts. Finally, we describe the laser setup and the spectroscopic scheme that we employed to record electronic photofragment spectra of cold biomolecular ions.

### 2.1. Overview of the tandem mass spectrometer

The experiments described in this thesis were conducted in a home-built tandem mass spectrometer equipped with a cold 22-pole ion trap<sup>1</sup> and a removable FAIMS unit.<sup>2</sup> The experimental apparatus is shown schematically in Figs. 2.1 and 2.2. An overview of the trajectory of the ions from their production at atmospheric pressure to their spectroscopic detection in vacuum will be given here, while some essential parts of the apparatus will be presented in more detail thereafter.

Ions are produced in the gas phase by electrospray ionization using a heated electrospray probe (H-ESI I, Thermo Fisher Scientific) and are sampled into the FAIMS analyzing region through a small pinhole on the entrance plate of the FAIMS assembly. The inset of Fig. 2.1 illustrates the FAIMS unit in more detail. A stream of gas of variable flow rate flows in between the entrance plate and the outer electrode of FAIMS (drying and carrier gas in inset of Fig. 2.1). Most of the gas exits from the pinhole of the entrance plate, helping to completely desolvate the ions before they are transmitted through the following stages of FAIMS and the mass spectrometer. Desolvated ions are carried by the remaining gas through the annular space between the two FAIMS electrodes, where a particular conformation is selected. The details of FAIMS separation are discussed in Chapter 3. The ions that are transmitted through FAIMS are drawn into the mass spectrometer through a glass capillary with metallized ends. Because of the large distance

between the FAIMS exit aperture and the orifice of the glass capillary, a metallic extension was built and fitted to the atmospheric pressure side of the capillary. The ions traverse a distance of  $\sim 0.5\text{mm}$  before they enter the extension. The nickel-coated surface of the capillary (and also the extension) is floated on the Outer Bias Voltage (OBV) of the FAIMS electrodes, so that maximum transmission of ions is achieved. If conformer selection is not needed, the FAIMS unit is removed and there is the possibility to use either the heated electrospray source or a nano-electrospray source (Proxeon Biosystems) for the production of ions. In this case, electrosprayed or nanosprayed ions are directly drawn into the first vacuum chamber of the mass spectrometer. The pressure in this region is  $\sim 1.9\text{ mbar}$ .

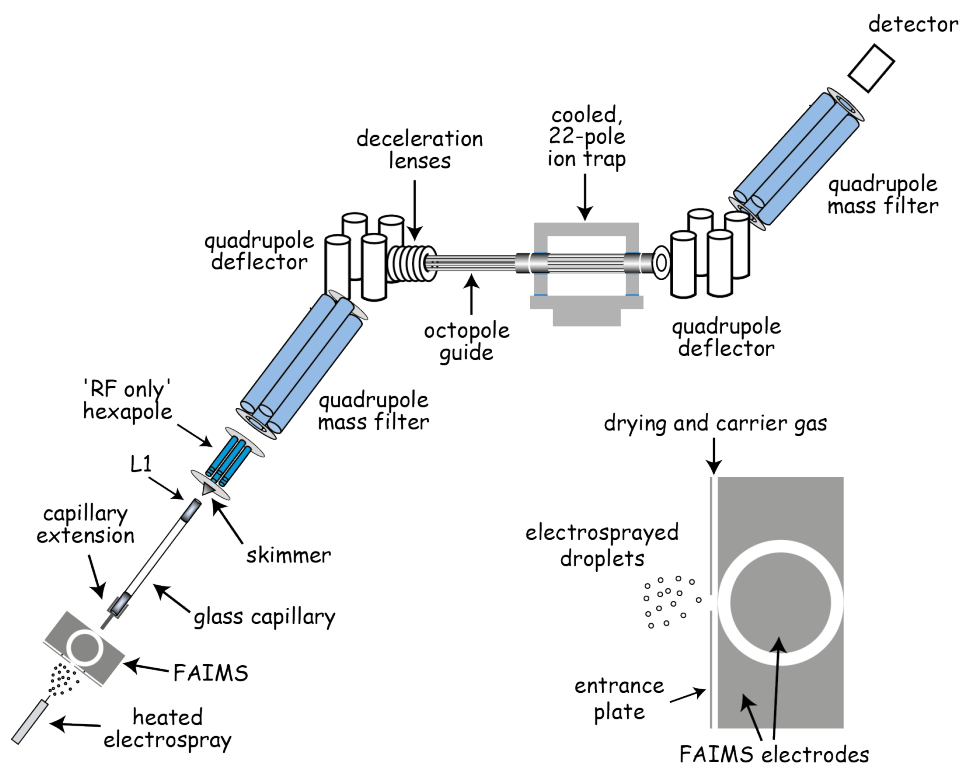


**Figure 2.1.** Illustration of the home-built tandem mass spectrometer. The spectrometer is equipped with a 22-pole ion trap, which is maintained at 6 K.

A voltage is applied on the vacuum end of the capillary (L1 in Fig 2.1). The voltage drop across the capillary and the skimmer defines the energy of the collisions of the ions with the background gas molecules in this area and their injection energy into the hexapole ion trap. Large voltage difference between these two elements increases the transmission of the ions, but also imparts energy on them *via* energetic collisions (collisional activation). This can lead to their conformational change or even their fragmentation. More details about this are given in Chapter 5 and 6, where spectra of bradykinin and ubiquitin are recorded as a function of the voltage of L1.

Subsequently, ions pass through a skimmer before they are accumulated in an RF-only (radio frequency) hexapole ion trap. Accumulation and trapping is achieved by raising the voltage of the exit electrode of the hexapole. Ions are then released in packets by lowering the voltage of the exit electrode periodically. The skimmer separates the first from the second vacuum stage while the hexapole traverses the second and the third vacuum stages. The pressure in these two stages is  $2 \cdot 10^{-2}$  mbar and  $4 \cdot 10^{-5}$  mbar, respectively. The section view of the tandem mass spectrometer along with the different vacuum stages is shown in Fig. 2.2.

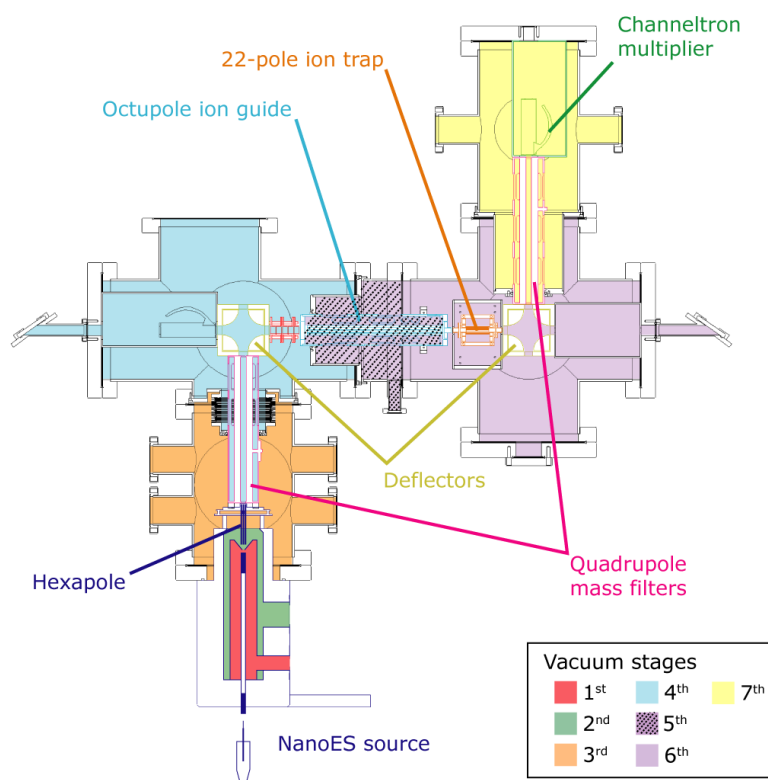


**Figure 2.2.** Section view of the tandem mass spectrometer, where the different vacuum stages are illustrated.

After some accumulation time in the hexapole, typically 40 ms, an ion packet is released and enters a mass-selecting quadrupole where only a particular  $m/z$  is allowed to be transmitted (the parent ion). The pressure in the chamber of the quadrupole mass filter is  $2.7 \cdot 10^{-7}$  mbar. After mass selection, the parent ions are turned  $90^\circ$  by a quadrupole deflector and guided through an RF-only octopole into the 22-pole ion trap. The pressure in the chamber of the octopole, which is the fifth vacuum stage, is  $3.7 \cdot 10^{-8}$  mbar while in the region of the 22-pole ion trap (sixth vacuum stage) is less than  $2 \cdot 10^{-9}$  mbar when He is not injected. The 22-pole ion trap is mounted on a close-cycle refrigerator and maintained at 6 K. A pulse of He is injected in the trap before the

arrival of the ion packet and is given sufficient time to equilibrate to the temperature of its housing. When the ions arrive in the 22-pole, they cool down in collisions with cold helium atoms.

Photofragment spectroscopy is performed on the cold ions and then parent and fragment ions are released from the trap, turned 90° in a second quadrupole deflector, mass selected in a second quadrupole mass filter and counted in a channeltron detector. The pressure in the seventh vacuum stage is less than  $2 \cdot 10^{-9}$  mbar.

## 2.2. Electrospray ionization

The difficulty of transferring intact large molecules into the gas phase stems from their low vapor pressure, and heating them may lead to their decomposition before they are volatilized. This problem was overcome with the advent of electrospray ionization (ESI), introduced by Dole<sup>3</sup> and further developed by Fenn and co-workers.<sup>4-6</sup> Electrospray ionization (ESI) is a soft ionization method in which ions are extracted from a solution into the gas phase.<sup>7</sup> The solution, typically of water/methanol solvent, is infused into a metallic needle at a fixed rate, on the order of tens of  $\mu\text{l}/\text{min}$ . Figure 2.3 illustrates the principle of ESI operation.

For the production of positive ions, a high voltage of 2-5 kV relative to a counter electrode is applied on the needle. As a result of the strong field present, positive charges are accumulated on the surface of the liquid and a so-called Taylor cone is formed at the tip of the needle.<sup>8</sup> When the coulombic repulsion between the charges overcomes the surface tension of the liquid, a fine mist of charged droplets is emitted from the needle. A flow of dry gas around the needle, the sheath gas (illustrated in blue in Fig. 2.3), can assist in the droplet formation.

The charged droplets fly in atmospheric pressure towards the counter electrode. Their radii are reduced because of collisions with the atmospheric gas that removes neutral solvent molecules from the droplets. A gas emerging from a pinhole on the counter electrode and flowing counter to the incoming droplets can assist in this process (countercurrent gas, not shown in Fig. 2.3). An essential part of the ESI probe that we use is a warm stream of gas, which is called auxiliary gas (Fig. 2.3), approaching the electrosprayed droplets from above. This gas helps in droplet desolvation. Also, when FAIMS is used, the carrier gas of the FAIMS assembly serves the same purpose (see inset of Fig. 2.1). As the volume of the droplets decreases, the charge density becomes larger, up to the point at which the coulombic repulsion equals the surface tension, called the Rayleigh limit.<sup>9</sup> At this point the droplet can break down into two or more droplets (droplet



fission) or a new Taylor cone can be formed from which smaller charged droplets are emitted. This process continues until very small charged droplets are produced.

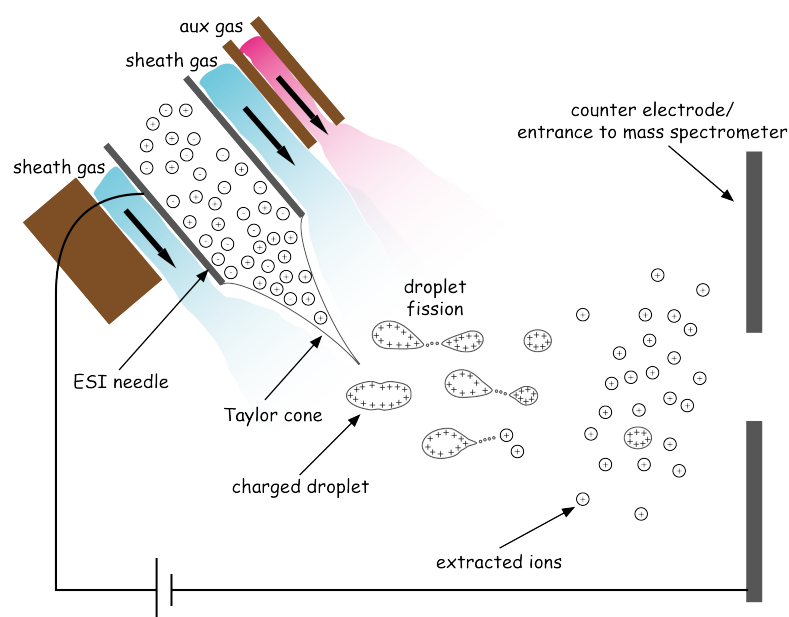


**Figure 2.3.** Schematic presentation of electro spray ionization (ESI). The tip of the H-ESI probe is shown on the left. The sheath and auxiliary gases are shown with blue and pink respectively. Several processes that happen during ESI are also illustrated.

Despite the research carried on concerning the ESI process, there is no consensus as to how the ions are formed from the charged droplets.<sup>10,11</sup> There are currently two models that explain this procedure. According to the charge residue model (CRM), the small droplets undergo desolvation until a stripped ion is left.<sup>3,12,13</sup> The ion evaporation model (IEM) states that ions evaporate from the surface of the small droplets.<sup>14,15</sup> Most likely, both mechanisms occur, with one prevailing over the other depending on the nature of the analyte and the composition of the solvent.<sup>13,16,17</sup>

In our set up we can either use an electro spray or a nanospray source.<sup>18,19</sup> The mechanism of ion production in nanospray is similar to that described above, however, there are some essential technical differences. The needles used for nanospray have a smaller diameter than those used for electro spray (1-2  $\mu\text{m}$  as opposed to  $\sim 100\mu\text{m}$ ), and the sample flow is much lower (on the order of tens of  $\text{nl}/\text{min}$ ) - hence the name nanospray. The voltage that is needed to initiate a jet of droplets from a Taylor cone is lower than that for electro spray. Smaller droplets are formed, without the aid of a sheath gas. The initial small size of the droplets does not require a warm gas to assist in the desolvation, although a counterflowing gas can sometimes stabilize the spray. Because of these reasons, solvents with a high surface tension and low organic content, or even

pure water can be used, a condition that is closer to physiological for proteins.<sup>20</sup> Whether or not there is a preference of ion formation *via* the CRM or the IEM in the two versions of electrospray and if this affects the nature of the produced ions (for example conformational preference in biomolecules) is unknown.

## 2.3. Ion transmission in the mass spectrometer

After their production, the ions enter the mass spectrometer through the capillary, pass the skimmer and are subjected to inhomogeneous radio-frequency (RF) alternating electric fields in the hexapole, the two quadrupoles, the octupole and the 22-pole ion trap. Fast oscillatory electric fields have the advantage that they can create potential minima in two or three dimensions as opposed to static electric fields where no real minima but rather saddle points can exist.<sup>21</sup> Because of this, these devices can trap or guide ions effectively.<sup>22</sup>

### 2.3.1. Quadrupole mass analyzers

The mass selection in quadrupole mass filters is based on the dependence of stable trajectories of ions on their  $m/z$ . The principle of operation has been described in detail in many textbooks and only a qualitative presentation will be given here.<sup>23,24</sup> These devices consist of four parallel rods which are placed so that they osculate the circumference of a circle of radius  $r_0$  and are parallel to one another and equally spaced, as is shown in Fig. 2.4. A voltage of the form  $\Phi_0 = \pm(U + V \cos \omega t)$  is applied on the pairs of opposite electrodes, with opposite polarity for the two pairs. In the above equation,  $U$  is the DC voltage,  $V$  is the peak of the alternating voltage and  $\omega$  is the RF-frequency.

Lets suppose first that the DC component of the voltage is zero ( $U=0$ ), i.e. the quadrupole is operated in RF-only mode. As a result of the voltage applied on the rods, an alternating electric field is established in the  $xy$  plane (Fig. 2.4). If electrodes of cylindrical cross-section are used, as is shown in the figure, the electric field approaches an ideal quadrupole field for a configuration in which  $r_0 = r/1.1486$ , where  $r$  is the radius of the electrodes.<sup>23</sup> In a field like this, ions that move across the  $z$  axis have stable oscillating trajectories in the  $xz$  plane but diverging trajectories in the  $yz$  plane for half a cycle of the waveform, where the electrodes have a fixed polarity. However,

the polarity changes with frequency  $\omega$ , and for the second half-cycle of the waveform the ions will be oscillating with stable trajectories in the  $yz$  plane but not in the  $xz$  plane. For a fast oscillating field (high  $\omega$ ), the ions will not have time to escape during their divergence from the  $z$  axis of the quadrupole and will be transmitted through the quadrupole, making the quadrupole operate as an ion guide. In other words, ions moving in the  $yz$  plane will be alternately diverging and converging to the  $z$  axis with frequency  $\omega$ . The same occurs for the motion of ions in the  $xz$  plane.

Mass discrimination comes when a small DC voltage ( $U \neq 0$  in the above equation) is added on top of the oscillating voltage, as is schematically shown in Fig. 2.4. The electrodes on the  $x$  axis have positive values of  $U$ , while those on the  $y$  axis negative. Thus, the field that is formed in the  $xy$  plane will consist of a static and an oscillating part. On the  $x$  axis, the poles will be most of the time at positive potential and only for a small amount of time on negative potential. This is where the mass of the ion influences whether its trajectory will be stable or not. Heavy ions, which are slowly accelerated, will be influenced by the average field and will thus be focused toward the  $z$  axis. During the time that the poles are at negative voltage, those heavy ions will not be influenced so much, and their divergence from the  $z$  axis will be negligible. On the other hand, very light ions will be influenced more during this time and will be accelerated towards the electrodes, where they are neutralized and lost. In this way, in the  $xz$  plane, heavy ions tend to converge while light ions tend to diverge from the axis.

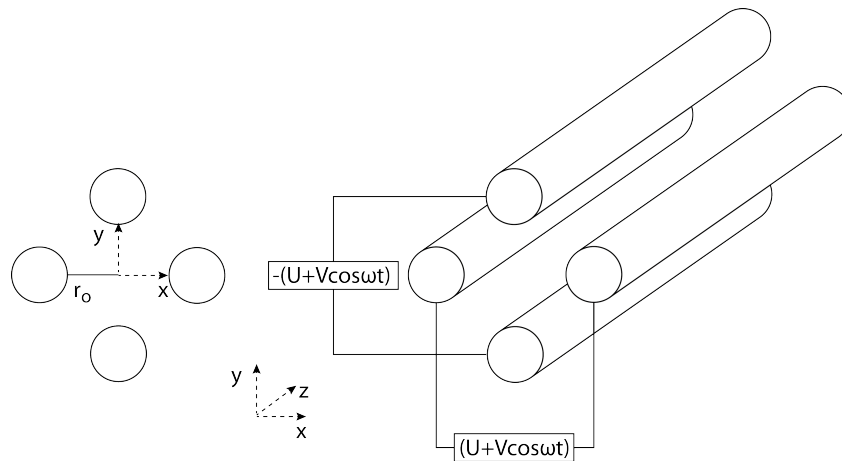


**Figure 2.4.** Schematic representation of a quadrupole mass filter/ion guide.

Consider now the ion motion in the  $yz$  plane. Most of the time the poles on the  $y$  axis will be on negative potential and only for a small amount of time on positive potential. Similarly, heavy ions will follow the time-averaged electric field and will be defocused from the  $z$  axis, while lighter ions respond faster to the oscillating field and thus have stable trajectories. Thus, on the  $yz$  plane, lighter ions tend to have more stable trajectories than heavier ones. It has been shown that

for a given value of  $U$ ,  $V$  and  $\omega$ , there is a range of  $m/z$  values that have stable trajectories through the quadrupole, while ions out of this range are lost.<sup>24</sup> This range can be minimized allowing the transmission of only those ions of a specific  $m/z$ . The conditions for stable trajectories for a specific  $m/z$  can be determined exactly by solving the equations of motion in a quadrupole field.<sup>24</sup>

### 2.3.2. Higher order multipoles

Quadrupole mass filters are a special case of multipoles for which the ion motion on the  $x$  axis is independent of the motion on the  $y$  axis. In higher order multipoles motion in the  $x$  and  $y$  directions can no longer be decoupled. Nevertheless, the ion's motion can be described by a rapidly oscillating motion superimposed on a smooth trajectory.<sup>22,25</sup> At high enough frequency, the smooth motion can be derived from a time-independent *effective potential*,  $V^*$ , which represents the time-averaged effect of the oscillatory field. In the case of a multiple of  $2n$  rods the effective potential is given by:<sup>22,26</sup>

$$V^*(r) = \frac{n^2}{4} \frac{q^2}{m\omega^2} \frac{V_0^2}{r_0^2} \left( \frac{r}{r_0} \right)^{2n-2} \quad (2.1)$$

where  $r$  is the distance from the central axis,  $q$  and  $m$  are the charge and mass of the ion,  $V_0$  and  $\omega$  are the amplitude and frequency of the oscillating voltage applied on the electrodes, and  $r_0$  is the inscribed radius of the  $2n$ -multipole. The inhomogeneity of this field provides the driving force (called *field gradient force*) that carries smoothly the ion to regions of weaker field. In addition, the volume of the field-free region in RF multipoles increases with the number of poles, while the effective potential rises steeper close to the poles. Ions spend most of the time in the field-free region where they undergo the smooth motion and only when they are in close proximity to the rods they sense the oscillating field, which causes them to experience a fast oscillating motion superimposed on their smooth trajectory.

The *adiabatic approximation*, which leads to the effective potential, requires that the change in the electric field that the ion experiences during the fast oscillation is much smaller than the electric field at the average position of the ion. Implied in this is that the RF frequency is high enough so that the amplitude of the fast oscillating motion is kept small. This is the condition for adiabaticity as defined by Gerlich, which is also expressed mathematically.<sup>21,22</sup> Under the adiabatic conditions, the RF field itself does not heat the ions.<sup>22,27</sup>

When RF-multipoles are used as trapping devices, the presence of a buffer gas is necessary to quench the translational energy of the ions entering the device. In the presence of a buffer gas,

ions can be warmed by above-thermal collisions driven by the RF-field, even when adiabatic conditions are met. The temperature of the ions can thus be increased above the temperature of the buffer gas. By minimizing the annular region where the wiggling motion is more pronounced, one minimizes the effect of RF-field on the energy distribution of the trapped ions.<sup>27</sup>

The octupole in our apparatus (see Fig. 2.1) is used as an ion guide, directing ions into the 22-pole. The hexapole and the 22-pole are RF-only multipole devices that are used for trapping. The hexapole is mainly used to pre-trap the continuously produced ions and form them in ion packets by releasing them periodically. In this way, the ESI source is made compatible with the pulsed nature of our experiments (because of the pulsed lasers). During their wiggling motion, collisions of the ions with the room temperature background gas in the hexapole may increase their internal energy. On the other hand, the 22-pole rests on a cold-head, which is maintained at 6K, and the buffer gas is thermalized to this temperature. Moreover, because of the steepness of the potential in the radial direction, the wiggling motion of the ions is limited to only a very small region close to the rods. Although there are still several other reasons that can cause the ions stored in a 22-pole trap to be heated above the buffer gas temperature (space charge effects, misalignment of the rods, high voltage on the electrodes used for longitudinal confinement etc.)<sup>22,27</sup>, it has been shown that ions trapped in a 22-pole can be effectively cooled, which makes this device ideal for use in the experiments described here.

## 2.4. Description of laser setup and spectroscopic schemes

### 2.4.1. Generation of ultraviolet radiation

The cold ions interact with laser irradiation inside the 22-pole trap. In the experiments presented here, electronic photofragment spectroscopy is used to record electronic excitation spectra of the cold, stored ions. Ultraviolet radiation is generated by frequency doubling the output of a Nd:YAG pumped dye laser. Different dyes were used, depending on the wavelength in the ultraviolet region of the electromagnetic spectrum that needed to be covered. The dyes are pumped by either the first (532nm) or the second (355nm) harmonic of the Nd:YAG fundamental (1064nm). The visible output of the tunable dye laser is passed through a beta barium borate (BBO) crystal for second harmonic generation. The BBO crystal is part of a system that, through

a feedback mechanism, automatically adjusts the crystal's rotation in order to find the phase-matching angle for maximum second harmonic generation efficiency as the dye laser is scanned (Inrad - Autotracker III). The ultraviolet output is separated from the remaining visible by reflection in two dichroic mirrors, focused by a lens and directed into the machine through a prism. The duration of the UV pulse is  $\sim 7$  ns while the pulse energy is kept  $\sim 1$ -2 mJ. The linewidth is  $\sim 0.07\text{cm}^{-1}$ .

## 2.4.2. Generation of infrared radiation

A TEA-CO<sub>2</sub> laser is used (Lumonics TEA-840) for the production of laser light in the 10.6  $\mu\text{m}$  region. The laser medium is a gas mixture composed of 8% CO<sub>2</sub>, 4% CO, 16% N<sub>2</sub> and 72% He. The CO<sub>2</sub> molecules are excited by collisional energy transfer from the N<sub>2</sub> molecules that are directly excited by electron impact from a discharge. TEA stands for *Transversely Excited Atmospheric* meaning that the discharge takes place perpendicular to the laser oscillation and that the laser is run at atmospheric pressure. The two vibrational bands used for laser transitions occur at 10.6  $\mu\text{m}$  ( $961\text{ cm}^{-1}$ ) and 9.6  $\mu\text{m}$  ( $1063.8\text{ cm}^{-1}$ ). These bands have rotational substructure, and a diffraction grating in the laser cavity can be used to select a single rovibrational line and make the laser operate on a specific wavelength within these bands.

The pulse from the CO<sub>2</sub> laser has a width of  $\sim 5\ \mu\text{s}$ , consisting of a leading highly intense spike of 100-200 ns and followed by lower intensity tail that lasts 4-5  $\mu\text{s}$ . The first part is produced by CO<sub>2</sub> molecules directly excited by the discharge while the second by those excited *via* collisional energy transfer from the N<sub>2</sub> molecules. Changing the relative content of the various gases in the mixture gives the ability to alter slightly the time profile of the pulse. The CO<sub>2</sub> laser output is focused by a ZnSe lens and directed into the machine from the side opposite to that of the UV laser with the use of gold mirrors.

## 2.4.3. Spectroscopic scheme

Photofragment spectroscopy is used for the recording of electronic spectra of the cold, trapped ions. The spectroscopic scheme is shown in Fig. 2.5. The UV laser excites the ions from the ground electronic state, S<sub>0</sub>, to the first excited electronic state, S<sub>1</sub>. In Fig. 2.5, MH<sup>+</sup> represents ions in the ground electronic state while MH<sup>+</sup>\* represents the initially excited ions in S<sub>1</sub>. MH<sup>+</sup>\*\* represents either ions that have relaxed from S<sub>1</sub> and find themselves either on S<sub>0</sub>, after internal

conversion (IC), or on another excited potential energy surface that crosses  $S_1$ . Depending on the electronic structure of the molecule under study, one process may dominate over the other.

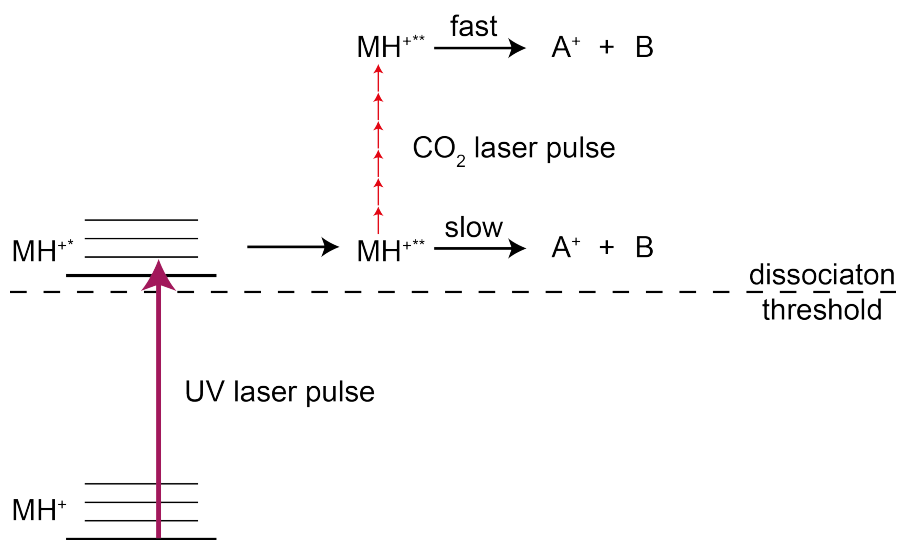


**Figure 2.5.** Spectroscopic scheme used in the experiments described in this thesis.

In IC, the ion undergoes a radiationless transition during which its electronic energy becomes vibrational energy on  $S_0$ . The ion finds itself in highly lying vibrational levels of the ground electronic state. Because of anharmonic coupling between the modes, the vibrational energy placed in one or several oscillators in the molecule does not remain localized i.e. the normal modes of vibration can not be treated as independent and energy is redistributed randomly between them. This process is called Intramolecular Vibrational Redistribution (IVR). When sufficient energy concentrates on one bond, this bond breaks. Dissociation is thus a statistical process. In molecules of increased size, the vibrational energy is redistributed over an increasing number of degrees of freedom. This results in a less frequent concentration of sufficient energy in a bond for its cleavage, and the dissociation slows down. It follows that an increase of the vibrational energy of the molecule increases the dissociation rate.

Because of the pulsed nature of our experiment, the time that the ions are trapped is limited to a few tens of milliseconds. This poses an upper time limit before which dissociation should occur in order for us to observe photofragments. To increase the vibrational energy of the UV excited ions, a pulse from a CO<sub>2</sub> laser is sent through the ion trap  $\sim 150$ ns after the UV pulse, to further excite them.<sup>28,29</sup> This may lead to an increase in the dissociation yield on the timescale of our experiment, improving the sensitivity but also pushing the limits of photofragment spectroscopy to the study of larger cold molecules.<sup>29,30</sup>

In addition to what may happen on the ground electronic surface, fragmentation can also occur from an excited electronic state. It has been shown that the CO<sub>2</sub> laser pulse mainly enhances the fragment that results from the loss of neutral side-chain of the UV chromophore, phenylalanine, tyrosine or tryptophan.<sup>30</sup> This involves dissociation of the C<sub>α</sub>-C<sub>β</sub> bond, which is not the weakest bond on S<sub>0</sub>, as it is not a preferred dissociation pathway in collision-induced dissociation (CID) experiments.<sup>31</sup> This suggests that a portion of the M<sup>+\*</sup> ions are not in the ground electronic state but in an excited state in which the C<sub>α</sub>-C<sub>β</sub> bond is the weakest bond. In this case, the added vibrational energy of the CO<sub>2</sub> pulse enhances this dissociation channel.

The detailed mechanism of the deactivation pathways after electronic excitation of the UV chromophores has been studied extensively<sup>32-34</sup> and is still under investigation in our group.<sup>30</sup> For the molecules that are presented in this thesis, electronic excitation leads to the neutral side chain loss of the UV chromophore, suggesting that at least a portion of the excited molecules are in an electronically excited state. Fragmentation in an electronically excited state is probably the reason why photofragment spectroscopy can be used to study species having very large molecular weights (and thus many vibrational degrees of freedom), such as ubiquitin. We present electronic photofragment spectra of ubiquitin in Chapter 6.

## 2.5. References

- (1) Rizzo, T. R.; Stearns, J. A.; Boyarkin, O. V. *Int. Rev. Phys. Chem.* **2009**, *28*, 481
- (2) Barnett, D. A.; Belford, M.; Dunyach, J.-J.; Purves, R. W. *J. Am. Soc. Mass Spectrom.* **2007**, *18*, 1653.
- (3) Dole, M.; Mack, L. L.; Hines, R. L.; Mobley, R. C.; Ferguson, L. D.; Alice, M. B. *J. Chem. Phys.* **1968**, *49*, 2240.
- (4) Yamashita, M.; Fenn, J. B. *J. Phys. Chem.* **1984**, *88*, 4451.
- (5) Fenn, J. B.; Mann, M.; Meng, C. K.; Wong, S. F.; Whitehouse, C. M. *Mass Spectrom. Rev.* **1990**, *9*, 37.
- (6) Fenn, J. B. *Angew. Chem., Int. Ed.* **2003**, *42*, 3871.
- (7) Fenn, J. B.; Mann, M.; Meng, C. K.; Wong, S. F.; Whitehouse, C. M. *Science* **1989**, *246*, 64.
- (8) Grimm, R. L.; Beauchamp, J. L. *J. Phys. Chem. B* **2005**, *109*, 8244.
- (9) Duft, D.; Achtzehn, T.; Muller, R.; Huber, B. A.; Leisner, T. *Nature* **2003**, *421*, 128.
- (10) Kebarle, P.; Peschke, M. *Anal. Chim. Acta* **2000**, *406*, 11.
- (11) Cole, R. B. *J. Mass Spectrom.* **2000**, *35*, 763.
- (12) Schmelzeisen-Redeker, G.; Bütfering, L.; Röllgen, F. W. *Int. J. Mass Spectrom. Ion Processes* **1989**, *90*, 139.
- (13) Rohner, T. C.; Lion, N.; Girault, H. H. *Phys. Chem. Chem. Phys.* **2004**, *6*, 3056.



- (14) Iribarne, J. V.; Thomson, B. A. *J. Chem. Phys.* **1976**, *64*, 2287.
- (15) Gaskell, S. J. *J. Mass Spectrom.* **1997**, *32*, 677.
- (16) Iavarone, A. T.; Williams, E. R. *J. Am. Chem. Soc.* **2003**, *125*, 2319.
- (17) Schermann, J.-P. *Spectroscopy and Modeling of Biomolecular Building Blocks*; Elsevier, 2008.
- (18) Wilm, M. S.; Mann, M. *Int. J. Mass Spectrom. Ion Processes* **1994**, *136*, 167.
- (19) Wilm, M.; Mann, M. *Anal. Chem.* **1996**, *68*, 1.
- (20) Li, J.; Taraszka, J. A.; Counterman, A. E.; Clemmer, D. E. *Int. J. Mass Spectrom.* **1999**, *185-187*, 37.
- (21) Teloy, E.; Gerlich, D. *Chem. Phys.* **1974**, *4*, 417.
- (22) Gerlich, D. *Adv. Chem. Phys.* **1992**, *82*, 1.
- (23) Campana, J. E. *Int. J. Mass Spectrom. Ion Phys.* **1980**, *33*, 101.
- (24) Dawson, P. H. *Mass Spectrom. Rev.* **1986**, *5*, 1.
- (25) Gerlich, D. *Phys. Scr.* **1995**, *T59*, 256.
- (26) Gerlich, D.; Horning, S. *Chem. Rev. (Washington, DC, U. S.)* **1992**, *92*, 1509.
- (27) Asvany, O.; Schlemmer, S. *Int. J. Mass Spectrom.* **2009**, *279*, 147.
- (28) Yeh, L. I.; Okumura, M.; Myers, J. D.; Price, J. M.; Lee, Y. T. *J. Chem. Phys.* **1989**, *91*, 7319.
- (29) Guidi, M.; Lorenz, U. J.; Papadopoulos, G.; Boyarkin, O. V.; Rizzo, T. R. *J. Phys. Chem. A* **2009**, *113*, 797.
- (30) Guidi, M. PhD Thesis, EPFL, 2010.
- (31) El Aribi, H.; Orlova, G.; Hopkinson, A. C.; Siu, K. W. M. *J. Phys. Chem. A* **2004**, *108*, 3844.
- (32) Lepere, V.; Lucas, B.; Barat, M.; Fayeton, J. A.; Picard, V. J.; Jouvét, C.; Carcabal, P.; Nielsen, I.; Dedonder-Lardeux, C.; Gregoire, G.; Fujii, A. *J. Chem. Phys.* **2007**, *127*, 134313.
- (33) Lucas, B.; Barat, M.; Fayeton, J. A.; Perot, M.; Jouvét, C.; Gregoire, G.; Nielsen, S. B. *J. Chem. Phys.* **2008**, *128*, 164302.
- (34) Pérot, M.; Lucas, B.; Barat, M.; Fayeton, J. A.; Jouvét, C. *J. Phys. Chem. A* **2009**, *114*, 3147.



## High-Field Asymmetric waveform Ion Mobility Spectrometry (FAIMS)

In this chapter we present the basic theory and instrumentation of high-Field Asymmetric waveform Ion Mobility Spectrometry (FAIMS). We start by briefly describing how Drift-Tube Ion Mobility Spectrometry (IMS) separates ions based on their shape by making use of a weak electric field. Then, we introduce the principle of ion separation in FAIMS that is accomplished by a combination of strong and weak electric fields, followed by an examination of the ion motion at the different field strengths. We then discuss various different FAIMS geometries that have been utilized along with the separation performance of each of them, as well as instrumental parameters that can be varied to change the balance between separation efficiency and sensitivity. We use these parameters in order to tune our FAIMS device in Chapters 4 and 5. We end this chapter with a comparison of FAIMS with IMS.

### 3.1. Ion separation in IMS

#### 3.1.1. Principle of operation

Drift-Tube Ion Mobility Spectrometry (DT-IMS, or more simply IMS) is an analytical technique that is being developed since the beginning of the 20th century.<sup>1</sup> It has been used in many applications, from detection of specific molecules and determination of the structure of biomolecules to the separation of complex mixtures in high-throughput applications like proteomics and metabolomics.<sup>1</sup> IMS has been the subject of several recent reviews covering a range of its applications and developments over the years.<sup>2-5</sup> Only the basic principle of its operation will be presented here.

In IMS an ensemble of ions is pulled through an inert buffer gas under the influence of a low, uniform electric field ( $E$ ).<sup>3,6-9</sup> The basic instrumentation for IMS experiments is a drift tube filled with buffer gas, having on one side a source for the ions and on the other a detector, illustrated in Fig. 3.1. The electric field is established along the length of the tube, parallel to its axis. The ions are injected into the drift tube as packets and move across the lines of the field. Their motion is hindered by collisions with the buffer gas molecules and the terminal velocity (or drift velocity -  $v_d$ ) that the ions acquire is directly proportional to the electric field<sup>10</sup> :

$$v_d = K \cdot E \quad (3.1)$$

where the constant  $K$  is called ion mobility. Provided that the field is low, the ion mobility is independent of the field. It depends only on the ion-buffer gas molecule pair and is connected to the collision cross-section,  $\Omega$ , via<sup>10</sup> :

$$K = \frac{3}{16} \left( \frac{2\pi}{\mu k_B T} \right)^{\frac{1}{2}} \frac{ze}{N\Omega} \quad (3.2)$$

where  $\mu$  is the reduced mass of the ion/buffer molecule pair,  $k_B$  is boltzmann's constant,  $T$  is the temperature of the buffer gas,  $N$  is the number density of the buffer gas and  $z$  is charge state of the ion.

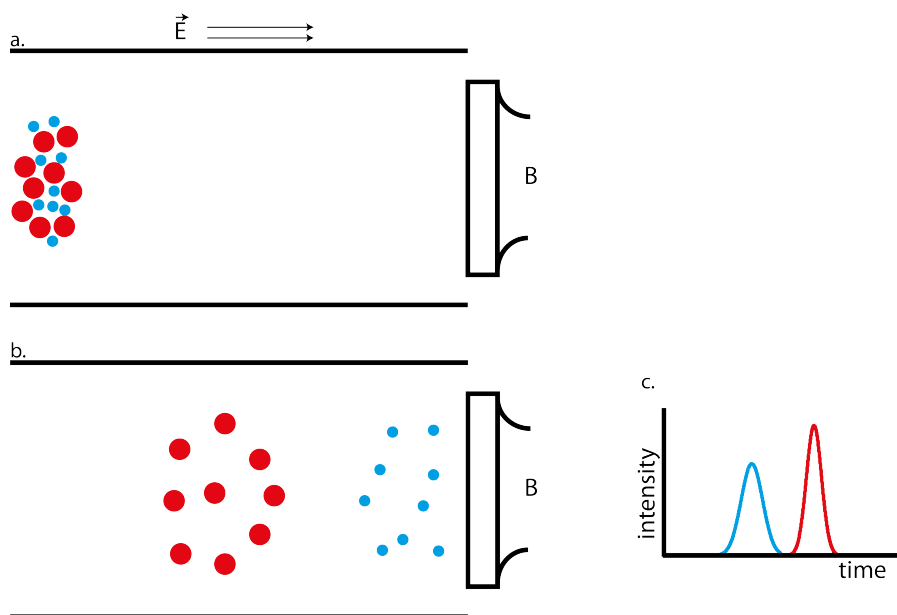


**Figure 3.1.** Illustration of ion separation in a Drift Tube Ion Mobility Spectrometer (DT-IMS). (a) A mixture of ions of large (red) and smaller (blue) collision cross-sections are introduced into a drift tube that is filled with a buffer gas. (b) The ions are separated according to their collision cross-sections as they move across the lines of the electric field ( $E$ ) towards the detector ( $B$ ). (c) An Arrival Time Distribution (ATD) spectrum acquired while recording the number of ions arriving at the detector as a function of time. Note that diffusion and ion-ion coulomb repulsion make the ion clouds expand during the separation.

Because of the dependence of  $K$  on  $\Omega$ , ions of different shape reach different drift velocities. This is the basis of ion separation in IMS, which is illustrated in Figs. 3.1a and 3.1b. Ions with extended structures have a larger cross-section than ions with compact structures, and thus they undergo more collisions with the buffer gas. Therefore, the two species will be separated in space as they drift through the gas and will reach the detector at different times (Fig. 3.1b). The time it takes for the ions to travel across the drift tube and reach the detector is called drift time,  $t_D$ . Recording the number of ions that arrive at the detector as a function of drift time yields an arrival time distribution (ATD), which is indicative of the species that were separated according to their different shapes (Fig. 3.1c).

Ions that exit the drift tube can also be mass selected by entering a time-of-flight (TOF) or a quadrupole mass spectrometer (QMS) before they reach the detector.<sup>11-14</sup> In this case, different peaks in the ATD reveal the presence of ions of the same  $m/z$  but with different shape, i.e. structural isomers. Exceptions to this are aggregates of  $n$  monomeric units, each of them carrying a charge of  $nz$ . These species appear at the same  $m/z$  and may have different cross sections than the  $nz$ -charged monomeric units, giving rise to separate peaks in the ATD that might erroneously be attributed to different conformers of the monomer.<sup>15</sup>

From the ATD one can calculate the ion mobilities corresponding to every peak (*via* equation 3.1) and associate it to a specific collision-cross section (*via* equation 3.2). The ions are free to rotate during their drift, so  $\Omega$  is the orientationally averaged collision cross section. Comparison of this experimental quantity to calculated ones from trial geometries generated by computers makes possible the assignment of a specific structure to an ion mobility value.<sup>8,16,17</sup>

### 3.1.2. Multidimensional IMS separations

Recently, techniques for multidimensional analysis of gas phase ions have emerged, in the form of IMS-IMS or IMS-IMS-IMS in conjunction with mass spectrometry.<sup>3</sup> This was greatly facilitated by the use of ion funnels<sup>18,19</sup> incorporated in between the ion mobility stages. Ion funnels refocus radially the ion cloud that is spread due to diffusion and ion-ion coulombic repulsion, improving ion transmission from one mobility stage to another. Also, ion funnels provide an effective way of collecting and injecting packets of ions from the source to the ion mobility stage and from the ion mobility stage to a time of flight stage for mass analysis.<sup>20</sup>

The use of two or three stages of IMS in tandem opened the way for a series of experiments, made possible for the first time.<sup>20,21</sup> For example, an ion population of a specific ion mobility (or

range of ion mobilities) separated in a first drift tube is selected and injected into a second drift tube for further separation. This can be done with the addition of an ion gate that allows or prevents ions from entering the ion funnel between the two stages.<sup>22,23</sup> Furthermore, the mobility-selected ions can be activated by controlling the voltage of injection into the subsequent mobility stage, inducing fragmentation or structural changes that can be readily followed in the subsequent IMS stage.<sup>3,21,24</sup>

Multidimensional ion mobility analyses provide also insight into the origin of the peak widths in an ATD. In certain cases, the width of a peak exceeds by far the one expected for a single conformer. The peak might appear broad because of the presence of many unresolved conformers with similar ion mobilities or because conformers with different mobilities are in a dynamic equilibrium i.e. they interconvert on the timescale of the separation.<sup>25,26</sup> By selecting a narrow range of mobilities from a broad peak and observe the evolution of the peak's width in a second IMS stage the two cases can be distinguished.<sup>23,27</sup>

## 3.2. Ion separation in FAIMS

### 3.2.1. Principle of operation

The mobility of an ion is not totally independent of the electric field,  $E$ , but depends on it, or more precisely, on  $E/N$ .<sup>10</sup> Expanding  $K$  as a power series on  $E/N$  gives<sup>10,28,29</sup> :

$$K(E) = K(0) \left[ 1 + a_1 \left( \frac{E}{N} \right)^2 + a_2 \left( \frac{E}{N} \right)^4 + \dots \right] \quad (3.3)$$

where  $K(E)$  and  $K(0)$  are the ion mobility at electric field  $E$  and zero, respectively.  $K(E)$  is also referred to as  $K_h$ , where  $h$  stands for high electric field, while  $K(0)$  simply  $K$ . The  $\alpha_n$  coefficients can be positive or negative and are related to the interaction potential between the ion and the buffer gas molecule. Only even terms appear on the expansion because of symmetry reasons, i.e. the change in the ion mobility has to be the same if the electric field changes direction.<sup>28</sup>

In IMS, typical values of the drift field are on the order of  $\sim 10$  V/cm for a low buffer gas pressure (2-5 Torr), but fields as high as  $\sim 200$  V/cm can be used if the pressure of the buffer gas is increased (200 Torr).<sup>25</sup> In this low  $E/N$  regime, the  $\alpha_n$  coefficients are negligible and the ion

mobility is essentially constant and equal to its value at zero field,  $K(0)$ . As the electric field is increased the  $\alpha_n$  coefficients become important, and the ion mobility deviates from its value at zero field. The deviation may be different for different species and this is the basis for ion separation in high-Field Asymmetric-waveform Ion Mobility Spectrometry (FAIMS), illustrated in Fig. 3.2.<sup>29</sup>

In FAIMS, an ensemble of ions is carried by a flow of gas (carrier gas) between two electrodes (Fig. 3.2a).<sup>30,31</sup> A periodic asymmetric voltage waveform is applied on one of the electrodes while the other is kept grounded. The maximum amplitude of the waveform is called the dispersion voltage (DV) (Fig. 3.2b). The waveform consists of a short high voltage component and a longer lower voltage component of opposite polarity combined in such a way so that the time-averaged voltage is zero. Thus the electric field that is established across the gap between the two electrodes has alternating segments of opposite directions and different magnitudes and is perpendicular to the gas flow.

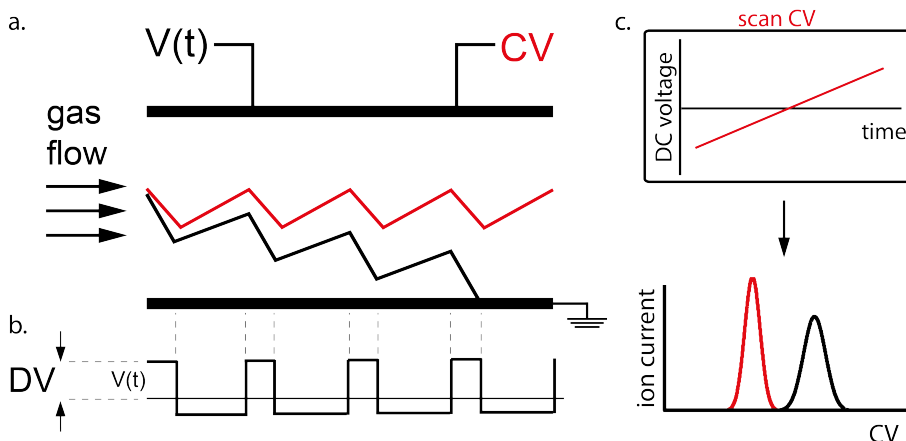


**Figure 3.2.** Illustration of ion separation in a high-Field Asymmetric-waveform Ion Mobility Spectrometer (FAIMS). (a) Two ions with different  $K(E/N)$  profiles enter the gap between the electrodes approximately at the median carried by a flow of gas. In the figure, their motion under the influence of the periodic asymmetric waveform is illustrated (b) A rectangular asymmetric waveform is applied on the upper electrode, while the lower is grounded. The peak amplitude of the waveform is the Dispersion Field (DV). At a given Compensation Voltage (CV) value, one of the ions is transmitted across the electrodes (red trajectory) while the other migrates towards the lower electrode (black trajectory). (c) Scanning the CV while detecting the number of ions that are transmitted yields a CV spectrum.

Under the influence of the alternating electric field, ions will oscillate between the electrodes as the gas carries them. For simplicity, suppose that ions enter the gap in the median (Fig. 3.2a). During the high voltage segment, an ion will migrate towards one of the electrodes with a velocity that is dictated by  $K(E)$  (black trajectory in Fig. 3.2a). During the opposite polarity lower voltage segment, the same ion will travel towards the other electrode but with a velocity

dictated by  $K(0)$ , since at low field the ion mobility is equal to  $K(0)$ . If we suppose that for this particular ion the mobility increases with increased electric field ( $K(E) > K(0)$ ), then it is clear that during the high voltage portion the distance that ion will travel away from the gap median and perpendicular to the gas flow will be longer than the distance on its way back, during the low voltage portion. This will result in a net displacement of the ion from the gap median, after a cycle of the waveform. After many cycles, the ion will eventually hit one of the electrodes and be neutralized and lost.

To compensate for this orthogonal drift and to ensure the transmission of the ion through the gap, a small DC voltage called the compensation voltage (CV) can be applied to either electrode. If there are two types of ions (black and red trajectories in Fig. 3.2a) with different dependencies of their mobility on the electric field, a distinct CV value will be needed for the transmission of each of them through the electrode gap. By monitoring the ion transmission through the gap as a function of the CV, one generates a Compensation Voltage spectrum (CV spectrum) that is indicative of the species present in the gas-phase sample (Fig. 3.2c).

It has been shown that for some peptides and proteins the difference in ion mobility at high and low fields is conformer dependent.<sup>32,33</sup> Ions that are transmitted through the FAIMS electrodes can be mass selected before they reach the detector. Thus, in this case, peaks in CV spectrum reveal the presence of different conformers.<sup>34</sup> In the same way as in DT-IMS, exceptions to this are aggregates that have the same  $m/z$ .<sup>35</sup> Phantom peaks can also be produced by charge stripping of higher charge states into the  $m/z$  channel that is being detected.<sup>34,36</sup>

There are several reasons why the ratio  $K_h/K$  is not constant over a range of  $E/N$  values, especially at high electric fields. The omnipresent reason, termed “standard high-field effect” by Shvartsburg, is the deviation of the relative velocity between the colliding partners (ion and buffer gas molecule),  $v_r$ , from the one calculated from the thermal equilibrium.<sup>29</sup> There are also other effects that influence the  $K(E/N)$  profile but their relative influence on the overall effect depends on the colliding partners, as the case may be. All these will be presented in the following sections.

### 3.2.2. The standard high-field effect

In the following we will calculate the drift velocity for two limiting cases. First, for the case where  $v_r$  is much smaller than the thermal motion of the gas phase ensemble (low  $E$ ) and second, where  $v_r$  is much larger than the thermal motion (very high  $E$ ). FAIMS operates in intermediate



field, which allows us to connect the drift velocity to the interaction potential between the ion and the buffer gas.<sup>29</sup>

An ion of mass  $m$  in a buffer gas of molecules of mass  $M$  under the influence of an electric field experiences a force that accelerates it between collisions. The energy and the momentum gained by interacting with the field are partially lost on each collision. Thus, the drift velocity of an ion is the macroscopic result of accelerations between collisions and decelerations during collisions. From the equations of momentum conservation and of momentum transfer during a collision we get<sup>10</sup> :

$$\nu_d = \xi \left( 1 + \frac{M}{m} \right) \frac{zeE}{M} \tau \quad (3.3)$$

where  $\tau$  is the time between collisions and  $\xi$  is a dimensionless quantity that absorbs results of inaccurate averaging.<sup>29</sup>

The time between collisions is given by :

$$\tau = \frac{1}{\langle \nu_r \rangle N \Omega} \quad (3.4)$$

The relative velocity between the collision partners can be approximated as :

$$\langle \nu_r \rangle^2 = \langle \nu \rangle^2 + \langle V \rangle^2 \quad (3.5)$$

where  $\nu$  and  $V$  is the velocity of the ions and the buffer gas molecules, respectively.

At low  $E/N$ , the motion of both the ions and the buffer gas molecules can be approximated to be thermal. Thus, the velocity distribution of the ion,  $\nu$ , is Maxwellian, defined by the temperature of the buffer gas. The ion motion is Brownian but with a small drift component across the lines of the field. This gives :

$$\langle \nu \rangle^2 + \langle V \rangle^2 = 3k_B T \left( \frac{1}{m} + \frac{1}{M} \right) \quad (3.6)$$

Substitution of equations 3.4, 3.5 and 3.6 into equation 3.3 gives :

$$\nu_d = \frac{\xi}{\sqrt{3}} \left( \frac{1}{\mu k_B T} \right)^{\frac{1}{2}} \frac{zeE}{N \Omega} \quad (3.7)$$

Equation 3.7 shows that under the low field condition, the drift velocity is directly proportional to the electric field. Substituting equation 3.7 into equation 3.1 and solving for  $K$  gives equation 3.2, for the right numeric value of  $\xi$ . On the other hand, in the limit of very high electric field, the ion's motion is no longer thermal. The thermal component of the ion's velocity

is negligible compared to the component caused by the field and for the same reason the mean velocity of the ion is much larger than the mean velocity of the buffer gas molecules :

$$\langle \nu \rangle \gg \langle V \rangle \quad (3.8)$$

From the equations of energy conservation and of energy transfer during collisions, we have :

$$\langle \nu \rangle^2 = \left( 1 + \frac{M}{m} \right) \nu_d^2 \quad (3.9)$$

Substituting equations 3.4, 3.5 and 3.9 into equation 3.3 and taking into account equation 3.8, we find :

$$\nu_d = \xi^{\frac{1}{2}} \left( \frac{1}{\mu M} \right)^{\frac{1}{4}} \left( \frac{zeE}{N\Omega} \right)^{\frac{1}{2}} \quad (3.10)$$

Equation 3.10 shows that at very high electric field the drift velocity scales as  $E^{1/2}$ . Thus, the mobility of an ion is always reduced at very high electric field compared to its value at low electric field i.e.  $K_h/K < 1$  at very high  $E$ .

However, FAIMS is operated at moderate electric fields, where the interaction potential between the ion and the buffer gas molecule may be important in the dynamics of collision. For example, for some ion/buffer molecule pairs the ion mobility increases initially with increasing electric field. To understand this behavior we need to compare the depth of the potential well,  $D$ , to the thermal energy available to the system,  $kT$ , in relation to the relative energy of the collision,  $\varepsilon_{rel}$ . If the potential between the ion and the buffer gas is shallow ( $kT > D$ ), the attractive forces between the collision partners are negligible. Collisions at large impact parameters will produce scattering at small deflection angles. Increasing the  $\varepsilon_{rel}$  (by increasing the electric field) in this case will gradually decrease the ion mobility because of the deviation of  $v_{rel}$  from thermal velocities, as shown above. However, the situation is different when the depth of the well is deep compared to the thermal energy ( $kT < D$ ). Here, the magnitude of  $\varepsilon_{rel}$  relative to  $D$  is important. For  $\varepsilon_{rel} < D$ , scattering produces large deflection angles and the neutral might also be captured in an orbit around the ion i.e. a large momentum transfer occurs. As the electric field is raised, so does  $\varepsilon_{rel}$  and the attractive forces between the colliding partners become less important, leading to smaller deflection angles. At this point, an increase in the mobility of the ion is observed. At even stronger field the mobility decreases.

For any depth of the potential well relative to  $kT$ , in collisions at small impact parameter, the relative energy of the collision,  $\varepsilon_{rel}$ , is not very critical for the momentum transfer, since mainly backscattering is observed.

Ions can be grouped into three types (A, B and C) according to their separation properties in FAIMS devices.<sup>31</sup> Types A and C correspond to ions for which their  $K_h/K$  ratio increases or

decreases, respectively, with increased electric field strength. For ions of type B,  $K_h/K$  initially increases to a maximum and then decreases at even higher electric field. The reason of the seemingly continuous increase in  $K_h/K$  for ions belonging to type A is the relatively low electric field that was used (i.e  $K_h/K$  reaches a maximum at even higher fields and then decreases).<sup>29</sup> Shvartsburg re-categorized ions into two groups. Those for which  $K_h/K$  decreases with increasing electric field (type 1) and those for which  $K_h/K$  shows an initial increase before the eventual decrease (type 2).

### 3.2.3. Clustering and declustering of ions

It has been proposed that one of the reasons for the deviation of  $K_h$  from  $K$  is the dependence of the degree of solvation of the ions with the buffer gas molecules on the electric field strength.<sup>37</sup> In other words clustering and declustering of the ions during the two different portions of the asymmetric waveform may contribute to the deviation.<sup>38</sup> During the low voltage portion, clustering of buffer gas molecules with the ion will increase its collision cross section. Under the influence of the high field the ion is heated by above-thermal collisions to an effective temperature,  $T_{eff}$ , which is given by:<sup>28</sup>

$$T_{eff} = T + \frac{M (KE)^2}{3k_B} \quad (3.11)$$

where  $T$  is the temperature of the buffer gas. This increased temperature can cause declustering, effectively decreasing the cross section.<sup>29</sup> As a result, the ion can have different cross sections during the two different field strengths, which clearly can lead to the change of its mobility.

Actually, this effect is the extreme case of the “standard high-field effect”, where, in a glancing collision of a slow ion with a neutral, the neutral may be captured in an orbit around the ion, depending on the depth of the interaction potential between them (clustering) while at very high  $v_{rel}$  the attractive forces are immaterial (declustering).<sup>29</sup>

### 3.2.4. Collisional and dipole alignment

As mentioned above, in DTIMS ions are free to rotate, and thus their drift time depends on their orientationally averaged collision cross section,  $\Omega_{avg}$ . In FAIMS, however, during the high voltage portion of the asymmetric waveform, the ions may be aligned with respect to the electric field.<sup>29</sup> There are two ways in which this can happen : collisional alignment and dipole alignment.

Both have as a consequence that during the low voltage portion the ions are characterized by  $\Omega_{avg}$ , while during the high voltage portion they can be aligned and so their collision cross section becomes directional,  $\Omega_{dir}$ .<sup>39</sup> For non-spherical ions,  $\Omega_{dir}$  and  $\Omega_{avg}$  will be different and this will also contribute in the difference between  $K_h$  and  $K$ .

Collisional alignment stems from the fact that ions have more collisions with the buffer gas molecules when they are oriented so that they have high values of  $\Omega_{dir}$  (Fig. 3.3). Since the ions can rotate and change their orientation in collisions, they will orient themselves so that  $\Omega_{dir}$  is minimized. This effect can only be prevalent at high  $E/N$  since only under this condition the collisions along the drift are greater in number than along other directions.

Ions can also be oriented in high electric fields by alignment of their dipole moment to the lines of the field. The effect was first proposed in FAIMS studies of very large proteins of MW>27kD like carbonic anhydrase II and alcohol dehydrogenase, which have extremely high dipole moments.<sup>39</sup> All peptides and proteins belong to type 1 ions, concerning their FAIMS properties. This means that their mobilities decrease with increasing electric field. However for the above proteins, it was found that they exhibit some conformers showing type 2 behavior, i.e. increase of mobility with increased electric field.<sup>39,40</sup> This was attributed to the reversible alignment of their dipole during their high field part of the waveform.<sup>29,40</sup>

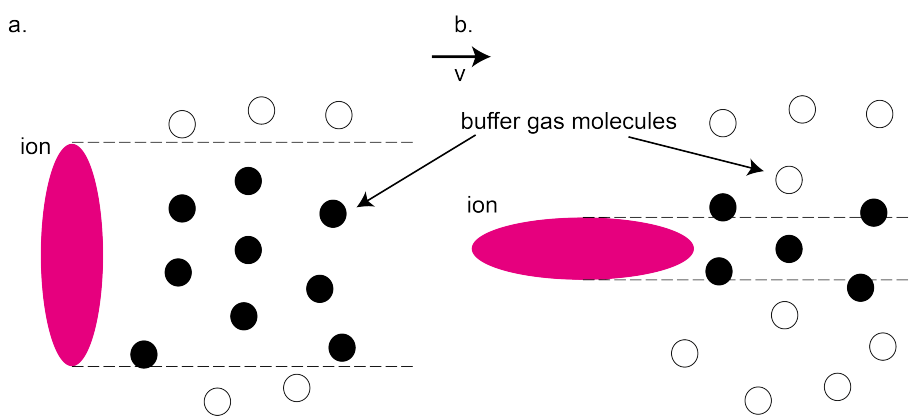


**Figure 3.3.** Collisional alignment of an ion under the influence of a high electric field. A non-spherical ion (pink) drifts through buffer gas (black and white). The ion has more collisions in orientations of higher  $\Omega_{dir}$  (a) than in lower (b). Those buffer gas molecules that collide with the ion in each case are designated black. (Adapted from ref. 24)

All dipoles tend to align at the presence of an electric field. In molecular species all polar bonds and net charges contribute to the dipole moment,  $p$ . Most proteins are expected to have large dipole moments because of the spatial ordering of the polar bonds and the distance between charges that increases with the size. Of course, the magnitude of the dipole moment depends on the spatial configuration of the atoms and bonds in a molecule (i.e. its conformation). Values for  $p$

can be from 100 D for small proteins to 10000 D for larger ones.<sup>39</sup> In the typical conditions used for FAIMS, the dipole moment should exceed 400 D in order to be aligned to the field. Proteins of mass larger than 30kD can have  $p > 400$  D and thus they may be aligned in FAIMS.<sup>39,40</sup> It was shown that because of the dipole alignment, the separation space for very large proteins is increased by an order of magnitude compared to smaller proteins, with the ions adopting a pendular motion during the high voltage portion of the asymmetric waveform.<sup>40</sup>

This might be a very important effect governing the properties of ion motion in very high electric fields, but it only becomes apparent for systems with high enough dipole moment, such as the proteins mentioned above. For the species mentioned in this thesis (bradykinin and ubiquitin) this effect is expected to be minimal, with the other factors prevailing in the determination of the  $K(E/N)$  profile.

### 3.3. FAIMS geometries

#### 3.3.1. Focusing in cylindrical geometries

The first paper on FAIMS in the English language appeared in 1993,<sup>30</sup> although the original report was a Soviet patent eleven years earlier.<sup>41</sup> In this paper, ion separation was done between two flat electrodes (the FAIMS electrodes), as shown in Fig. 3.2.<sup>30</sup> Later it was found that the sensitivity of the separation is improved when it takes place in the gap between two concentric electrodes, illustrated in Fig. 3.4.<sup>42,43</sup> The design of FAIMS of cylindrical geometry was subsequently characterized mass spectrometrically, showing some unexpected results.<sup>31</sup> Contrary to what was anticipated intuitively, increase of the DV did not lead to a decrease the transmitted ion signal because of larger spacial dispersion of the ions but to a striking increase.<sup>31,44</sup> Moreover, the width of the peaks in the CV spectrum increased with increased DV.<sup>29,44</sup> Also, inverting the DV polarity did not lead to an inversion of the polarity in the CV values that was needed for the transmission of specific ions, as would be logically required.<sup>31</sup> These findings were rationalized in terms of the focusing properties of cylindrical FAIMS devices.<sup>44</sup>

The electric field that is established between two parallel electrodes when a voltage difference is applied across them is homogeneous i.e. it has a constant value across the gap. Thus, ions experience a constant force, irrespective of their position in the gap. The situation is different

for electrodes of curved geometry (Fig. 3.4). There the electric field is inhomogeneous, and its magnitude depends on the distance  $r$  from the center :

$$E(r) = \frac{V}{r \ln \frac{R_{in}}{R_{out}}} \quad (3.12)$$

where  $V$  is the voltage applied to the inner electrode, and  $R_{in}$  and  $R_{out}$  are the outer radius of the inner electrode and the inner radius of the outer electrode, respectively. It is obvious that the CV voltage will also be a function of  $r$ . Thus, ions that are spread across  $r$  in the analytical gap will experience a different force from the field that is established because of the application of the DV and CV voltages, depending on their position. It has been shown that, at a given CV, ions that meet the condition of transmission through the electrodes are also focused in the gap median after a full cycle of the waveform (i.e. ions closer to the inner electrode are pushed toward the gap median while ions closer to the outer electrode are attracted toward the gap median).<sup>44,45</sup> The strength of focusing depends on the slope of  $K(E/N)$  over the range of the applied  $E$ .<sup>44</sup> In section 4.5, using the results obtained in this thesis with a cylindrical FAIMS device, we will show how the inhomogeneity of the field leads to focusing of the ions in the gap.

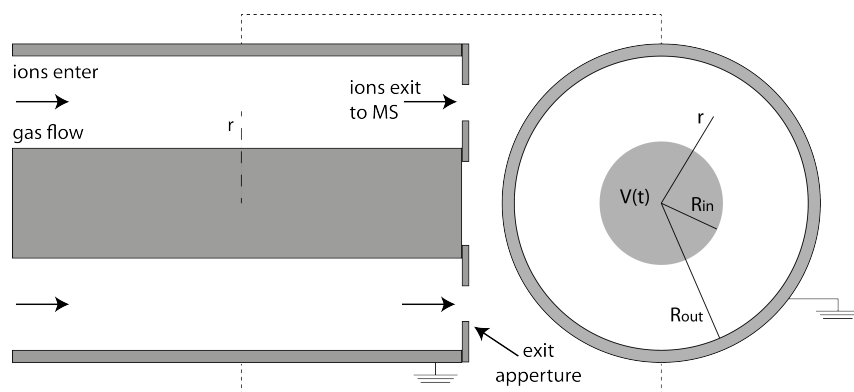


**Figure 3.4.** Cross-sectional view of a high-field Asymmetric-waveform Ion Mobility Spectrometer of cylindrical symmetry. Left: cross-section along the axis of the inner electrode (axis of symmetry). Right: cross-section perpendicular to the axis of symmetry. The asymmetric waveform ( $V(t)$ ) is applied on the inner electrode, while the outer is grounded.  $R_{in}$  is the radius of the inner electrode while  $R_{out}$  is the radius of the outer electrode.  $r$  defines the distance from the axis of the inner electrode

The property of atmospheric pressure ion focusing explained the unexpected behavior in FAIMS devices of cylindrical geometry. Increasing the DV leads to an increase in the inhomogeneity of the field across the gap, and focusing becomes tighter, hence the increase in the ion signal.<sup>44</sup> Reversing DV's polarity leads to defocusing for the particular ion.<sup>44</sup> Moreover, the inhomogeneity of the field gives rise to different deviations of  $K_h$  from  $K$  for ions of a specific

species that are found at different  $r$  (which is translated as different CV values that are needed for transmission of the ions). However, these ions are not lost to the electrodes since they are focused in the gap median. There is thus an expansion in the CV values that lead to stable trajectories at higher DV values.<sup>44,46</sup> This leads to an increase of the width of the peaks in the CV spectrum. In section 4.5 we will present a more rigorous proof of this.

Since ion focusing is a consequence of the inhomogeneity of the field, it does not hold for electrodes of flat geometry.<sup>47,48</sup> In the flat geometry the ions that are transmitted at exactly the CV value that is applied have stable trajectories but these are spread across the gap and only a part of them will be sampled by the mass spectrometer. On the other hand, in the cylindrical geometry, ions that are spread across the gap (across  $r$ ) will be focused and transmitted, increasing the sensitivity. However, as mentioned above, focusing leads to an expansion in the values of CV that lead to stable trajectories which increases the width of the peaks and thus reduces the resolution of the device.<sup>47,49</sup> So, for the FAIMS of cylindrical geometry, increased sensitivity comes at the expense of resolution, and there is a balance between them which is controlled by the curvature of the electrodes (for all the other parameters fixed, as discussed below).<sup>46</sup>

There are also some other aspects of FAIMS operation that are associated with the focusing property of these devices. For a given DV, ions with strong  $K(E/N)$  dependence will be focused tighter than ions with weaker  $K(E/N)$  profiles.<sup>44,47,50,51</sup> This leads to a discrimination in sensitivity against the latter ions. As a consequence, care should be taken when comparing the peaks in a CV spectrum: higher intensity might mean higher abundance of a specific ion, but it might also mean tighter focusing. Also, the expansion in the CV's that lead to stable trajectories in the gap will be larger for ions with strong  $K(E/N)$  dependence. This means that ions transmitted at low  $|CV|$  (weak  $K(E/N)$  dependence) appear to exhibit sharper peaks in the CV spectra as compared to ions transmitted at higher  $|CV|$ , which undergo a stronger focusing.<sup>44</sup>

### 3.3.2. “dome” FAIMS

An electrode design that has been widely used in FAIMS is the so-called “dome” geometry, shown in Fig. 3.5.<sup>52-57</sup> In this design, the two electrodes are cylindrical and concentric but the inner electrode is machined to a hemispherical end with the same diameter as the cylindrical part, while the inner side of the outer electrode has a concave end.<sup>58,59</sup> The advantage of the “dome” design over the previous cylindrical is that the transmission efficiency from the ESI source to a mass spectrometer is increased since all stable trajectories in the gap are focused in front of the

spherical tip.<sup>52</sup> The “dome” FAIMS device has also been used as an ion trapping device, where ions were captured at the tip of the hemispherical part, showing that by using the FAIMS principle it is possible to confine ions at atmospheric pressure and room temperature.<sup>44,60,61</sup>

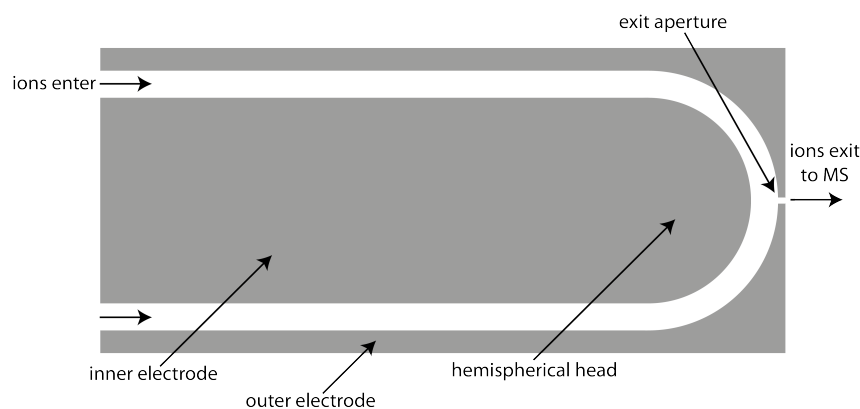


**Figure 3.5.** Cross-sectional view of a high-Field Asymmetric-waveform Ion Mobility Spectrometer of “dome” geometry. Both electrodes are of cylindrical symmetry but the inner terminates with a hemispherical cap while the outer with a concave end of the same radius as the hemispherical part. Ions are carried by a flow of gas around the inner electrode towards the tip of the hemispherical cap. Those of stable trajectories are drawn into the vacuum of the mass spectrometer (MS) through the exit aperture.

The ion motion in the cylindrical part is the same as that discussed in the previous section, with the electric field focusing the ions in the gap median. The electric field in the hemispherical part is slightly different from the cylindrical part and has been modeled numerically.<sup>61</sup> When the gaps in the cylindrical and in the hemispherical parts have the same width, a higher field gradient in the latter focuses strongly all the ions that were transmitted through the former, increasing the ion transmission.<sup>29,61</sup> The longitudinal displacement of the inner electrode changes the electric field gradient in the hemispherical part and has been shown to control the resolution/sensitivity balance.<sup>58</sup> The “dome” FAIMS can be thought of as a combination of two FAIMS devices, a cylindrical one and a spherical one used “in-tandem”.<sup>29</sup> Because they have slightly different separation properties, their combination can potentially increase the resolution of the separation.<sup>29,58</sup>

### 3.3.3. “side-to-side” FAIMS

Guevremont has also introduced the “side-to-side” FAIMS, which is illustrated in Fig. 3.6.<sup>61</sup> This FAIMS geometry was used for the experiments that we present in this thesis. In this configuration, the two electrodes are cylindrical and concentric, and the ion separation takes place



in the annular gap between the two electrodes, like in all the other cylindrical designs.<sup>62</sup> However, the ion entrance and exit apertures are located on the outer electrode, at opposite sides of the inner electrode. Ions enter the gap and the gas flow carries them around the inner electrode to the outlet of the FAIMS device. Ion losses along the length of the inner cylinder are minimized because the carrier gas hinders the ions from moving in this dimension and directs them towards the exit aperture.<sup>61</sup> This design of FAIMS was first used in a tandem FAIMS-FAIMS configuration coupled to a time-of-flight mass spectrometer (TOFMS).<sup>61</sup> The first FAIMS stage was of “side-to-side” geometry with low curvature of the electrodes, and thus a better separation efficiency. It was used to select ions for transmission into the second stage that consisted of a “dome” FAIMS optimized to trap the ions.<sup>61</sup> Lowering the number of background ions because of selection in the first stage allowed for great improvement in ion trapping times over the previous FAIMS trapping device that consisted of a “dome” FAIMS only.<sup>60</sup>

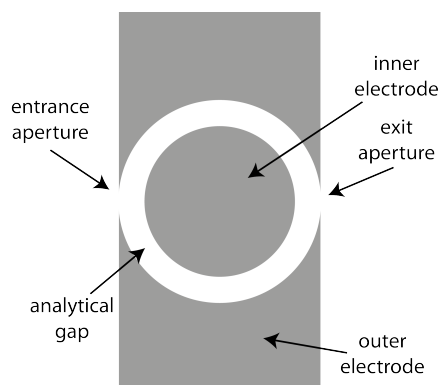


**Figure 3.6.** Cross-sectional view of a high-field Asymmetric-waveform Ion Mobility Spectrometer of “side-to-side” geometry. The analytical gap is the annular region between the two electrodes.

This FAIMS design was commercially developed and used in many applications.<sup>62,63</sup> However, when used with mass spectrometers or ion sources that produce heat (like a heated electrospray source or a mass spectrometer comprising a heated capillary), the CV values for transmittance of the ions changed with time, which required a temperature equilibration for stable operating conditions.<sup>62</sup> This led to a further development of the “side-to-side” FAIMS system with active, independent control of the temperatures of the two electrodes.<sup>64</sup> Temperature control is accomplished by flowing heated compressed air through holes drilled into the FAIMS electrodes. Temperatures are stabilized after ~5 min.<sup>64</sup>

Another advantage of being able to control the temperature of the electrodes independently is that one can establish a temperature gradient across the gap.<sup>64</sup> The usefulness of this will be obvious shortly. It was shown that the focusing in curved electrodes is a consequence of the

inhomogeneity of the electric field in the gap.<sup>44</sup> This inhomogeneity causes the ratio of  $K_h/K$  to change across the analytical gap as a function of  $r$ , *via* equation 3.3. It is exactly this variation in  $K_h/K$  that focuses the ions that meet the condition of transmission. Yet, the ion mobility depends on the electric field through  $E/N$ , where  $N$  is the number density of the buffer gas (carrier gas) molecules.<sup>10</sup> Thus, if  $N$  is changed across the gap so that (in an ideal situation)  $E/N$  remains stable, the ratio  $K_h/K$  will be a constant of  $r$  across the gap and so the focusing property and all its consequences will be lost.<sup>29,64</sup>

The gradient in the number density of buffer gas molecules across the gap can be produced by establishing a temperature gradient between the two electrodes.<sup>64</sup> In an ideal gas approximation,  $N$  scales as  $1/T$ . The voltage is applied on the inner electrode, so by equation 3.12 the electric field is stronger closer to the inner electrode. This means that in order to have  $E/N$  (and thus  $K_h/K$ ) stable across the gap, the inner electrode has to be kept at a lower temperature than the outer one. It has been shown that by doing this, the focusing properties of the device could be reduced, decreasing the sensitivity but increasing the resolution.<sup>64</sup> The magnitude of the temperature gradient provides a way to control the resolution of the instrument. On the other hand, establishing the temperature gradient the other way around has the same effect as increasing the curvature of FAIMS and so the sensitivity is enhanced while the resolution diminishes.<sup>64</sup> The independent, active temperature control of the two electrodes has proven to be a fast and easy way to tune the resolution/sensitivity balance.

### 3.4. Parameters that govern FAIMS performance

Although most of the instrumental parameters that govern FAIMS performance were determined empirically, a better understanding and rationalization of their effects on the separation metrics came only after modeling them computationally.<sup>45,49,65</sup> In initial computations the main features of ion separation, focusing and trapping were explained and predicted.<sup>44,60</sup> However, these models did not include ion-ion repulsion and diffusion.<sup>44,60</sup> Subsequent models took into account these effects and also shed light on the effects of instrumental parameters on the resolution and sensitivity of the separation.<sup>45,46,49</sup>

These parameters include the shape of the electrodes, the analytical gap width, the frequency and the form of the waveform, the carrier gas flow speed and the length of the gap and also the carrier's gas composition.<sup>49</sup> Some of them can be adjusted without much effort (e.g. *via* a

computer program) while for others mechanical intervention is required.<sup>46</sup> In the following, these parameters will be presented briefly.

### 3.4.1. The asymmetric waveform

The rectangular asymmetric waveform that was shown in Fig. 3.2 for illustrative purposes is difficult to implement.<sup>29</sup> In spite of this, such waveforms were modeled and were proven to be ideal for FAIMS operation.<sup>66,67</sup> Also, recently, nearly rectangular waveforms have been produced and applied to FAIMS but their frequency and amplitude were limited.<sup>68</sup> The most frequent asymmetric waveform that is applied across the FAIMS electrodes consists of a sinusoidal waveform plus its scaled harmonic phase shifted by 90°. This can be described mathematically by:<sup>69,70</sup>

$$V(t) = CV + \frac{2}{3}DV \sin(\omega t) + \frac{1}{3}DV \sin(2\omega t - \frac{\pi}{2}) \quad (3.13)$$

where  $CV$  is the Compensation Voltage,  $DV$  the Dispersion Voltage and  $\omega$  is the frequency of the waveform. This waveform is plotted in Fig. 3.7. The amplitude of the oscillations that the ions undergo in the gap is defined by  $\omega$ . Decrease of the frequency of the waveform leads to an increase of the motion's amplitude.<sup>49</sup> The turning point of the oscillations are brought closer to the electrodes, resulting in larger ion losses which decrease the sensitivity. This ion loss mechanism is enhanced for ions displaced from the gap median, which are those that cause the peaks to be wider. Consequently, the resolution is increased. Inversely, increasing  $\omega$  reduces the amplitude of the ions' oscillatory motion causing an increase in the number of the stable trajectories, even for ions that are a bit displaced from the gap median. The sensitivity is increased at the expense of resolution.<sup>49</sup>

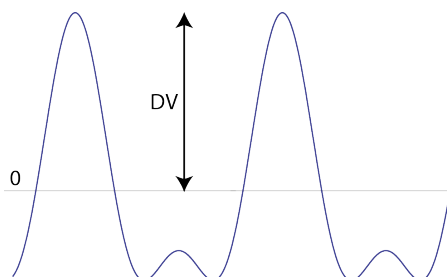


**Figure 3.7.** Typical asymmetric waveform applied on the FAIMS electrodes. The time dependent waveform of eq. 3.13 is plotted for  $CV=0$ .

Typical frequencies that are employed for the waveform shown above are 750 kHz,<sup>64</sup> but frequencies as low as 200 kHz<sup>31</sup> and as high as 28.5 MHz have also been used.<sup>71</sup>

### 3.4.2. The analytical gap width

The impact of modifying the analytical gap width on the resolution/sensitivity balance is expected to be similar to changing the frequency of the asymmetric waveform.<sup>29,49</sup> Smaller gap width leads to larger losses in the electrodes because of the ion's oscillatory motion, thus decreasing their transmittance through FAIMS. However, this happens preferentially for the ions that are displaced from the gap median and so the resolution of the instrument is increased.<sup>49</sup> This has also proven to be the case experimentally.<sup>46,72</sup>

It should be noted, however, that decreasing the gap width at constant DV cannot be considered exactly equivalent to reducing the asymmetric waveform's frequency,  $\omega$ .<sup>72</sup> This is because the former will also increase the electric field strength in the analytical gap and hence the  $K_h/K$  ratio for a specific ion, which improves the resolution *per se*.

### 3.4.3. The carrier gas flow speed/length of the gap

The ions are carried through the FAIMS electrodes by the gas that flows between them. Thus, the gas flow speed defines the residence time for the ions in the analytical gap,  $t_{res}$ .<sup>49</sup> For a constant gas flow, the residence time is increased with increased length of the FAIMS electrodes. Therefore, reducing the gas flow is equivalent to increasing the length of the gap.<sup>45</sup>

The longer the ion cloud is subjected to the oscillatory motion in the analytical gap, the better the separation since ions with the "wrong" CV have more time to drift towards one of the electrodes and be lost. Moreover, diffusion and ion-ion repulsion will lead to expansion in the ion cloud and thus ions further away from the gap median will be disproportionately lost, reducing the width of the peaks.<sup>45,49</sup> Consequently, increased residence times of the ions in the analytical gap reduces the transmission while increases the resolution.

It should be noted that this is strictly correct for FAIMS of flat geometry. In curved geometries, where there is focusing of the ions, an increase in the residence time after focusing has completed is not expected to have an effect in the resolution/sensitivity balance.

In the initial modeling of the effect of changing the gas flow on the resolution/sensitivity performance of FAIMS, a uniform gas flow in the analytical gap was assumed.<sup>45,49</sup> Shvartsburg *et. al.* improved the model by including realistic gas flow, where the flow drops dramatically close to the electrodes while reaches its maximum at the gap median.<sup>73</sup> This means that the further away ions are from the gap median the slower they are carried though the FAIMS electrodes. However, this seemed to have a minor effect in the resolution, probably because ions that are close to the electrodes are lost anyway.<sup>73</sup>

### 3.4.4. The composition of the carrier gas

The most frequently used carrier gas in FAIMS is N<sub>2</sub>,<sup>35,55,74</sup> although O<sub>2</sub>, CO<sub>2</sub>, N<sub>2</sub>O and SF<sub>6</sub> have also been used.<sup>75</sup> Changing the carrier gas alters the interaction potential with the ion and hence modifies the  $K(E/N)$  dependence.<sup>29</sup> Combinations of gases in various ratios have also been used as a FAIMS medium, mainly N<sub>2</sub>/He<sup>34,54,64,76,77</sup> but also N<sub>2</sub>/O<sub>2</sub>,<sup>53</sup> N<sub>2</sub>/CO<sub>2</sub>,<sup>53,57</sup> N<sub>2</sub>/He/CO<sub>2</sub><sup>78</sup> and more recently N<sub>2</sub>/H<sub>2</sub>.<sup>79</sup> The effect of adding small amounts of water or organic vapors in the carrier gas has also been studied.<sup>37,80,81</sup>

The mobility of an ion in a mixture of gas,  $K_{mix}$ , can be estimated from Blanc's law, which relates  $K_{mix}$  to the mobility of an ion in the individual gases,  $K_i$ . In mathematical formulation:<sup>82</sup>

$$\frac{1}{K_{mix}} = \frac{\chi_1}{K_1} + \frac{\chi_2}{K_2} + \dots \quad (3.14)$$

where  $\chi_i$  is the molar fractional population of the  $i^{th}$  gas in the mixture. For the phthalic acid anion and the Cs<sup>+</sup> ion in a gas mixture of N<sub>2</sub>/O<sub>2</sub> of various ratios, it was found that the experimental CV values are exactly the ones that are expected according to the above law.<sup>53,83</sup> However, deviation from Blanc's law were observed for a mixture of N<sub>2</sub>/CO<sub>2</sub>.<sup>53</sup> Moreover, the deviation was isomer dependent, and this effect led to the baseline separation of the o-, m-, and p-phthalic acid in a 95/5 mixture of N<sub>2</sub>/CO<sub>2</sub>.<sup>53</sup> The use of mixtures for carrier gas proved to be of great advantage in FAIMS, improving the resolution but also the sensitivity, because of non-Blanc behavior of the ions.<sup>54,59</sup> Nevertheless, non-Blanc deviations may also lead to a reduction of the separation space, so that species that are separated in pure N<sub>2</sub> overlap in mixtures of N<sub>2</sub>/CO<sub>2</sub>.<sup>78</sup>

The behavior of ions in gas mixtures was studied by Shvartsburg *et. al.* in a model they introduced where they were able to calculate high-field ion mobilities in gas mixtures.<sup>83</sup> Based on physical phenomena underlying the ion's motion under the influence of a strong electric field in a

mixture of gases, they predicted that stronger non-Blanc phenomena should be expected in binary mixtures of gases with large difference in masses and collision cross-sections, in accordance to experiments.<sup>83</sup> They also proposed the use of He/SF<sub>6</sub> mixture as the ultimate carrier gas for FAIMS.<sup>83</sup> A model of complexation of ions with buffer gas molecules and dissociation of the clusters, in-phase with the asymmetric waveform, has also been proposed to explain the unexpected behavior of ions in gas mixtures or upon addition of vapors.<sup>37</sup> This would modify strongly the K(E/N) profile of an ion, expanding the separation space and thus improving the resolution.<sup>80</sup> Probably the two effects are additive and should both be taken into account.<sup>29</sup>

### 3.4.5. Instrumental modifications for high-resolution FAIMS

Since FAIMS can be used for a variety of applications, its optimum performance depends on the specific task, and the above parameters can be optimized accordingly. For example, in applications where a high resolution is needed, such as the separation of conformers, use of a FAIMS unit with flat electrodes is preferable. However, most commercially available FAIMS devices that are used in conjunction with mass spectrometers comprise the cylindrical geometry. The reason for this is that the focusing in these geometries reduced ion losses and increases the transmission of ions in the vacuum chamber. Nevertheless, the need to develop differential mobility spectrometers with high resolution and sensitivity remains.

To avoid the discrimination effects in curved gaps, interest has mainly been focused in improving the design of flat electrode FAIMS devices. Shvartsburg et. al. constructed a new planar analyzer with longer length, permitting longer residence times for the ions and thus higher resolution.<sup>48</sup> This design incorporated an ion funnel to improve the transmission efficiency from the FAIMS to the MS stage.<sup>14,18</sup> In addition, the sensitivity was improved by opening 11 circular holes in a “slit” orientation instead of a single aperture of the same area as an exit outlet for the ions from the FAIMS stage to the ion funnel. The “slit” captured the ribbon-shaped ion beam formed in FAIMS and proved to increase the transmittance by as much as 250%.<sup>48</sup> In another version of this instrument, a “slit” aperture was also opened in the front interface of FAIMS in order to couple it to multi-emitter electrospray ionization comprising up to 19 emitters, increasing the ion current in the analytical gap.<sup>84</sup> Doing this increased the sensitivity of the FAIMS device at equal resolution.

Use of He/N<sub>2</sub> mixtures for carrier gas with He content up to 75% further improved the resolution of the instrument.<sup>36,76</sup> However, the amount of He was limited to less than 80% to

avoid electrical breakdown in the gap.<sup>76</sup> More recently, better resolution was achieved by the use of H<sub>2</sub>/N<sub>2</sub> mixture with up to 90% H<sub>2</sub>.<sup>79</sup>

Enhanced resolution was achieved by increasing the DV (and thus the dispersion field) by 35% with the use of only 50% He in the carrier gas.<sup>85</sup> Further increase of the DV was prohibited because of electrical breakdown.<sup>85</sup> The effect of the residence time of the ion on the resolution was also studied experimentally by changing the carrier gas flow.<sup>86</sup> It was shown that by increasing  $t_{res}$  four times there was a corresponding two times enhancement in the resolution.<sup>86</sup>

It should be noted here that increases in the RF field or in the time that the ion is subjected to this field ( $t_{res}$ ) can induce heating of the ions in FAIMS, which can lead to their isomerization or dissociation, a situation that, in general, is not desired.<sup>29</sup>

### 3.5. Comparison of IMS with FAIMS

Conventional IMS separates conformers of ions according to their absolute ion mobilities in a time-independent low electric field. FAIMS separation is based on the difference in the ion mobility value at high and low field, making use of a time-dependent electric field. FAIMS is also called differential ion mobility because it measures the *change* in this quantity ( $K$ ) as a function of the electric field.

Absolute mobilities can be directly connected to collision cross-sections, *via* equation 3.2, and thus, as mentioned above, to specific conformations. On the other hand, calculating the dependence of the ion mobility on the electric field for a specific ion (or conformation of ion) in a buffer gas is not trivial because of the difficulty in modeling all of the above parameters. In other words, drift times ( $t_D$ ) in IMS are readily correlated to structural properties of the ion while CV values do not. Thus, while it may be possible to separate different conformers using FAIMS, it is impossible to obtain information on the ion geometries from the CV values alone.

However, the fact that CV values do not directly relate to the size of the ion is what makes FAIMS such a powerful analytical technique. In IMS, the cross-section of an ion correlates to its size and thus to its mass.<sup>87-89</sup> However, the  $K(E/N)$  profile of two ions of the same mass may be completely different.<sup>52,89</sup> This renders FAIMS more orthogonal to MS than IMS. FAIMS-MS has been shown to separate isobaric species as well as conformers of proteins that are indistinguishable by their drift time in IMS-MS studies.<sup>48,52</sup> Despite the fact that this advantage of FAIMS-MS is mitigated by the inability to obtain direct structural information, this can be

extracted when FAIMS separation of isomers done in tandem with different techniques such as H/D exchange or energy-loss experiments.<sup>32-34</sup> Also, since the change in a quantity does not depend on the value of the quantity itself, FAIMS is orthogonal to IMS.<sup>29</sup> This has been realized in two-dimensional separations in the form of FAIMS-IMS-MS, increasing the separation space for complex mixtures<sup>56,77</sup> but also detecting conformers that are invisible by the use of either technique alone.<sup>90</sup>

FAIMS can be used as an ion filter that continuously separates and transmits ions of a specific type into the mass spectrometer. Moreover, FAIMS functions at atmospheric pressure and room temperature. This makes it easy to use with electrospray ionization, as a part of the atmospheric pressure source, but also convenient to remove from and mount it on a mass spectrometer without breaking vacuum.<sup>54</sup> On the other hand, IMS requires accumulation of ions prior to their injection into the drift tube for separation, and the ions are released in packets. Thus, ion trapping is required between atmospheric pressure ionization sources and the drift tube, and interfacing to a mass spectrometer is more complex than in the case of FAIMS.

A major disadvantage of FAIMS is that during the separation process ions are inevitably heated by above-thermal collisions. According to the “standard high-field effect”, the deviation of  $K_h$  from  $K$  results from the shift of the relative velocity of the ion-gas molecule,  $v_{rel}$ , to higher velocities than those of the buffer gas. In other words, separation in FAIMS happens because the ions are heated translationally to  $T_{eff}$ . Thus, the energy imparted on an ion upon collisions is transferred into its vibrations and may induce isomerization (see Chapters 4 and 5). This heating is negligible in drift tube IMS where low electric fields are used and collisions in the gas phase ensemble (ions and buffer gas molecules) are thermal.

### 3.6. References

- (1) Eiceman, G. A.; Karpas, Z. *Ion Mobility Spectrometry*; Taylor & Francis Group: Boca Raton, FL, 2005.
- (2) Kanu, A. B.; Dwivedi, P.; Tam, M.; Matz, L.; Hill, H. H. J. *J. Mass Spectrom.* **2008**, *43*, 1.
- (3) Bohrer, B. C.; Merenbloom, S. I.; Koeniger, S. L.; Hilderbrand, A. E.; Clemmer, D. E. *Annu. Rev. Anal. Chem.* **2008**, *1*, 293.
- (4) Uetrecht, C.; Rose, R. J.; van Duijn, E.; Lorenzen, K.; Heck, A. J. R. *Chem. Soc. Rev.* **2010**, *39*, 1633.
- (5) Jurneczko, E.; Barran, P. E. *Analyst* **2011**, *136*, 20.
- (6) Kemper, P.; Bowers, M. J. *Am. Soc. Mass Spectrom.* **1990**, *1*, 197.



- (7) von Helden, G.; Wyttenbach, T.; Bowers, M. T. *Science* **1995**, *267*, 1483.
- (8) Bowers, M. T.; Kemper, P. R.; von Helden, G.; Vankoppen, P. A. M. *Science* **1993**, *260*, 1446.
- (9) Jarrold, M. F. *Annu. Rev. Phys. Chem.* **2000**, *51*, 179.
- (10) Mason, E. A.; McDaniel, E. W. *Transport Properties Of Ions In Gases*; Wiley: New York, 1988.
- (11) Hoaglund, C. S.; Valentine, S. J.; Sporleder, C. R.; Reilly, J. P.; Clemmer, D. E. *Anal. Chem.* **1998**, *70*, 2236.
- (12) Jarrold, M. F. *J. Phys. Chem.* **1995**, *99*, 11.
- (13) Gillig, K. J.; Ruotolo, B.; Stone, E. G.; Russell, D. H.; Fuhrer, K.; Gonin, M.; Schultz, A. J. *Anal. Chem.* **2000**, *72*, 3965.
- (14) Tang, K.; Shvartsburg, A. A.; Lee, H.-N.; Prior, D. C.; Buschbach, M. A.; Li, F.; Tolmachev, A. V.; Anderson, G. A.; Smith, R. D. *Anal. Chem.* **2005**, *77*, 3330.
- (15) Counterman, A. E.; Valentine, S. J.; Srebalus, C. A.; Henderson, S. C.; Hoaglund, C. S.; Clemmer, D. E. *J. Am. Soc. Mass Spectrom.* **1998**, *9*, 743.
- (16) Shvartsburg, A. A.; Jarrold, M. F. *Chem. Phys. Lett.* **1996**, *261*, 86.
- (17) Mesleh, M. F.; Hunter, J. M.; Shvartsburg, A. A.; Schatz, G. C.; Jarrold, M. F. *J. Phys. Chem.* **1996**, *100*, 16082.
- (18) Kim, T.; Tolmachev, A. V.; Harkewicz, R.; Prior, D. C.; Anderson, G.; Udseth, H. R.; Smith, R. D.; Bailey, T. H.; Rakov, S.; Futrell, J. H. *Anal. Chem.* **2000**, *72*, 2247.
- (19) Kim, T.; Tang, K.; Udseth, H. R.; Smith, R. D. *Anal. Chem.* **2001**, *73*, 4162.
- (20) Koeniger, S. L.; Merenbloom, S. I.; Valentine, S. J.; Jarrold, M. F.; Udseth, H. R.; Smith, R. D.; Clemmer, D. E. *Anal. Chem.* **2006**, *78*, 4161.
- (21) Merenbloom, S. I.; Koeniger, S. L.; Valentine, S. J.; Plasencia, M. D.; Clemmer, D. E. *Anal. Chem.* **2006**, *78*, 2802.
- (22) Merenbloom, S. I.; Bohrer, B. C.; Koeniger, S. L.; Clemmer, D. E. *Anal. Chem.* **2006**, *79*, 515.
- (23) Koeniger, S. L.; Merenbloom, S. I.; Clemmer, D. E. *J. Phys. Chem. B* **2006**, *110*, 7017.
- (24) Pierson, N. A.; Valentine, S. J.; Clemmer, D. E. *J. Phys. Chem. B* **2010**, *114*, 7777.
- (25) Dugourd, P.; Hudgins, R. R.; Clemmer, D. E.; Jarrold, M. F. *Rev. Sci. Instrum.* **1997**, *68*, 1122.
- (26) Gidden, J.; Wyttenbach, T.; Batka, J. J.; Weis, P.; Jackson, A. T.; Scrivens, J. H.; Bowers, M. T. *J. Am. Chem. Soc.* **1999**, *121*, 1421.
- (27) Koeniger, S.; Clemmer, D. E. *J. Am. Soc. Mass Spectrom.* **2007**, *18*, 322.
- (28) Revercomb, H. E.; Mason, E. A. *Anal. Chem.* **1975**, *47*, 970.
- (29) Shvartsburg, A. A. *Differential Ion Mobility Spectrometry*; CRC Press: Boca Raton FL, 2009.
- (30) Buryakov, I. A.; Krylov, E. V.; Nazarov, E. G.; Rasulev, U. K. *Int. J. Mass Spectrom. Ion Processes* **1993**, *128*, 143.
- (31) Purves, R. W.; Guevremont, R.; Day, S.; Pipich, C. W.; Matyjaszczyk, M. S. *Rev. Sci. Instrum.* **1998**, *69*, 4094.
- (32) Purves, R. W.; Barnett, D. A.; Ells, B.; Guevremont, R. *J. Am. Soc. Mass Spectrom.* **2000**, *11*, 738.
- (33) Purves, R. W.; Barnett, D. A.; Ells, B.; Guevremont, R. *Rapid Commun. Mass Spectrom.* **2001**, *15*, 1453.
- (34) Purves, R. W.; Barnett, D. A.; Ells, B.; Guevremont, R. *J. Am. Soc. Mass Spectrom.* **2001**, *12*, 894.
- (35) Guevremont, R.; Purves, R. W. *J. Am. Soc. Mass Spectrom.* **1999**, *10*, 492.

- (36) Shvartsburg, A. A.; Tang, K.; Smith, R. D. *Anal. Chem.* **2010**, *82*, 32.
- (37) Krylova, N.; Krylov, E.; Eiceman, G. A.; Stone, J. A. *J. Phys. Chem. A* **2003**, *107*, 3648.
- (38) Nazarov, E. G.; Coy, S. L.; Krylov, E. V.; Miller, R. A.; Eiceman, G. A. *Anal. Chem.* **2006**, *78*, 7697.
- (39) Shvartsburg, A. A.; Bryskiewicz, T.; Purves, R. W.; Tang, K.; Guevremont, R.; Smith, R. D. *J. Phys. Chem. B* **2006**, *110*, 21966.
- (40) Shvartsburg, A. A.; Noskov, S. Y.; Purves, R. W.; Smith, R. D. *Proc. Natl. Acad. Sci. U. S. A.* **2009**.
- (41) Gorshkov, M. P. USSR, 1982; USSR Inventor's Certificate 966,583.
- (42) Carnahan, B.; Tarassov, A. U.S.A., 1995; U.S. Patent Number 5 420 424.
- (43) Krylov, E., V. *Tech. Phys.* **1999**, *44*, 113.
- (44) Guevremont, R.; Purves, R. W. *Rev. Sci. Instrum.* **1999**, *70*, 1370.
- (45) Shvartsburg, A. A.; Tang, K.; Smith, R. D. *J. Am. Soc. Mass Spectrom.* **2004**, *15*, 1487.
- (46) Guevremont, R.; Purves, R. *J. Am. Soc. Mass Spectrom.* **2005**, *16*, 349.
- (47) Krylov, E. V. *Int. J. Mass Spectrom.* **2003**, *225*, 39.
- (48) Shvartsburg, A. A.; Li, F.; Tang, K.; Smith, R. D. *Anal. Chem.* **2006**, *78*, 3706.
- (49) Shvartsburg, A. A.; Tang, K.; Smith, R. D. *J. Am. Soc. Mass Spectrom.* **2005**, *16*, 2.
- (50) Barnett, D. A.; Guevremont, R.; Purves, R. W. *Appl. Spectrosc.* **1999**, *53*, 1367.
- (51) Schneider, B. B.; Covey, T. R.; Coy, S. L.; Krylov, E. V.; Nazarov, E. G. *Int. J. Mass Spectrom.* **2010**, *298*, 45.
- (52) Guevremont, R.; Barnett, D. A.; Purves, R. W.; Vandermeij, J. *Anal. Chem.* **2000**, *72*, 4577.
- (53) Barnett, D. A.; Purves, R. W.; Ells, B.; Guevremont, R. *J. Mass Spectrom.* **2000**, *35*, 976.
- (54) Barnett, D.; Ells, B.; Guevremont, R.; Purves, R. *J. Am. Soc. Mass Spectrom.* **2002**, *13*, 1282.
- (55) Gabryelski, W.; Froese, K. *J. Am. Soc. Mass Spectrom.* **2003**, *14*, 265.
- (56) Tang, K.; Li, F.; Shvartsburg, A. A.; Strittmatter, E. F.; Smith, R. D. *Anal. Chem.* **2005**, *77*, 6381.
- (57) Beach, D. G.; Gabryelski, W. *Anal. Chem.* **2011**, *83*, 9107.
- (58) Guevremont, R.; Thekkadath, G.; Hilton, C. *J. Am. Soc. Mass Spectrom.* **2005**, *16*, 948.
- (59) Guevremont, R. *J. Chromatogr. A* **2004**, *1058*, 3.
- (60) Guevremont, R.; Purves, R. W.; Barnett, D. A.; Ding, L. *Int. J. Mass Spectrom.* **1999**, *193*, 45.
- (61) Guevremont, R.; Ding, L.; Ells, B.; Barnett, D. A.; Purves, R. W. *J. Am. Soc. Mass Spectrom.* **2001**, *12*, 1320.
- (62) Kapron, T., James; Jemal, M.; Duncan, G.; Kolakowski, B.; Purves, R. *Rapid Commun. Mass Spectrom.* **2005**, *19*, 1979.
- (63) Kapron, T., James; Wu, J.; Mauriala, T.; Clark, P.; Purves, W., Randy; Bateman, P., Kevin *Rapid Commun. Mass Spectrom.* **2006**, *20*, 1504.
- (64) Barnett, D. A.; Belford, M.; Dunyach, J.-J.; Purves, R. W. *J. Am. Soc. Mass Spectrom.* **2007**, *18*, 1653.
- (65) Shvartsburg, A. A.; Smith, R. D. *J. Am. Soc. Mass Spectrom.* **2007**, *18*, 1672.
- (66) Krylov, E. V.; Nazarov, E. G.; Miller, R. A. *Int. J. Mass Spectrom.* **2007**, *266*, 76.
- (67) Shvartsburg, A. A.; Smith, R. D. *J. Am. Soc. Mass Spectrom.* **2008**, *19*, 1286.

- (68) Papanastasiou, D.; Wollnik, H.; Rico, G.; Tadjimukhamedov, F.; Mueller, W.; Eiceman, G. A. *J. Phys. Chem. A* **2008**, *112*, 3638.
- (69) Viehland, L. A.; Guevremont, R.; Purves, R. W.; Barnett, D. A. *Int. J. Mass Spectrom.* **2000**, *197*, 123.
- (70) Guevremont, R.; Barnett, D. A.; Purves, R. W.; Viehland, L. A. *J. Chem. Phys.* **2001**, *114*, 10270.
- (71) Shvartsburg, A. A.; Smith, R. D.; Wilks, A.; Koehl, A.; Ruiz-Alonso, D.; Boyle, B. *Anal. Chem.* **2009**, *81*, 6489.
- (72) Barnett, D. A.; Ouellette, R. J. *Rapid Commun. Mass Spectrom.* **2011**, *25*, 1959.
- (73) Shvartsburg, A. A.; Tang, K.; Smith, R. D. *J. Am. Soc. Mass Spectrom.* **2005**, *16*, 1447.
- (74) Purves, R. W.; Guevremont, R. *Anal. Chem.* **1999**, *71*, 2346.
- (75) Barnett, D. A.; Ells, B.; Guevremont, R.; Purves, R. W.; Viehland, L. A. *J. Am. Soc. Mass Spectrom.* **2000**, *11*, 1125.
- (76) Shvartsburg, A. A.; Danielson, W. F.; Smith, R. D. *Anal. Chem.* **2010**, *82*, 2456.
- (77) Shvartsburg, A. A.; Tang, K.; Smith, R. D. In *Mass Spectrometry of Proteins and Peptides: Methods and Protocols* 2008; Vol. 492, p 417.
- (78) Cui, M.; Ding, L.; Mester, Z. *Anal. Chem.* **2003**, *75*, 5847.
- (79) Shvartsburg, A. A.; Smith, R. D. *Anal. Chem.* **2011**, *83*, 9159.
- (80) Eiceman, G. A.; Krylov, E. V.; Krylova, N. S.; Nazarov, E. G.; Miller, R. A. *Anal. Chem.* **2004**, *76*, 4937.
- (81) Rorrer, L. C.; Yost, R. A. *Int. J. Mass Spectrom.* **2011**, *300*, 173.
- (82) Sandler, S. I.; Mason, E. A. *J. Chem. Phys.* **1968**, *48*, 2873.
- (83) Shvartsburg, A. A.; Tang, K.; Smith, R. D. *Anal. Chem.* **2004**, *76*, 7366.
- (84) Mabrouki, R.; Kelly, R. T.; Prior, D. C.; Shvartsburg, A. A.; Tang, K.; Smith, R. D. *J. Am. Soc. Mass Spectrom.* **2009**, *20*, 1768.
- (85) Shvartsburg, A. A.; Prior, D. C.; Tang, K.; Smith, R. D. *Anal. Chem.* **2010**, *82*, 7649.
- (86) Shvartsburg, A. A.; Smith, R. D. *Anal. Chem.* **2010**, *83*, 23.
- (87) Ruotolo, B. T.; Gillig, K. J.; Stone, E. G.; Russell, D. H. *J. Chromatogr. B* **2002**, *782*, 385.
- (88) Shvartsburg, A.; Siu, K.; Clemmer, D. *J. Am. Soc. Mass Spectrom.* **2001**, *12*, 885.
- (89) Shvartsburg, A. A.; Mashkevich, S. V.; Smith, R. D. *J. Phys. Chem. A* **2006**, *110*, 2663.
- (90) Shvartsburg, A. A.; Li, F.; Tang, K.; Smith, R. D. *Anal. Chem.* **2006**, *78*, 3304.



## Spectroscopy of mobility-selected biomolecular ions

In this chapter we present experiments that combine high-Field Asymmetric-waveform Ion Mobility Spectrometry (FAIMS), which separates conformational isomers of biomolecular ions, with electronic spectroscopy in a cold, radio-frequency ion trap. We first describe the problem of spectral congestion that may arise when cold ion spectroscopy is employed to study large peptides and small proteins and then how this can be mitigated with the help of ion mobility techniques. Then, we show the feasibility, but also the advantages and the limitations of the marriage of the two techniques by performing experiments on a small but conformationally complex peptide. Most of the results that we present here were published recently.<sup>1</sup>

### 4.1. Introduction

Over the last several years both electronic and vibrational spectroscopy have been used extensively to characterize the structural and photophysical properties of biomolecular ions in the gas phase.<sup>2-9</sup> When the ions are cooled to low temperatures their spectra become greatly simplified, allowing the identification of individual conformational isomers, which typically have slightly different electronic and vibrational transitions frequencies.<sup>10-12</sup> The measurement of conformation-specific infrared spectra via IR-UV double resonance and its comparison with theory has been one of the primary means of determining the structure of gas phase biomolecules.<sup>13-22</sup> However, as the size and complexity of the molecules increase, the electronic spectra become increasingly complex and congested, hindering their interpretation but also the application of IR-UV double resonance. To allow analysis of the spectra and to push our technique to larger molecules, it is necessary to examine the potential causes of spectral congestion.

The features in an electronic spectrum may arise from vibrational progressions of low-frequency vibrations that couple to the electronic transition of the molecule. The number of low-

frequency vibrations increases with the size of the molecule. Vibrations that have good Franck-Condon factors will contribute to the electronic spectrum leading to its complexity and congestion. Figure 4.1 shows electronic photofragment spectra of PheH<sup>+</sup> (a), Ac-Phe-(Ala)<sub>5</sub>-Lys-H<sup>+</sup> (b) and Ac-Phe-(Ala)<sub>10</sub>-Lys-H<sup>+</sup> (c) cooled to 10 K in a radio-frequency ion trap, recorded by Stearns *et al.*<sup>14,15,23</sup> The latter two ions form stable helices in the gas phase.<sup>14,24-26</sup> All spectra of Fig. 4.1 exhibit sharp ( $\sim 2$  cm<sup>-1</sup>), well-resolved features. While the size of the molecule increases from traces (a) to (c) the spectrum does not seem to become much more complex. These data suggest that the number of Franck-Condon active modes does not increase with molecular size, indicating that the electronic chromophore is a probe of its local environment. Therefore, we don't expect low-frequency vibronic activity to be the main contribution to spectral congestion as the size of the biomolecule is increased.

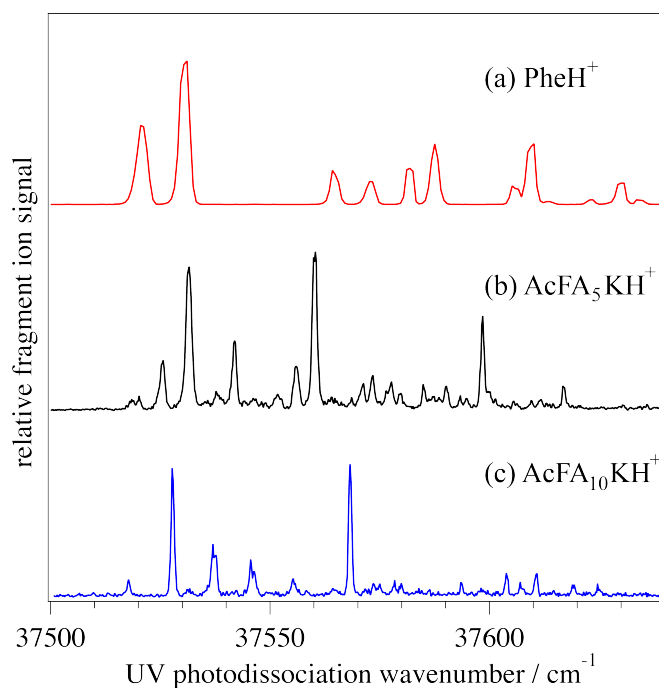


**Figure 4.1.** Electronic photofragment excitation spectra of (a) PheH<sup>+</sup>; (b) AcFA<sub>5</sub>KH<sup>+</sup>; and (c) AcFA<sub>10</sub>KH<sup>+</sup>.

Broadening of individual transitions in an electronic spectrum may also lead to its congestion. This may result from fast decay of the initially excited electronic state. The photophysics of the excited-state is molecule and in some cases conformation dependent.<sup>27</sup> While this is not the case for both cold phenylalanine (shown in Fig. 4.1a) and tyrosine,<sup>15</sup> the electronic spectrum of cold tryptophan is sensitive to its local environment, exhibiting two broad bands ( $\sim 350$  cm<sup>-1</sup>) when in the proximity of a charge<sup>10</sup> and sharp features ( $\sim 2$  cm<sup>-1</sup>) when the charge is blocked.<sup>28</sup> While probing the right electronic chromophores in biomolecules may allow for the

recording of highly-resolved electronic spectra, for proteins carrying a plethora of aromatic amino acids that may interact or their transitions may overlap this will certainly be a limitation of our technique.<sup>29</sup>

A third source of spectral congestion is conformational heterogeneity. Even at the low temperatures attainable in a cold ion trap, a number of stable conformations can be populated. Different conformers have slightly different and partially overlapping electronic spectra.<sup>18</sup> The electronic spectrum that one obtains is a weighted composite of the individual spectra of the conformations. Their number will increase with the size of the molecule, and we expect this to be the main reason of spectral congestion. Electronic transitions that are (even partially) overlapping in the electronic spectrum inhibit the use of IR-UV double-resonance, rendering the detailed spectroscopic analysis difficult. In such cases one needs additional “dimensions” in which to disperse the spectra and alleviate the overlap of spectral bands.

A way out of this problem is to use the “dimension” of ion mobility spectrometry (IMS)<sup>30-32</sup> in order to disperse gas-phase conformers prior to spectroscopic interrogation. In this way, a complex electronic spectrum could be decomposed into contributions from different conformers or conformational families separated by mobility. In other words, ion mobility can be used as a conformational filter for spectroscopy.

IMS techniques have been used in conjunction with photoelectron spectroscopy in the past.<sup>33-35</sup> Part of the work done during this thesis was to determine whether ion mobility can be used in conjunction with photofragment spectroscopy of ions cooled in a radio-frequency ion trap. The feasibility of the marriage of these two techniques is in question because the separation of conformers takes place typically at room temperature and then the selected conformation cools down to the temperature of the trap. If during the cooling process there is conformational redistribution, there will be no gain from the separation step and the UV spectrum will be as congested as without separation. In a first step of investigating the coupling of the two techniques we use high-Field Asymmetric waveform Ion Mobility Spectrometry (FAIMS) in conjunction with cold ion spectroscopy. As described in Chapter 3, FAIMS separates ions based on the difference in their mobility at high and low electric field and *not* on absolute mobilities. Despite some disadvantages of FAIMS over drift tube IMS, it was preferred in these initial studies because it is commercially available as a stand-alone device and it is more easily coupled to our home-built machine.

The ability to separate different conformations of biomolecules before injection into a cold ion trap is not only important for spectroscopic studies, but also for studies of conformational isomerization. While isomerization dynamics can be investigated in mixtures of several

conformers,<sup>36-39</sup> having the ability to physically isolate a single conformer before energizing the molecule (e.g. *via* optical pumping) allows the isomerization products to be detected on a zero background, which greatly enhances the sensitivity of this technique.

In addition to using ion mobility as a conformational filter for cold ion spectroscopy and conformational isomerization studies, one can also exploit the coupling between these two techniques in the inverse sense. Ion mobility separates ions based upon their shape, either by detecting the difference in drift time through a finite pressure of gas, or, in the case of FAIMS, by their difference in mobility at high and low electric field. In either case, one would like to have sufficient resolution to distinguish different conformational sub-families. Because spectra of cold ions are extremely sensitive to the overall conformation, using a spectroscopic probe to detect the ions after separation, either in a conventional drift tube or in a FAIMS device, has the potential to detect and resolve conformer sub-populations that are hiding underneath a broad mobility peak.<sup>40-</sup>

42

## 4.2. Coupling of ion mobility and cold ion spectroscopy

We first describe the general experimental approach of coupling ion mobility and cold ion spectroscopy and explain the type of information that can be obtained. Because this approach should be perfectly applicable for both drift-tube ion mobility spectrometry (IMS) and differential ion mobility (i.e., FAIMS), we describe it here in the general case, where we used the term ion mobility to represent either a drift time in IMS or the compensation voltage in FAIMS.

Consider the relatively simple case in which a biomolecular ion exists in only two stable conformations in the isolated, low temperature environment of a cold ion trap. Each of these conformers will have different electronic spectra, but because the same chromophore is responsible for the absorption of UV radiation the spectra are likely to overlap. This is represented schematically in the top panel of Fig. 4.2. Since we measure electronic spectra by photofragment spectroscopy,<sup>18</sup> we plot the total fragment ion signal as a function of the UV dissociation laser wavenumber. Even with only two stable conformers populated in the ion trap, the presence of just a few low-frequency vibrational progressions for each conformer can lead to a significantly congested spectrum. However, if the two conformers giving rise to this schematic spectrum have different ion mobilities, as illustrated in the middle panel of Fig. 4.2, one can use this difference to filter the conformers before injection into the ion trap, giving rise to simplified spectra (lower panel).



There are several requirements for such a scheme to work as cleanly as is illustrated in Fig. 4.2. First, and most obviously, the better the resolution in the ion mobility spectrum the better one's ability to completely remove a particular conformer before making spectroscopic measurements. As the number of stable conformers present in the gas phase sample increases it will be more difficult to separate them by ion mobility. Nevertheless, even separation into "families" of conformers with similar ion mobility can help simplify spectra.

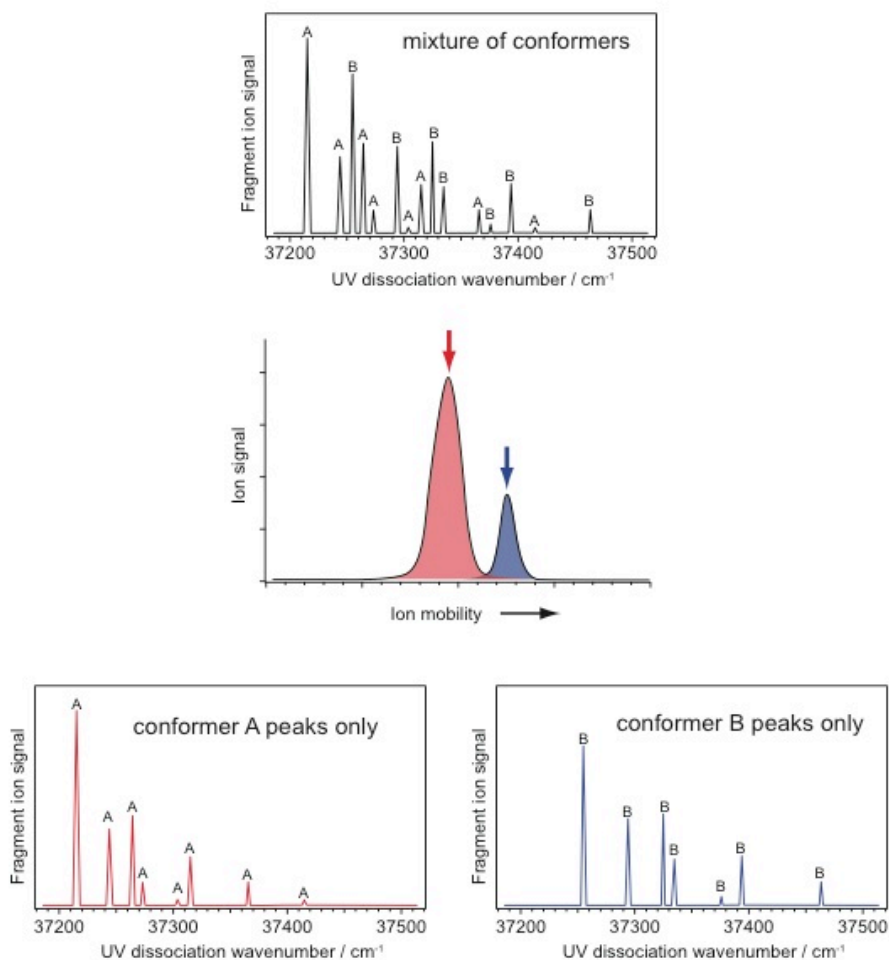


**Figure 4.2.** Schematic figure illustrating the principle of using ion mobility as a conformational filter to simplify a congested electronic spectrum. Top panel: A fabricated electronic spectrum of a small peptide that exhibits features arising from two different stable conformers, A and B. Middle panel: Ion mobility spectrum in which conformers A and B are completely resolved. Bottom panel: (left) Electronic spectrum obtained after filling the cold ion trap with only those ions having a mobility corresponding to the red peak; (right) Electronic spectrum of those ions having a mobility corresponding to the blue peak

In addition to needing sufficient resolution in the ion mobility separation process, it is important that the isolated conformers do not undergo conformational isomerization afterwards, otherwise the advantages gained by the separation will be lost. Since ion mobility is typically

performed at room temperature, the ions have a significant amount of thermal energy during the separation process and can in principle isomerize if the barriers are low. The fact that ion mobility spectra show distinct peaks indicates that there are many instances in which at least certain families of conformations do not isomerize during the separation process. Nevertheless, to be able to use ion mobility as a conformational filter for spectroscopy, one must ensure that isomerization does not occur downstream from the separation process, and this requires paying particular attention to the energies imparted to the ions both during and after separation. In the particular case of FAIMS, subjection of the ions to high electric fields during separation can lead to collisional heating. The energy thus imparted to the ions may cause them to isomerize either in the FAIMS device, in which case they may be filtered out, or after the ions exit the FAIMS electrodes, in which case the conformational selection will be partially scrambled. As will be described below, our data on  $[bk + 2H]^{2+}$  does indeed show evidence of conformational isomerization, and this partially compromises the degree to which we can separate the spectral contributions of different conformational families.

A second reason to couple ion mobility with cold ion spectroscopy is to use the latter as a “high-resolution”, conformationally sensitive detector for the former, either in the case of IMS or in FAIMS. Consider the situation shown schematically in the top panel of Fig. 4.3, in which an ion mobility spectrum exhibits no resolved peaks and is broader than expected given the resolving power of the instrument. Within such a feature, it is likely that there will be conformational sub-populations of molecules that have similar but not identical structure and hence mobility. Rather than detecting the *total* signal after ion mobility separation we can cool the ions in a cold ion trap and detect *only* those that have UV absorption at a particular fixed frequency (middle panel of Fig. 4.3). This would allow us to decompose the mobility peak into the contributions from the different conformational sub-populations (lower panel of Fig. 4.3).

For this approach to work two conditions must be met. First, to get complete separation of the components in the ion mobility spectrum, the features in the electronic spectrum corresponding to the different conformers must be fully resolved and assigned to different conformers, which can be done using hole-burning techniques.<sup>43-45</sup> This becomes increasingly difficult as the number of stable conformations present in the sample increases. However, if one wants simply to detect the presence of different sub-populations within an ion mobility peak, it is not necessary to achieve complete spectral separation of the conformers. In fact, any type of spectroscopic detection that favors one conformer over another would change the shape of the ion mobility spectrum and allow the detection of separate conformer sub-populations. This means that even IRMPD spectroscopy of room temperature samples at relatively low resolution could

potentially be used to detect the presence of different conformational families within an unresolved ion mobility peak.

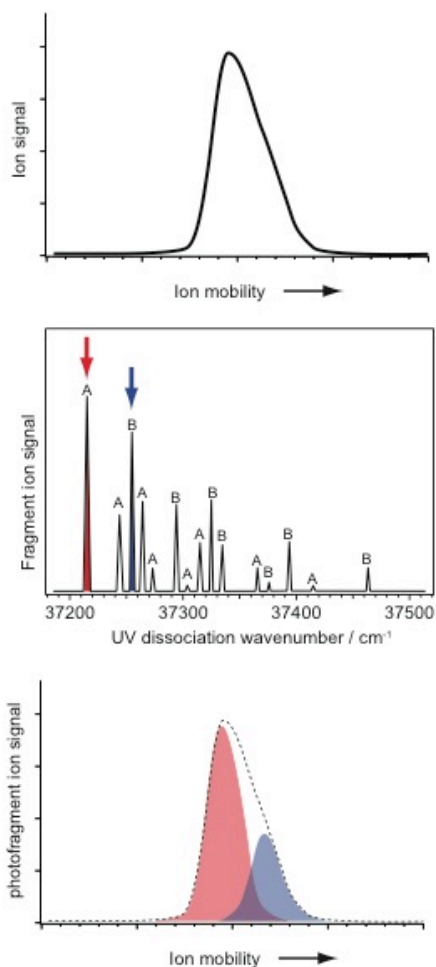


**Figure 4.3.** Schematic figure illustrating the principle of using cold ion spectroscopy as a conformationally sensitive detector for ion mobility. Top panel: A fabricated ion mobility spectrum of a small peptide showing a hint of an unresolved shoulder arising from different conformers or conformational families. Middle panel: Electronic photofragment spectrum of the peptide in a cold ion trap showing two different resolved conformer peaks that can be used to detect the ions after ion mobility separation. Bottom panel: Ion mobility spectrum of the peptide detected after cooling the sample in the ion trap and photodissociating conformer A (red) or conformer B (blue) *via* the bands in the UV spectrum indicated in the middle panel. The total ion mobility signal is indicated in the bottom panel as a dashed line.

The second requirement for this approach to work is that the different conformers not undergo conformational isomerization after ion mobility separation (in the same way as described above). If one is simply trying to detect the presence of different sub-populations within an ion mobility peak and not necessarily separate them, some degree of isomerization would be tolerable. However to separate the contributions from different conformer sub-populations completely, one

would have to avoid all downstream isomerization due to the internal energy already in the molecule or imparted to the molecule when it is stopped by collisions in the cold ion trap.

### 4.3. Bradykinin and its structure in the gas phase

Bradykinin is a nona-peptide with the sequence Arg-Pro-Pro-Gly-Phe-Ser-Pro-Phe-Arg.<sup>46</sup> It is a member of the kinins, a family of vasoactive peptides with a very diverse physiological activity.<sup>47</sup> Bradykinin has been extensively investigated because of its antithrombogenic and antihypertensive effects.<sup>47</sup> On the other hand, it can cause inflammations like allergic rhinitis and asthma and symptoms like swelling and pain.<sup>48</sup> It is believed that a central part of its biologic activity is associated with a  $\beta$ -turn adopted by the Ser-Pro-Phe-Arg residues of the C-terminus,<sup>49</sup> which is stabilized in many different solution environments.<sup>50</sup> The Arg-Pro-Pro-Gly-Phe sequence at the N-terminus seems to be unstructured and it can lead to a large number of conformational preferences.<sup>51,52</sup>

Bradykinin contains 2 basic residues (2 arginines) plus the N-terminal amino group that can be protonated, but also the carboxylic group at the C-terminus that can be deprotonated. It has long served as a model peptide in mass spectrometry and ion mobility. Selected charge states of bradykinin have been investigated by several methods like collision-induced dissociation (CID) in a Fourier transform Ion Cyclotron Resonance (FT-ICR) mass spectrometer,<sup>53</sup> H/D exchange,<sup>54,55</sup> Blackbody Infrared Radiative Dissociation (BIRD),<sup>56,57</sup> reactions with hydroiodic acid in an ion trap,<sup>58</sup> ion mobility spectrometry (IMS),<sup>51,59-64</sup> and Field Asymmetric-waveform Ion Mobility Spectrometry (FAIMS).<sup>65-70</sup>

Using matrix-assisted laser desorption ionization (MALDI) in conjunction with IMS, Bowers and coworkers investigated bradykinin (bk) in its singly charged  $[\text{bk} + \text{H}]^+$ , sodiated  $[\text{bk} + \text{Na}]^+$  and doubly sodiated  $[\text{bk} - \text{H} + 2\text{Na}]^+$  forms.<sup>59</sup> They found that the three different forms exhibit similar cross-sections that were invariable with a change in temperature from 80 to 600 K, while the arrival time distributions were slightly broader than those calculated for simple structures. They explained their results by the presence of a few conformers with very similar cross-sections that at high temperature interconvert rapidly. Bradykinin in its singly protonated state can have either one of the arginines protonated or be a zwitterion where the two arginines are protonated while the C-terminus deprotonated. Extensive calculations by Wytttenbach *et. al.* showed that the most stable structures of all three isomers of  $[\text{bk} + \text{H}]^+$  have very similar cross-

section and the experiment cannot distinguish between them.<sup>59</sup> However, BIRD studies<sup>56</sup> and predictions from theoretical calculations<sup>71</sup> consent to singly protonated bradykinin being a zwitterion in the gas phase.

While at the time only one feature was shown in the arrival time distribution of  $[\text{bk} + 2\text{H}]^{2+}$ ,<sup>60,62</sup> reactions with hydroiodic acid suggested at least two stable conformations for this protonation state.<sup>58</sup> This was also proposed by FAIMS studies in which a device of “dome” geometry was used.<sup>65</sup> In addition, when FAIMS was combined with H/D exchange four conformers were revealed.<sup>65</sup> Shvartsburg *et. al.* constructed high-resolution planar FAIMS devices and identified six conformers of  $[\text{bk} + 2\text{H}]^{2+}$ , some of them being products of extensive isomerization.<sup>66-68</sup> Recently, the construction of higher resolution drift tube IMS mass spectrometers also revealed the presence of two conformations for  $[\text{bk} + 2\text{H}]^{2+}$ , with very similar cross-sections.<sup>63,72</sup> Doubly protonated bradykinin can also exist in two forms, one non-zwitterionic where the two arginines are protonated and one zwitterionic where the two arginines plus the N-terminus are protonated while the C-terminus is deprotonated.<sup>64</sup> However, recent theoretical calculations by Siu and coworkers predict that doubly charged bradykinin exist as a zwitterion in the gas phase.<sup>71,73</sup> Yet,  $[\text{bk} + 2\text{H}]^{2+}$  shows a plethora of conformations in the gas phase, the exact nature of which is not clear.<sup>74</sup>

Theoretical calculations of  $[\text{bk} + 3\text{H}]^{3+}$  showed that the most stable structures are non-zwitterionic, with the two arginines and the N-terminal amino group protonated.<sup>71</sup> Early IMS studies showed one feature in the arrival time distribution of  $[\text{bk} + 3\text{H}]^{3+}$  exhibiting a cross section ~20% larger than  $[\text{bk} + 2\text{H}]^{2+}$ .<sup>60</sup> Higher resolution measurements revealed the presence of three conformations.<sup>72,75</sup> In two-dimensional IMS, Pierson *et. al.* identified at least six stable structures.<sup>63</sup> Moreover, the number of features in the arrival time distribution was found to depend on the solution used to generate gas phase ions of  $[\text{bk} + 3\text{H}]^{3+}$ , exhibiting as many as eight structures co-existing in certain cases, indicating the conformational heterogeneity of this peptide.<sup>51</sup>

To demonstrate the feasibility of coupling FAIMS with cold-ion spectroscopy we have chosen to investigate the doubly protonated form of the peptide bradykinin (bk). From a spectroscopic perspective, the electronic spectrum of bradykinin exhibits an extensive degree of conformational heterogeneity, providing a challenge for spectral decomposition techniques. On the other hand, as mentioned above, FAIMS can readily separate conformations of  $[\text{bk} + 2\text{H}]^{2+}$ . Doubly-protonated bradykinin thus provides an ideal testing ground for the coupling of differential ion mobility with cold ion spectroscopy.

## 4.4. Experimental details

To demonstrate the principles described above for coupling FAIMS and cold ion spectroscopy, we have incorporated a “side-to-side” cylindrical FAIMS device (Thermo Fisher Scientific) into our cold-ion photofragment tandem mass spectrometer.<sup>76,77</sup> Doubly protonated bradykinin ions are produced by ESI of a 20  $\mu\text{M}$  solution in 49.5:49.5:1 (% volume) water:methanol:acetic acid. For the investigation of the transmission through FAIMS and the optimization of its separation capabilities, a number of FAIMS parameters are varied and tuned like the temperature of the electrodes, the flow of the carrier gas and its composition. CV spectra are recorded as a function of the above parameters. Ions that are transmitted through FAIMS are mass-selected, trapped and counted. The CV is varied slowly during a CV scan (3-5 Volts/min). The UV laser is operated at a frequency of 10Hz and its energy is kept at  $\sim 1.5$  mJ/pulse. We increase the fragmentation yield after UV excitation by irradiation with a CO<sub>2</sub> laser.<sup>78,79</sup> The CO<sub>2</sub> laser is operated at 10Hz and is tuned at the 9P20 rovibrational line of CO<sub>2</sub> molecules. The pulse of the CO<sub>2</sub> laser is delayed 150ns after the UV pulse. The only laser-induced fragment ions observed are those resulting from the loss of neutral phenylalanine side-chain. Electronic spectra are recorded by measuring the number of fragment ions as a function of the UV laser frequency. CV spectra are recorded by measuring the number of trapped parent ions (without the use of lasers) or fragment ions (when combined with spectroscopy) as a function of the compensation voltage. Electronic spectra are normalized by the number of parent ions and the UV laser power.

## 4.5. Bradykinin in “side-to-side” FAIMS

The first step in these studies is to optimize the transmission of  $[\text{bk} + 2\text{H}]^{2+}$  through the FAIMS electrodes and to investigate the separation capabilities of our device. Figure 4.4 shows compensation voltage (CV) spectra of  $[\text{bk} + 2\text{H}]^{2+}$  recorded as a function of the dispersion voltage (DV) of the waveform that is applied between the FAIMS electrodes. The carrier gas is 100% N<sub>2</sub> and the electrodes are kept at room temperature. At -2500 V (Fig. 4.4, black trace) the CV spectrum shows one broad peak with maximum at  $\sim -2$  V. This non-zero value of CV is a consequence of the change in the mobility of  $[\text{bk} + 2\text{H}]^{2+}$  ions at high electric field,  $K_h$ , compared to its value at low electric field,  $K$ . This translates to a net drift of the ions towards one of the electrodes, and a negative CV value needs to be applied for the ions to be transmitted. For values

of CV lower than -5 V or higher than +1 V, the ions are forced to the electrodes and no transmission is observed. As the DV is increased, the peak maximum appears at more negative CV values, a result of a further increase in the deviation of  $K_h$  from  $K$ . Moreover, the sensitivity is increased (from  $\sim 2000$  counts at -2500 V to  $\sim 3250$  counts at -5000 V) but also the peak becomes wider. These are the results of atmospheric pressure ion focusing in cylindrical FAIMS devices.<sup>80,81</sup>

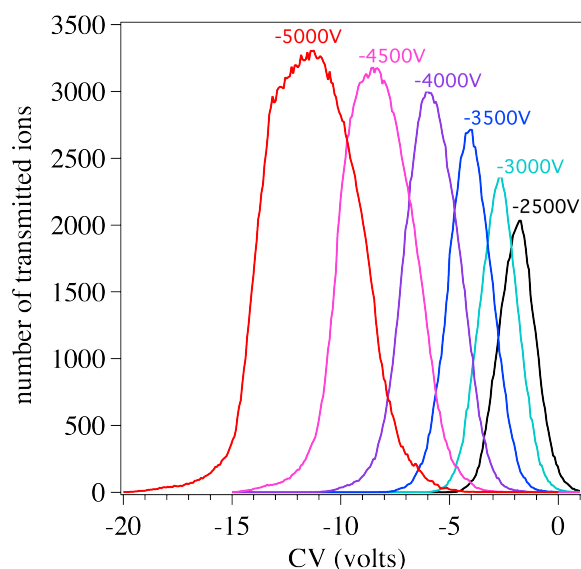


**Figure 4.4.** CV spectra of  $[bk + 2H]^{2+}$  as a function of the DV voltage. The spectra are recorded at DV values between -2500 V and -5000 V with intervals of 500 V.

To explain focusing in FAIMS better, we use the data of Fig. 4.4 to construct a CV/DV<sup>81</sup> plot shown in Fig. 4.5a. This plot shows the optimal combinations of CV and DV for which the  $[bk + 2H]^{2+}$  ions experience no net motion from the application of the asymmetric waveform. In order to construct the (CV, DV) pairs for balancing conditions from Fig. 4.4, for a given DV we choose the CV for which transmission is maximized. Consider first a situation in which the separation of  $[bk + 2H]^{2+}$  ions is done using a flat-electrode FAIMS, where the electric field is uniform in the analytical gap. In this case, only if the correct CV is applied (for a given DV) the ion will balance and not migrate towards one of the electrodes. These are the (CV, DV) combinations that fall on the curve of Fig. 4.5a. For example, for DV = -4000 V, if CV = -5.9 V the ions will balance between the electrodes (circled trace in Fig. 4.5a). For more negative CV values (below the circled trace of Fig. 4.5a), the  $[bk + 2H]^{2+}$  ions are attracted towards the electrode that carries the CV/DV, while for less negative values (above the circled trace of Fig. 4.5a), the  $[bk + 2H]^{2+}$  ions are moving towards the grounded electrode. Because the ions

migrate towards the electrodes even for very small deviations from  $CV = -5.9$  V, very narrow peaks can be observed for sufficient separation time.

The situation is different in the case of our cylindrical FAIMS device, where the application of the CV and DV voltages establish an inhomogeneous field across the analytical gap. The compensation (CF) and dispersion fields (DF) (established by the CV and DV, respectively) can be calculated as a function of the distance from the center of the device ( $r$ ) using equation 3.12 for inner and outer electrodes radii of 6.5 mm and 9 mm, respectively. The black curve of Fig. 4.5b shows the balancing conditions for the calculated CF and DF, assuming that the optimal transmission conditions occur at the gap median ( $r = 7.7$  mm). For example for  $DV = -4000$  V and  $CV = -5.9$  V, the fields at the gap median is  $DF = -15950$  V/cm and  $CF = -23.5$  V/cm (circled trace in Fig. 4.5b). For the same values of DV and CV, the “actual” DF and CF across the gap can also be calculated using equation (3.12) as a function of  $r$ . For example at  $r = 6.5$  mm (at the inner electrode),  $DF = -18895$  V/cm and  $CF = -27.9$  V/cm and at  $r = 9$  mm (at the outer electrode),  $DF = -13647$  V/cm and  $CF = -20.1$  V/cm. The “actual” DF ( $r$ ) and CF ( $r$ ) are plotted against each other forming the red trace (ii) superimposed on the black curve of Fig. 4.5b. Now suppose that for the above CV and DV conditions a  $[bk + 2H]^{2+}$  ion is close to the inner electrode ( $r \approx 6.5$  mm). As shown by the rightmost marker of trace (ii) the “actual” (DF, CF) at this  $r$  is (-18895 V/cm, -27.9 V/cm). However, at this DF, the CF needed to balance the ion is -39.5 V/cm, more negative than the “actual” CF at this point. This makes the ion move away from the inner electrode and toward the gap median. Respectively, an ion close to the outer electrode ( $r \approx 9$  mm) experiences actual (DF, CF) values of (-13647 V/cm, -20.1 V/cm) while at this DF the CF that would balance the ion is -16 V/cm. As a result the ion moves away from the outer electrode and towards the gap median. Thus, in FAIMS of cylindrical geometry ions that are spread across  $r$  focus toward the gap median, increasing the transmission efficiency.

Figure 4.5b also shows the “actual” fields across the gap at  $DV = -3000$  V and  $CV = -2.8$  V (trace (i)) superimposed on the curve of the “balanced” fields. The vertical distance between the red and black curves of Fig. 4.5b is the difference between the actual and the balanced fields at a specific radius in the analytical gap, and gives the strength of ion focusing. This is stronger for a larger value of applied DV, as can be seen by comparison of the vertical distances of traces (i) and (ii) from the balanced curve. This explains the increased sensitivity as the DV is increased. Moreover, a CV scan corresponds to the vertical movement of the red traces from the top of Fig. 4.5b downwards. Intersection between the red and black traces permits stable trajectories in the analytical gap. As can be seen by comparison of traces (i) and (ii), the CF range of stable trajectories is larger in the latter case, where the DF is stronger. Thus, there is an expansion of the



CV values that lead to stable trajectories in the gap at high DVs. This explains the larger width of the peaks in the CV spectra of  $[bk + 2H]^{2+}$  as the DV is increased.

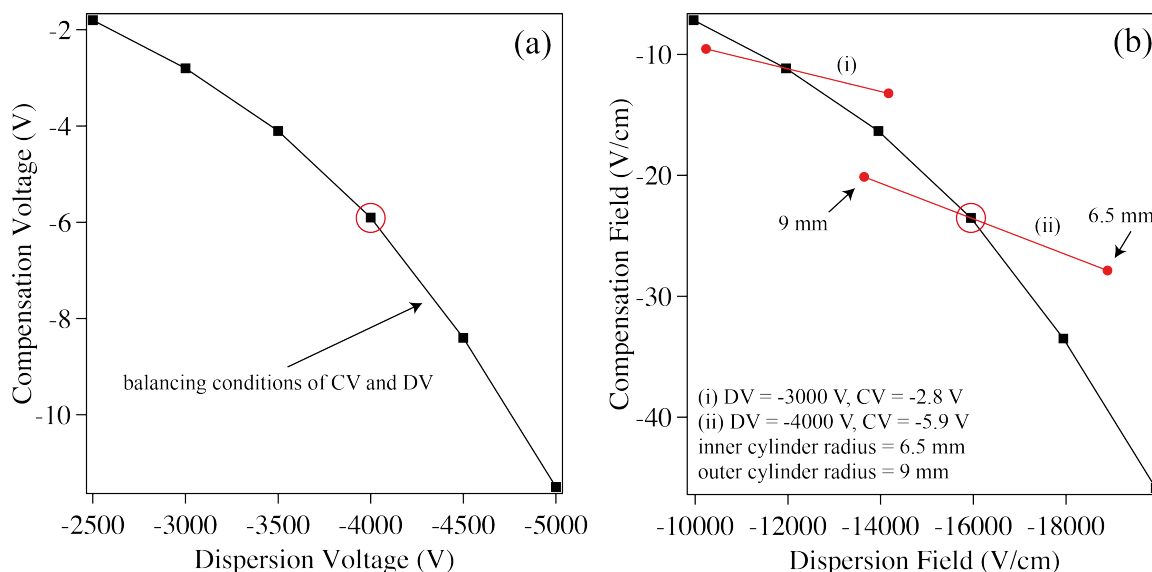


**Figure 4.5.** (a) CV/DV and (b) CF/DF plot that shows conditions of balance for the  $[bk + 2H]^{2+}$  ions, determined experimentally; the red traces of (b) are calculated electric fields across the analytical gap for  $9 \text{ mm} < r < 6.5 \text{ mm}$  and (i) DV = -3000 V and CV = -2.8 V and (ii) DV = -4000 V and CV = -5.9 V,.

Although the inhomogeneity of the field increases the width of the peaks of Fig. 4.4 at higher DVs, a second reason may contribute to that. This is the presence of several different isomers of  $[bk + 2H]^{2+}$  that only at higher DV values begin to separate, owing to their different deviations of  $K_h$  from  $K$ . The asymmetry of the peak in the CV spectrum recorded at -5000V (Fig. 4.4, light blue trace) might be an indication of this.

As explained in a Chapter 3, establishing a temperature gradient across the analytical gap in FAIMS of cylindrical geometry gives us the ability to tune the resolution/sensitivity balance. In this version of FAIMS, the asymmetric waveform is applied on the inner electrode. The electric field that is established across the gap is inhomogeneous, with higher values closer to the inner electrode. Thus, the  $E/N$  ratio decreases with increased distance from the inner electrode, and as a result ions are focused in the gap median.<sup>81</sup> Application of a temperature gradient creates a density gradient that changes  $N$  in the denominator of  $E/N$  so that focusing becomes stronger or weaker, depending on the direction of the gradient. Figure 4.6a shows CV spectra recorded as a function of the temperature difference between the inner and the outer electrode of FAIMS. The outer electrode is kept at 30 °C while the temperature of the inner electrode is increased. In this case, stronger focusing is observed for larger difference between the temperatures of the

electrodes. Figure 4.6a shows all the characteristics of increasing the focusing: peaks become more intense and wider.

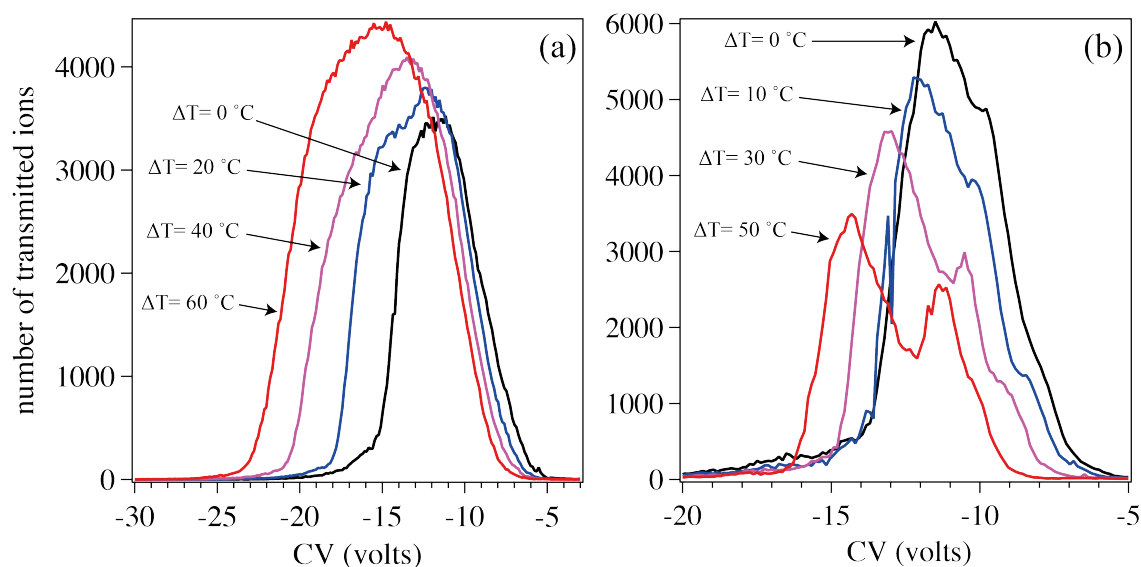


**Figure 4.6.** CV spectra of  $[bk + 2H]^{2+}$  recorded at different temperature gradients across the gap; (a) the temperature of the outer electrode is kept at 30 °C, while this of the inner electrode is 30, 50, 70 and 90 °C, for the black, blue, violet and red traces, respectively; (b) the temperature of the inner electrode is kept at 30 °C, while this of the outer electrode is 30, 40, 60 and 80 °C, for the black, blue, violet and red traces, respectively.

If the temperature varies the other way around, increasing from the outer to the inner electrode, then the opposite effect should be observed: the resolution should increase but at the expense of sensitivity. In this case, the temperature gradient should act against ion focusing, effectively offsetting the curvature. Figure 4.6b shows CV spectra recorded as a function of increased temperature difference between the inner and the outer electrode, with the inner electrode kept at 30 °C while the temperature of the outer electrode is increased. By inspection of the spectra shown in Fig. 4.6b, two things are apparent. The first is that the overall signal decreases as the temperature difference is increased. Second, and most strikingly, is that the CV spectrum gradually changes shape as the magnitude of the gradient is increased. The broad peak with the shoulder in the spectrum acquired with no temperature gradient (black trace, Fig. 4.6b) evolves into two partially resolved peaks at  $\Delta T = 50$  °C (violet spectrum, Fig. 4.6b). This spectrum is similar to the CV spectrum originally obtained by Guevremont *et. al.* using a “dome” FAIMS geometry.<sup>65</sup> In that work they performed H/D exchange on ions transmitted at different values of the compensation voltage. Since the deuteration pattern of the ions measured after FAIMS separation depended upon the CV, they concluded that the features in the spectrum

correspond to different conformations of the molecule. We note that while FAIMS<sup>65</sup> as well as kinetic studies of gas phase reactions of  $[\text{bk}+2\text{H}]^{2+}$  with hydroiodic acid<sup>58</sup> indicated the existence of at least two conformations of  $[\text{bk}+2\text{H}]^{2+}$ , gas-phase conformers of this ion were until recently unresolved with IMS.<sup>60</sup> However, with the construction of higher resolution ion mobility spectrometers it has become possible to partially resolve these two features in the drift time spectrum.<sup>63,72</sup> On the basis of this comparison, which we later confirm spectroscopically, we attribute the two peaks in the violet trace of Fig. 4.6b to two different conformational families of gas-phase  $[\text{bk} + 2\text{H}]^{2+}$ . We emphasize that these are conformational *families* since multiple conformations might be hidden within these features. The smaller shoulder on the higher CV side of the distributions of Fig. 4.6b is analyzed in Fig. 4.8.

Both of the black traces of Figs. 4.6a and 4.6b are recorded with no temperature gradient across the gap. However, the second displays a shoulder at higher CV values. We attribute this difference to the slightly different conditions used in obtaining these spectra. The composition of the carrier gas in the former case was 100% N<sub>2</sub>, while in the latter case it was a mixture of N<sub>2</sub> with 10% He. The inclusion of helium increases the resolution so that the shoulder is revealed.<sup>70</sup> Figure 4.7a shows the effect of the He content of the carrier gas on the CV spectrum. The temperature of the inner electrode is 30 °C while this of the outer 95 °C. From comparison of the traces of Fig. 4.7a it is evident that the whole distribution shifts to lower values of CV as the He percentage is increased. This is attributed to non-blanc behavior that can raise absolute CV values, consistent to previous studies where the He content is varied.<sup>67,82</sup> Moreover, the two partially resolved peaks move further apart, a consequence of the conformer dependent change of the  $K(E)$  profile.<sup>67,83</sup> Also, the overall transmission decreases with increased He content, as has been observed before.<sup>67</sup> The relative intensities of the two peaks also change with He content. These reflect the populations of the different conformers present in the gas phase sample. This change may be a consequence of conformational isomerization during the separation process, which becomes stronger at higher He content.<sup>70,84</sup>

The effect of the flow of the carrier gas on the CV spectrum is shown in Fig. 4.7b. The content of the He in the carrier gas is 25%, while the temperature difference between the electrodes is 65 °C. The gas flow defines the residence time of the ions between the electrodes and thus the duration of the separation. As the gas flow is decreased, the resolution becomes better, as is seen from the better separation of the two species in Fig. 4.7b. However, the signal decreases dramatically because the increased separation time leads to larger ion losses. The change in the relative abundances of the conformers may be attributed to heating during the separation that causes isomerization. For a longer the residence time (longer heating), the

conformers may undergo structural change and thus the CV value at which they are transmitted can change. Thus the ions may be eliminated from the analytical gap. The thresholds for this process may be different for the different conformers so that disproportional elimination of ions changes the relative intensities of the peaks.<sup>69</sup>

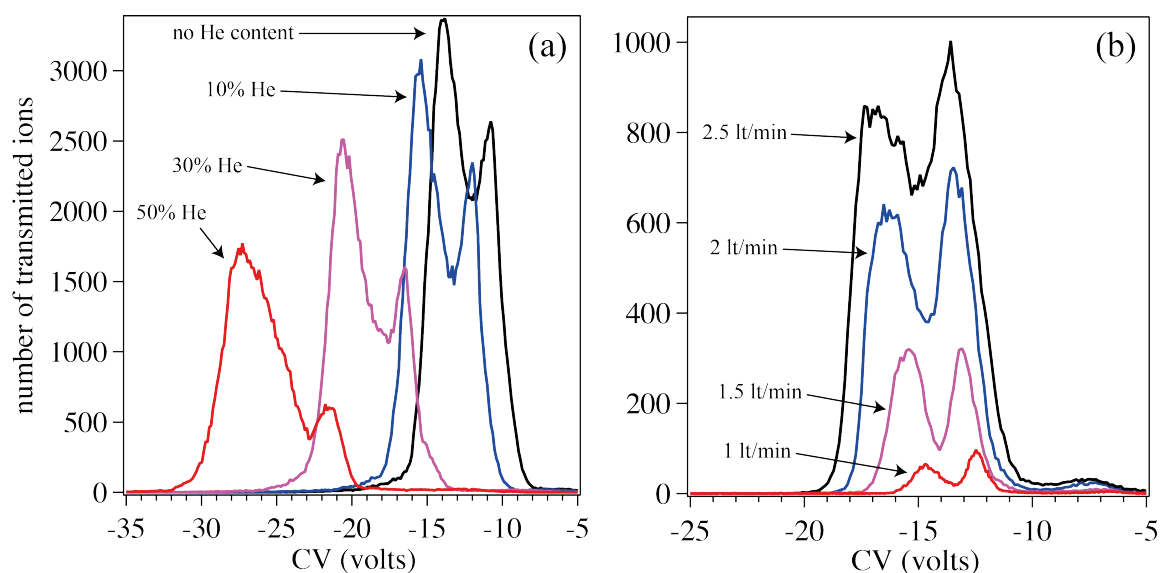


**Figure 4.7.** CV spectra of  $[bk + 2H]^{2+}$  recorded: (a) as a function of the He content of the carrier gas; (b) as a function of the carrier gas flow.

Another phenomenon that is observed by inspection of the traces of Fig. 4.7b is that the whole distribution moves slightly to higher values of CV as the carrier gas flow is decreased. The control that we have over the gas flow (in lt/min) concerns the total flow through a line that provides the gas for desolvation but also the gas that carries ions through the FAIMS electrodes. Most of the carrier gas is used for the first purpose.<sup>76</sup> On the other hand, the conductance of the capillary of our mass spectrometer is  $\sim 1$  lt/min. It seems that, as we decrease the gas flow, the mass spectrometer compensates for the missing gas by pumping it from the atmosphere, which is rich in  $N_2$ . As a result, the He content in the carrier gas decreases with decreased flow, and the features move to slightly higher values of CV.

In addition to the two partially resolved peaks, the spectra of Fig. 4.7b exhibit a third feature at  $CV \sim -7$  volts. The appearance of this feature depends strongly on the spray conditions. We attribute this to chemical noise that is produced from the electrospray ionization that is transmitted at this CV when detecting mass/charge of 531 ( $m/z$  of  $[bk + 2H]^{2+}$  is 531). The red trace of Fig. 4.8 is a CV spectrum recorded from a blank sample while detecting  $m/z$  531 in the mass spectrometer. For comparison, a CV spectrum of doubly protonated bradykinin is included (black trace, Fig 4.8). We thus assign the peak at -7 volts to chemical noise.

The blue trace of Fig. 4.8 is a CV spectrum recorded from a solution of bradykinin, but in this case the triply protonated form of this molecule ( $[\text{bk} + 3\text{H}]^{3+}$ ,  $m/z$  354.3) is detected in the mass spectrometer. The spectrum shows one peak at  $\text{CV} = -13.7$  V, exactly at the same position where a shoulder appears in the black trace, acquired when detecting  $[\text{bk} + 2\text{H}]^{2+}$  with  $m/z$  531. This feature also appears as a shoulder in the spectra of Fig. 4.6b and it depends strongly on the spray conditions. We attribute the shoulder of the black trace of Fig. 4.8 to  $[\text{bk} + 3\text{H}]^{3+}$  that is transmitted at this CV but gets charged reduced *via* proton stripping in the analytical gap and is detected as  $[\text{bk} + 2\text{H}]^{2+}$ ,<sup>85</sup> in agreement with other published results on the same system.<sup>70</sup>

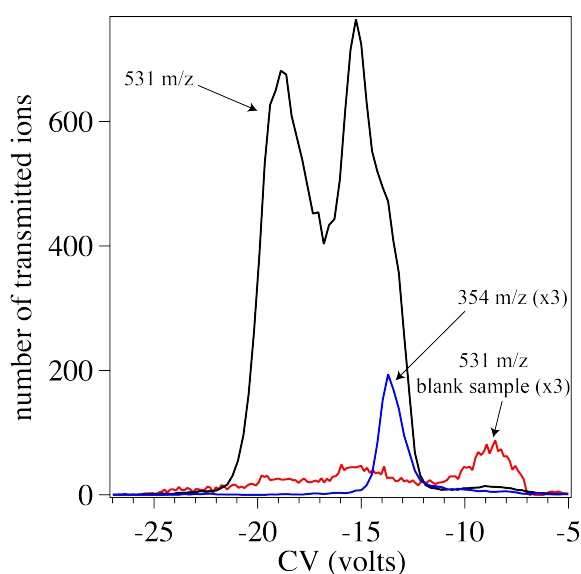


**Figure 4.8.** CV spectra recorded while monitoring  $m/z$  531 ( $[\text{bk} + 2\text{H}]^{2+}$ ),  $m/z$  354 ( $[\text{bk} + 3\text{H}]^{3+}$ ) from electrospaying solution of bradykinin, in the black and blue traces respectively. The red trace is a CV spectrum recorded by electrospaying a blank solution.

Having examined the effect of various FAIMS parameters in the separation of the device, we now show our use of FAIMS as a conformational filter for cold ion spectroscopy.

## 4.6. FAIMS as a conformational filter for cold ion spectroscopy

Figure 4.9 compares electronic photofragment spectra of  $[\text{bk} + 2\text{H}]^{2+}$  (Fig 4.9b, black trace) and  $\text{Ac-Phe-(Ala)}_5\text{Lys-H}^+$  (Fig 4.9a, red trace), at the origin of the electronic band. The spectrum of  $\text{Ac-Phe-(Ala)}_5\text{Lys-H}^+$  shows a number of sharp bands across  $100\text{ cm}^{-1}$ . Stearns *et. al.* used IR-

UV double resonance spectroscopy and identified four stable conformations giving rise to the transitions of the red spectrum.<sup>23</sup> On the other hand, the spectrum of  $[\text{bk} + 2\text{H}]^{2+}$  appears highly congested over a larger wavenumber region. It exhibits a large number of sharp features with a number of them resting on a broad band. Svendsen *et. al.* employed double resonance spectroscopy to show that there are at least five stable conformations of  $[\text{bk} + 2\text{H}]^{2+}$  contributing to the black spectrum.<sup>74</sup> This shows a high degree of conformational heterogeneity and we attribute the spectral congestion in the spectrum of Fig. 4.9b to the large number of conformations of  $[\text{bk} + 2\text{H}]^{2+}$  ions that are stable at the temperature of our trap.

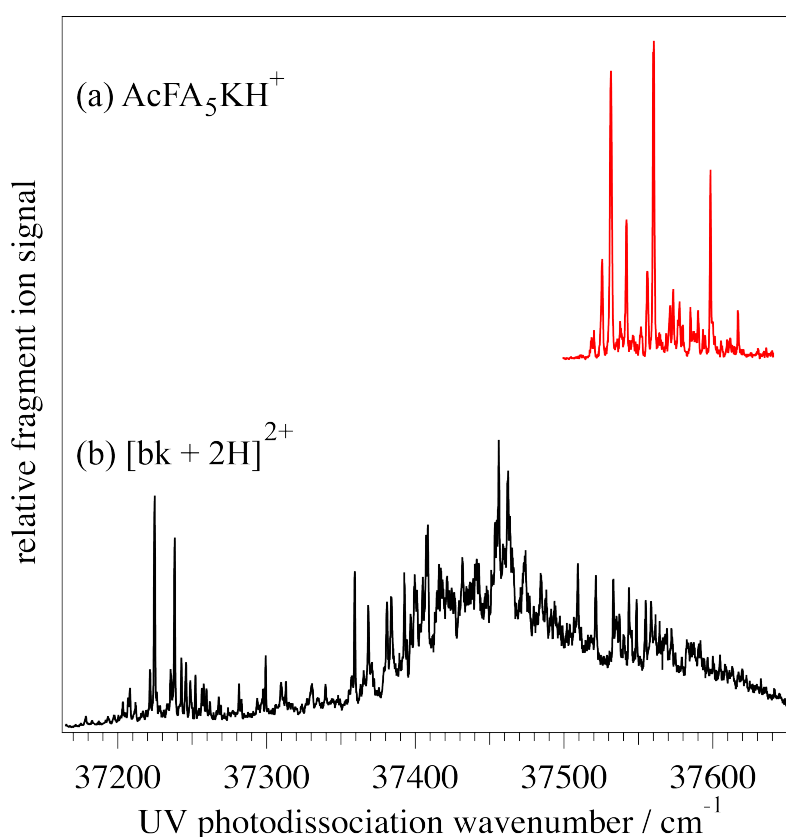


**Figure 4.9.** Electronic photofragment excitation spectrum of (a)  $\text{AcFA}_5\text{KH}^+$ ; and (b)  $[\text{bk} + 2\text{H}]^{2+}$ .

To investigate if we can simplify the congested spectrum of  $[\text{bk} + 2\text{H}]^{2+}$  by separating them into conformational families, we pass the electrosprayed ions through the FAIMS electrodes prior to their laser interrogation. We adopt those parameters in the FAIMS device for which the two conformational families are well resolved while the amount of the transmitted ions allows us to perform photofragment spectroscopy. The temperature of the inner electrode is held at 30 °C while of the outer at 85 °C, establishing thus a gradient of  $\Delta T=55$  °C. The carrier gas contains 90%  $\text{N}_2$  and 10% He and is provided at a flow of 1.9 lt/min. The DV used is -4600 V. Figure

4.10 shows the CV spectrum of  $[\text{bk} + 2\text{H}]^{2+}$  recorded with the above parameters. We refer to the peak transmitted at -13.3 V as conformer family A and that at -10.4 V conformer family B.

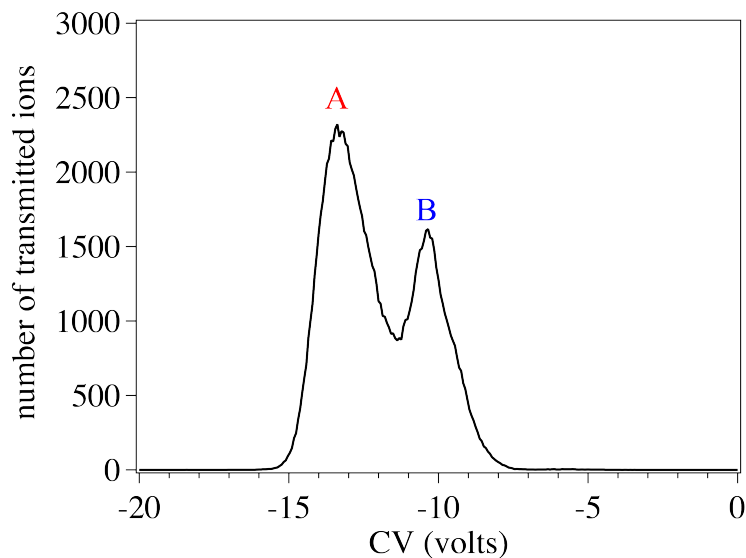


**Figure 4.10.** CV spectrum of  $[\text{bk} + 2\text{H}]^{2+}$ . The temperature of the inner electrode is kept at 30 °C, while this of the outer electrode at 85 °C.

Having shown that we can at least partially separate  $[\text{bk} + 2\text{H}]^{2+}$  conformers in our FAIMS device, we now proceed to demonstrate the ability to reduce conformational heterogeneity in the electronic spectrum by filtering out certain conformational families before injecting them into our cold ion trap. Figure 4.11 displays the ultraviolet photofragment spectrum of cold, doubly protonated bradykinin. In Fig. 4.11a we show the spectrum obtained without FAIMS separation for comparison. The traces in figures 4.11b and 4.11c have been recorded with FAIMS separation using CV values of -10.4 V and -13.3 V respectively, such that only one of the conformational families are transmitted into the mass spectrometer and injected into the cold trap.

Several things become apparent upon comparison of the spectra. First, the electronic spectra obtained for the different CV values are clearly different. Some peaks in the spectrum of Fig. 4.11b appear to be completely absent from the spectrum of Fig. 4.11c and vice versa. The expanded view of a portion of these spectra shown in Fig. 4.12 demonstrates this more clearly. This can occur only if the FAIMS process has separated the stream of  $[\text{bk} + 2\text{H}]^{2+}$  ions from the electrospray source into conformational families (A or B) that are selectively transmitted to the cold ion trap for spectroscopic interrogation. The spectrum shown in Fig. 4.11a appears to be a weighted composite of those in Figs. 4.11b and 4.11c, with no peaks in the former that do not appear in the latter two. This implies that all populated conformations ultimately get transmitted at a CV value of either -13.3 V or -10.4 V. While using our FAIMS device only two peaks are

observed, higher resolution FAIMS studies of  $[\text{bk} + 2\text{H}]^{2+}$  exhibit a greater number of features,<sup>66</sup> consistent with the IR-UV double resonance studies of Svendsen *et. al.*<sup>74</sup> This confirms that within the peaks in the CV spectrum of Fig. 4.10 there is indeed a distribution of conformers.

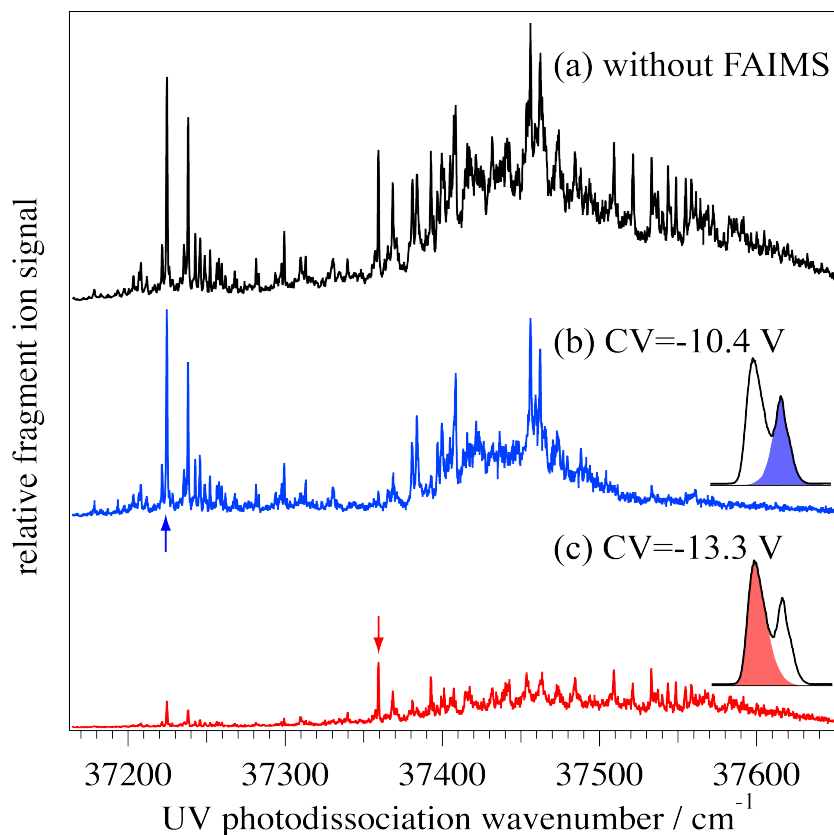


**Figure 4.11.** Electronic photofragment excitation spectrum of  $[\text{bk} + 2\text{H}]^{2+}$  obtained (a) without FAIMS separation; (b) with FAIMS separation transmitting ions at CV=-10.4 V; and (c) with FAIMS separation transmitting ions at CV=-13.3 V. The red and blue arrows are explained in the caption of Fig. 4.14.

On the other hand, there are some common features in the spectra of Fig. 4.11b and Fig. 4.11c. Figure 4.13 shows an expanded view of the electronic spectra of Figs. 4.11b and 4.11c in the lower frequency region. Here one can see that all the peaks appearing in the spectrum of Fig. 4.11b also appear in 4.11c but with much lower intensity. As mentioned in section 4.2, this cross-conformer contamination can be the result of two phenomena. First, of the low resolution in the separation step, with the two species only partially separated, as is the case here. When the CV is set to a value corresponding to a peak, most of the ions that are transmitted belong to the species that give rise to this peak. However, the tail of the nearby feature in the CV spectrum, which belong to another species, may reach as far as the CV value that is currently probed, unavoidably leading to the introduction of the both species into the mass spectrometer and their appearance in



the electronic spectrum. Second, this contamination can be the result of conformational isomerization, which is described in more detail below.

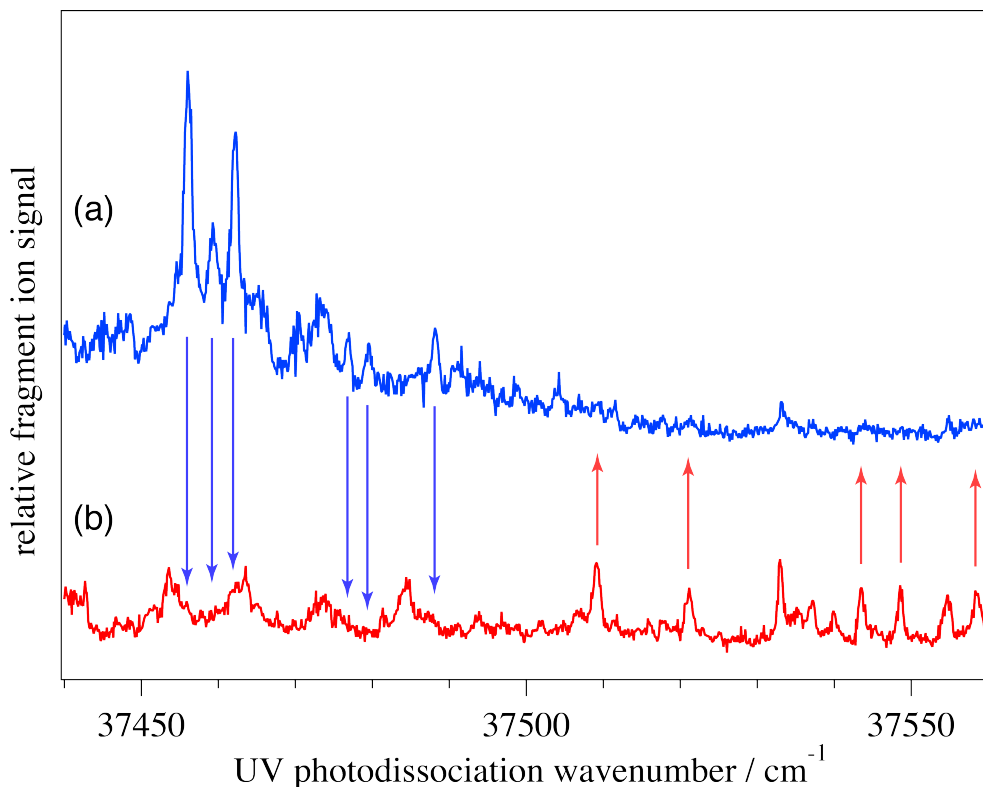


**Figure 4.12.** A portion of the electronic photofragment excitation spectra of Fig. 4.11 shown at higher resolution with (a)  $CV=-13.3$  V; (b) at  $CV=-10.4$  V. The blue downward pointing arrows indicate some of the peaks that appear prominently in the upper spectrum but absent in the lower, while the red upward pointing arrows show some of those appearing only in the lower spectrum.

In the process of separation by FAIMS, the parent ions will be heated by collisions with the bath gas during the high voltage portion of the asymmetric waveform.<sup>83,86</sup> In addition to this field-driven heating of the ions, in the case of our cylindrical FAIMS we explicitly heat the two electrodes to maintain a density gradient in the carrier gas, and this will heat the ions as well. Both types of heating can lead to conformational isomerization. If isomerization of the ion being transmitted at a particular CV occurs within the FAIMS region and the new conformer has a sufficiently different CV, the isomerization products (i.e., new conformation(s)) should be filtered out, unless isomerization occurs just before exiting. However, if isomerization is slow compared to the residence time between the FAIMS electrodes, some ions will be energized in this region but then isomerize downstream. Since these will not be filtered out they will appear in the cold ion spectrum. In addition, after exiting FAIMS ions may be energized internally by collisions in

the hexapole ion trap or upon injection into the cold ion trap, and this can also induce isomerization, partially scrambling the conformer distribution.

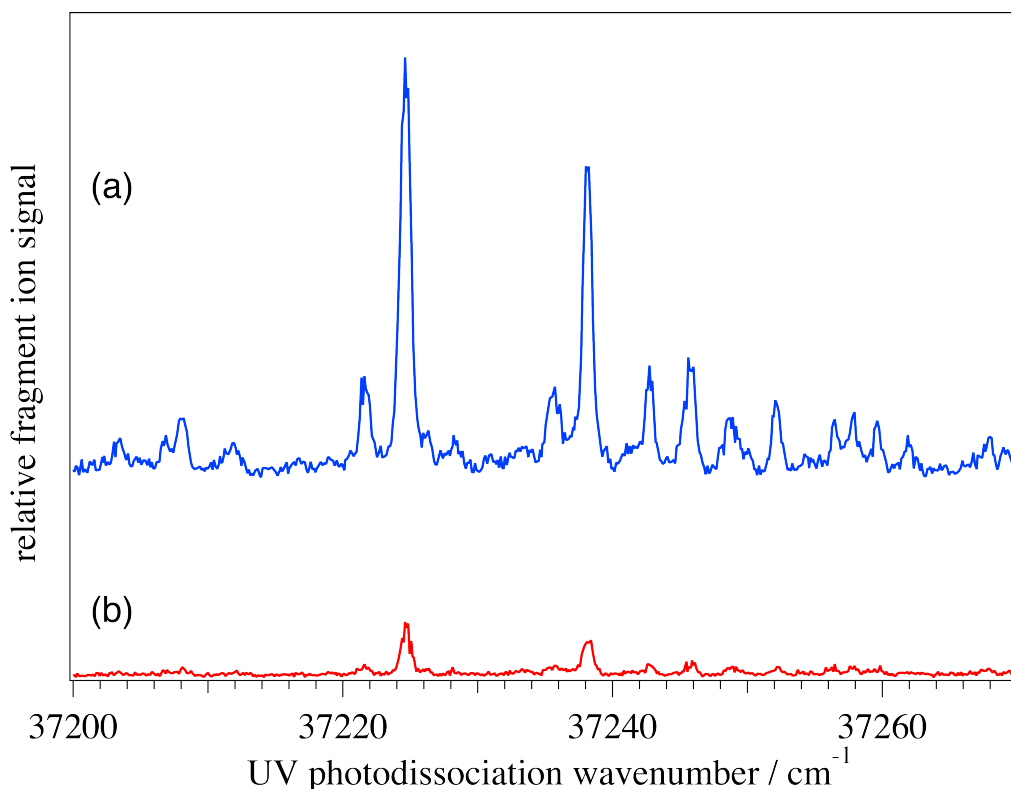


**Figure 4.13.** Expanded view of the lower frequency portion of the electronic photofragment excitation spectra of Fig. 4.11 with (a) CV=-13.3 V; (b) at CV=-10.4 V.

To distinguish between these two phenomena that mix up the conformers and result in contaminated spectra, we undertook a series of experiments in two studies that are presented in Chapter 5. The first resides in trying to achieve base-line resolution of the two conformational families in our FAIMS device. The second, in decreasing the heating during and after FAIMS resolution so as to reduce structural transitions. These studies suggest that the two conformational families of gas phase  $[\text{bk} + 2\text{H}]^{2+}$  interconvert after FAIMS separation, partially scrambling the conformational distribution. In kinetic studies of gas-phase reactions of  $[\text{bk} + 2\text{H}]^{2+}$  with hydroiodic acid, Schaaff *et. al.* also proposed the existence of two distinct conformations of the parent molecules with different reaction rates that interconvert upon gentle activation.<sup>58</sup> The IR-UV double-resonance studies of Svendsen *et. al.* suggest that these are two conformational families rather than simply two conformers.<sup>74</sup>

## 4.7. Cold ion spectroscopy as a high resolution ion mobility detector

Having demonstrated that FAIMS can be successfully used as a conformational filter for cold ion spectroscopy, we now demonstrate a second dimension in the coupling of these two techniques – using cold ion spectroscopy as a conformationally sensitive detector for ion mobility, and in our specific case, for FAIMS. Figure 4.14 shows conformation-specific CV spectra of doubly protonated bradykinin recorded using the following approach. After passing the ions through the FAIMS electrodes at a particular CV, we send them through the first stages of our mass spectrometer and into our cold, 22-pole ion trap, where after cooling they are irradiated by a UV laser pulse and then dissociated by the CO<sub>2</sub> laser.<sup>79</sup> The UV laser frequency is set to a peak in the cold spectrum associated with a particular conformer. The red and blue spectra of Fig. 4.14 show the photofragment ion signal recorded at different UV frequencies as a function of the CV of the transmitted parent ions. The dotted black trace is the normal CV spectrum recorded by monitoring the parent ion transmission through FAIMS. The heights of the red and blue traces are arbitrarily scaled such that the main peak matches the amplitude of the normal CV spectrum. This compensates for, among other things, the difference in the detection sensitivity of the cold ions *via* transitions of different oscillator strength.

The data of Fig. 4.14 clearly demonstrate that detecting the ion transmission through FAIMS in a conformer-specific way changes the shape of the CV spectrum. With the UV laser frequency set on a transition from one of the conformers associated with family A (red curve), the peak at CV=-13.3 V, which is associated with family A is enhanced relative to the one at -10.4 V, which is associated with family B. When the UV laser is set on a transition of family B (blue curve) the inverse occurs. While the overall shape of the CV spectrum changes quite dramatically, the peaks associated with the different conformational families are not cleanly separated insofar as intensity remains at the CV of the family that was not explicitly probed.

The spectroscopic transitions used for selective detection of a particular conformer appear to be clean and well resolved, although it is possible that a small amount of intensity may arise from spectral overlap with transitions from other conformations. Apart from the occurrence of an accidental coincidence between strong transitions of two conformers, we estimate that the small background from transitions of other conformers overlapping the main probe transition would give rise to at best a few percent of ion signal. In Chapter 5 we show that the major source of residual signal at CV values other than that of the probed conformer family results from isomerization

from other conformers into the one being probed. Nevertheless, it is clear that we can selectively detect different conformer sub-populations using a spectroscopic probe.

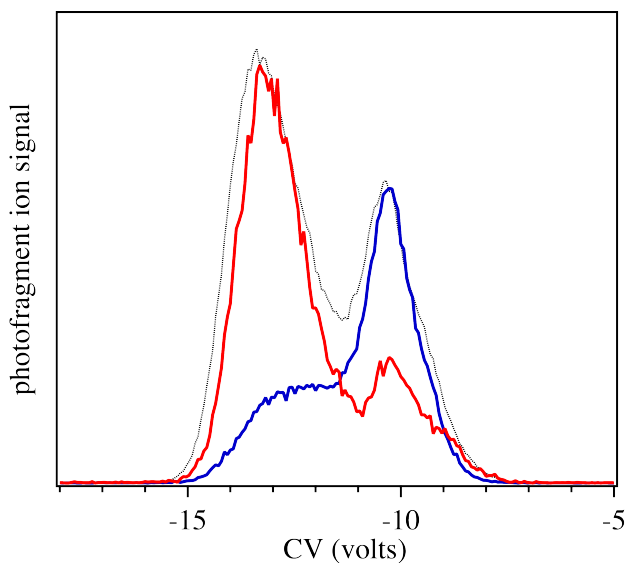


**Figure 4.14.** CV spectrum of  $[\text{bk} + 2\text{H}]^{2+}$  by detecting ions by photofragment spectroscopy in the cold ion trap. The red trace is the result of detecting ions *via* a transition of conformer family A at  $37359\text{ cm}^{-1}$  (red arrow Fig. 4.11) while the blue trace comes from detecting conformer family B at  $37224\text{ cm}^{-1}$  (blue arrow Fig. 4.11). The dotted black line is the normal CV spectrum detecting all transmitted ions of  $[\text{bk} + 2\text{H}]^{2+}$ , reproduced from Fig. 4.10.

It is interesting to note that the smaller peak in the CV curve of Fig. 4.14 detected *via* a transition of conformer B (blue trace) does not occur precisely at the same CV peak as in the normal CV spectrum (black dotted trace) or that obtained by probing conformer family A (red trace), and it seems to be broader. Higher resolution FAIMS spectra<sup>66</sup> as well as conformation-specific IR spectra<sup>74</sup> suggest that there are at least 5-6 stable conformers of  $[\text{bk} + 2\text{H}]^{2+}$ . The two main features in the CV spectrum must therefore represent not single conformers but a family of several conformers with similar differential ion mobility. It is likely that the barriers for isomerization from different conformers in family A into the probed conformer in family B are different, and the smaller broad peak on the blue trace of Fig. 4.14 may come from a subset of the “unresolved” conformers of family A. We should note that the appearance of a broad peak in the CV spectrum between conformer families A and B could also result from isomerization that occurs on the timescale of the FAIMS separation, similar to the situation in IMS.<sup>87</sup>

The advantages of using cold ion spectroscopy as a detector for ion mobility become more evident in a case where an ion mobility peak is unresolved. To demonstrate these advantages we can intentionally reduce the resolution of the FAIMS separation by eliminating the temperature gradient across the electrodes, as we demonstrated in section 4.5.<sup>76,83</sup> The CV spectrum of  $[\text{bk} +$

$2\text{H}]^{2+}$  taken under these conditions is shown in Fig. 4.15. The dotted black trace shows the CV spectrum obtained by detecting the total transmitted ion current at the  $[\text{bk} + 2\text{H}]^{2+}$  mass, while the red and blue traces correspond to CV spectra of those ions transmitted, cooled and detected *via* photofragment spectroscopy at transitions corresponding to conformer families A and B respectively. While the normal CV spectrum exhibits a structured shoulder, families A and B are no longer clearly resolved. Selective detection *via* photofragment spectroscopy of the cold ions can clearly pull out individual conformer contributions from this unresolved spectrum. Because the average temperature of the FAIMS electrodes, and hence the carrier gas, are lower in this measurement, it appears that the degree of cross-conformer contamination in the spectroscopically detected CV spectra is less than that in Fig. 4.15. The additional peak that appears at CV=-9.4 V in the spectrum of conformer family A comes from  $[\text{bk} + 3\text{H}]^{3+}$  that loses a proton during FAIMS separation and then isomerizes to conformer family A.

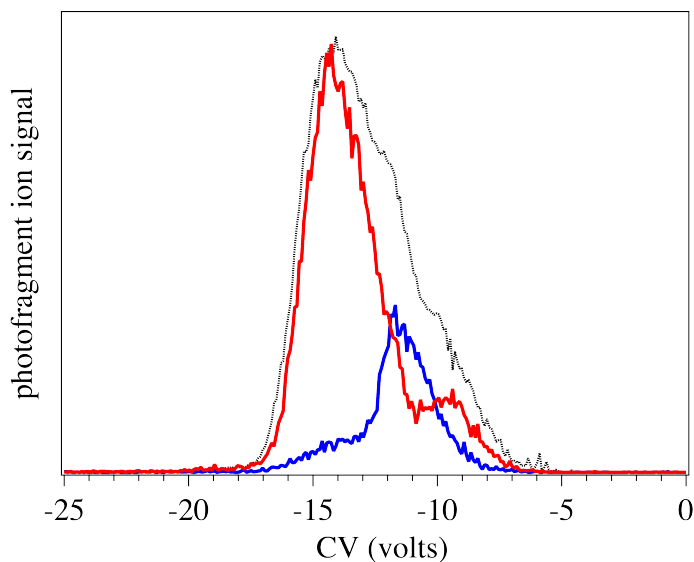


**Figure 4.15.** CV spectrum of  $[\text{bk} + 2\text{H}]^{2+}$  under intentionally reduced FAIMS resolution. The red trace is the result of detecting ions *via* a transition of conformer family A at  $37359\text{ cm}^{-1}$  (red arrow Fig. 4.11) while the blue trace comes from detecting conformer family B at  $37224\text{ cm}^{-1}$  (blue arrow Fig. 4.11). The dotted black line is the normal CV spectrum detecting all transmitted ions of  $[\text{bk} + 2\text{H}]^{2+}$ .

## 4.8. Conclusions

In this chapter we demonstrated experiments where differential ion mobility (i.e. FAIMS) was coupled to cold ion spectroscopy, using doubly protonated bradykinin as a test case. The spectrum of  $[\text{bk} + 2\text{H}]^{2+}$  is highly congested but individual features are still resolved and IR-UV

double resonance spectroscopy can be used successfully.<sup>74</sup> However, the data presented in this chapter show the feasibility, advantages and limitations of coupling the two techniques. While our FAIMS apparatus does not have sufficient resolution to separate all of the  $[\text{bk} + 2\text{H}]^{2+}$  conformers, even separation of conformational families allows us to begin to pull apart the complex electronic spectrum. We also demonstrated that the use of cold ion spectroscopy as a detector for ion mobility shows great promise in being able to decompose unresolved mobility spectra into components arising from distinct conformers. In both implementations of this technique, the major limitation seems to be isomerization of the ions after separation by FAIMS, and much of this is induced by the energy imparted to the ions during the separation process. From this point of view FAIMS is less than ideal, since subjecting the ions to high electric fields invariably energizes them in collisions with the carrier gas. However, cold ion spectroscopy can serve as a diagnostic of FAIMS, by observing the nascent conformational distribution as it is reflected in the electronic spectrum. In Chapter 5 we use  $[\text{bk} + 2\text{H}]^{2+}$  as a probe molecule to shed some light into the cross-conformer contamination that was observed in the individual spectra of the families.

In favorable cases, even with the limited resolution of our FAIMS device, we can prepare samples that consist of a single conformational family. The ability to do this has the potential to simplify studies of conformational isomerization in which one conformer is selectively pumped by laser excitation to explore the connectivity of different regions of conformational space and the heights of the barriers between them.<sup>36-39</sup>

While the work reported herein has used differential ion mobility rather than drift-tube ion mobility, the principles described here should hold equally well for the latter. Issues of conformational isomerization during the separation process will be equally important in coupling cold ion spectroscopy to IMS, but the field strengths used in the drift tube are significantly lower than in FAIMS,<sup>30,31,88</sup> and thus conformational isomerization should be much easier to control. The fact that the conformers of many molecules can be separated by IMS suggests that there are entire classes of molecules that don't isomerize at room temperature.<sup>89</sup> Moreover, adding a conformer-specific spectroscopic probe to IMS can potentially decompose a broad arrival time distribution into contributions from ions of very similar cross-sections.<sup>40</sup> This will lead to a better determination of drift times (and thus cross sections), improving the calculation of molecular shape for a given conformation.

Finally, from an analytical point of view, adding new dimensions to both ion mobility and laser spectroscopy could provide powerful fingerprints with which to identify gas phase biological molecules.

## 4.9. References

- (1) Papadopoulos, G.; Svendsen, A.; Boyarkin, O. V.; Rizzo, T. R. *Faraday Discuss.* **2011**, *150*, 243.
- (2) Nolting, D.; Marian, C.; Weinkauff, R. *Phys. Chem. Chem. Phys.* **2004**, *6*, 2633.
- (3) Kang, H.; Jouvét, C.; Dedonder-Lardeux, C.; Martrenchard, S.; Gregoire, G.; Desfrancois, C.; Schermann, J. P.; Barat, M.; Fayeton, J. A. *Phys. Chem. Chem. Phys.* **2005**, *7*, 394.
- (4) Oh, H.; Breuker, K.; Sze, S. K.; Ge, Y.; Carpenter, B. K.; McLafferty, F. W. *Proc. Natl. Acad. Sci. U. S. A.* **2002**, *99*, 15863.
- (5) Kamariotis, A.; Boyarkin, O. V.; Mercier, S. R.; Beck, R. D.; Bush, M. F.; Williams, E. R.; Rizzo, T. R. *J. Am. Chem. Soc.* **2005**, *128*, 905.
- (6) Oomens, J.; Polfer, N.; Moore, D. T.; van der Meer, L.; Marshall, A. G.; Eyler, J. R.; Meijer, G.; von Helden, G. *Phys. Chem. Chem. Phys.* **2005**, *7*, 1345.
- (7) Vaden, T. D.; de Boer, T. S. J. A.; Simons, J. P.; Snoek, L. C. *Phys. Chem. Chem. Phys.* **2008**, *10*, 1443.
- (8) Kamrath, M. Z.; Garand, E.; Jordan, P. A.; Leavitt, C. M.; Wolk, A. B.; Van Stipdonk, M. J.; Miller, S. J.; Johnson, M. A. *J. Am. Chem. Soc.* **2011**, *133*, 6440.
- (9) Rodrigo, C. P.; James, W. H.; Zwier, T. S. *J. Am. Chem. Soc.* **2011**, *133*, 2632.
- (10) Boyarkin, O. V.; Mercier, S. R.; Kamariotis, A.; Rizzo, T. R. *J. Am. Chem. Soc.* **2006**, *128*, 2816.
- (11) Nagornova, N. S.; Rizzo, T. R.; Boyarkin, O. V. *J. Am. Chem. Soc.* **2010**, *132*, 4040.
- (12) Nagornova, N. S.; Guglielmi, M.; Doemer, M.; Tavernelli, I.; Rothlisberger, U.; Rizzo, T. R.; Boyarkin, O. V. *Angew. Chem., Int. Ed.* **2011**, *50*, 5383.
- (13) Simons, J. P. *Mol. Phys.* **2009**, *107*, 2435.
- (14) Stearns, J. A.; Boyarkin, O. V.; Rizzo, T. R. *J. Am. Chem. Soc.* **2007**, *129*, 13820.
- (15) Stearns, J. A.; Mercier, S.; Seaiby, C.; Guidi, M.; Boyarkin, O. V.; Rizzo, T. R. *J. Am. Chem. Soc.* **2007**, *129*, 11814.
- (16) James, W. H.; Baquero, E. E.; Shubert, V. A.; Choi, S. H.; Gellman, S. H.; Zwier, T. S. *J. Am. Chem. Soc.* **2009**, *131*, 6574.
- (17) Fricke, H.; Funk, A.; Schrader, T.; Gerhards, M. *J. Am. Chem. Soc.* **2008**, *130*, 4692.
- (18) Rizzo, T. R.; Stearns, J. A.; Boyarkin, O. V. *Int. Rev. Phys. Chem.* **2009**, *28*, 481
- (19) Inokuchi, Y.; Kobayashi, Y.; Ito, T.; Ebata, T. *J. Phys. Chem. A* **2007**, *111*, 3209.
- (20) Abo-Riziq, A.; Crews, B. O.; Callahan, M. P.; Grace, L.; de Vries, M. S. *Angew. Chem., Int. Ed.* **2006**, *45*, 5166.
- (21) Chin, W.; PiuZZi, F.; Dognon, J. P.; Dimicoli, L.; Tardivel, B.; Mons, M. *J. Am. Chem. Soc.* **2005**, *127*, 11900.
- (22) Plutzer, C.; Hunig, I.; Kleinermanns, K. *Phys. Chem. Chem. Phys.* **2003**, *5*, 1158.
- (23) Stearns, J. A.; Seaiby, C.; Boyarkin, O. V.; Rizzo, T. R. *Phys. Chem. Chem. Phys.* **2009**, *11*, 125.
- (24) Hudgins, R. R.; Ratner, M. A.; Jarrold, M. F. *J. Am. Chem. Soc.* **1998**, *120*, 12974.
- (25) Jarrold, M. F. *Phys. Chem. Chem. Phys.* **2007**, *9*, 1659.
- (26) Rossi, M.; Blum, V.; Kupser, P.; von Helden, G.; Bierau, F.; Pagel, K.; Meijer, G.; Scheffler, M. *J. Phys. Chem. Lett.* **2010**, *1*, 3465.
- (27) Dian, B. C.; Longarte, A.; Mercier, S.; Evans, D. A.; Wales, D. J.; Zwier, T. S. *J. Chem. Phys.* **2002**, *117*, 10688.
- (28) Mercier, S. R.; Boyarkin, O. V.; Kamariotis, A.; Guglielmi, M.; Tavernelli, I.; Cascella, M.; Rothlisberger, U.; Rizzo, T. R. *J. Am. Chem. Soc.* **2006**, *128*, 16938.

- (29) Guidi, M. PhD Thesis, EPFL, 2010.
- (30) Bowers, M. T.; Kemper, P. R.; von Helden, G.; Vankoppen, P. A. M. *Science* **1993**, *260*, 1446.
- (31) Clemmer, D. E.; Jarrold, M. F. *J. Mass Spectrom.* **1997**, *32*, 577.
- (32) Jarrold, M. F. *Annu. Rev. Phys. Chem.* **2000**, *51*, 179.
- (33) Fromherz, R.; Ganteför, G.; Shvartsburg, A. A. *Phys. Rev. Lett.* **2002**, *89*, 083001.
- (34) Vonderach, M.; Ehrler, O. T.; Weis, P.; Kappes, M. M. *Anal. Chem.* **2011**, *83*, 1108.
- (35) Vonderach, M.; Ehrler, O. T.; Matheis, K.; Karpuschkin, T.; Papalazarou, E.; Brunet, C.; Antoine, R.; Weis, P.; Hampe, O.; Kappes, M. M.; Dugourd, P. *Phys. Chem. Chem. Phys.* **2011**, *13*.
- (36) Dian, B. C.; Longarte, A.; Zwier, T. S. *Science* **2002**, *296*, 2369.
- (37) Dian, B. C.; Clarkson, J. R.; Zwier, T. S. *Science* **2004**, *303*, 1169.
- (38) Dian, B. C.; Longarte, A.; Winter, R. P.; Zwier, T. S. *J. Chem. Phys.* **2004**, *120*, 133.
- (39) Dian, B. C.; Florio, G. M.; Clarkson, J. R.; Longarte, A.; Zwier, T. S. *J. Chem. Phys.* **2004**, *120*, 9033.
- (40) Koeniger, S. L.; Merenbloom, S. I.; Clemmer, D. E. *J. Phys. Chem. B* **2006**, *110*, 7017.
- (41) Koeniger, S.; Clemmer, D. *J. Am. Soc. Mass Spectrom.* **2007**, *18*, 322.
- (42) Purves, R. W.; Barnett, D. A.; Guevremont, R. *Int. J. Mass Spectrom.* **2000**, *197*, 163.
- (43) Carney, J. R.; Zwier, T. S. *J. Phys. Chem. A* **2000**, *104*, 8677.
- (44) Zwier, T. S. *J. Phys. Chem. A* **2006**, *110*, 4133.
- (45) Hünig, I.; Seefeld, K. A.; Kleinermanns, K. *Chem. Phys. Lett.* **2003**, *369*, 173.
- (46) Bhoola, K. D.; Figueroa, C. D.; Worthy, K. *Pharmacol. Rev.* **1992**, *44*, 1.
- (47) Maurer, M.; Bader, M.; Bas, M.; Bossi, F.; Cicardi, M.; Cugno, M.; Howarth, P.; Kaplan, A.; Kojda, G.; Leeb-Lundberg, F.; Lötvall, J.; Magerl, M. *Allergy* **2011**, *66*, 1397.
- (48) Kaplan, A. P.; Joseph, K.; Silverberg, M. *J. Allergy Clin. Immunol.* **2002**, *109*, 195.
- (49) Salvino, J. M.; Seoane, P. R.; Dolle, R. E. *J. Comput. Chem.* **1993**, *14*, 438.
- (50) Young, J. K.; Hicks, R. P. *Biopolymers* **1994**, *34*, 611.
- (51) Pierson, N. A.; Chen, L.; Valentine, S. J.; Russell, D. H.; Clemmer, D. E. *J. Am. Chem. Soc.* **2011**, *133*, 13810.
- (52) Cann, J. R.; Stewart, J. M.; Matsueda, G. R. *Biochemistry* **1973**, *12*, 3780.
- (53) Heck, A. J. R.; Derrick, P. J. *Anal. Chem.* **1997**, *69*, 3603.
- (54) Freitas, M.; Marshall, A. *Int. J. Mass Spectrom.* **1999**, *182–183*, 221.
- (55) Herrmann, K. A.; Kuppannan, K.; Wysocki, V. H. *Int. J. Mass Spectrom.* **2006**, *249–250*, 93.
- (56) Schnier, P. D.; Price, W. D.; Jockusch, R. A.; Williams, E. R. *J. Am. Chem. Soc.* **1996**, *118*, 7178.
- (57) Price, W. D.; Schnier, P. D.; Williams, E. R. *Anal. Chem.* **1996**, *68*, 859.
- (58) Schaaff, T. G.; Stephenson, J. L.; McLuckey, S. A. *J. Am. Chem. Soc.* **1999**, *121*, 8907.
- (59) Wyttenbach, T.; von Helden, G.; Bowers, M. T. *J. Am. Chem. Soc.* **1996**, *118*, 8355.
- (60) Counterman, A. E.; Valentine, S. J.; Srebalus, C. A.; Henderson, S. C.; Hoaglund, C. S.; Clemmer, D. E. *J. Am. Soc. Mass Spectrom.* **1998**, *9*, 743.
- (61) Hoaglund, C. S.; Valentine, S. J.; Sporleder, C. R.; Reilly, J. P.; Clemmer, D. E. *Anal. Chem.* **1998**, *70*, 2236.
- (62) Wu, C.; Klasmeier, J.; Hill, H. H. *Rapid Commun. Mass Spectrom.* **1999**, *13*, 1138.
- (63) Pierson, N. A.; Valentine, S. J.; Clemmer, D. E. *J. Phys. Chem. B* **2010**, *114*, 7777.



- (64) Gill, A. C.; Jennings, K. R.; Wyttenbach, T.; Bowers, M. T. *Int. J. Mass Spectrom.* **2000**, *195-196*, 685.
- (65) Purves, W. R.; Barnett, A. D.; Ells, B.; Guevremont, R. *Rapid Commun. Mass Spectrom.* **2001**, *15*, 1453.
- (66) Shvartsburg, A. A.; Li, F.; Tang, K.; Smith, R. D. *Anal. Chem.* **2006**, *78*, 3706.
- (67) Shvartsburg, A. A.; Danielson, W. F.; Smith, R. D. *Anal. Chem.* **2010**, *82*, 2456.
- (68) Shvartsburg, A. A.; Prior, D. C.; Tang, K.; Smith, R. D. *Anal. Chem.* **2010**, *82*, 7649.
- (69) Shvartsburg, A. A.; Smith, R. D. *Anal. Chem.* **2010**, *83*, 23.
- (70) Shvartsburg, A. A.; Tang, K.; Smith, R. D. *Anal. Chem.* **2010**, *82*, 32.
- (71) Rodriquez, C. F.; Orlova, G.; Guo, Y.; Li, X.; Siu, C.-K.; Hopkinson, A. C.; Siu, K. W. *M. J. Phys. Chem. B* **2006**, *110*, 7528.
- (72) Kemper, P. R.; Dupuis, N. F.; Bowers, M. T. *Int. J. Mass Spectrom.* **2009**, *287*, 46.
- (73) Siu, C.-K.; Guo, Y.; Saminathan, I. S.; Hopkinson, A. C.; Siu, K. W. *M. J. Phys. Chem. B* **2009**, *114*, 1204.
- (74) Svendsen, A.; Boyarkin, O. V.; Rizzo, T. R. *in preparation* **2012**.
- (75) Guo, Y.; Wang, J.; Javahery, G.; Thomson, B. A.; Siu, K. W. *M. Anal. Chem.* **2004**, *77*, 266.
- (76) Barnett, D. A.; Belford, M.; Dunyach, J.-J.; Purves, R. W. *J. Am. Soc. Mass Spectrom.* **2007**, *18*, 1653.
- (77) Robinson, E. W.; Shvartsburg, A. A.; Tang, K.; Smith, R. D. *Anal. Chem.* **2008**, *80*, 7508.
- (78) Yeh, L. I.; Okumura, M.; Myers, J. D.; Price, J. M.; Lee, Y. T. *J. Chem. Phys.* **1989**, *91*, 7319.
- (79) Guidi, M.; Lorenz, U. J.; Papadopoulos, G.; Boyarkin, O. V.; Rizzo, T. R. *J. Phys. Chem. A* **2009**, *113*, 797.
- (80) Purves, R. W.; Guevremont, R.; Day, S.; Pipich, C. W.; Matyjaszczyk, M. S. *Rev. Sci. Instrum.* **1998**, *69*, 4094.
- (81) Guevremont, R.; Purves, R. W. *Rev. Sci. Instrum.* **1999**, *70*, 1370.
- (82) Shvartsburg, A. A.; Tang, K.; Smith, R. D. *Anal. Chem.* **2004**, *76*, 7366.
- (83) Shvartsburg, A. A. *Differential Ion Mobility Spectrometry*; CRC Press: Boca Raton FL, 2009.
- (84) Baker, E. S.; Clowers, B. H.; Li, F.; Tang, K.; Tolmachev, A. V.; Prior, D. C.; Belov, M. E.; Smith, R. D. *J. Am. Soc. Mass Spectrom.* **2007**, *18*, 1176.
- (85) Purves, R. W.; Barnett, D. A.; Ells, B.; Guevremont, R. *J. Am. Soc. Mass Spectrom.* **2001**, *12*, 894.
- (86) Shvartsburg, A. A.; Li, F.; Tang, K.; Smith, R. D. *Anal. Chem.* **2007**, *79*, 1523.
- (87) Dugourd, P.; Hudgins, R. R.; Clemmer, D. E.; Jarrold, M. F. *Rev. Sci. Instrum.* **1997**, *68*, 1122.
- (88) von Helden, G.; Wyttenbach, T.; Bowers, M. T. *Science* **1995**, *267*, 1483.
- (89) Clemmer, D. E.; Hudgins, R. R.; Jarrold, M. F. *J. Am. Chem. Soc.* **1995**, *117*, 10141.



## Using the conformational distribution of bradykinin as a probe of isomerization

In this chapter we use the conformational distribution of  $[\text{bk} + 2\text{H}]^{2+}$  to investigate processes that impart energy on the ions after their production in the gas phase. We first measure the electronic spectra of doubly protonated bradykinin as a function of its injection energy into our mass spectrometer, without the use of FAIMS. Upon increase of the injection voltage, we induce conformational isomerization, which is observed as changes in the relative intensities of the peaks in the electronic spectra. We then use this feature to investigate the cross-conformer contamination that we observe in the electronic spectra of a FAIMS-selected conformational family of  $[\text{bk} + 2\text{H}]^{2+}$ . We do this by changing a few parameters of the separation process and observing the resulting conformational distribution of  $[\text{bk} + 2\text{H}]^{2+}$ , as it is reflected in the electronic spectrum. Finally, we use FAIMS as a conformational filter for isomerization studies, where the selected family is collisionally activated. At high injection energies we produce what seems to be a gas-phase quasi-equilibrium distribution of conformers. This distribution is different from the one produced initially by electrospray, indicating that some of the initially produced conformers appear to be kinetically trapped and may represent conformations that are stable in solution. Most of the results that we present here were published recently.<sup>1</sup>

### 5.1. Introduction

Bradykinin is a nona-peptide that possesses a high degree of flexibility in solution.<sup>2</sup> Electrospray ionization of a bradykinin solution produces a variety of gas phase structures for the doubly protonated state.<sup>3</sup> This conformational heterogeneity is reflected in its congested electronic spectrum, exhibiting a number of features originating from different structural isomers.<sup>4</sup> In Chapter 4, we showed that it is possible to use Field Asymmetric waveform Ion Mobility Spectrometry (FAIMS) to separate the electrosprayed bradykinin ions in two conformational

families and record electronic spectra for each of them. Although the family-selected electronic spectra are clearly different, we observed some cross-conformer contamination. It is well known that ions are energized during their separation in FAIMS, and this can lead to their isomerization from one conformational family to the other, either during or after the separation. Conformational isomerization of ions during FAIMS separation has also been observed in two-dimensional FAIMS-IMS separations,<sup>5</sup> where the degree of isomerization induced during FAIMS separation was investigated by comparing ubiquitin ions that have passed through a FAIMS separation stage with those that have been introduced directly into an IMS drift tube.<sup>5</sup> It was found that for most charge states some structural transitions occur, with a net effect similar to that when heating the ions to ~75 °C prior to their introduction into the IMS stage.<sup>5</sup> In addition, using the cylindrical FAIMS device, we could not achieve a complete (base-line) separation in our FAIMS device, which might also be the cause of the contamination that we observe. Both of the above can contribute to the conformational contamination.

To disentangle the two possible sources of the cross-conformer contamination we conducted two series of experiments, using  $[\text{bk} + 2\text{H}]^{2+}$  ions as a probe. First, we demonstrate a way to increase the resolution of our FAIMS device and subsequently we record electronic spectra corresponding to the baseline-separated peaks. Second, we decrease the amount of energy that we impart on the ions during the separation process, and we look at the corresponding conformational distribution by inspecting the electronic spectra. The results of these investigations demonstrate that the contamination is not a result of incomplete spatial separation in the FAIMS stage but rather comes from energizing the ions during the FAIMS separation and/or in subsequent collisions in the mass spectrometer.

In the following we will investigate the origin of this contamination, but before that, we will examine the conformational distribution of doubly protonated bradykinin in the gas phase, without the use of FAIMS separation.

## 5.2. Experimental details

The experimental procedure in these series of experiments is similar to the one described in Chapter 4 and only the additional elements will be mentioned. In our “side-to-side” FAIMS<sup>6-8</sup> we used two sets of electrodes with different spacings (and hence different analytical gap widths). The first electrode set, which has an electrode gap of 2.5 mm, is the standard one used in the

FAIMS unit. All the results in Chapter 4 were obtained using this electrode set. Here, we use a DV of -5000 Volts, and a carrier gas of either 90% N<sub>2</sub> and 10% He or 100% N<sub>2</sub>. We perform experiments with and without establishing a temperature gradient across the analytical gap of FAIMS, depending on the resolution/heating that is needed for a particular experiment.<sup>6,9</sup> The second electrode set has an analytical gap of 1 mm. For this set, we use a DV of -2500 V and no temperature gradient across the analytical gap.

The ions that are transmitted through the FAIMS device are introduced into the cold ion trap tandem mass spectrometer,<sup>10-12</sup> which is described in detail in Chapter 2. We can use the voltage drop between the exit of the capillary (L1 in Fig. 5.1) and the skimmer to vary the collision energy of the ions with the background gas upon injection, since the pressure in this region is 1.7 mbar. In the initial collisions of the ions with the background gas, part of their kinetic energy is converted to internal energy and the ions heat up. Subsequently, the ions are thermalized to the temperature of the background gas. This heating/cooling cycle can serve as an annealing process that may lead to structural transitions.<sup>13-15</sup> The amount of heating depends on the kinetic energy of the colliding partners and thus on the injection voltage. Electronic photofragment spectra are recorded as a function of the injection voltage. For experiments where no FAIMS selection is needed, the FAIMS device is removed from the mass spectrometer and the electrosprayed ions were directly injected into vacuum through the glass capillary.

### 5.3. Gas phase conformational distribution of [bk + 2H]<sup>2+</sup> without FAIMS

We first demonstrate the effect of the injection voltage<sup>16</sup> of cold [bk + 2H]<sup>2+</sup> on the UV photofragment spectrum when no FAIMS separation is used. These spectra are shown in Fig. 5.1. The traces (e) to (a) display spectra recorded with increasing ion injection energy into the hexapole trap by increasing the voltage on the capillary exit. The voltage difference between the capillary and the skimmer is shown on the left of each trace. The spectrum of Fig. 5.1(f) was recorded under as gentle conditions in the mass spectrometer as possible that still sustains ion transmission. This means that there were no large differences in the voltages of the ion optics that are used to transfer the ions across the higher-pressure regions of the mass spectrometer. In addition, ions were not pre-trapped in the hexapole, and their translational energy entering the hexapole and the 22-pole was less than 1eV. All the spectra in Fig. 5.1 are congested, exhibiting a

large number of sharp transitions. Svendsen et. al used an IR-UV double resonance spectroscopic scheme to record conformer-specific vibrational spectra of double protonated bradykinin.<sup>4</sup> These data indicate that there are at least five different stable conformations at the temperature of the trap that all contribute to the acquired spectra. Conformational heterogeneity is thus a major source of congestion in the spectra of Fig. 5.1, consistent with what one would predict on the basis of high-resolution FAIMS measurements.<sup>17</sup>

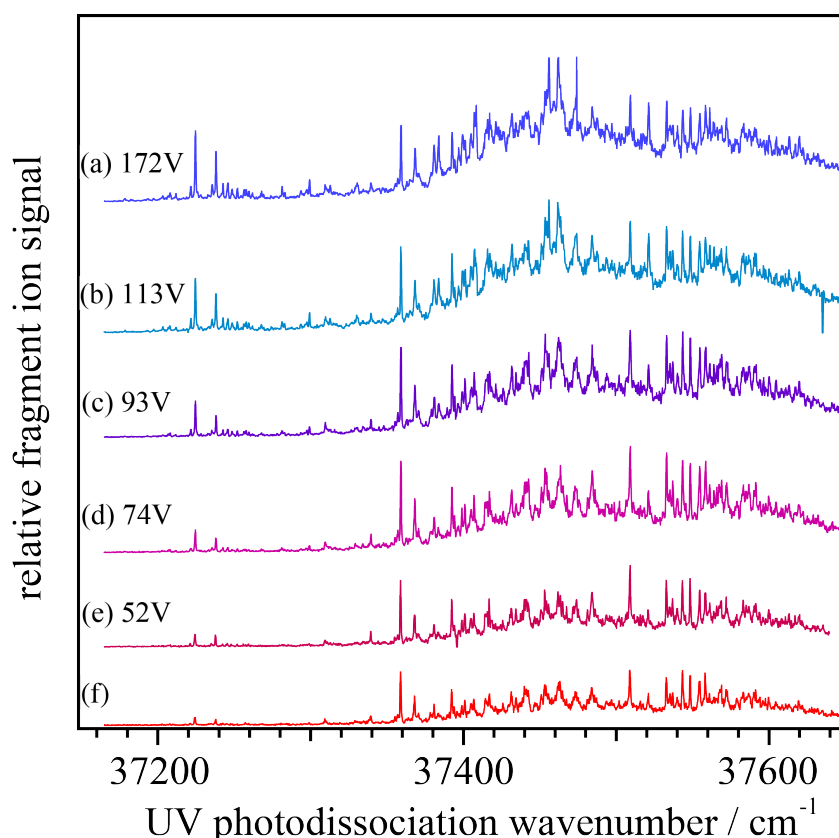


**Figure 5.1.** Electronic photofragment excitation spectra of  $[bk+2H]^{2+}$  obtained (a)-(e) with variable injection voltage of the ions into the hexapole ion trap, (f) under very gentle conditions (see text). Spectra are normalized by the number of parent ions.

The spectra of Fig. 5.1 clearly show that upon increase of the ion injection energy some peaks change in relative intensity. For example the two transitions around  $37230\text{ cm}^{-1}$  and the transitions around  $37380\text{ cm}^{-1}$  increase in intensity compared to the peak at  $\sim 37360\text{ cm}^{-1}$ . Data from IR-UV double resonance spectroscopy with the UV laser set on the features at  $\sim 37230\text{ cm}^{-1}$  and at  $\sim 37360\text{ cm}^{-1}$ , indicate that these transitions originate from different conformations.<sup>4</sup> Since the intensity of a peak depends upon the population of the initial state probed by the UV laser, the increase of the intensity of a feature at a fixed temperature reveals an increase in conformer population that gives rise to it. A change in the relative populations of a given distribution over a

number of stable conformations would necessarily involve energizing the ion population above the barrier to isomerization.

The voltage drop between the capillary and the skimmer determines the injection energy of the ions, and thus the average energy of their collisions with the background gas in this region. In our case, the increase in population of a particular conformer involves an annealing process in which the ions are first energized in initial collisions with the background gas and then cooled in collisions both with background gas in the hexapole and with cold He in the 22-pole ion trap so that the “hot” ion population relaxes into a different distribution. The increase in the intensities of the peaks around  $37230\text{ cm}^{-1}$ ,  $37380\text{ cm}^{-1}$  and  $37460\text{ cm}^{-1}$  with increased injection energy is indicative of such a process. Over the range represented in Fig. 5.1, the higher the collisional activation, the larger the fraction of ions that change their conformation *via* this annealing process.

In Chapter 4, we used FAIMS to divide the stream of the electrosprayed  $[\text{bk}+2\text{H}]^{2+}$  ions into two families, A and B.<sup>18</sup> Interestingly, all the peaks of Fig. 5.1 that increase in intensity originate from the conformers that constitute family B, while those whose intensity is nearly independent of the injection voltage come from family A.

The fact that peaks of family B increase so significantly in intensity during the annealing process raises the question of whether the family of conformers that they represent is initially produced in the electrospray process or becomes populated only in the gas phase upon annealing. To answer this question we recorded a UV photofragment spectrum of cold  $[\text{bk}+2\text{H}]^{2+}$  under the gentlest conditions possible in our mass spectrometer (Fig. 5.1(f)). This spectrum shows that characteristic peaks of family B around  $37230\text{ cm}^{-1}$  and  $37380\text{ cm}^{-1}$  do appear but with very low intensities. This indicates that the conformers of family B are indeed present, albeit with low relative population. The conformers that give rise to the prominent peaks in Fig. 5.1(f), belonging to family A, are significantly populated without annealing and appear to be those predominantly formed in the electrospray process.

One could argue that the conditions that we employ for the transfer of ions into the 22-pole trap are not gentle enough, and that this induces their partial isomerization from the initially produced A family to B, which is a family of conformers that becomes stable in the gas phase. Another possibility may be that family A spontaneously decays to family B. However, data presented further below indicate that both of these possibilities can be excluded. We thus believe that the spectrum of Fig. 5.1(f) reflects the distribution of populations between the two conformational families as they are produced in the electrospray process, which may in fact represent the distribution in solution before electrospraying.<sup>19</sup> This would imply that in solution there are two structural families with different stabilities and thus different populations. When

solvent is removed, the less populated family gives rise to conformational family B and the more populated to A. At the same time, the desolvation stabilizes the structures that form family B while leaves kinetically trapped those that form family A, since a barrier on the potential energy surface inhibits isomerization from A to B. Consistent with this interpretation is that when we increase the injection energy of the ions in our mass spectrometer we provide the necessary energy to overcome this barrier. To what extent conformational families A and B produced by electrospray are related to their solution counterparts is an open question,<sup>19</sup> however, studies indicate that there is at least a memory of the solution conformational distribution in the nascent electrospray distribution.<sup>20</sup> In section 5.5, we further investigate this scenario by first separating the conformational families using FAIMS before spectroscopically probing the final conformational distribution in our cold ion trap.

## 5.4. Investigation of the cross-conformer contamination

### 5.4.1. Introduction

Figure 5.2 shows a CV spectrum of  $[\text{bk}+2\text{H}]^{2+}$  with the temperature of inner electrode held at 35 °C while that of the outer electrode at 95 °C, establishing thus a temperature gradient of 60 °C. The spectrum exhibits two partially resolved peaks, one at -20.4V and one at -16.1V. It is similar to the spectrum optimized for a good balance between resolution and sensitivity that was shown in Fig 4.10.<sup>18</sup> However, the whole spectrum is shifted to lower CV values, and the features are spread over a wider range of CV values. There are two reasons for this. First, the dispersion voltage (DV) used here is -5000 V as opposed to -4600 V.<sup>18</sup> Higher value of DV induces a larger migration of the ions away from the gap median because of the larger deviation in their mobility at high electric field  $K_h$  from its value at low electric field  $K$ . Thus, a more negative CV value is needed to keep the ions in the gap median. The second reason is that because of the higher temperature gradient across the gap, the average temperature is greater in the present experiment. Hence, the number density of the carrier gas is smaller and, since ion mobility depends on the electric field through  $E/N$ ,<sup>9,21</sup> the difference between  $K_h$  and  $K$  will be greater. As a result, more negative CV values are needed for the transmission of the ions through the FAIMS electrodes.



We showed in Chapter 4 that the two features in the CV spectrum give rise to distinct electronic spectra.<sup>18</sup> Following our previous notation, we refer to the peak transmitted at -20.4 V as conformational family A and the one at -16.1 V as conformational family B.

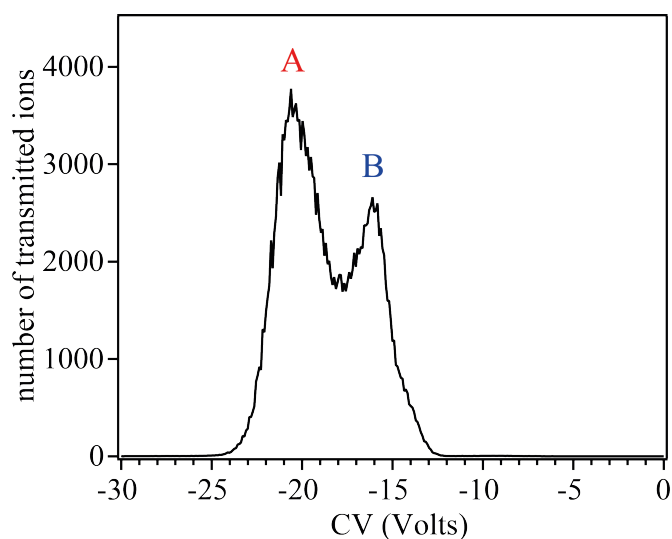


**Figure 5.2.** CV spectrum of [bk+2H]<sup>2+</sup> using a DV of -5 kV and a temperature gradient of 60 °C across the analytical gap.

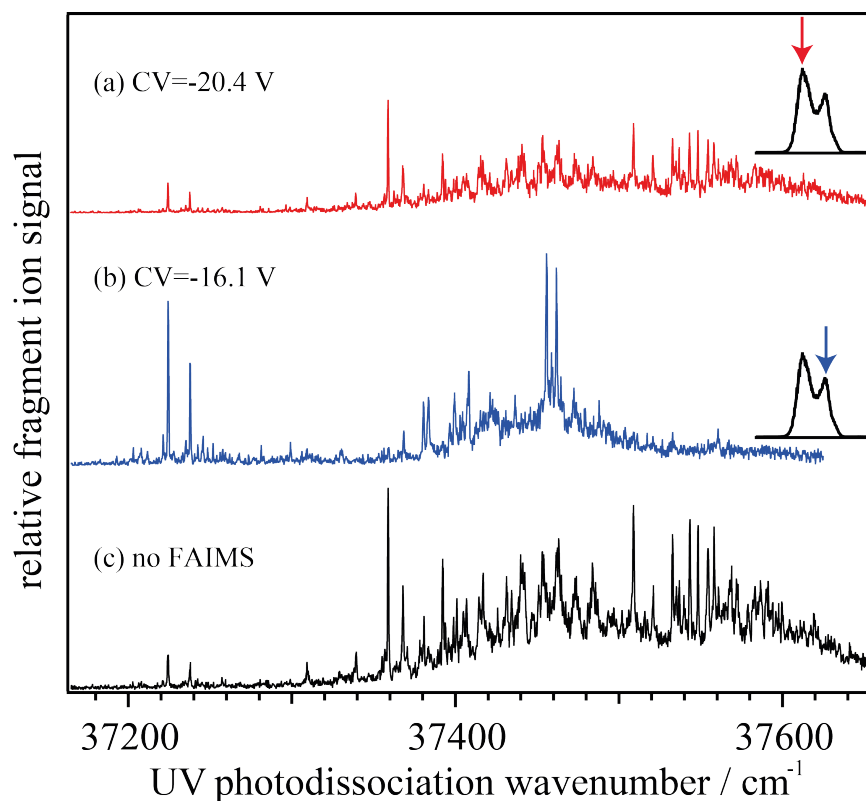


**Figure 5.3.** Electronic photofragment excitation spectra of [bk+2H]<sup>2+</sup> obtained (a) with FAIMS separation transmitting ions at CV=-20.4 V; (b) with FAIMS separation transmitting ions at CV=-16.1 V; (c) without FAIMS separation and under gentle conditions in the mass spectrometer.

Figure 5.3 displays UV photofragment spectra of cold  $[\text{bk}+2\text{H}]^{2+}$  in combination with FAIMS. The traces in Figs. 5.3a and 5.3b are recorded with the electrosprayed ions passing through the FAIMS electrodes and transmitted at CV values of -20.4 V and -16.1 V respectively. For comparison, the spectrum recorded under gentle conditions without the use of FAIMS is included (Fig. 5.3c). The spectra of Fig. 5.3a and 5.3b are also recorded with low injection energy (L1:40 V) so that collisional energy imparted to the ions is minimized. For the most part, the two spectra are distinct and represent the two conformational families.

Nevertheless, the spectrum of conformational family A (Fig. 5.4a) contains the peaks originating from conformers of the B family, but with much lower intensity than in the spectrum of Fig. 5.4b.<sup>18</sup> On the other hand, the spectrum of Fig. 5.4b is a conformationally clean spectrum of the B family, as it shows no trace of feature arising from A family. In the following, the origin of the cross-conformer contamination in the former case will be addressed.<sup>18</sup>

## 5.4.2. Increasing FAIMS resolution

In the CV spectrum of Fig. 5.2 it is shown that the two conformational families are only partially separated. Inevitably, the ion population that is transmitted through FAIMS at a CV value corresponding to one of the peaks in Fig. 5.2 will contain some contamination from the other conformational family. As a result, the electronic photofragment spectrum of this conformationally mixed ionic population will be composed of contributions from both families. However, for a small amount of contamination, the intensities corresponding to the transitions from the contaminant may be undetectable. To investigate if the cross-conformer contamination stems from the partial separation of the two families, we increase the resolution of our FAIMS device to better spatially separate the two conformational families and thus allow into the mass spectrometer a conformationally “cleaner” ionic population.

One way to improve the resolution is to decrease the width of the analytical gap.<sup>9,22-24</sup> To this end, we removed the inner electrode of the FAIMS device and replaced it with one of larger diameter. In the original electrode set (set 1) the inner electrode has a diameter of 13 mm while in the new set (set 2) this has been increased to 16 mm. In both sets the outer electrode has an inner diameter of 18 mm and thus the analytical gap is reduced from 2.5 mm to 1 mm. Figure 5.4 shows these two sets of electrodes schematically. With electrode set 1 we used -5000 V, which translates to an electric field of 20 kV/cm in the gap median at the peak of the waveform. With electrode set 2 we used -2500 V, the lowest possible value of DV allowed from the FAIMS electronics, which

produces an electric field of 25 kV/cm at the median. Figure 5.5 shows CV spectra of  $[\text{bk}+2\text{H}]^{2+}$  recorded with the two electrode sets. Figure 5.5a repeats the spectrum of Fig. 5.2, which is recorded with set 1 and a temperature gradient of 60 °C, while Fig. 5.5b shows the spectrum recorded with set 2 for which no temperature gradient was used.

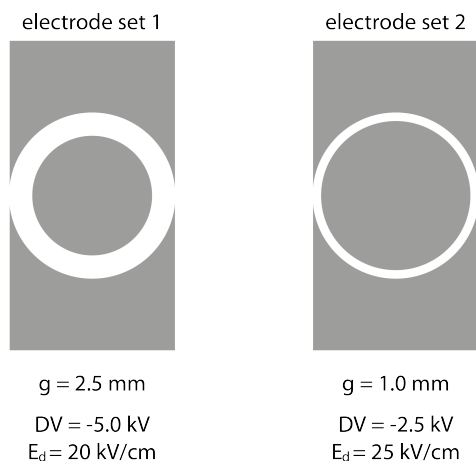


**Figure 5.4.** Schematic presentation of the two sets of electrodes that were used in FAIMS separation. The electrode set 1 and 2, shown left and right respectively, differ by diameter of the inner electrode. The analytical gap width ( $g$ ) as well as the dispersive voltage ( $DV$ ) used and the electric field ( $E_d$ ) in the median of the gap created by this particular DV is shown underneath each pair of electrodes for comparison.

From comparison of the spectra of Fig. 5.5, it is evident that the resolution of the FAIMS device is greatly enhanced for the electrode set 2 compared to electrode set 1, with the two conformational families almost base-line resolved. On the other hand, the number of transmitted ions decreases for both families, as expected when decreasing the width of the analytical gap (see Section 3.4.2). Interestingly, the relative intensities of the two peaks are different in the two spectra of Fig. 5.5, with the relative number of transmitted ions of the B family being larger in the case of set 1. In set 2 the difference in the CV values of the two families is larger than the width of the individual peaks. In this case, isomerization of an ion from family A to family B and vice versa is accompanied by a relatively large change in the CV value for which the ion is transmitted. Thus, the newly isomerized ion does not satisfy the condition for stable trajectory, and is filtered out. In set 1, where we observe only partial separation of the two families, isomerization will lead to a change in the CV value of the ion, but this newly formed isomer may have a stable trajectory in the analytical gap. In this case the population that undergoes isomerization is not lost but rather adds to the conformational family it's isomerizing into. In conclusion, isomerization in electrode set 1 leads to stable trajectory for the isomerized species while in electrode set 2 leads to unstable

trajectory. We believe that this is the reason why the relative intensities of the two families are different in the two electrode sets.

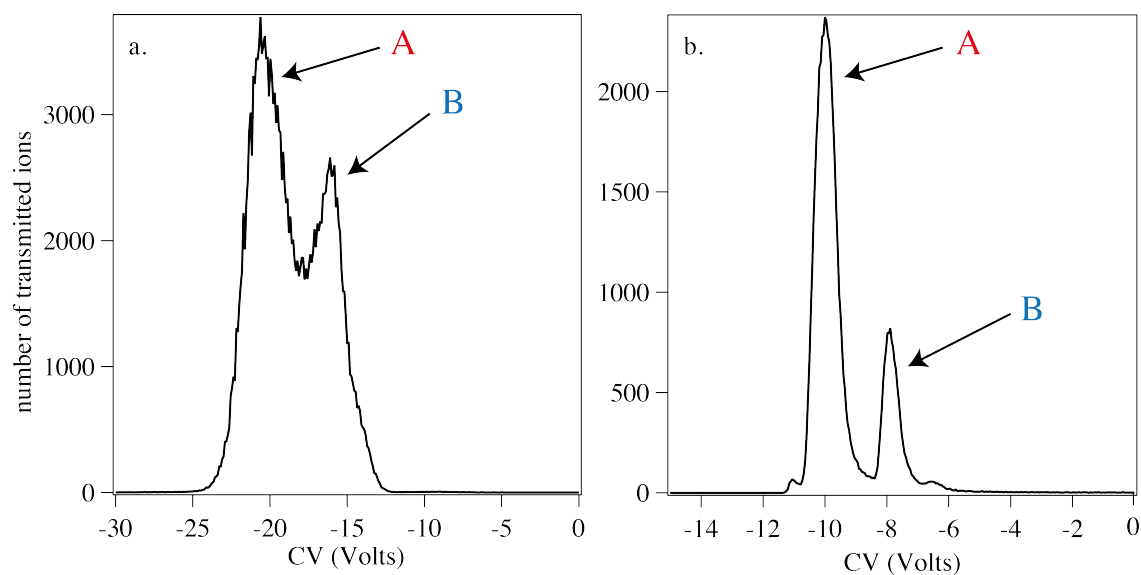


**Figure 5.5.** CV spectra of  $[bk+2H]^{2+}$  using the two sets of electrodes shown in Fig. 5.5. a: CV spectrum of Fig. 5.2 recorded with electrode set 1, b: CV spectrum recorded with electrode set 2. The peaks corresponding to conformational families A and B are also shown.

To investigate whether a base line separation of the two families in FAIMS leads to spectra free from conformational contamination, we used electronic photofragment spectroscopy to probe the ions transmitted at the two CV values corresponding to the peaks in the CV spectrum of Fig. 5.5b. Figures 5.6b and 5.6c shows UV photofragment spectra of cold  $[bk+2H]^{2+}$ , recorded with the ions passing through the electrode set 2 and with the CV set at -10 V and -7.9 V, respectively. For comparison, we include the spectra of conformational families A and B recorded with electrode set 1 and with a temperature gradient across the analytical gap (Figs. 5.6a and 5.6d, respectively). In the spectrum that probes conformational family A (Fig. 5.6b) the characteristic peaks of conformational family B are also present with high intensities. Comparison of the Figs. 5.6a and 5.6b shows that in the latter case the degree of contamination is higher, despite the much better resolution in the FAIMS stage. This indicates that the cross-conformer contamination is not a result of poor separation in the FAIMS stage, but must be caused by conformational isomerization after the FAIMS stage. On the other hand, the spectrum of conformational family B recorded with electrode set 2 (Fig. 5.6c) is almost the same as that recorded with electrode set 1 (Fig. 5.6d). The absence of characteristic peaks of the A conformational family in the spectrum

probing family B (Fig. 5.6c) may indicate that isomerization from B to A has a higher barrier than from A to B.

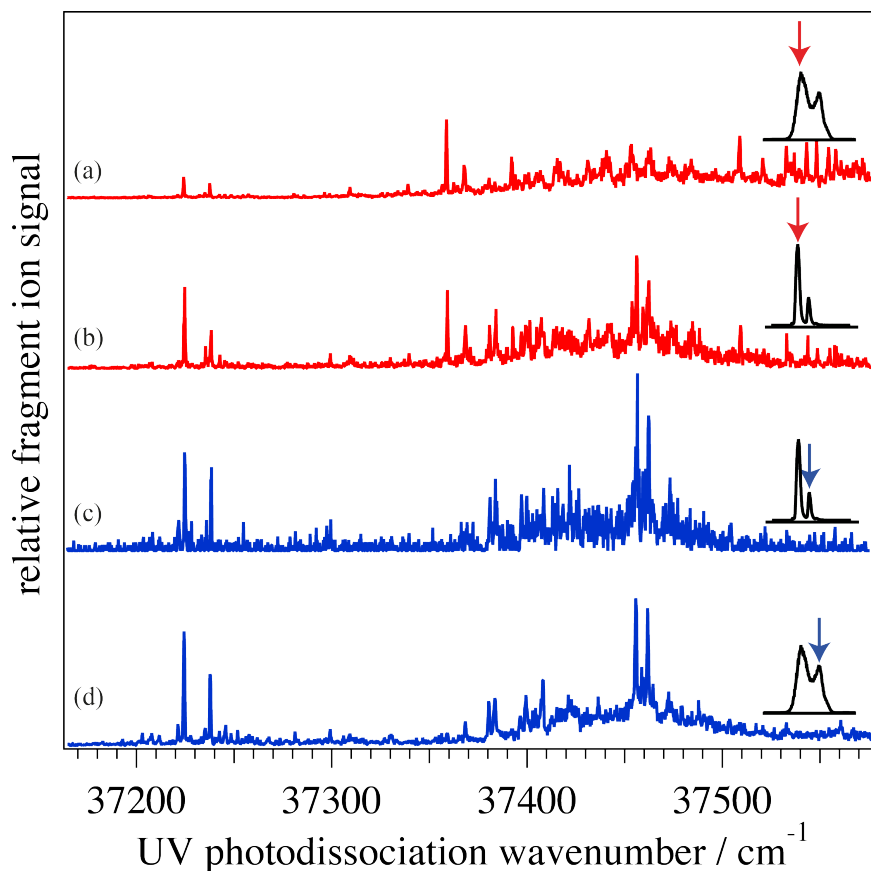


**Figure 5.6.** Electronic photofragment excitation spectra of  $[bk+2H]^{2+}$  obtained with FAIMS comprising : (a), (d) electrode set 1 with CV = -20.4 V and CV = -16.1 V, respectively; (b), (c) electrode set 2 with CV = -10 V and CV = -7.9 V, respectively.

In order to reduce the energy imparted to the ions during the FAIMS separation, we conducted all the following experiments with the electrode set 1.

### 5.4.3. Reducing heating in FAIMS

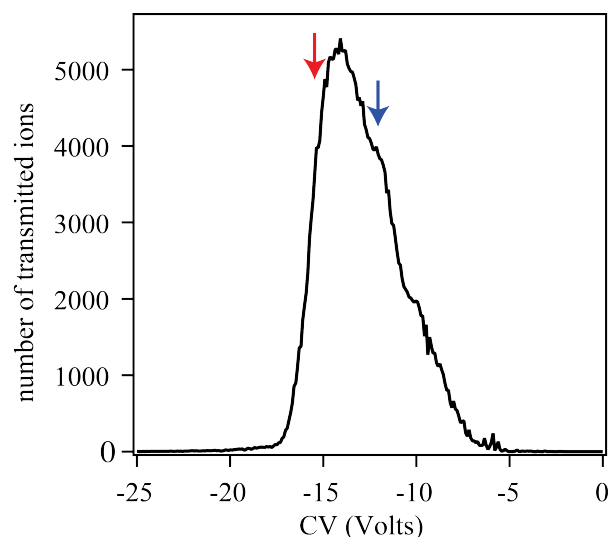
As discussed in the previous section, ions can be energized during their passage through FAIMS in energetic collisions with the carrier gas, driven by the RF-field. In our case, we also use a temperature gradient across the FAIMS electrodes in order to increase the resolution of our device.<sup>6,9</sup> While doing this allows partial separation of the ions into two conformational families, the increased temperature will raise the average energy imparted to the ions in collisions with the

carrier gas. Thus, ions exiting FAIMS will be warm and, consequently, likely to isomerize downstream from the separation stage during their transfer to the 22-pole.

Heating of the ions during the FAIMS separation may not pose a problem when FAIMS is used as a stand-alone device for detecting the number of conformations of a biomolecular ion, although in cases of extreme heating, extended unfolding may lead to erroneous conclusions about the number of conformations initially produced by electrospray.<sup>25</sup> However, when FAIMS is used in conjunction with other methods, where a selected conformation is isolated for a subsequent experiment, the heating effect is undesirable and must be diminished. As discussed by Shvartsburg et al.,<sup>5</sup> reducing the magnitude of the DV would lower the amount of field heating in FAIMS. However, this would also decrease the resolution of FAIMS. A solution that would not affect the resolution would be to cool the FAIMS unit to compensate for the heating, which was estimated to be ~75 °C using a flat electrode FAIMS device.<sup>5</sup> In the case of the cylindrical geometry FAIMS device, we are obliged to maintain a temperature gradient across the two electrodes in order to achieve an acceptable resolution. This means that the amount of cooling would have to be more than 60°C lower in order to incorporate the necessary temperature difference between the electrodes. The realization of this is hindered by experimental difficulties.

In order to investigate the effect of the temperature during the separation, we used our FAIMS device without a temperature gradient and recorded the spectrum of the ions transmitted at two different values of the CV. Figure 5.7 shows a CV spectrum of  $[\text{bk}+2\text{H}]^{2+}$  with both of the electrodes held at 35 °C. The spectrum exhibits one peak at -14.1 V with a shoulder at -11.9 V. The smaller shoulder at -10.2 V arises from a charge reduction of  $[\text{bk}+3\text{H}]^{3+}$  in the FAIMS device, which results in its detection as  $[\text{bk}+2\text{H}]^{2+}$ ,<sup>18,25,26</sup> as was shown in Chapter 4. As the temperature gradient is increased, the peak and the shoulder become increasingly resolved and the CV spectrum approaches the one shown in Fig. 5.2. We thus attribute the main peak in Fig. 5.7 (-14.1 V) to conformational family A and the shoulder (-11.9 V) to conformational family B.

Although the two conformational families are not even partially resolved in this CV spectrum, operating FAIMS at reduced average temperature minimizes the thermal heating of the ions during the separation. It may be possible, by setting the CV off the main peak to more negative values of the compensating voltage (<-15 V), to introduce conformational family A selectively into our mass spectrometer. This is because at  $\text{CV} < -15$  V the contribution of conformational family B (shoulder, -11.9 V) will be reduced. Moreover, the ions of conformational family A exiting FAIMS will be heated less and thus be less likely to isomerize downstream.



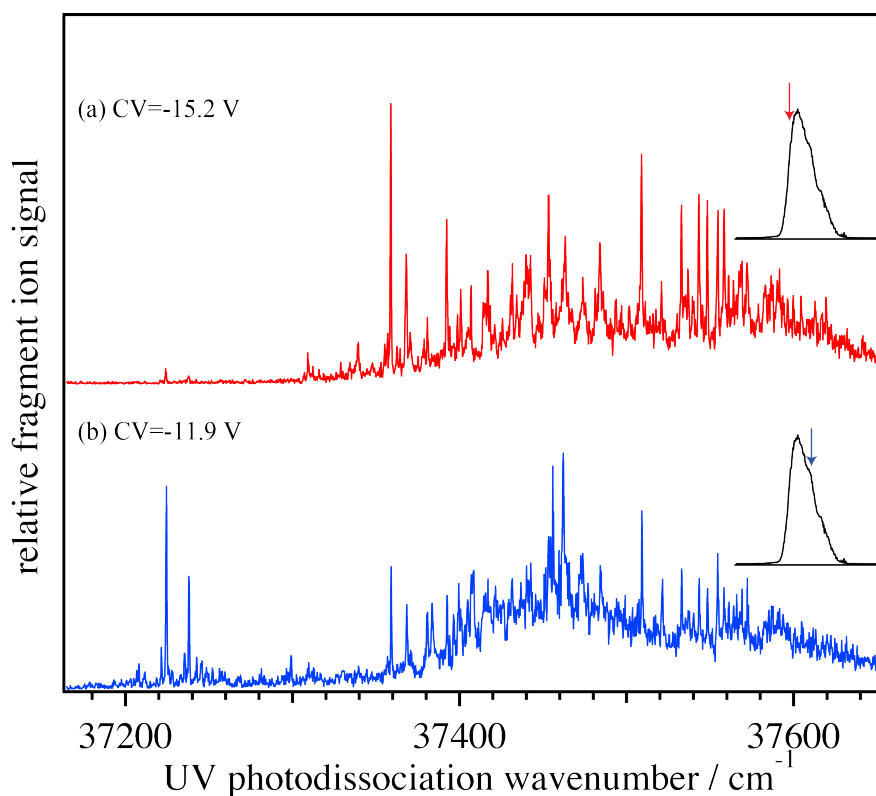
**Figure 5.7.** CV spectrum of  $[bk+2H]^{2+}$  using a DV of -5 kV and no temperature gradient across the analytical gap. The temperature of both electrodes is 35 °C. The red and blue arrows are explained in the text.

Figure 5.8a shows the photofragment spectrum of  $[bk+2H]^{2+}$  when the CV is set to -15.2 V (red arrow, Fig. 5.7), while Fig. 5.8b shows the spectrum when the CV is set to -11.9 V (blue arrow, Fig. 5.7), both of which are recorded with no temperature gradient between the FAIMS electrodes. Indeed, the spectrum of conformational family A (Fig. 5.8a) appears conformationally cleaner than that of Fig. 5.3a, exhibiting almost no intensity for peaks belonging to family B. Thus, contrary to what might have been expected, better conformational separation in FAIMS does not necessarily produce conformationally cleaner spectra, because the increased resolution is obtained by using a temperature gradient, which energizes the ions during FAIMS separation. The energized ions isomerize more rapidly in the mass spectrometer, producing the cross-conformer contamination demonstrated in the spectrum of Fig. 5.3a.

The electronic spectrum of  $[bk+2H]^{2+}$  exiting FAIMS at a CV value of -11.9 V (Fig. 5.8b) appears to be a composite of the two conformational families. At this CV, which corresponds to the unresolved shoulder belonging to conformer family B, it is impossible to avoid the transmission of ions of the more abundant conformational family A.<sup>18</sup>

Figures 5.9a and 5.9b compares the spectra of conformational family A recorded with and without the temperature gradient used across the analytical gap of FAIMS. Figure 5.9c is the spectrum of  $[bk+2H]^{2+}$  without FAIMS separation, recorded under very gentle conditions in the mass spectrometer, included for comparison. It should be noted that spectra of Figs. 5.9a and 5.9b are recorded under the same conditions in the mass spectrometer, but not in FAIMS. The carrier gas used for the separation contains 10% He in Fig. 5.9a, while in Fig. 5.9b pure N<sub>2</sub> is used. Use of a mixture of He/N<sub>2</sub> in FAIMS separations has been shown to increase the resolution of the

separation<sup>27</sup> but at the same time heats the ions.<sup>28</sup> However, we estimate the amount of ion heating in a 90/10 N<sub>2</sub>/He mixture to be about 4 °C greater than in a 100% N<sub>2</sub> carrier gas, and thus negligible compared to the increase in the mean temperature when we use a temperature gradient to improve the resolution.<sup>27</sup> This means that the comparison between Figs. 5.9a and 5.9b reveals the effect of the temperature gradient on the relative population of the conformations.



**Figure 5.8.** Electronic photofragment excitation spectra of [bk+2H]<sup>2+</sup> obtained (a) with FAIMS separation transmitting ions at CV=-15.2 V; (b) with FAIMS separation transmitting ions at CV=-11.9 V; In the spectra (a) and (b) FAIMS is used without temperature gradient.

The fact that we can record a conformationally clean spectrum of the A family (Fig. 5.9b) suggests that the ions do not spontaneously isomerize to conformational family B, at least on the timescale of their transfer to the 22-pole ion trap where they are cooled. Moreover, the conditions we employ for recording the spectrum of Fig. 5.9b are “harsher” than those of spectrum of Fig. 5.9c (no FAIMS), and still the amount of cross-conformer contamination is negligible. This means peaks of conformational family B appear in this spectrum of Fig. 5.9c because conformers belonging to family B are initially produced in the electrosprayed ion population and not because of isomerization from family A.



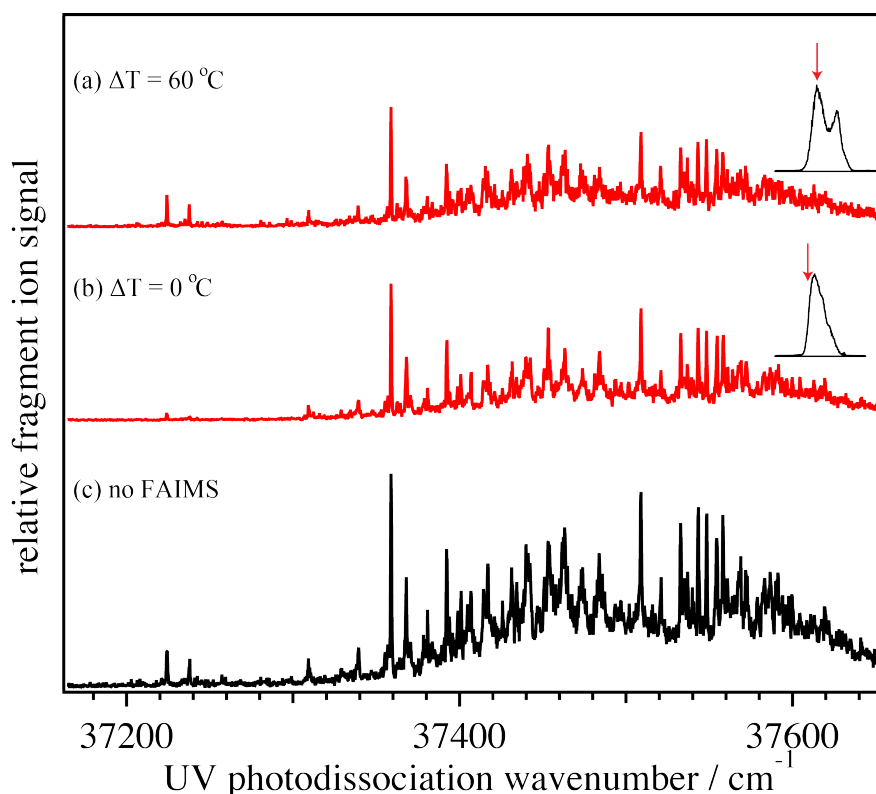


**Figure 5.9.** Electronic photofragment excitation spectra of  $[\text{bk}+2\text{H}]^{2+}$  obtained (a) conformational family A selected using FAIMS with  $\Delta T = 60\text{ }^{\circ}\text{C}$ ; (b) conformational family A selected using FAIMS with  $\Delta T = 0\text{ }^{\circ}\text{C}$ ; (c) without FAIMS separation and under very gentle conditions in the mass spectrometer.

## 5.5. Quasi-equilibrium distribution in the gas phase

To examine conformational isomerization further, we investigated the effect of annealing the FAIMS-selected ion population by collisionally activating the ions followed by cooling to 10 K in our 22-pole ion trap. The ion activation step is achieved by changing the potential difference between the capillary exit (L1) and the skimmer (see Fig. 2.1), which changes the collisional energy of the ions as they enter the hexapole ion trap. Figure 5.10 shows UV spectra of the ion population after they have been cooled and trapped in our 22-pole as a function of increased injection energy into the hexapole. The left and right panels of Fig. 5.10 show spectra when only conformational family A or B respectively is introduced into the mass spectrometer. The selection of conformational families is performed with a temperature gradient established between the FAIMS electrodes, which causes a small amount of contamination of conformer family B into A

even at low injection voltage, as is evident from spectrum Fig 5.11d (left panel), where characteristic peaks of family B appear at low intensity.

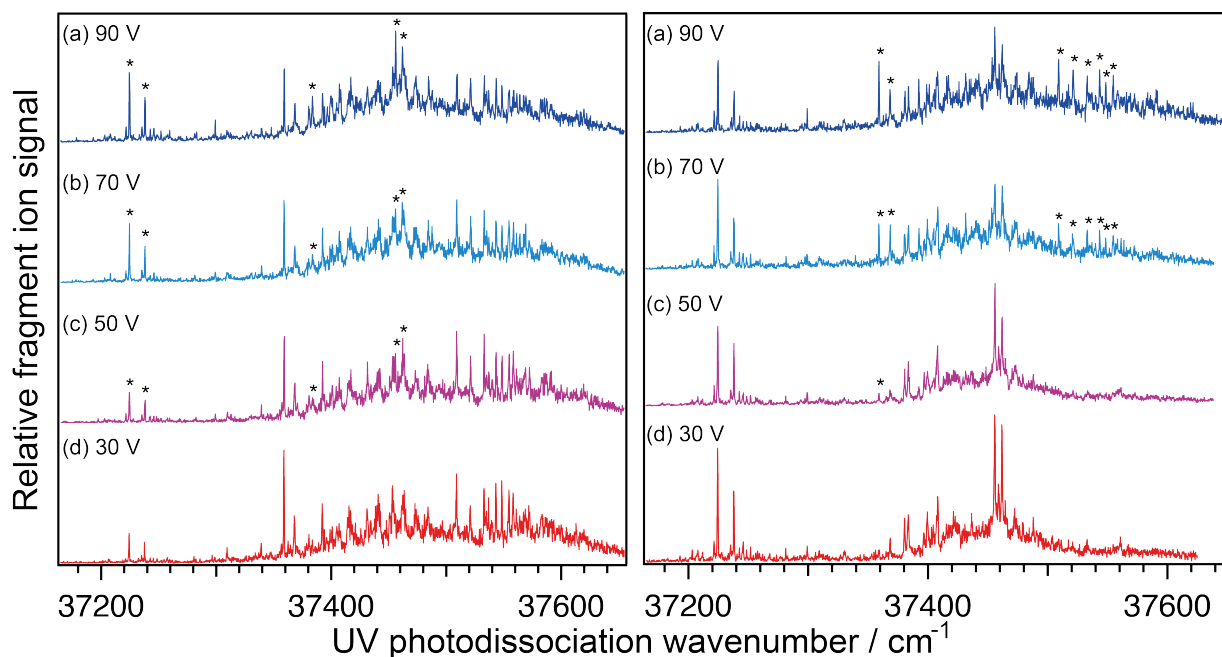


**Figure 5.10.** Electronic photofragment excitation spectra of  $[bk+2H]^{2+}$  recorded as a function of the injection voltage into the hexapole ion trap. One conformational family is initially introduced into the mass spectrometer: left--conformational family A; right--conformational family B.

As one can clearly see in Fig. 5.10, for each conformational family, the characteristic peaks of the other family, indicated by asterisks, increase in intensity upon increase of the injection energy. This can only happen if an increased fraction of the FAIMS-selected population is excited above the barrier to isomerization from one family to the other, so that when the population is quenched in the hexapole or the cold ion trap, a new distribution is formed. At high injection energy the spectra of the relaxed population of ions in the cold trap are almost indistinguishable (Fig. 5.10a, left and right panels). This means that the same conformational distribution of ions is formed, irrespective of which conformational family we introduce into the mass spectrometer. This is indicative of a quasi-equilibrium that is established between the two conformational families.<sup>29</sup> We use the term quasi-equilibrium because the temperature at which the starting structures are heated during the collisional activation is unknown. Figure 5.11 compares the quasi-equilibrium conformational distribution (Fig. 5.11a) with the electrospray source distribution, when no conformational separation is used (Fig 5.11b). It is clear that the two distributions are different.

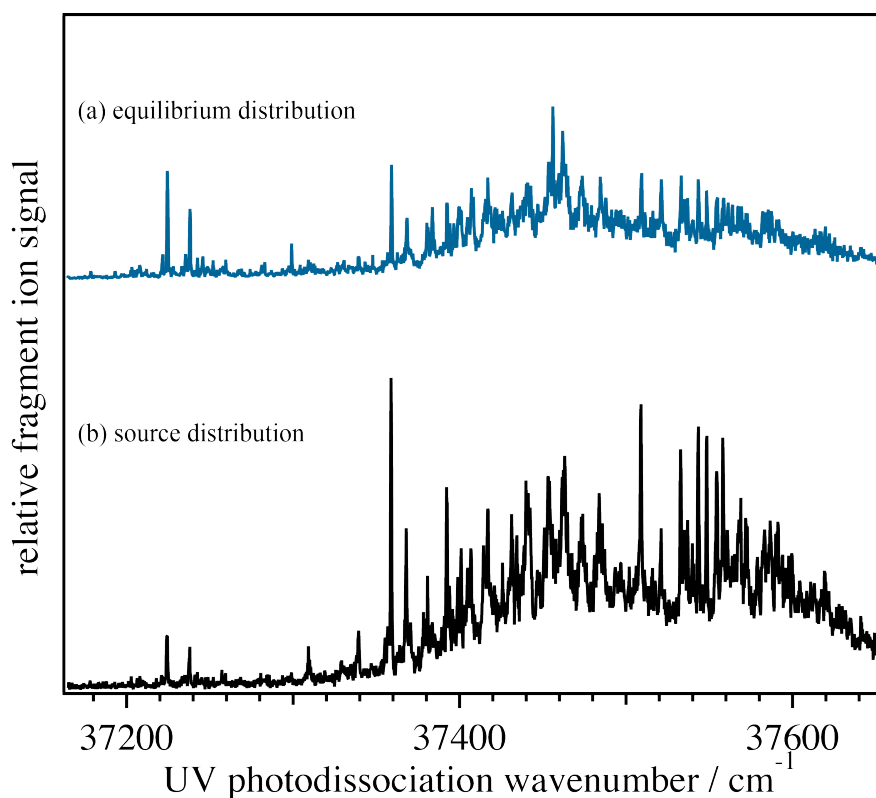


**Figure 5.11.** Electronic photofragment excitation spectra of  $[bk+2H]^{2+}$  that reflect: (a) the quasi-equilibrium conformational distribution in the gas phase; (b) the conformational distribution formed at the ESI source.

## 5.6. Kinetic-trapping of ions and implications concerning their solution structure

Recently, Pierson et al. investigated the dynamics of conformational isomerization of  $[bk+3H]^{3+}$  using two-dimensional ion mobility spectrometry in an IMS-IMS-MS configuration,<sup>29</sup> with an activation region in between the two mobility stages. They were able to separate six conformers of the  $[bk+3H]^{3+}$  ion in the first stage and then selectively activate each of them and measure the subsequent distribution of conformers in the second stage as a function of the activation voltage. They demonstrate that at high activation voltage the distribution is always the same, independent of the starting structure,<sup>29</sup> indicating that a quasi-equilibrium is established between the conformers at high energies. They also observe that the gas-phase quasi-equilibrium distribution of  $[bk+3H]^{3+}$  conformers is different than the distribution initially produced by the electrospray source.<sup>29</sup>

In our experiment we use a two-dimensional technique to study the same phenomenon but, instead of using a stage of IMS as a second dimension to probe the emerging distribution after ion activation, we use electronic photofragment spectroscopy. It seems that for both  $[\text{bk}+2\text{H}]^{2+}$ , as described here, as well as for  $[\text{bk}+3\text{H}]^{3+}$ , as shown in the work of Pierson et al.,<sup>29</sup> electrospray produces a conformational distribution of ions that are kinetically trapped. Providing energy to the system induces isomerization such that the conformer populations approach gas-phase equilibrium.

There is a growing amount of evidence which shows that electrospray ionization (ESI) can produce, under certain conditions, gas phase biomolecules in metastable structures.<sup>29-32</sup> These structures have limited lifetime before they isomerize into more stable conformations in the absence of solvent.<sup>33</sup> This can range from several milliseconds<sup>30,34,35</sup> to several seconds.<sup>36</sup> In any case, it seems that for certain systems the produced structures do not isomerize on the experimental time scale unless their internal energy is increased. Since these kinetically trapped structures are directly produced from the solution and are not equilibrated gas phase structures, they may be closely related to the solution phase conformations.<sup>19,20</sup> In favor of this argument are experiments that show, in many cases, that the nascent, gas-phase conformational distribution depends upon the solvent composition used in the electrospray process.<sup>20,37,38</sup> Moreover, cross-sections determined for low charge states of several proteins are similar to what one would calculate for the crystal or for the native structure in solution.<sup>19,39,40</sup> While this does not prove that the electrosprayed distribution is the same as that in solution, it clearly demonstrates that the gas-phase distribution retains a memory of the solution conditions from which it was produced. The mechanism of electrospray formation of these kinetically trapped ions is not clear, although there is evidence that large multiply charged species like proteins are produced *via* the charge residue model.<sup>41</sup> In this model the naked ion is formed by sequential evaporation of solvent molecules.<sup>42-44</sup> This may lead to an evaporating cooling mechanism where conformations that exist in solution are “frozen” and thus preserved during the desolvation process.<sup>45</sup> If this interpretation is true, there can be important information in the conformational distribution initially produced by electrospray and probing the ions right after their production might provide insight into the structures that they adopt in solution.

## 5.7. Conclusions

In this chapter we demonstrated how the conformational distribution of  $[\text{bk}+2\text{H}]^{2+}$  can be used as a sensitive probe of heating processes that may occur after its production by electrospray. By changing some parameters during the FAIMS separation while observing the resulting conformational distribution, we investigated the origin of the cross-conformer contamination that we observed in a family-selected electronic spectrum of  $[\text{bk}+2\text{H}]^{2+}$ . We also used FAIMS to select one conformational family of  $[\text{bk}+2\text{H}]^{2+}$  at a time and collisionally activate the ion population in our mass spectrometer. Upon intense collisional activation both families produce the same conformational distribution, indicating that gas phase quasi-equilibrium is established. This is different from the conformational distribution as it is produced by the source indicating that some structures are produced in metastable states.

On the other hand, the fact that the initial conformational distribution of electrosprayed ions can be different from the gas-phase quasi-equilibrium distribution is highly significant for studies of biological molecules in the gas-phase. The use of vibrational spectroscopy to determine ion structure is accomplished by comparing a measured infrared spectrum with a calculated one.<sup>11</sup> To determine the latter, a conformational search is typically performed using classical force fields, and then the energies of the most stable structures are refined using density functional theory. One then calculates the spectra of the lowest energy structures and compares them to experiment. Since the calculations are done for isolated molecules, the structures determined by this approach should be the lowest energy gas phase structures. However, if the experiments do not produce the lowest energy gas-phase structures, this can inhibit finding a match between calculations and experiment and lead to erroneous conclusions. From an experimental point of view, this problem can be overcome by annealing the initially formed conformer distribution as described in both our work here on  $[\text{bk}+2\text{H}]^{2+}$ , as well as that of Pierson et al. for  $[\text{bk}+3\text{H}]^{3+}$ .<sup>29</sup>

By adding a spectroscopic dimension to ion mobility, our approach should help elucidate the connection between gas-phase and solution-phase structures. The extreme sensitivity of our conformer-specific, IR-UV spectroscopic techniques puts high demands on the accuracy of calculated structures and spectra.<sup>46</sup> However, Svendsen *et. al.* have not yet succeeded in obtaining an acceptable match with measured vibrational spectra of  $[\text{bk}+2\text{H}]^{2+}$  conformers.<sup>4</sup> Nevertheless, high-resolution spectroscopy will be key to understanding the connection between the gas-phase and solution.

## 5.8. References

- (1) Papadopoulos, G.; Svendsen, A.; Boyarkin, O.; Rizzo, T. *J. Am. Soc. Mass Spectrom.* **2012**, *23*, 1173.
- (2) Cann, J. R.; Stewart, J. M.; Matsueda, G. R. *Biochemistry* **1973**, *12*, 3780.
- (3) Purves, W. R.; Barnett, A. D.; Ells, B.; Guevremont, R. *Rapid Commun. Mass Spectrom.* **2001**, *15*, 1453.
- (4) Svendsen, A.; Boyarkin, O. V.; Rizzo, T. R. *in preparation* **2012**.
- (5) Shvartsburg, A. A.; Li, F.; Tang, K.; Smith, R. D. *Anal. Chem.* **2007**, *79*, 1523.
- (6) Barnett, D. A.; Belford, M.; Dunyach, J.-J.; Purves, R. W. *J. Am. Soc. Mass Spectrom.* **2007**, *18*, 1653.
- (7) Robinson, E. W.; Shvartsburg, A. A.; Tang, K.; Smith, R. D. *Anal. Chem.* **2008**, *80*, 7508.
- (8) Aksenov, A. A.; Kapron, T. *J. Rapid Commun. Mass Spectrom.* **2010**, *24*, 1392.
- (9) Shvartsburg, A. A. *Differential Ion Mobility Spectrometry*; CRC Press: Boca Raton FL, 2009.
- (10) Stearns, J. A.; Mercier, S.; Seaiby, C.; Guidi, M.; Boyarkin, O. V.; Rizzo, T. R. *J. Am. Chem. Soc.* **2007**, *129*, 11814.
- (11) Rizzo, T. R.; Stearns, J. A.; Boyarkin, O. V. *Int. Rev. Phys. Chem.* **2009**, *28*, 481
- (12) Mercier, S. R.; Boyarkin, O. V.; Kamariotis, A.; Guglielmi, M.; Tavernelli, I.; Cascella, M.; Rothlisberger, U.; Rizzo, T. R. *J. Am. Chem. Soc.* **2006**, *128*, 16938.
- (13) Jarrold, M. F.; Honea, E. C. *J. Am. Chem. Soc.* **1992**, *114*, 459.
- (14) Hunter, J. M.; Fye, J. L.; Jarrold, M. F. *J. Chem. Phys.* **1993**, *99*, 1785.
- (15) Shelimov, K. B.; Jarrold, M. F. *J. Am. Chem. Soc.* **1996**, *118*, 10313.
- (16) Clemmer, D. E.; Jarrold, M. F. *J. Mass Spectrom.* **1997**, *32*, 577.
- (17) Shvartsburg, A. A.; Li, F.; Tang, K.; Smith, R. D. *Anal. Chem.* **2006**, *78*, 3706.
- (18) Papadopoulos, G.; Svendsen, A.; Boyarkin, O. V.; Rizzo, T. R. *Faraday Discuss.* **2011**, *150*, 243.
- (19) Wyttenbach, T.; Bowers, M. T. *J. Phys. Chem. B* **2011**, *115*, 12266.
- (20) Pierson, N. A.; Chen, L.; Valentine, S. J.; Russell, D. H.; Clemmer, D. E. *J. Am. Chem. Soc.* **2011**, *133*, 13810.
- (21) Mason, E. A.; McDaniel, E. W. *Transport Properties Of Ions In Gases*; Wiley: New York, 1988.
- (22) Barnett, D. A.; Ouellette, R. J. *Rapid Commun. Mass Spectrom.* **2011**, *25*, 1959.
- (23) Guevremont, R.; Purves, R. *J. Am. Soc. Mass Spectrom.* **2005**, *16*, 349.
- (24) Shvartsburg, A. A.; Tang, K.; Smith, R. D. *J. Am. Soc. Mass Spectrom.* **2005**, *16*, 2.
- (25) Shvartsburg, A. A.; Tang, K.; Smith, R. D. *Anal. Chem.* **2010**, *82*, 32.
- (26) Purves, R. W.; Barnett, D. A.; Ells, B.; Guevremont, R. *J. Am. Soc. Mass Spectrom.* **2001**, *12*, 894.
- (27) Shvartsburg, A. A.; Danielson, W. F.; Smith, R. D. *Anal. Chem.* **2010**, *82*, 2456.
- (28) Baker, E. S.; Clowers, B. H.; Li, F.; Tang, K.; Tolmachev, A. V.; Prior, D. C.; Belov, M. E.; Smith, R. D. *J. Am. Soc. Mass Spectrom.* **2007**, *18*, 1176.
- (29) Pierson, N. A.; Valentine, S. J.; Clemmer, D. E. *J. Phys. Chem. B* **2010**, *114*, 7777.
- (30) Koeniger, S. L.; Merenbloom, S. I.; Clemmer, D. E. *J. Phys. Chem. B* **2006**, *110*, 7017.
- (31) Koeniger, S.; Clemmer, D. *J. Am. Soc. Mass Spectrom.* **2007**, *18*, 322.
- (32) van der Spoel, D.; Marklund, E. G.; Larsson, D. S. D.; Caleman, C. *Macromol. Biosci.* **2011**, *11*, 50.

- (33) Breuker, K.; McLafferty, F. W. *Proc. Natl. Acad. Sci. U. S. A.* **2008**, *105*, 18145.
- (34) Myung, S.; Badman, E. R.; Lee, Y. J.; Clemmer, D. E. *J. Phys. Chem. A* **2002**, *106*, 9976.
- (35) Badman, E. R.; Hoaglund-Hyzer, C. S.; Clemmer, D. E. *Anal. Chem.* **2001**, *73*, 6000.
- (36) Breuker, K.; Brüscheiler, S.; Tollinger, M. *Angew. Chem., Int. Ed.* **2011**, *50*, 873.
- (37) Li, J.; Taraszka, J. A.; Counterman, A. E.; Clemmer, D. E. *Int. J. Mass Spectrom.* **1999**, *185-187*, 37.
- (38) Purves, R. W.; Barnett, D. A.; Guevremont, R. *Int. J. Mass Spectrom.* **2000**, *197*, 163.
- (39) Shelimov, K. B.; Clemmer, D. E.; Hudgins, R. R.; Jarrold, M. F. *J. Am. Chem. Soc.* **1997**, *119*, 2240.
- (40) Valentine, S. J.; Anderson, J. G.; Ellington, A. D.; Clemmer, D. E. *J. Phys. Chem. B* **1997**, *101*, 3891.
- (41) Fernandez de la Mora, J. *Anal. Chim. Acta* **2000**, *406*, 93.
- (42) Dole, M.; Mack, L. L.; Hines, R. L.; Mobley, R. C.; Ferguson, L. D.; Alice, M. B. *J. Chem. Phys.* **1968**, *49*, 2240.
- (43) Schmelzeisen-Redeker, G.; Bütfering, L.; Röllgen, F. W. *Int. J. Mass Spectrom. Ion Processes* **1989**, *90*, 139.
- (44) Rohner, T. C.; Lion, N.; Girault, H. H. *Phys. Chem. Chem. Phys.* **2004**, *6*, 3056.
- (45) Lee, S.-W.; Freivogel, P.; Schindler, T.; Beauchamp, J. L. *J. Am. Chem. Soc.* **1998**, *120*, 11758.
- (46) Nagornova, N. S.; Guglielmi, M.; Doemer, M.; Tavernelli, I.; Rothlisberger, U.; Rizzo, T. R.; Boyarkin, O. V. *Angew. Chem., Int. Ed.* **2011**, *50*, 5383.





# Electronic photofragment spectroscopy of cold ubiquitin

In this chapter we show the potential but also the limitations of our spectroscopic approach in investigating small, naturally occurring proteins. First, we describe the complications that we face in the application of our spectroscopic technique to systems of increasing size. Then we move on to apply it to ubiquitin, a protein of 76 amino acids. We present electronic photofragment spectra of various protonation states of ubiquitin and we compare our results to those acquired by other techniques, mainly ion mobility spectrometry. Although some of the results obtained may be important in characterizing ubiquitin in the gas phase, these experiments are at an early stage and the application of photofragment spectroscopy on cold proteins needs more investigation.

## 6.1. Introduction

There are many obstacles we are confronted with in the application of our technique to study increasingly large and complicated biomolecular ions. One of them is the requirement that the electronically excited molecules have to dissociate in order for us to observe absorption. If the dissociation happens on the ground electronic state after internal conversion from the excited state, the rate of the dissociation is expected to decrease with increasing the size of the molecule.<sup>1,2</sup> The timescale of the dissociation, then, becomes a limiting factor in the application of our technique. We can partly overcome this hurdle by further exciting the ions with a use of a CO<sub>2</sub> laser in order to increase their internal energy and thus increase their dissociation rate.<sup>3</sup> On the other hand, if dissociation happens on an excited electronic surface, it may be possible to observe fragmentation immediately after absorption of a photon, irrespective of the size of the molecule.

If we achieve laser-induced fragmentation and record a photofragment spectrum of a large biomolecule, the complexity of the spectrum might prohibit us from extracting any information. We have described the possible sources of spectral congestion in Chapter 4. However, this

discussion concerned biomolecules of a few amino acids that can effectively be cooled in our ion trap ( $\sim 10$  K).<sup>4-8</sup> However, for the study of larger systems, the question concerning our technique is: as the size of ions is increased, to what extent buffer gas cooling can remove their internal energy, on a given time window? Larger ions may have increased internal temperature at the moment of laser interrogation, which may be a problem for two reasons. First, large and flexible ions can adopt a multitude of structures, the number of which increases with temperature. Individual spectra of all those conformers will contribute to the spectrum, leading to its congestion. Second, the internal temperature of an ion influences the intensity of hot bands, which is another source of complexity and congestion of the spectrum. Thus, low internal temperature of the ions is essential for our approach.

On the other hand, even at very low internal ionic temperatures, the problem of conformational heterogeneity remains, depending on the cooling rate in the ion trap. As we showed in Chapters 4 and 5, the electronic spectrum of cold bradykinin is congested because of this reason. In this case, however, individual transitions could still be identified and the spectral congestion did not prohibit the application of IR-UV double resonance spectroscopy.<sup>9</sup> Nevertheless, for larger and more complex biomolecules the question that rises is: at what molecular size conformational heterogeneity will cause the spectrum of a cold molecule to be so congested that it will be mandatory to use ion mobility techniques in order to record simplified spectra of selected conformational types?

In this chapter we present electronic photofragment spectra of a small protein. In doing so, we also try to answer the above questions concerning the application of our technique to the study of biomolecules of increased size. The molecule that we use as a test is ubiquitin and the reasons for this choice are presented below.

## 6.2. Ubiquitin and its structure in the gas phase

Ubiquitin (ub) is a small protein of 76 amino acids that has a molecular weight of 8565.<sup>10</sup> It is found in all eukaryotic living cells (hence the name ubiquitin) and its primary structure is highly conserved across a number of completely different organisms.<sup>11,12</sup> Physiologically, ubiquitin plays a central role in protein regulation in the cell.<sup>13</sup> In the ubiquitin proteasome pathway, it tags other proteins by covalently binding to them (ubiquitination), starting a cascade of events that leads to their degradation.<sup>14,15</sup> Ubiquitin has a highly compact crystal structure and native solution

structure (called “the *N* state”) determined by x-ray diffraction and NMR respectively.<sup>10,12,16,17</sup> It consists of a five-stranded  $\beta$ -sheet, two helical segments (a larger one of an  $\alpha$ -helix and a smaller one of a  $3_{10}$  helix) and seven turns.<sup>12,17</sup> In denaturing solutions it adopts a partially unfolded state (called “the *A* state”) which is also well characterized.<sup>18,19</sup> It consists of an antiparallel  $\beta$ -sheet and a helix at the N-terminus, showing that elements of the native state survive in such conditions. On the other hand, the C-terminus, being rich in  $\beta$ -strand in the native form, undergoes a methanol-induced transition that stabilizes an  $\alpha$ -helix for the residues 39-72.<sup>19</sup>

Ubiquitin contains 12 basic residues (7 lysines, 4 arginines and 1 histidine) plus the N terminal amino group that can be protonated, and so it can exist in several charge states in the gas phase. Extensive studies of selected charge states have been performed by mass spectrometry (MS) in combination with Ion Mobility Spectrometry (IMS),<sup>20-28</sup> H/D exchange,<sup>27,29,30</sup> Electron Capture Dissociation (ECD),<sup>31,32</sup> Field Asymmetric-waveform Ion Mobility Spectrometry (FAIMS)<sup>33-36</sup> and spectroscopy.<sup>37,38</sup> Its dissociation behavior under a variety of activating methods has also been investigated.<sup>39-42</sup> Most of the above studies revealed a number of structural isomers coexisting for each charge state. In addition, since these methods probe different physical properties, their separation capabilities are complementary (i.e., some conformers inseparable by one method are readily separated by another). This was exploited in two-dimensional separations employing combinations of these techniques.<sup>36,43,44</sup>

IMS-MS studies of selected charge states ranging from  $[\text{ub} + 6\text{H}]^{6+}$  to  $[\text{ub} + 13\text{H}]^{13+}$  revealed arrival time distributions spanning compact, partially unfolded and elongated structures.<sup>20,21</sup> The distribution of features for each conformational type were broad, indicating the presence of different conformers with very similar cross sections or interconversion between them that occurs on the time scale of the separation.<sup>21</sup> These studies showed that the collision cross-section correlates with the charge state of the ion.<sup>20</sup> The lower charge states appear to be dominated by native-like compact conformations while the higher charge states adopt more open and extended structures. This was explained purely electrostatically -- the increased coulombic repulsion between charges drives higher charge states to adopt more open conformations. Ions of intermediate charge states appear to populate more than one conformational type.

In FAIMS studies of ubiquitin, Guevremont and coworkers found that higher charge states populate one conformational type, while lower charge states several.<sup>34</sup> They also performed ion retarding potential measurements on selected conformers in a triple quadrupole mass spectrometer in order to measure collision cross-sections for each conformer.<sup>33</sup> They were able to make direct comparison between FAIMS and IMS studies of this system, showing that the two techniques can identify the same conformational types with a remarkably good agreement in the values of cross-

sections that each technique provides.<sup>33</sup> Moreover, FAIMS resolved some additional conformers having identical cross-sections.<sup>33</sup>

Contrary to other proteins,<sup>45</sup> ubiquitin does not possess structure stabilizing disulfide bonds, and this makes it richer in the conformational types it can adopt but also more amenable to structural changes after its production in the gas phase. It was shown that upon increase of the injection voltage into the drift tube, the compact structures appear to unfold.<sup>20,46</sup> The same was shown for compact conformers separated by FAIMS that were subsequently collisionally activated.<sup>33</sup> Increased temperature of the capillary at the vacuum interface had the same effect.<sup>21</sup>

The structural evolution of compact conformers after their formation in the gas phase was also investigated with IMS.<sup>23</sup> In this approach, ions were stored for variable amounts of time in an ion trap before being injected in a drift tube for structural analysis. In the case of  $[\text{ub} + 6\text{H}]^{6+}$ , the compact structures seem to be stable over the 30s of the trapping time.<sup>23</sup> On the other hand,  $[\text{ub} + 8\text{H}]^{8+}$  charge state unfolds rapidly into two elongated structures. These persist for 30s and may correlate with the two structures of the same species observed in an Fourier transform ion cyclotron resonance mass spectrometer (FTICR) after 1h of trapping.<sup>47</sup> For the  $[\text{ub} + 7\text{H}]^{7+}$  charge state, two types of compact structures were identified having similar cross sections but differing in their rates of unfolding.<sup>23</sup> However, both of the compact structures (or families of structures) appeared to be stable for the first ~30 ms of trapping.<sup>23</sup> More recent results suggest that the lifetime of these structures may be even longer.<sup>28</sup>

In some initial IMS and FAIMS studies, the electrospray solvent composition seemed to have an effect on the structural types produced,<sup>21,34</sup> indicating either that some memory of the solvent structure is retained in the gas phase or that different solvents influence the production of ions during the electrospray process and thereby the resulting conformational distribution. However, Bowers and coworkers recently showed that the arrival time distributions of ubiquitin ions sprayed from a variety of different solutions do not differ substantially.<sup>28</sup> They proposed that the solution structure is preserved upon desolvation and that the number of the charges that the ions pick up during the electrospray process depends on the degree of unfolding in solution.

Recently, Clemmer and coworkers introduced multi-dimensional ion mobility separations<sup>24-26,48-50</sup> in which an ion gate at the end of a drift tube can select a slice out of a broad arrival time distribution and inject it to a second drift tube for further separation.<sup>24,26</sup> The resulting conformational transitions can be followed in a “state-to-state” manner as a function of the injection energy into the second drift tube.<sup>26,51</sup> In the case of  $[\text{ub} + 7\text{H}]^{7+}$ , the arrival time shows a continuous distribution that is dominated mainly by compact structures but also contains some partially folded structures.<sup>21,23,26</sup> Narrow slices taken across the entire broad distribution in the

drift tube retained their width during their drift through the second tube when injected at low energies.<sup>24</sup> This indicated that many unresolved conformers with similar cross-sections are responsible for the large width of the initial distribution, and that these conformations are stable and do not interconvert on the timescale of the second separation (~20ms).<sup>24</sup> On the other hand, when different slices of compact conformers were injected into the second IMS with increased energy, unfolding occurred for all of them, but the resulting distributions were slightly different.<sup>25</sup> This indicated that some structural elements are conserved in the unfolding process.<sup>25</sup>

Clemmer and coworkers carried out analogous experiments for the high charge states of ubiquitin.<sup>26</sup> Four resolvable elongated states were found for the +12 state in agreement with earlier FAIMS measurements of the same system.<sup>35</sup> Two conformations were identified for the +11 with a broad signal of unresolved structures, and only one for the +13 state.<sup>26</sup> Some parts from the initial distributions were shown to belong to conformers that are stable on the time scale of their travel through the second drift tube. Upon collisional activation, structural transitions were observed indicating that there is a number of elongated states initially produced that are kinetically trapped.<sup>26</sup>

Spectroscopic studies of gas phase ubiquitin are limited.<sup>37,38</sup> McLafferty and co workers have performed infrared multiple photon dissociation spectroscopy on ECD-reduced [ub + zH]<sup>(z-1)+</sup> in a Fourier transform ion cyclotron resonance mass spectrometer (FT-ICR).<sup>37</sup> They found spectroscopic signatures of hydrogen bonding that indicate the presence of tertiary structure for ions of  $6 < z < 9$ .<sup>37</sup> However, their experiment involves timescales of several seconds during which drastic structural changes can happen.<sup>52</sup> Dugourd and coworkers have introduced a technique that can be used to obtain electronic spectra of large deprotonated proteins in the gas phase, and applied it to ubiquitin, among other proteins.<sup>2,38</sup> This can be used as an alternative to photofragmentation spectroscopy, and it involves monitoring of the photoinduced electron detachment channel as a function of the laser excitation wavelength.<sup>38</sup> However, this technique has been applied on room-temperature species where a multitude of conformers are expected to be present. Moreover, photodetachment may lead to an ultrafast deactivation of the excited state that reduces its lifetime and broadens the transitions.

From the above we conclude that ubiquitin is a well-characterized small protein that shows a wealth of conformations for each charge state, which is typical for small proteins of this size. Our spectroscopic techniques are put to the test by recording electronic photofragment spectra of cold ubiquitin. These experiments have the potential to provide spectroscopic signatures of structural changes in the gas phase by recording spectra as a function of the injection voltage into our mass spectrometer. On the other hand, some structures of this complex system are produced in

metastable, kinetically trapped states that persist for several milliseconds, making it an ideal system for future combinations of ion mobility spectrometry and spectroscopy. Moreover, our spectroscopic technique can provide detailed information on the gas phase structure of biomolecular ions, which can potentially shed some light on the question of whether kinetically trapped ions do indeed resemble solution phase structures or not.

### 6.3. Experimental details

For the experiments that we describe in this chapter we used nano electrospray ionization (nESI) to produce ubiquitin ions in the gas phase. Bovine ubiquitin was purchased by Sigma Aldrich. For the production of the low charge states (+6 to +9) we used a 10 $\mu$ M solution of 50:50 (% volume) water:acetonitrile and for the production of high charge states (+8 to +13) a 10 $\mu$ M solution of 49:49:2 (% volume) water:acetonitrile:acetic acid. The laser setup was the same as described in Chapter 4. For all charge states investigated, the only laser-induced fragment ions observed are those resulting from the loss of neutral phenylalanine (or tyrosine) side-chain. We vary the collisional energy of the ions and their injection energy into the hexapole ion trap by tuning voltage drop between the exit of the capillary (L1) and the skimmer.

### 6.4. nESI mass spectra of ubiquitin

Figure 6.1 shows nano electrospray mass spectra of bovine ubiquitin. Fig. 6.1a and 6.1b were recorded using a 50:50 (% volume) water:acetonitrile solution while for Fig. 6.1c 2% of acetic acid was added.

In the spectrum of Fig. 6.1c, the charge state distribution corresponds to ubiquitin with an excess of 8 to 13 protons,  $[\text{ub} + z\text{H}]^{z+}$  ( $z=8-13$ ), peaking at  $z=12$ . It is in agreement with the ESI spectra published in the literature using the same solution with acid,<sup>20,21</sup> and it is virtually the same when methanol is used instead of acetonitrile.<sup>28,53</sup> In the spectra of Fig. 6.1a and 6.1b, where we use a solution where no acid is added, the distribution displays only the lower charge states. The peaks correspond to ubiquitin that accommodates 6 to 9 protons,  $[\text{ub} + z\text{H}]^{z+}$  ( $z=6-9$ ), peaking at  $z=7$  and  $z=8$ , for traces (a) and (b) respectively. These spectra are similar to ESI mass spectra

from aqueous or water:methanol solutions.<sup>28</sup> The voltage we apply on the nanospray needle is higher in trace (b) than in trace (a). This seems to shift slightly the distribution to higher charge states, indicating that the source conditions can be adjusted to optimize for one charge state over the others, within a given charge state distribution.

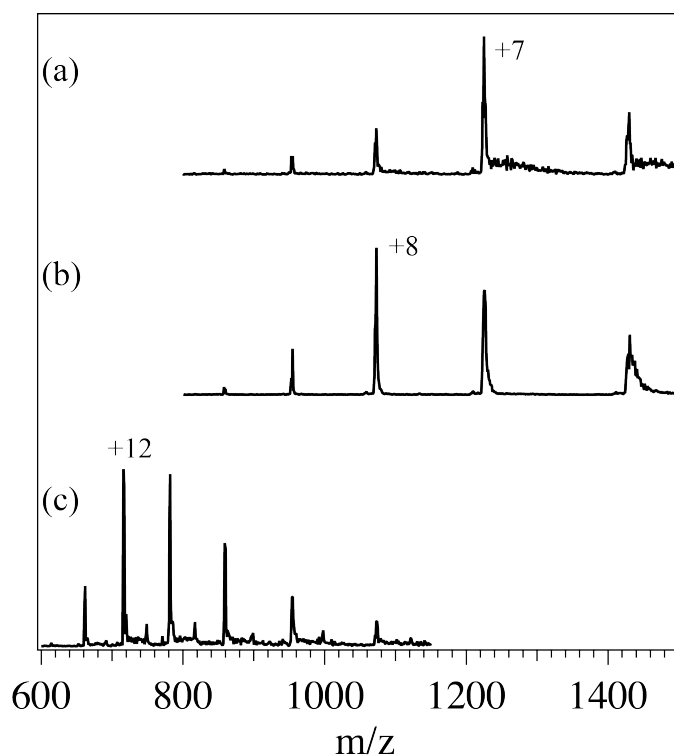


**Figure 6.1.** Nano electrospray ionization mass spectra of bovine ubiquitin sprayed out of a: (a) and (b) 50:50 water:acetonitrile solution; (c) 49:49:2 water:acetonitrile:acetic acid of 10  $\mu$ M in ubiquitin. Trace (b) is recorded with a higher voltage applied on the nanospray needle than trace (a).

## 6.5. Photofragmentation spectra of ubiquitin in phe and tyr absorption regions

Having shown that we can produce various charge states of ubiquitin in the gas phase, we go on to select one of them, trap the ions in our cold 22-pole and irradiate them with lasers to see if we can produce a fragment and thus record a photofragment spectrum. We select the  $[\text{ub} + 12\text{H}]^{12+}$  state as a parent molecule ( $m/z$  714) and scan the UV laser in the region where the amino acid phenylalanine absorbs (ubiquitin contains two phenylalanines and one tyrosine) while detecting the fragmentation channel corresponding to loss of neutral phenylalanine side chain ( $m/z$  707) as a potential laser induced fragment signal. Based on our experience with other molecules,

we anticipate the possibility of loss of the aromatic side chain, since fragmentation seems to proceed from an electronically excited state<sup>54-57</sup> and may occur independent of the size of the molecule. As in the case of bradykinin shown in Chapters 4 and 5, a CO<sub>2</sub> laser is used to enhance the fragmentation.

Figure 6.2 displays the ultraviolet electronic photofragment mass spectrum of [ub + 12H]<sup>12+</sup> after it has been cooled in our 22-pole ion trap. The spectrum consists of a number of sharp features that sit on a broad background. The sharp features indicate that the [ub + 12H]<sup>12+</sup> ions are cooled effectively in collisions with He upon trapping in the cold trap. The width of the main peak at 37504 cm<sup>-1</sup> is 2.5 cm<sup>-1</sup>, as measured between the violet bars shown in Fig. 6.2.

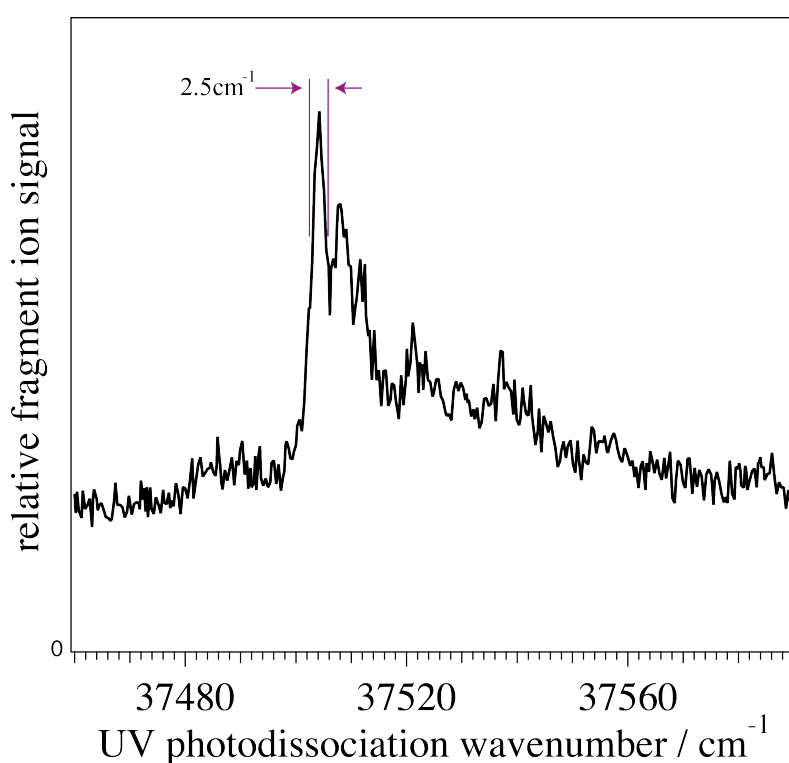


**Figure 6.2.** Electronic photofragment excitation spectrum of [ub + 12H]<sup>12+</sup> (m/z 714) recorded by scanning the UV laser monitoring the fragment that results from loss of neutral phe side chain loss (m/z 707).

The broad photofragmentation signal of Fig 6.2 comes from vibronic activity of the tyrosine amino acid, as shown before in our lab for molecules that possess both aromatic amino acids.<sup>8</sup> The band origin of electronic absorption of bare, cold tyrosine occurs at ~ 35080 cm<sup>-1</sup>, while that of phenylalanine is at ~ 37520 cm<sup>-1</sup>.<sup>58,59</sup> The electronic spectra of both amino acids exhibit sharp features, with that of tyrosine being more congested.<sup>59</sup> For small cold peptides of seven amino acids that contain both chromophores, the spectrum at the region ~ 37500 cm<sup>-1</sup> shows sharp lines from transitions of phenylalanine that rest on a broad photofragment signal coming from vibronic



activity of the tyrosine chromophore.<sup>8</sup> The spectrum we acquire for  $[\text{ub} + 12\text{H}]^{12+}$  (Fig. 6.2) shows similar characteristics.

We also emphasize that the sharp, intense peak in the spectrum of Fig. 6.2 at  $37504\text{ cm}^{-1}$  is very close to the band origin of cold, bare phenylalanine ( $37520\text{ cm}^{-1}$ ).<sup>59</sup> This indicates that the phenylalanine that is responsible for these transitions in ubiquitin has little interaction with its surroundings, suggesting that it may be a “surface” residue rather than embedded inside the protein edifice.

To investigate if laser irradiation  $[\text{ub} + 12\text{H}]^{12+}$  ions produces additional fragments, we recorded a photofragment mass spectrum, shown in Fig. 6.3. The black trace of Fig. 6.3 is recorded without laser irradiation of the trapped ions. The red trace is recorded with the lasers irradiating the ions where the UV is set at  $37504\text{ cm}^{-1}$  while the  $\text{CO}_2$  laser follows the UV pulse and assists in the fragmentation.<sup>3</sup> The blue trace is the difference spectrum that illustrates more clearly the influence of the laser irradiation. It exhibits a laser induced peak at  $\sim m/z\ 707$  that appears only as a “wing” of the parent mass ( $\sim m/z\ 715$ ) in the red trace. Apart from this fragment, we don’t observe any other photofragmentation across the range from 4 to 1000  $m/z$  units (only the range from  $\sim 560$  to 800  $m/z$  is shown in Fig. 6.3).

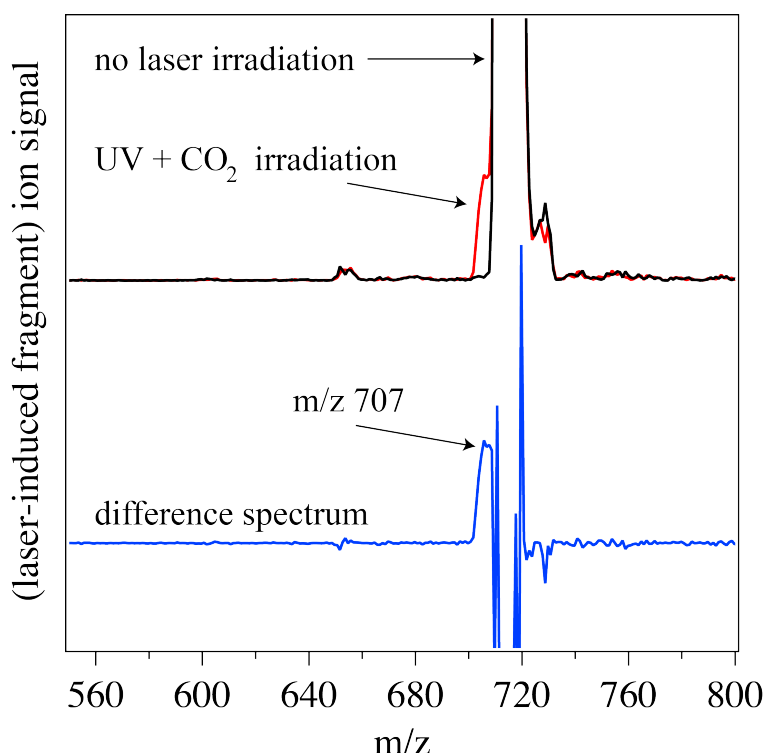


**Figure 6.3.** Fragment mass spectrum of  $[\text{ub} + 12\text{H}]^{12+}$  recorded with the lasers on (red trace), and with the lasers off (black trace) and the lasers on-lasers off difference spectrum (blue). The  $\text{CO}_2$  laser assists in the fragmentation.

We monitored this laser-induced signal ( $\sim m/z$  707) to record the spectrum of Fig. 6.2. In fact, the photofragment that we observe might as well be the one that corresponds to the side chain loss of tyr ( $\sim m/z$  706), since at this wavelength the tyrosine also absorbs the laser radiation. However, because of the high charge state of the parent, the two fragment channels are indistinguishable.

Figure 6.4 shows the electronic photofragment spectrum of  $[\text{ub} + 12\text{H}]^{12+}$  at the tyrosine band origin. The red trace of Fig. 6.4 is the spectrum acquired when the  $\text{CO}_2$  laser is used 150ns after the UV laser to enhance the fragmentation signal. The blue trace is the fragmentation signal induced by the UV laser only. Two things are apparent by inspection of the spectra of Fig. 6.4. First, that a photofragment spectrum can be recorded by using the UV laser only. This will be addressed in Section 6.6. Second, that the spectrum of  $[\text{ub} + 12\text{H}]^{12+}$  at the band origin has no resolvable features. We attribute this to the many conformations of  $[\text{ub} + 12\text{H}]^{12+}$  that are populated combined with the low frequency vibrational progressions characteristic of the electronic spectrum of tyrosine.<sup>58-60</sup>

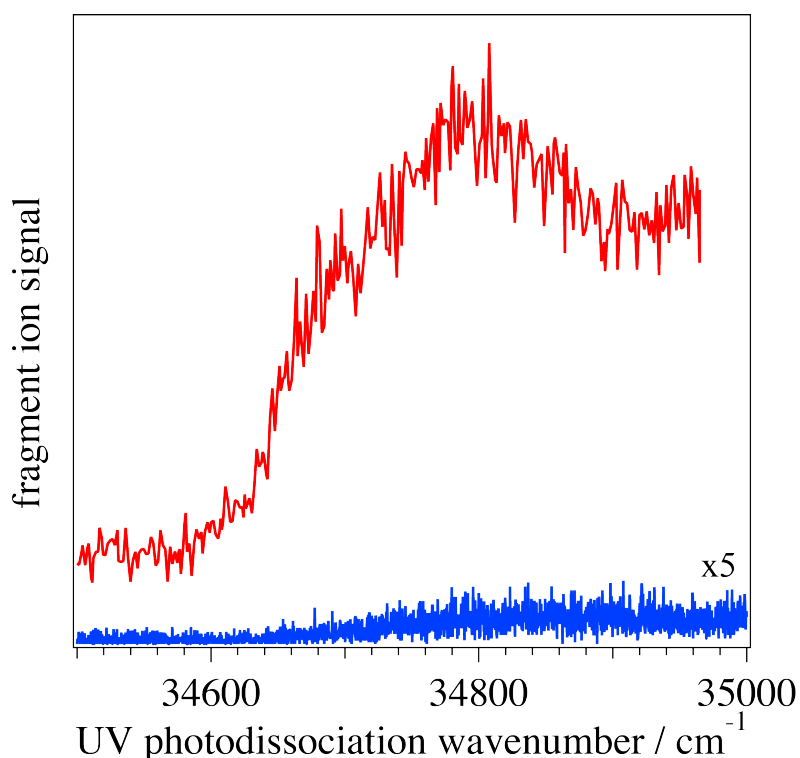


**Figure 6.4.** Electronic photofragment excitation spectrum of  $[\text{ub} + 12\text{H}]^{12+}$  by UV only fragmentation (blue trace), and by UV excitation assisted by IRMPD (red trace).

A number of elongated conformational types for the  $[\text{ub} + 12\text{H}]^{12+}$  ions have been detected by H/D exchange,<sup>29,47,61</sup> FAIMS,<sup>33-35</sup> IMS<sup>26</sup> as well as two-dimensional separations such as

FAIMS-H/D exchange<sup>36</sup> and FAIMS-IMS.<sup>43</sup> Even if the number of conformational types revealed by the above studies is 2-4, they may contain more than one conformation. In each of them, tyrosine finds itself in slightly different environments, and electronic transitions occurring at slightly different energies lead to overlapping peaks in the electronic spectrum. This, in combination with the low frequency vibrations in the electronic spectrum of tyrosine<sup>59</sup> leads to spectral congestion of such a large extent that the spectrum appears broad. If this explanation is true, the use of ion mobility techniques to separate the conformers prior to their interrogation with the lasers may simplify the spectrum in this region. For the rest of the chapter we will concentrate in the region  $\sim 37500\text{ cm}^{-1}$ , where the transitions associated with absorption from the phenylalanines are sharp.

## 6.6. UV fragmentation vs UV excitation assisted by IRMPD

Figure 6.4 shows that we can record an electronic photofragmentation spectrum of  $[\text{ub} + 12\text{H}]^{12+}$  by using only the UV laser. However, UV-only fragmentation was not detected when the laser was set in the phenylalanine absorption region at  $37504\text{ cm}^{-1}$ , even though  $[\text{ub} + 12\text{H}]^{12+}$  ions absorb the UV photon at this wavelength, as is seen in the spectrum of Fig. 6.2. To better understand this phenomenon, we recorded UV photofragmentation spectra of  $[\text{ub} + 12\text{H}]^{12+}$  in the region of  $37500\text{ cm}^{-1}$  with and without assistance from the  $\text{CO}_2$  laser. The spectra are shown in Fig. 6.5. Both lasers are used for the red trace, while only the UV laser for the blue trace. The fragment mass channel that we monitored is  $\sim m/z\ 706$ . We can extract several pieces of information from Fig. 6.5. First and most strikingly, the two spectra are completely different. This is in stark contrast to all the cases where a  $\text{CO}_2$  laser was used to enhance the fragmentation yield of UV excited ions by infrared multiple photon dissociation (IRMPD).<sup>3,8</sup> The blue trace exhibits one peak at  $37538\text{ cm}^{-1}$  with FWHM of  $2.8\text{ cm}^{-1}$  and some structure to the high energy side of that peak. Second, and in relation to the first, at  $37504\text{ cm}^{-1}$  where a peak appears in the  $\text{CO}_2$  laser assisted spectrum (Fig. 6.2) there is no UV-only fragmentation. Third, the red spectrum of Fig. 6.5 and the spectrum of Fig. 6.2 exhibit different relative intensities of the sharp features. This is a consequence of the different injection energy used in the two experiments and will be addressed in Section 6.8.

Stearns *et. al.* have previously shown in our lab that cold, bare, protonated tyrosine produces two major photofragments upon electronic excitation.<sup>59</sup> One of the fragments corresponds to the loss of CO + H<sub>2</sub>O and it is also a fragment observed in collision-induced dissociation (CID),<sup>62</sup> pointing to a fragmentation process that occurs in the ground electronic state after internal conversion. The second fragment is the loss of tyrosine side chain radical, which is only a minor product in CID and is believed to arise from dissociation directly on an excited state after electronic excitation.<sup>54-57</sup> Moreover, they identified four stable conformers of protonated tyrosine at the temperature of our trap (10 K)<sup>59</sup> which exhibit different relative intensities of the two photofragments.<sup>59</sup> Correspondingly, the two electronic spectra recorded by monitoring each of the fragments exhibit the same transitions but with different relative intensities for the different conformers.<sup>59</sup> This pointed to conformers having different excited state fragmentation yields.

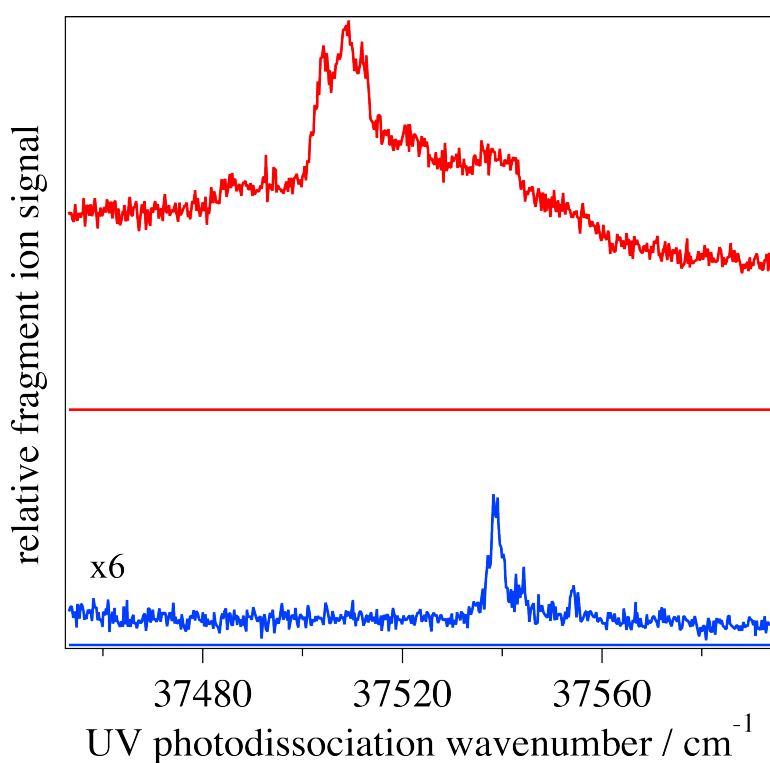


**Figure 6.5.** Electronic photofragment excitation spectrum of [ub + 12H]<sup>12+</sup> by UV only fragmentation (blue trace), and by UV excitation assisted by the IRMPD (red trace).

Here, we use the CO<sub>2</sub> laser to further excite the UV pre-excited ions by absorption of multiple IR photons.<sup>3</sup> Studies on the application of this technique to small peptides indicate that the major enhancement in the dissociation yield involves the excited state fragmentation channel (side chain loss of the UV chromophore amino acid).<sup>3,8</sup> In the case of ubiquitin, dissociation must occur exclusively on an electronically excited state, since only the neutral side chain loss is

observed. Mercier *et. al.* have shown that in the case of tryptophan, the local environment of the chromophore can shift the relative positions of different electronic states and thus influence the excited state dynamics.<sup>63</sup> A change in the crossing points of the initially excited state with other electronic states will control the branching ratio between the different deactivation pathways, one of which may be fragmentation. Antoine *et. al.* also pointed that different excited state fragmentation efficiencies may stem from different structures that the excited ion may adopt.<sup>64</sup> Thus only transitions that originate from conformers that fragment efficiently on the excited state will appear in the electronic photofragmentation spectrum.

It could be that the transitions around  $37510\text{ cm}^{-1}$  and those around  $37540\text{ cm}^{-1}$  originate from different conformational types of  $[\text{ub} + 12\text{H}]^{12+}$ . Upon UV irradiation, the ions are excited but only some conformers fragment giving rise to the latter transitions, while others seem to be in a state where no crossing to the fragmentation channel occurs. In the experiment where the  $\text{CO}_2$  laser is used, the latter ions also absorb the IR photons and fragment, producing thus a spectrum with no discrimination against some conformational types, like the red spectrum of Fig. 6.5. However, in this case differences between relative intensities of transitions originating from different conformational types may reflect differences in the populations that are in the excited state at the moment of the  $\text{CO}_2$  laser irradiation.

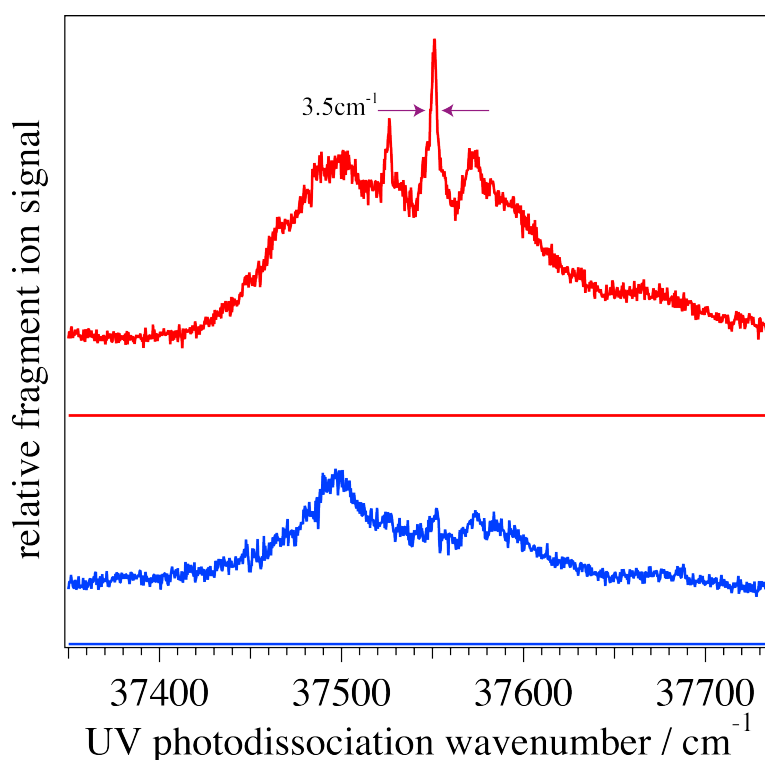


**Figure 6.6.** Electronic photofragment excitation spectrum of  $[\text{ub} + 7\text{H}]^{7+}$  by UV only fragmentation (blue trace), and by UV excitation assisted by the IRMPD (red trace).

We observe the same phenomenon in the electronic photofragment spectrum of  $[\text{ub} + 7\text{H}]^{7+}$  ( $\sim m/z$  1225), albeit to a smaller extent, as shown in Fig. 6.6. For the blue trace only the UV laser is used to illuminate the ions while for the red trace the  $\text{CO}_2$  laser assists in the fragmentation. The laser induced fragment that we monitor in both traces is  $\sim m/z$  1209 corresponding to the loss of the neutral aromatic side chain. The fragment mass spectrum with the UV laser set at  $37551 \text{ cm}^{-1}$  is shown in Fig. 6.7. The red and blue traces are recorded with and without the use of the  $\text{CO}_2$  laser, respectively. From the traces of Fig. 6.7 it seems that the  $\text{CO}_2$  laser enhances but also broadens the laser induced fragmentation, suggesting that more photofragments are produced in this case. However, the resolution of our mass filter doesn't allow their identification.

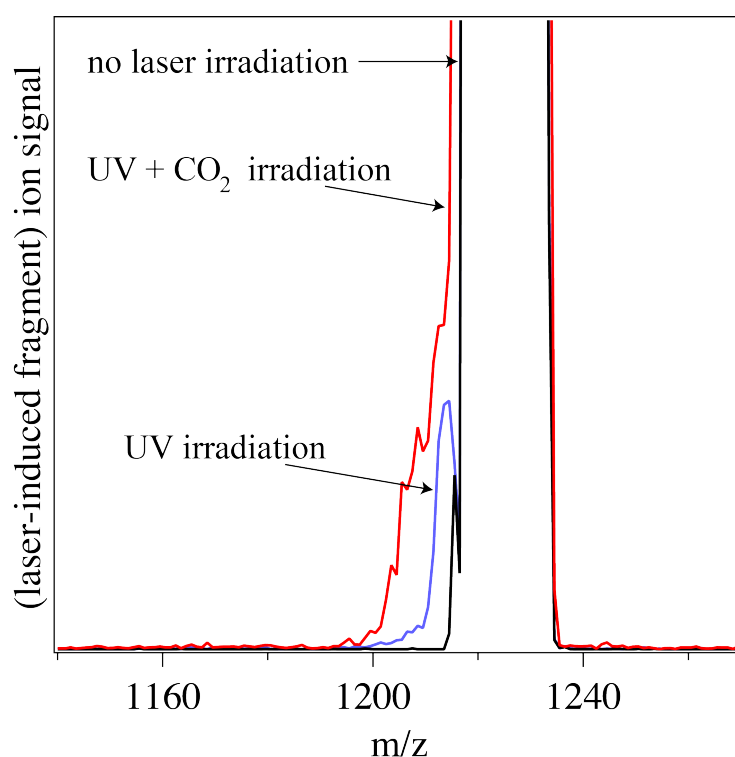


**Figure 6.7.** Fragment mass spectrum of  $[\text{ub} + 7\text{H}]^{7+}$  recorded with both lasers on (red trace), with only the UV laser on (blue trace), and the lasers off (black trace).

The electronic photofragment spectrum of  $[\text{ub} + 7\text{H}]^{7+}$  shown in the red trace of Fig. 6.6 exhibits similar characteristics as that of  $[\text{ub} + 12\text{H}]^{12+}$  shown in Fig. 6.2 i.e a number of sharp features that rest on top of a broad photofragment signal. The width of the peak at  $\sim 37551 \text{ cm}^{-1}$  is  $3.5 \text{ cm}^{-1}$ , measured at the height of the violet arrow shown in Fig. 6.6. The spectrum recorded with the UV laser only (blue trace) shows the same features as the one recorded with the addition of the  $\text{CO}_2$  laser (red spectrum), but the intensities of the sharp peaks are greatly reduced. If the model we proposed above is correct, the sharp features in the spectrum of  $[\text{ub} + 7\text{H}]^{7+}$  must arise

from conformers that show decreased fragmentation upon UV-only excitation because of their excited state dynamics. It should be noted that the UV-only fragmentation efficiency of  $[\text{ub} + 7\text{H}]^{7+}$  ions is superior than that of the  $[\text{ub} + 12\text{H}]^{12+}$  ions.

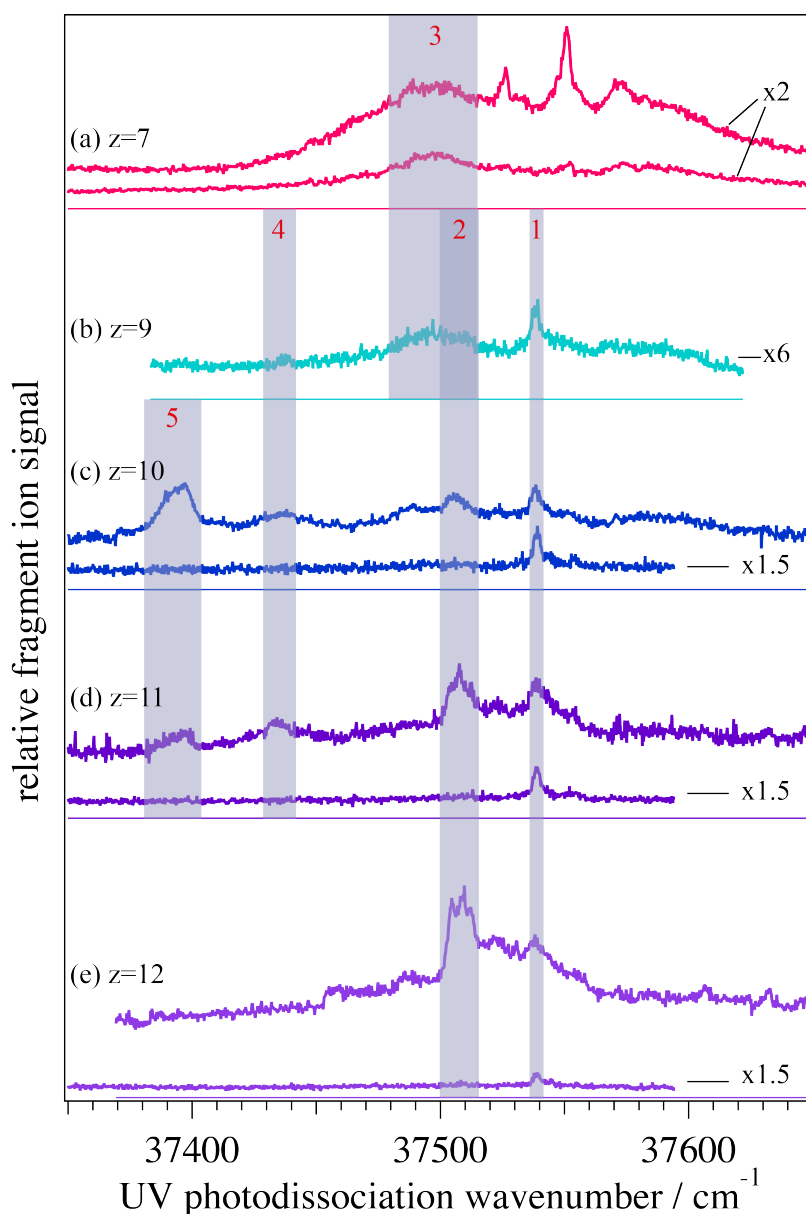
## 6.7. Spectra of different charge states of ubiquitin

Figure 6.8 shows electronic photofragment spectra of  $[\text{ub} + z\text{H}]^{z+}$  with  $z = 7, 9, 10, 11, 12$  for the traces (a) to (e) respectively, recorded with the  $\text{CO}_2$  laser assisting in the fragmentation. For all charge states except the +9, the UV-only photofragment spectrum is included. The spectra are recorded by varying the UV laser frequency while monitoring the fragment that results from the side chain loss of tyrosine or phenylalanine, for every charge state. Spectra of individual charge states will be presented in more detail in the following section and only some general characteristics will be discussed here. The grey transparent ribbons in Fig. 6.8 (numbered 1-5, from right to left) are explained in the text.

The UV-only spectra of the  $[\text{ub} + 10\text{H}]^{10+}$ ,  $[\text{ub} + 11\text{H}]^{11+}$  and  $[\text{ub} + 12\text{H}]^{12+}$  (traces c to e of Fig. 6.8) are very similar, exhibiting one peak at  $\sim 37539 \text{ cm}^{-1}$  and differing only in the fragmentation efficiency, which increases from the +12 to +10 states. This may indicate that this feature rises from a well-conserved conformational moiety across these charge states. This peak seems to correlate with the feature that is visible at the same wavenumber in the UV+ $\text{CO}_2$  photofragment spectra of the states +12 to +9, covered by the grey transparent ribbon (ribbon 1). In the UV+ $\text{CO}_2$  photofragment spectra, the region  $\sim 37510 \text{ cm}^{-1}$  is also common across these charge states (ribbon 2) but with decreasing intensity from +12 to +9, relative to the feature at  $\sim 37539 \text{ cm}^{-1}$ . This may indicate that one structural motif prevails over the other as the charge state is decreased. In fact, coulomb repulsion between the charges sites in the molecule increases from  $[\text{ub} + 9\text{H}]^{9+}$  to  $[\text{ub} + 12\text{H}]^{12+}$ , inducing transitions to more elongated structures.<sup>20,21,26</sup> The increase in intensity of the band  $\sim 37510 \text{ cm}^{-1}$  across these charge states may be indicative of an increased fraction of the ubiquitin ions that are unfolded.

The UV-only and UV- $\text{CO}_2$  photofragment spectra of  $[\text{ub} + 7\text{H}]^{7+}$  (top trace of Fig. 6.8) appear to be different than the corresponding spectra of the other charge states. The broad spectral feature around  $\sim 37500 \text{ cm}^{-1}$  seems to be common between the  $[\text{ub} + 7\text{H}]^{7+}$  and  $[\text{ub} + 9\text{H}]^{9+}$  charge states, with increased relative intensity for  $[\text{ub} + 7\text{H}]^{7+}$ . This may be a spectral signature of more compact structures, the relative population of which increase as the charge state is decreased.

Other gray ribbons in Fig. 6.8 indicate bands that are common across a number of charge states. For example, the common band at  $\sim 37390 \text{ cm}^{-1}$  between  $[\text{ub} + 10\text{H}]^{10+}$  and  $[\text{ub} + 11\text{H}]^{11+}$  may indicate a common structural motif between these charge states. However, it is difficult to extract any other information of the general structure of ubiquitin from these data alone, since for every charge state the conformational distribution across compact, partially folded and elongated structures depends on the injection energy of the ions into the mass spectrometer.<sup>25,26,51</sup> In the following section, we present spectra of individual charge states into the mass spectrometer as a function of the injection voltage.



**Figure 6.8.** Electronic photofragment excitation spectra of  $[\text{ub} + z\text{H}]^{z+}$  with  $z=7, 9, 10, 11$  and  $12$  for the traces (a) to (e). In every section, the lower and upper traces are the UV-only and UV+CO<sub>2</sub> spectra, respectively.



## 6.8. The influence of the injection voltage

In the electronic photofragment spectra of the  $[\text{ub} + 12\text{H}]^{12+}$  and  $[\text{ub} + 11\text{H}]^{11+}$  (traces e and d of Fig. 6.8) we can observe some sub-structure in the band around  $\sim 37510 \text{ cm}^{-1}$ . Moreover, the transitions that constitute the sub-structure in the spectra of  $[\text{ub} + 12\text{H}]^{12+}$  shown in Fig. 6.2 and Fig. 6.5 (red trace) exhibit different relative intensities. As we mentioned above, we recorded the two latter spectra with different injection voltages of the ions into the hexapole ion trap of our mass spectrometer. To further investigate this influence, we recorded spectra as function of the injection voltage for several charge states. Figure 6.9 shows these spectra for  $[\text{ub} + 12\text{H}]^{12+}$  (left panel) and  $[\text{ub} + 11\text{H}]^{11+}$  (right panel). The injection voltage is shown at the left of each trace. At 16.6V (light blue trace), the spectra for both charge states have no sharp features. IMS studies of  $[\text{ub} + 12\text{H}]^{12+}$  injected gently into the drift tube show four resolvable peaks with cross-sections ranging from  $1750 \text{ \AA}$  to  $2100 \text{ \AA}$  (which classifies them as elongated structures) with only one of them being significantly populated.<sup>26</sup> For  $[\text{ub} + 11\text{H}]^{11+}$ , two sharp features are found in the same range of cross-sections but also a distribution of unresolved structures, all elongated.<sup>26</sup> The band around  $\sim 37510 \text{ cm}^{-1}$  may be a spectral indication that the structures of both charge states are elongated.

Studies with two-dimensional IMS of both charge states where slices from the initial IMS distribution were injected gently into the second drift tube, show that some structural types are stable while others interconvert to conformers with higher or lower cross-sections.<sup>26</sup> Upon activation, the selected family interconverts to one or more of the four structural types that were initially identified. The grey ribbon in left panel of Fig. 6.9 shows that upon increase of the injection voltage a sharp feature at  $37504 \text{ cm}^{-1}$  emerges out of the broad band in the electronic photofragment spectrum of  $[\text{ub} + 12\text{H}]^{12+}$ . The spectrum remains virtually the same when recorded at injection voltages higher than 80 V. Taking into account the results from the IMS studies, we conclude that collisional activation changes the relative populations of the initially formed four elongated structural types favoring a particular conformer that gives rise to the transition at  $37504 \text{ cm}^{-1}$ .

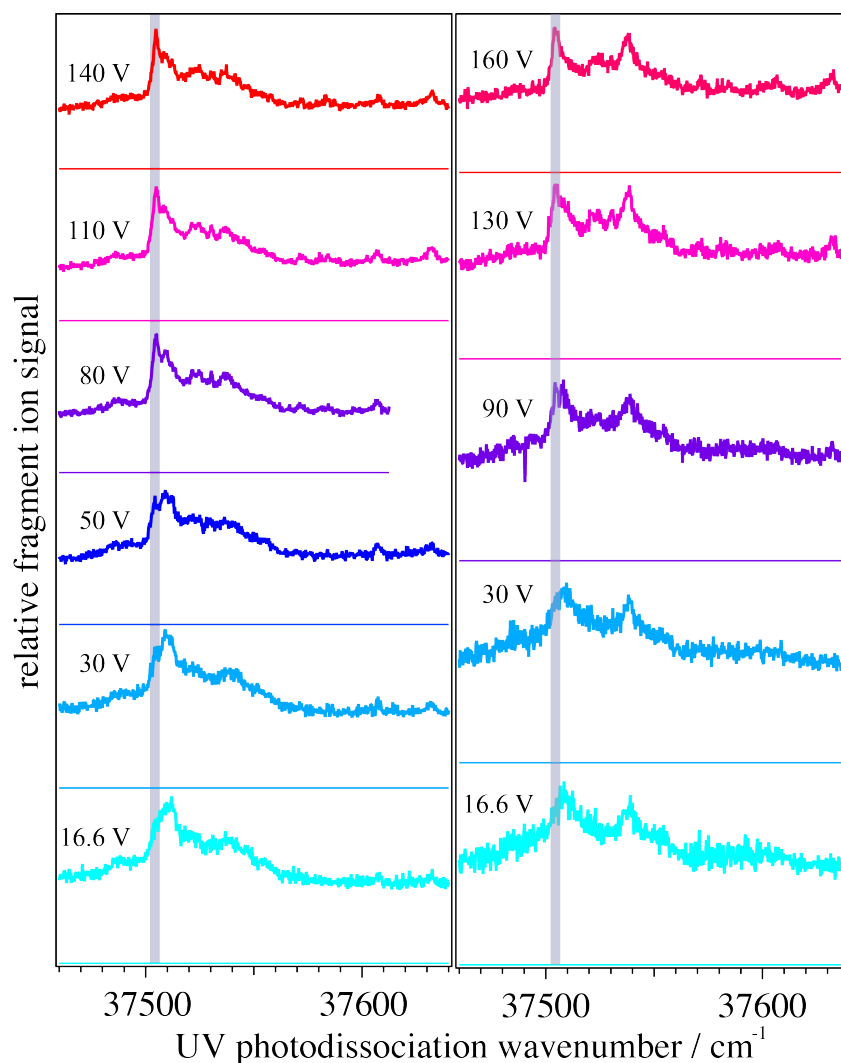


**Figure 6.9.** Electronic photofragment excitation spectra of  $[\text{ub} + 12\text{H}]^{12+}$  (left panel) and  $[\text{ub} + 11\text{H}]^{11+}$  (right panel) recorded as a function of increased injection energy into the hexapole ion trap.

IMS-IMS studies of  $[\text{ub} + 11\text{H}]^{11+}$  reveal that upon selection and activation of ions out of the initial distribution, the resulting distribution shows that the conformers that are formed have collision cross-sections that coincide with the peaks of the initial distribution.<sup>26</sup> In the photofragment electronic spectrum of  $[\text{ub} + 11\text{H}]^{11+}$  (Fig. 6.9, right panel) a peak at  $37504 \text{ cm}^{-1}$  grows in intensity upon increase of the injection voltage. It seems that collisional activation leads to a redistribution of populations over the initially formed structural types favoring a conformation from which the transition at  $37504 \text{ cm}^{-1}$  originates. In both spectra of  $[\text{ub} + 11\text{H}]^{11+}$  and  $[\text{ub} + 12\text{H}]^{12+}$ , the sharp feature that emerges is at the same frequency, suggesting that the phenylalanine that is responsible for this transition finds itself in the same environment in the two species. ECD data of McLafferty and colleagues<sup>32</sup> but also data from H/D exchange studies of Marshall and coworkers<sup>47</sup> suggest some populations of both  $[\text{ub} + 11\text{H}]^{11+}$  and  $[\text{ub} + 12\text{H}]^{12+}$  have very similar

structures. Our experiment may provide evidence that the transition at  $37504\text{ cm}^{-1}$  originates from this population and that it becomes dominant at high collisional energies.

Figure 6.10 shows the photofragment excitation spectra of  $[\text{ub} + 10\text{H}]^{11+}$  as a function of the injection voltage of the ions into the hexapole ion trap. The spectrum changes only slightly with varied injection energy. Contrary to the charge states shown in Fig. 6.9,  $[\text{ub} + 10\text{H}]^{11+}$  ions do not seem to undergo any significant structural change across the injection voltages presented in Fig. 6.10. However, the poor signal-to-noise ratio does not allow us to draw definite conclusions.

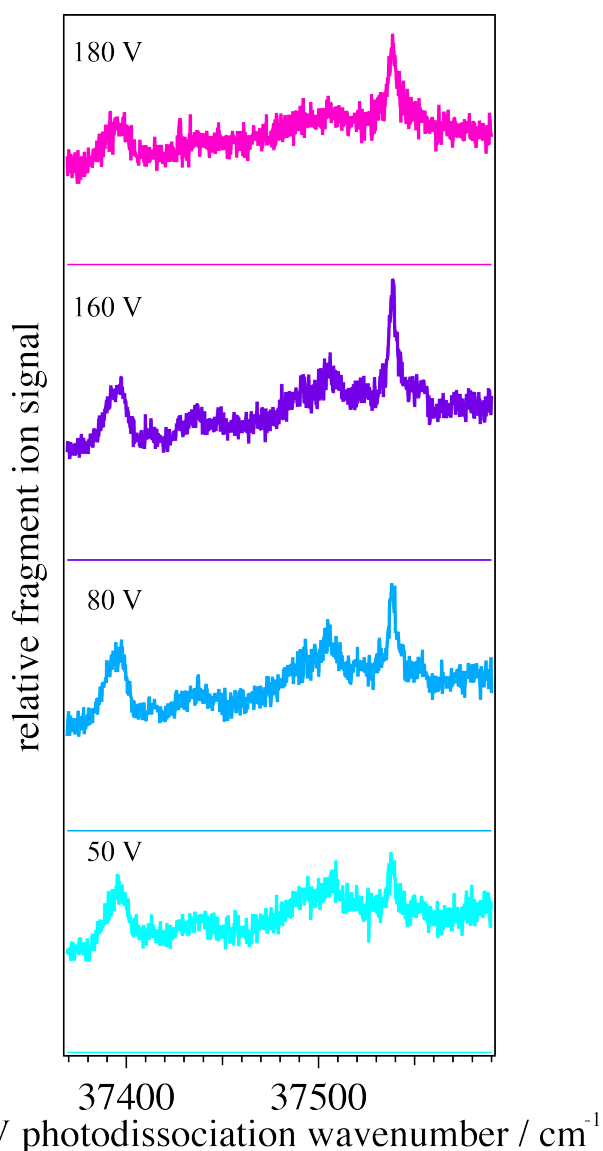


**Figure 6.10.** Electronic photofragment excitation spectra of  $[\text{ub} + 10\text{H}]^{10+}$  recorded as a function of increased injection energy into the hexapole ion trap.

The case of  $[\text{ub} + 7\text{H}]^{7+}$  is of particular interest for the following reasons. IMS studies have shown that this charge states exists in a variety of structural types, ranging from compact to

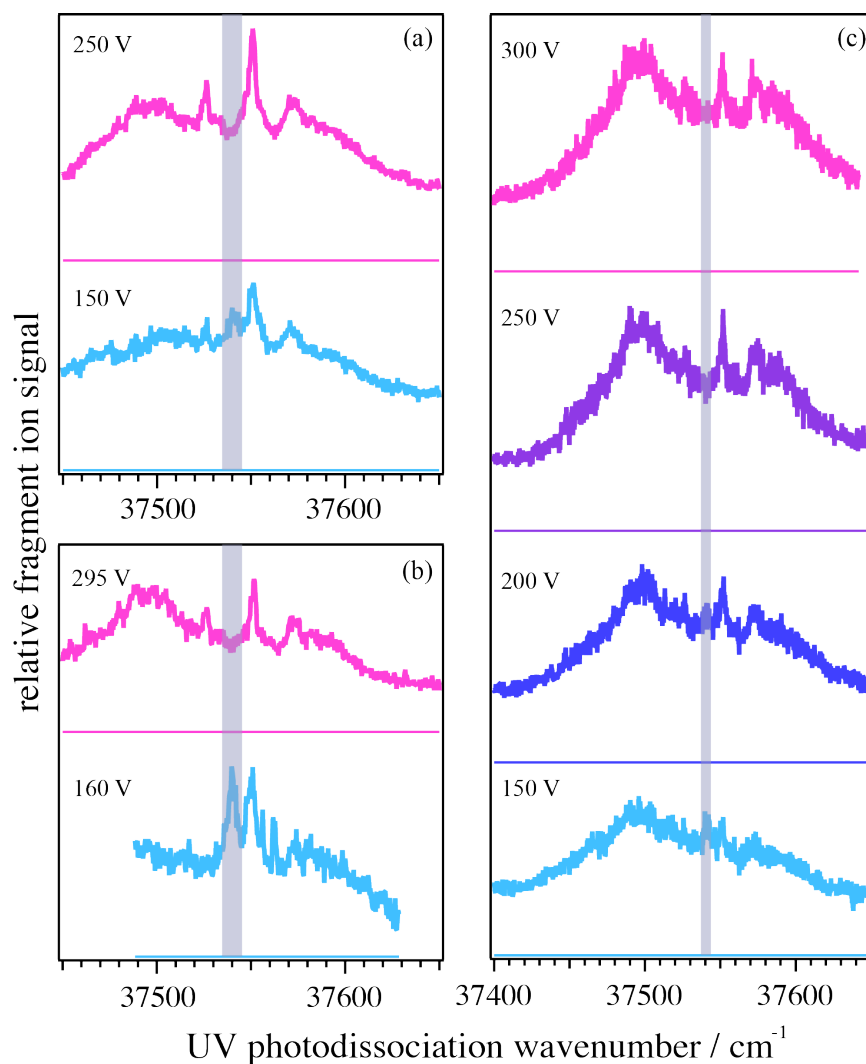
partially unfolded to elongated.<sup>21,26,28</sup> The distribution of their arrival time in a drift tube shows a continuous signal across these structural types with significant population of the compact structures ( $\sim 80\%$ ).<sup>25,26</sup> On the other hand, two-dimensional IMS has shown that all of these conformers retain their structures for at least 10 – 20ms after their production in the gas phase.<sup>24</sup> Thus,  $[\text{ub} + 7\text{H}]^{7+}$  ions show a plethora of completely different structural isomers, that under gentle conditions do not interconvert, and so their spectroscopic signatures will contribute in the spectrum. Moreover, upon collisional activation compact conformers interconvert to more elongated ones<sup>25</sup> and this could be followed spectroscopically.

Figure 6.11a shows electronic photofragment spectra of  $[\text{ub} + 7\text{H}]^{7+}$  at two different injection voltages into the hexapole ion trap. The injection voltage is shown on the left of each trace. The two traces are clearly different with an additional feature appearing at  $37540\text{ cm}^{-1}$  in the spectrum recorded with lower collisional activation, while the three transitions at  $37526\text{ cm}^{-1}$ ,  $37551\text{ cm}^{-1}$  and  $37570\text{ cm}^{-1}$  decrease in intensity. It seems that the conformer(s) associated with the latter transitions appear to be favored at high injection voltages. Thus, the three transitions may originate from elongated conformers of  $[\text{ub} + 7\text{H}]^{7+}$  ions. Moreover, since the transition at  $37540\text{ cm}^{-1}$  appears at less intense conditions of collisional activation, it should originate from a less unfolded conformer.

In our mass spectrometer, we vary the collisional activation by changing the capillary/skimmer voltage drop. Thus the change in the energy of the collisions of the ions with the background gas is not decoupled from their transmission efficiency from the source to the cold trap. To perform photofragment spectroscopy, at least 1000-2000 ions are necessary, limiting the range of injection voltage that we can use. In the case of  $[\text{ub} + 7\text{H}]^{7+}$  the acceptable voltage range is larger than  $\sim 150\text{ V}$ , a value which should promote at least partial unfolding of the majority of compact structures, considering the background pressure in the capillary/skimmer region ( $1.7\text{ mbar}$ ).<sup>25</sup> Thus, the transition at  $37540\text{ cm}^{-1}$  can be attributed to a partially folded conformer that unfolds upon increase of the injection voltage or to an elongated molecule that changes its conformation at even higher collisional activation.

Another important aspect that we observe is that the electronic photofragment spectrum of  $[\text{ub} + 7\text{H}]^{7+}$  depends on the source configuration. Panels (b) and (c) of Fig. 6.11 show photofragment electronic spectra of  $[\text{ub} + 7\text{H}]^{7+}$  recorded at slightly different source conditions. Although the upper traces of panels (b) and (c) are typical spectra for  $[\text{ub} + 7\text{H}]^{7+}$  recorded at high injection energies, they are clearly different than the upper trace of panel (a), showing lower intensities for the sharp features relative to the broader band at  $\sim 37500\text{ cm}^{-1}$ . On the other hand, when the spectrum is recorded under more gentle conditions, we observe the transition at  $\sim 37540$

$\text{cm}^{-1}$ , as is evident from the lower traces of panels (b) and (c). Although changes in source configuration may translate to different conformational distribution or degree of desolvation of the produced ions when they reach the capillary/skimmer region, we have to undergo a more detailed investigation of these effects before drawing definite conclusions.



**Figure 6.11.** Electronic photofragment excitation spectra of  $[\text{ub} + 7\text{H}]^{7+}$  recorded as a function of increased injection energy into the hexapole ion trap. Panels (a)-(c) correspond to different source configurations used for the production of the ions.

## 6.9. Conclusions

We have employed photofragment spectroscopy to record electronic spectra of cold, protonated ubiquitin in the gas phase. The application of this method is possible in small proteins of this size because fragmentation seems to occur from an excited electronic state after absorption of the laser radiation. However, the fragmentation yield is structure dependent, rendering the technique sensitive to only a portion of the conformational distribution. We partially overcome this by the use of a CO<sub>2</sub> laser that assists in the dissociation of conformers with no UV-only induced excited state fragmentation. We have recorded spectra of several different protonation states of ubiquitin in the spectral region where phenylalanine absorbs. All of them exhibit some sharp features on top of a broad photofragment signal. The sharp transitions indicate that the ions are cold, while the broad band rises from vibronic activity of the tyrosine amino acid. Based on ion mobility studies we found a band in the spectrum that may be an indication of higher content of elongated structures. Interestingly, the spectrum at the spectral region where tyrosine absorbs (the band origin) is devoid of clearly resolved features. We attribute this to the large number of conformational isomers that have similar and partially overlapping electronic spectra, in combination with the low frequency vibronic activity of tyrosine. All these contribute to the acquired spectrum leading to its spectral congestion. The use of ion mobility to separate the ionic ensemble into conformations (or conformational families) prior to their interrogation with laser spectroscopy may lead to a simplification of the spectrum. Attempts towards this direction are currently being undertaken in our laboratory.

We also recorded spectra of individual charge states as a function of their injection energy into the hexapole ion trap of our machine. We inspected differences in intensities of the features in individual spectra and we attributed them to changes in the relative populations of the conformers from which they originate. These studies give us the possibility to follow structural transitions by spectroscopic means and as a function of the collision energy. We mainly compared our data with similar studies of this system by multidimensional ion mobility spectrometry, pioneered by Clemmer and co-workers.<sup>24-26</sup> However, while in these studies a precursor conformation (or conformational family) can be selected and monitored, in our experiment all the conformers contribute to the spectrum making it difficult to resolve transitions originating from different structures. We believe that a combination of the two techniques is essential for the detailed investigation of the structural evolution of ubiquitin ions after their production from electrospray ionization.

## 6.10. References

- (1) Griffin, L. L.; McAdoo, D. J. *J. Am. Soc. Mass Spectrom.* **1993**, *4*, 11.
- (2) Antoine, R.; Dugourd, P. *Phys. Chem. Chem. Phys.* **2011**, *13*.
- (3) Guidi, M.; Lorenz, U. J.; Papadopoulos, G.; Boyarkin, O. V.; Rizzo, T. R. *J. Phys. Chem. A* **2009**, *113*, 797.
- (4) Stearns, J. A.; Boyarkin, O. V.; Rizzo, T. R. *J. Am. Chem. Soc.* **2007**, *129*, 13820.
- (5) Rizzo, T. R.; Stearns, J. A.; Boyarkin, O. V. *Int. Rev. Phys. Chem.* **2009**, *28*, 481
- (6) Nagornova, N. S.; Rizzo, T. R.; Boyarkin, O. V. *J. Am. Chem. Soc.* **2010**, *132*, 4040.
- (7) Nagornova, N. S.; Guglielmi, M.; Doemer, M.; Tavernelli, I.; Rothlisberger, U.; Rizzo, T. R.; Boyarkin, O. V. *Angew. Chem., Int. Ed.* **2011**, *50*, 5383.
- (8) Guidi, M. PhD Thesis, EPFL, 2010.
- (9) Svendsen, A.; Boyarkin, O. V.; Rizzo, T. R. *in preparation* **2012**.
- (10) Vijay-Kumar, S.; Bugg, C. E.; Wilkinson, K. D.; Cook, W. J. *Proc. Natl. Acad. Sci. U. S. A.* **1985**, *82*, 3582.
- (11) Goldstein, G.; Scheid, M.; Hammerling, U.; Schlesinger, D. H.; Niall, H. D.; Boyse, E. A. *Proc. Natl. Acad. Sci. U. S. A.* **1975**, *72*, 11.
- (12) Vijay-Kumar, S.; Bugg, C. E.; Cook, W. J. *J. Mol. Biol.* **1987**, *194*, 531.
- (13) Baek, K.-H. *Exp. Mol. Med.* **2003**, *35*, 1.
- (14) Ciechanover, A.; Ben-Saadon, R. *Trends Cell Biol.* **2004**, *14*, 103.
- (15) Gao, M.; Karin, M. *Mol. Cell* **2005**, *19*, 581.
- (16) Weber, P. L.; Brown, S. C.; Mueller, L. *Biochemistry* **1987**, *26*, 7282.
- (17) Di Stefano, D. L.; Wand, A. J. *Biochemistry* **1987**, *26*, 7272.
- (18) Harding, M. M.; Williams, D. H.; Woolfson, D. N. *Biochemistry* **1991**, *30*, 3120.
- (19) Brutscher, B.; Brüscheweiler, R.; Ernst, R. R. *Biochemistry* **1997**, *36*, 13043.
- (20) Valentine, S.; Counterman, A.; Clemmer, D. J. *J. Am. Soc. Mass Spectrom.* **1997**, *8*, 954.
- (21) Li, J.; Taraszka, J. A.; Counterman, A. E.; Clemmer, D. E. *Int. J. Mass Spectrom.* **1999**, *185-187*, 37.
- (22) Badman, E.; Hoaglund-Hyzer, C.; Clemmer, D. J. *J. Am. Soc. Mass Spectrom.* **2002**, *13*, 719.
- (23) Myung, S.; Badman, E. R.; Lee, Y. J.; Clemmer, D. E. *J. Phys. Chem. A* **2002**, *106*, 9976.
- (24) Koeniger, S. L.; Merenbloom, S. I.; Clemmer, D. E. *J. Phys. Chem. B* **2006**, *110*, 7017.
- (25) Koeniger, S. L.; Merenbloom, S. I.; Sevugarajan, S.; Clemmer, D. E. *J. Am. Chem. Soc.* **2006**, *128*, 11713.
- (26) Koeniger, S.; Clemmer, D. J. *J. Am. Soc. Mass Spectrom.* **2007**, *18*, 322.
- (27) Bohrer, B. C.; Atlasevich, N.; Clemmer, D. E. *J. Phys. Chem. B* **2011**, *115*, 4509.
- (28) Wyttenbach, T.; Bowers, M. T. *J. Phys. Chem. B* **2011**, *115*, 12266.
- (29) Cassidy, C. J.; Carr, S. R. *J. Mass Spectrom.* **1996**, *31*, 247.
- (30) Geller, O.; Lifshitz, C. *J. Phys. Chem. A* **2005**, *109*, 2217.
- (31) Zubarev, R. A.; Horn, D. M.; Fridriksson, E. K.; Kelleher, N. L.; Kruger, N. A.; Lewis, M. A.; Carpenter, B. K.; McLafferty, F. W. *Anal. Chem.* **2000**, *72*, 563.
- (32) Breuker, K.; Oh, H.; Horn, D. M.; Cerda, B. A.; McLafferty, F. W. *J. Am. Chem. Soc.* **2002**, *124*, 6407.
- (33) Purves, R. W.; Barnett, D. A.; Ells, B.; Guevremont, R. *J. Am. Soc. Mass Spectrom.* **2000**, *11*, 738.

- (34) Purves, R. W.; Barnett, D. A.; Guevremont, R. *Int. J. Mass Spectrom.* **2000**, *197*, 163.
- (35) Purves, R. W.; Barnett, D. A.; Ells, B.; Guevremont, R. *J. Am. Soc. Mass Spectrom.* **2001**, *12*, 894.
- (36) Robinson, E. W.; Williams, E. R. *J. Am. Soc. Mass Spectrom.* **2005**, *16*, 1427.
- (37) Oh, H.; Breuker, K.; Sze, S. K.; Ge, Y.; Carpenter, B. K.; McLafferty, F. W. *Proc. Natl. Acad. Sci. U. S. A.* **2002**, *99*, 15863.
- (38) Bellina, B.; Compagnon, I.; Joly, L.; Albrieux, F.; Allouche, A. R.; Bertorelle, F.; Lemoine, J.; Antoine, R.; Dugourd, P. *Int. J. Mass Spectrom.* **2010**, *297*, 36.
- (39) Horn, D. M.; Zubarev, R. A.; McLafferty, F. W. *Proc. Natl. Acad. Sci. U. S. A.* **2000**, *97*, 10313.
- (40) Loo, J. A.; Edmonds, C. G.; Smith, R. D. *Anal. Chem.* **1993**, *65*, 425.
- (41) Little, D. P.; Speir, J. P.; Senko, M. W.; Oconnor, P. B.; McLafferty, F. W. *Anal. Chem.* **1994**, *66*, 2809.
- (42) Jockusch, R. A.; Schnier, P. D.; Price, W. D.; Strittmatter, E. F.; Demirev, P. A.; Williams, E. R. *Anal. Chem.* **1997**, *69*, 1119.
- (43) Shvartsburg, A. A.; Li, F.; Tang, K.; Smith, R. D. *Anal. Chem.* **2006**, *78*, 3304.
- (44) Robinson, E.; Leib, R.; Williams, E. *J. Am. Soc. Mass Spectrom.* **2006**, *17*, 1470.
- (45) Shelimov, K. B.; Clemmer, D. E.; Hudgins, R. R.; Jarrold, M. F. *J. Am. Chem. Soc.* **1997**, *119*, 2240.
- (46) Wyttenbach, T.; Kemper, P. R.; Bowers, M. T. *Int. J. Mass Spectrom.* **2001**, *212*, 13.
- (47) Freitas, M. A.; Hendrickson, C. L.; Emmett, M. R.; Marshall, A. G. *Int. J. Mass Spectrom.* **1999**, *185-187*, 565.
- (48) Koeniger, S. L.; Merenbloom, S. I.; Valentine, S. J.; Jarrold, M. F.; Udseth, H. R.; Smith, R. D.; Clemmer, D. E. *Anal. Chem.* **2006**, *78*, 4161.
- (49) Merenbloom, S. I.; Koeniger, S. L.; Valentine, S. J.; Plasencia, M. D.; Clemmer, D. E. *Anal. Chem.* **2006**, *78*, 2802.
- (50) Merenbloom, S. I.; Bohrer, B. C.; Koeniger, S. L.; Clemmer, D. E. *Anal. Chem.* **2006**, *79*, 515.
- (51) Bohrer, B. C.; Merenbloom, S. I.; Koeniger, S. L.; Hilderbrand, A. E.; Clemmer, D. E. *Annu. Rev. Anal. Chem.* **2008**, *1*, 293.
- (52) Breuker, K.; McLafferty, F. W. *Proc. Natl. Acad. Sci. U. S. A.* **2008**, *105*, 18145.
- (53) Katta, V.; Chait, B. T. *J. Am. Chem. Soc.* **1993**, *115*, 6317.
- (54) Kang, H.; Jouvét, C.; Dedonder-Lardeux, C.; Martrenchard, S.; Gregoire, G.; Desfrancois, C.; Schermann, J. P.; Barat, M.; Fayeton, J. A. *Phys. Chem. Chem. Phys.* **2005**, *7*, 394.
- (55) Tabarin, T.; Antoine, R.; Broyer, M.; Dugourd, P. *Rapid Commun. Mass Spectrom.* **2005**, *19*, 2883.
- (56) Joly, L.; Antoine, R.; Broyer, M.; Dugourd, P.; Lemoine, J. *J. Mass Spectrom.* **2007**, *42*, 818.
- (57) Lucas, B.; Barat, M.; Fayeton, J. A.; Perot, M.; Jouvét, C.; Gregoire, G.; Nielsen, S. B. *J. Chem. Phys.* **2008**, *128*, 164302.
- (58) Boyarkin, O. V.; Mercier, S. R.; Kamariotis, A.; Rizzo, T. R. *J. Am. Chem. Soc.* **2006**, *128*, 2816.
- (59) Stearns, J. A.; Mercier, S.; Seaiby, C.; Guidi, M.; Boyarkin, O. V.; Rizzo, T. R. *J. Am. Chem. Soc.* **2007**, *129*, 11814.
- (60) Stearns, J. A.; Guidi, M.; Boyarkin, O. V.; Rizzo, T. R. *J. Chem. Phys.* **2007**, *127*, 154322.
- (61) Zhang, X.; Cassady, C. *J. Am. Soc. Mass Spectrom.* **1996**, *7*, 1211.



- (62) El Aribi, H.; Orlova, G.; Hopkinson, A. C.; Siu, K. W. M. *J. Phys. Chem. A* **2004**, *108*, 3844.
- (63) Mercier, S. R.; Boyarkin, O. V.; Kamariotis, A.; Guglielmi, M.; Tavernelli, I.; Cascella, M.; Rothlisberger, U.; Rizzo, T. R. *J. Am. Chem. Soc.* **2006**, *128*, 16938.
- (64) Antoine, R.; Broyer, M.; Chamot-Rooke, J.; Dedonder, C.; Desfrancois, C.; Dugourd, P.; Grégoire, G.; Jouvét, C.; Onidas, D.; Poulain, P.; Tabarin, T.; van der Rest, G. *Rapid Commun. Mass Spectrom.* **2006**, *20*, 1648.



## Conclusions and perspectives

While photofragment spectroscopy has been successfully used to study the structural and photophysical properties of small, cold peptides, its application to larger systems is hindered by their increased structural complexity. Using our spectroscopic method, structural determination relies on the comparison of the experimentally obtained of conformer-specific vibrational spectra (recorded *via* IR-UV double resonance) to calculated ones.<sup>1</sup> As a first step for this, it is necessary to record a highly resolved electronic spectrum in which transitions originating from different conformers are clearly separated. This is increasingly difficult for large and complex molecules, where a plethora of stable conformers can lead to congestion of the electronic spectra. To overcome this problem, we proposed combining our spectroscopic methods with ion mobility techniques in order to disperse the conformations of complex systems in an additional dimension prior to their spectroscopic investigation. We demonstrated the feasibility of this approach by performing a proof-of-principle experiment using FAIMS for conformer separation and selection. We showed that the spectrum of a conformationally complex peptide can be simplified by exclusively introducing a selected conformational population into our cold trap. In the inverse sense, we used our spectroscopic tools to decompose a mobility spectrum, showing the versatility of the two techniques when used *in tandem*. Moreover, we showed the potential of laser spectroscopy to provide insight into heating processes during the FAIMS separation.

We also tested the limits of photofragment spectroscopy by presenting preliminary experiments in which we investigated a small protein of 76 amino acids. We showed that for molecules of this size conformational heterogeneity congests the electronic spectrum to a substantial extent. Several charge states of ubiquitin exhibit spectra with mainly broad bands and only a few sharp features. Spectral congestion to such a large extent inhibits the use of IR-UV double resonance, clearly showing the limitation of our spectroscopic methods in recording conformer-specific vibrational spectra. On the other hand, collisional activation can induce structural transitions that leave their spectroscopic “traces” in the electronic spectra and thus can be readily followed. Although some general structural characteristics of the protein can be

inferred from the spectra, the use of laser spectroscopy alone is unable to provide detailed structural information. However, a combination with ion mobility techniques may simplify the electronic spectra of molecules of this size and allow for the use of double-resonance techniques.

Two questions are raised at this point. First, will a vibrational spectrum of a molecule of this size be sufficient for detailed structural determination? And second, to which accuracy can theoretical calculations predict the structure and spectra of molecules of this size? If the use of ion mobility separation leads to a limited number of features in the electronic spectrum, this will allow for the recording of conformer-specific vibrational spectra *via* IR-UV double resonance. However, the number of, for example, N-H oscillators in a protein of this size is large, and they will all contribute to the vibrational spectrum. This will lead to its congestion and may impede comparison with theory. On the other hand, we can use the information gained from the separation step to confine the search of the conformational space in theoretical calculations. Although in these experiments we used FAIMS in which every conformation (or conformational family) is characterized by a CV value, the use of drift tube IMS will yield collision cross sections that can be readily associated with a structural type. In this way, the conformer-specific vibrational spectrum together with a collision cross section may facilitate comparison with theory.

However, we are skeptical about the ability of theoretical calculations to predict structures and spectra with great certainty. This is where the importance of providing an experimentally obtained vibrational spectrum comes. Theoretical methods can be tested against these experimental data,<sup>1</sup> and in this way they can be improved. While high-resolution vibrational data are not expected from applying our spectroscopic scheme to proteins, smaller molecules can be used to help towards this direction.

The combination of the two techniques can also simplify isomerization studies performed inside an ion trap<sup>2</sup> by reducing the number of conformers stored in it.<sup>3</sup> In these experiments, photoexcitation can selectively energize a single conformation and induce a transfer of the initial population into different conformers,<sup>3</sup> while the resulting conformational distribution can be probed spectroscopically. These experiments give direct information on the connectivity between different conformers and also on the barriers of isomerization. However, in situations where a number of conformations are initially present, the treatment of the data is difficult.<sup>2-4</sup> In a combination of two techniques and with an ideal mobility separation, a single conformation can be stored in the cold trap. In this case, because of the initial presence of a single conformer, transfer of population will occur to minima in the potential energy surface where there was no occupation before the laser excitation. This will make the experiment background free, leading to a much easier treatment of the spectroscopic data. While two-dimensional IMS techniques can be used for

similar experiments,<sup>5-7</sup> the amount of energy that is imparted on the selected ions is not precisely determined, making the calculation of isomerization barrier heights impossible. However, one can imagine an experiment where a selected conformation from a first drift stage is energized by a laser pulse (and thus by a precise amount of energy) while the nascent distribution is detected in a second drift tube. This combination will improve the accuracy of the above experiments.

The plethora of conformations that a solvent-free biomolecule can adopt may be intermediates in its folding pathway<sup>8</sup> towards a native, biologically active state, or conformational substates<sup>9</sup> that are essential for its function. Knowledge of the detailed structures of the gas phase biomolecules is thus of fundamental importance. We anticipate that the combination of the techniques of ion mobility and cold ion spectroscopy proposed in this work will help in this direction, probing systems of increased size and complexity.

## 7.1. References

- (1) Rizzo, T. R.; Stearns, J. A.; Boyarkin, O. V. *Int. Rev. Phys. Chem.* **2009**, *28*, 481
- (2) Dian, B. C.; Longarte, A.; Zwier, T. S. *Science* **2002**, *296*, 2369.
- (3) Seaiby, C. PhD Thesis, EPFL.
- (4) Dian, B. C.; Longarte, A.; Winter, R. P.; Zwier, T. S. *J. Chem. Phys.* **2004**, *120*, 133.
- (5) Koeniger, S. L.; Merenbloom, S. I.; Valentine, S. J.; Jarrold, M. F.; Udseth, H. R.; Smith, R. D.; Clemmer, D. E. *Anal. Chem.* **2006**, *78*, 4161.
- (6) Koeniger, S. L.; Merenbloom, S. I.; Sevugarajan, S.; Clemmer, D. E. *J. Am. Chem. Soc.* **2006**, *128*, 11713.
- (7) Koeniger, S.; Clemmer, D. *J. Am. Soc. Mass Spectrom.* **2007**, *18*, 322.
- (8) Wolynes, P. G. *Proc. Natl. Acad. Sci. U. S. A.* **1995**, *92*, 2426.
- (9) Frauenfelder, H. *The Physics of Proteins: An Introduction to Biological Physics and Molecular Biophysics*; Springer, 2010.



# List of abbreviations

ATD: arrival time distribution  
BIRD: blackbody infrared radiative dissociation  
CD: circular dichroism  
CID: collision-induced dissociation  
CRM: charge residue model  
CV: compensation voltage  
DC: direct current  
DT-IMS: drift tube ion mobility spectrometry  
DV: dispersion voltage  
ECD: electron capture dissociation  
ESI: electrospray ionization  
FT-ICR: Fourier transform ion cyclotron resonance  
FTIR: Fourier transform infrared  
FAIMS: high-field asymmetric waveform ion mobility spectrometry  
FWHM: full width at half maximum  
IC: internal conversion  
IEM: ion evaporation model  
IMS: ion mobility spectrometry  
IVR: intramolecular vibrational redistribution  
IRMPD: infrared multiphoton dissociation  
IR: infrared  
m/z: mass-to-charge ratio  
MALDI: matrix-assisted laser desorption/ionization  
MS: mass spectrometry  
NMR: nuclear magnetic resonance  
OBV: outer bias voltage  
QMS: quadrupole mass spectrometry  
OPO: optical parametric oscillator  
RF: radio-frequency  
TEA: transversely excited atmospheric  
TOF: time-of-flight  
UV: ultraviolet  
YAG: yttrium aluminum garnet





# Curriculum vitae

Georgios Papadopoulos

Born on 18 December 1980 in Athens, Greece

## Education

- 2007-2012 Ph.D. thesis in Physical Chemistry at the Ecole Polytechnique Fédérale de Lausanne, Switzerland
- Title: A combination of cold-ion spectroscopy and ion mobility for the study of complex peptides and small proteins.
- 2004-2006 MSc. thesis in Applied Molecular Spectroscopy at the University of Crete, Greece  
MSc. Applied Molecular Spectroscopy, Department of Chemistry, Laboratory of Biophysical Chemistry
- Title: FT-IR study of myoglobin and caa<sub>3</sub> oxidoreductase from *Thermus Thermophilus*.
- 1998-2004 Undergraduate studies in chemistry at the University of Crete, Greece

## Languages

Greek (native), English (fluent), French (intermediate), German (basic)

## Publications

1. E. Pinakoulaki, K. Koutsoupakis, S. Stavarakis, M. Aggelaki, G. Papadopoulos, V. Daskalakis, C. Varotsis. “*Structural Dynamics of Heme-Copper Oxidases and Nitric Oxide Reductases: Time-resolved Step-Scan Fourier Transform Infrared and Time-resolved Resonance Raman Studies*”, *Journal of Raman Spectroscopy*. **36**, 337-349 (2005).
2. M. Guidi, U. J. Lorenz, G. Papadopoulos, O. V. Boyarkin, and T. R. Rizzo, “*Spectroscopy of Protonated Peptides Assisted by Infrared Multiple Photon Excitation*”, *Journal of Physical Chemistry A*, **113**, 797 (2009).
3. G. Papadopoulos, A. Svendsen, O. V. Boyarkine, T. R. Rizzo, “*Spectroscopy of mobility-selected biomolecular ions*”, *Faraday Discussions*, **150**, 243 (2011).
4. G. Papadopoulos, A. Svendsen, O. V. Boyarkine, T. R. Rizzo, “*Conformational distribution of bradykinin [bk+2H]<sup>2+</sup> revealed by cold ion spectroscopy coupled with FAIMS*”, *Journal of the American Society for Mass Spectrometry*, **23**, 1173 (2012).



# Acknowledgments

I would like to thank Prof. Thomas Rizzo for accepting me in his group five years ago and for his constant support, understanding and patience over those years. Most importantly, for his enthusiastic interest in my project and for his enjoyment when discussing my results. Time spent with Tom in the lab, on late afternoons, trying to optimize signals and understand the data is unforgettable. It was a pleasure.

Marianne Dang for her kind concern and for taking care of all of us - life in Lausanne would be much more difficult without her. Dr. Oleg Boyarkine, who was always there for proposing solutions to all the possible problems in the lab and for answering my questions. Dr. Jaime Stearns, Dr. Monia Guidi and Dr. Caroline Seaiby for explaining to me how the machine works and for helping me in the first steps trying to use it. Dr. Annette Svendsen for her enthusiasm, for her deep knowledge of the scientific instruments we use (I hope I wasn't a black box user..) and for very useful discussions concerning my project. Dr. Sandra Brünken for spending time with me in projects that didn't yield many results. Dr. Ulrich Lorenz for scientific, artistic but also "stupid" discussions. And for the hikes, beers and unsuccessful pizzas (good thing we never invited Monia..). Dr. Natalia Nagornova for sharing the office for the first months and for trying to understand together the science that we were expected to do. Dr. Tobias Wassermann for endless discussions in Lausanne (and in Boston!). All the past and present members of the LCPM for creating a friendly atmosphere where coming to work is a pleasure. And of course for being friends.

Dr. Bruce Yoder for.. it goes without saying..

Dr. Gert von Helden, Prof. David Clemmer, Prof. Yury Tsybin and Dr. Ruud Hovius for accepting to be members of the jury for this thesis, and for the very interesting discussion during the private exam.

Last, but not least, I would like to thank my parents, family and friends in Lausanne and abroad, for always being there for me when I need them and, most importantly, when I don't. This was possible also because of you.

